sustainability

Special Issue Reprint

Sustainable Management and Regulation of Agricultural Water Resources in the Context of Global Climate Change

Edited by
Xiaolin Yang, Wenfeng Liu and Wen Yin

mdpi.com/journal/sustainability

MDPI

Sustainable Management and Regulation of Agricultural Water Resources in the Context of Global Climate Change

Sustainable Management and Regulation of Agricultural Water Resources in the Context of Global Climate Change

Guest Editors

Xiaolin Yang
Wenfeng Liu
Wen Yin

MDPI

Basel • Beijing • Wuhan • Barcelona • Belgrade • Novi Sad • Cluj • Manchester

Guest Editors

Xiaolin Yang
College of Water Resources and Civil Engineering
China Agricultural University
Beijng
China

Wenfeng Liu
College of Water Resources and Civil Engineering
China Agricultural University
Beijing
China

Wen Yin
College of Agronomy
Gansu Agricultural University
Beijing
China

Editorial Office
MDPI AG
Grosspeteranlage 5
4052 Basel, Switzerland

This is a reprint of the Special Issue, published open access by the journal *Sustainability* (ISSN 2071-1050), freely accessible at: www.mdpi.com/journal/sustainability/special_issues/3067302Q67.

For citation purposes, cite each article independently as indicated on the article page online and using the guide below:

Lastname, A.A.; Lastname, B.B. Article Title. *Journal Name* **Year**, *Volume Number*, Page Range.

ISBN 978-3-7258-3732-8 (Hbk)
ISBN 978-3-7258-3731-1 (PDF)
https://doi.org/10.3390/books978-3-7258-3731-1

Contents

sustainability

MDPI

Editorial

Sustainable Management and Regulation of Agricultural Water Resources in the Context of Global Climate Change

Wen Yin [1,*], Xiaolin Yang [2,*] and Wenfeng Liu [2]

[1] State Key Laboratory of Aridland Crop Science, College of Agronomy, Gansu Agricultural University, Lanzhou 730070, China
[2] College of Water Resources & Civil Engineering, China Agricultural University, Beijing 100083, China; wenfeng.liu@cau.edu.cn
* Correspondence: yinwen@gsau.edu.cn (W.Y.); yangxiaolin429@cau.edu.cn (X.Y.)

Water is the lifeblood of agriculture, a sector that sustains global food security and livelihoods. However, the increasing complexity of water management in agriculture, exacerbated by global climate change, poses significant challenges to the sustainability of this vital resource. Specifically, climate change has intensified the risks associated with agricultural water management, particularly in regions already grappling with water scarcity [1]. While certain aspects of climate change, such as increased precipitation and elevated CO_2 concentrations, may offer localized benefits, the overarching impacts—reduced water availability, more frequent extreme weather events, and shifting precipitation patterns—threaten agricultural productivity and water security. Moreover, as the global population continues to grow, the demand for food and water is increasing, placing additional pressure on already strained water resources [2]. In addition, climate change exacerbates these pressures by altering precipitation patterns, increasing the frequency and severity of extreme weather events, and raising temperatures, all of which impact agricultural water use [3]. Consequently, in regions where water scarcity is already a concern, these changes pose significant economic and social challenges. Despite some localized benefits, the overall impact of climate change on agricultural water management is overwhelmingly negative, necessitating the development of robust adaptation strategies [4].

In this context, developing adaptation strategies through sustainable water management and regulation is not just a necessity but an imperative. Therefore, this Special Issue seeks to advance our understanding of the risks and adaptation strategies in agricultural water management, with the goal of enhancing the efficient use of limited water resources and ensuring food security in a changing climate. To achieve this, this Special Issue aims to address these challenges by exploring historical and future trends in crop evapotranspiration and irrigation requirements, evaluating the effectiveness of various agronomic and policy measures, and proposing sustainable pathways for adapting to future climate change. Ultimately, the goal is to enhance our understanding of the risks and opportunities associated with agricultural water management under climate change and to provide policymakers with the knowledge needed to formulate effective strategies for reducing the vulnerability of the agricultural sector and increasing its resilience. As a result, we can better prepare for the impacts of climate change and ensure the continued availability of water resources for agricultural production, thereby safeguarding global food security and livelihoods.

In the first paper of this Special Issue, Yunquan Zhang and Peiling Yang discuss a simulation-based optimization model for controlling soil salinization in the Hetao irrigation district in northwest China. Their results provide water shortage and water distribution

check for updates

Received: 17 March 2025
Accepted: 19 March 2025
Published: 20 March 2025

Citation: Yin, W.; Yang, X.; Liu, W. Sustainable Management and Regulation of Agricultural Water Resources in the Context of Global Climate Change. *Sustainability* **2025**, *17*, 2760. https://doi.org/10.3390/su17062760

targets for multiple water sources and levels across five irrigation areas in the HID. These targets were used as the main input parameters for the SALTMOD model, which is based on the principle of water and salt balance. The outputs included data on groundwater mineralization and depth. Their findings revealed that (1) integrated interval two-stage robust stochastic programming and the SALTMOD model can be coupled to simulate a model under uncertainty; (2) systemic risk issues were effectively considered; and (3) the proposed method can be applied to the HID to address soil salinization control. This approach is particularly applicable to arid and semiarid regions facing similar challenges (Contribution 1). Similarly, Pan Li, Wen Yin, Guiping Chen, Yao Guo, Zhilong Fan, Falong Hu, Fuxue Feng, Hong Fan, and Wei He conducted a comprehensive evaluation of yield, resource utilization efficiency, carbon emissions, and economic benefits based on the crop rotation of maize with different wheat straw-returning methods. They concluded that no tillage with 25–30 cm tall wheat straw mulching is a sustainable maize management practice for increasing economic benefits and improving environmental impacts in arid irrigated areas (Contribution 2). This finding highlights the importance of adopting conservation agriculture practices to enhance sustainability in water-scarce regions.

In another study, Xin Zhang, Jianheng Zhang, Jiaxin Xue, and Guiyan Wang confirmed that the S086 variety, combined with a total irrigation water amount of 165 mm, could achieve the dual goals of high crop yields and water use efficiency, thereby reducing groundwater depletion (Contribution 3). This research underscores the potential of crop breeding and precision irrigation technologies to optimize water use in agriculture. Furthermore, Vinod Phogat, Jirka Šimůnek, Paul Petrie, Tim Pitt, and Vilim Filipović used a process-based biophysical numerical model to evaluate water balance and nitrogen (N) dynamics in soils under rainfed wheat cultivation at low- (219 mm, Pygery) and medium-rainfall (392 mm, Yeelanna) sites in South Australia over two seasons. Their results suggest that combining water balance and N modeling can optimize wheat production while minimizing N losses in rainfed agriculture (Contribution 4). This approach provides a valuable tool for managing water and nutrient resources in rainfed systems, which are particularly vulnerable to climate variability. Additionally, Ahmed A. Abdelmoneim, Roula Khadra, Angela Elkamouh, Bilal Derardja, and Giovanna Dragonetti investigated the field validation of a low-cost IoT soil moisture tensiometer prototype, comparing weather-based irrigation to soil moisture-based irrigation in terms of yield and crop water productivity. They noted that while the sensors were deployed for two months during the lettuce crop season, further investigation is needed to assess their long-term reliability and maintenance requirements (Contribution 5). This study not only highlights the potential of IoT-based technologies to improve irrigation efficiency but also emphasizes the need for robust and durable sensor systems.

In another significant contribution, Waqas Ahmed, Suhail Ahmed, Jehangir F. Punthakey, Ghulam Hussain Dars, Muhammad Shafqat Ejaz, Abdul Latif Qureshi, and Michael Mitchell used MODFLOW 2005 to quantify the groundwater budget of the Northern Rohri Canal Command Area under RCP 4.5 and 8.5 climatic scenarios. Their estimates suggest that a sustainable yield of approximately 3 ± 0.3 BCM per year should be maintained to ensure adaptive groundwater reserves during droughts while reducing waterlogging impacts (Contribution 6). This research provides critical insights for managing groundwater resources in regions facing both water scarcity and waterlogging. Moreover, Natalia Julio, Amaya Álvez, Rodrigo Castillo, Kimberly Iglesias, Diego Rivera, Fernando Ochoa, and Ricardo Figueroa analyzed legal approaches and management mechanisms in Chile, highlighting the need for River Basin Boards with broader planning powers to incorporate diverse stakeholders and improve water governance (Contribution 7). Their findings underscore the importance of inclusive and adaptive governance structures for managing water

resources in a changing climate. In a different context, Krzysztof Kud, Aleksandra Badora, and Marian Woźniak used a diagnostic survey method in southeastern Poland to assess the social awareness of water management under climate change. Their findings revealed a lack of awareness about natural water retention methods, with respondents favoring outdated technical solutions like flood embankments and large dams (Contribution 8). This study highlights the need for public education and engagement to promote sustainable water management practices.

Additionally, Edson Costa-Filho, José L. Chávez, and Huihui Zhang evaluated remote sensing (RS) algorithms for estimating maize evapotranspiration (ETa) in semiarid regions. They found that the MSR5 proximal platform provided optimal data, emphasizing the need to improve RS data quality from sub-optimal platforms for sustainable irrigation management (Contribution 9). This research not only demonstrates the potential of remote sensing technologies to enhance irrigation efficiency but also calls for advancements in data quality and accessibility. Finally, Andrzej Brandyk, Ryszard Oleszczuk, Grzegorz Majewski, Mariusz Barszcz, and Katarzyna Rozbicka present a conceptual model for managing drainage/irrigation systems, which demonstrates close alignment with Modflow simulations and offers potential for calibration in polder areas (Contribution 10). This model provides a practical tool for managing water resources in low-lying agricultural areas, which are particularly vulnerable to flooding and waterlogging.

Climate change is expected to have profound impacts on agricultural water management, particularly in regions that are already water-stressed. One of the most significant impacts is the alteration in precipitation patterns, which can lead to both increased drought frequency and more intense rainfall events. These changes can reduce water availability for irrigation, increase the risk of crop failure, and exacerbate soil erosion. Additionally, higher temperatures can elevate evapotranspiration rates, further straining water resources. The Intergovernmental Panel on Climate Change (IPCC) has projected that water availability will decline in many regions, particularly in the subtropics and mid-latitude areas [1]. For example, in the Mediterranean region, water availability is expected to decrease by 20–30% by the end of the century, threatening the productivity of water-intense crops like rice and cotton [5]. Furthermore, extreme weather events such as droughts, floods, and heatwaves are becoming more frequent and severe, leading to crop failures, soil degradation, and economic losses. For instance, the 2012 drought in the United States caused significant reductions in corn and soybean yields [6], while the 2010 Russian heatwave reduced wheat production by 30%, contributing to a global spike in food prices [7].

In addition to these direct impacts, climate change also affects water quality, further complicating agricultural water management. For example, higher temperatures can increase the growth of harmful algae in water bodies [8], while more intense rainfall events can lead to the increased runoff of agricultural chemicals into water sources [9]. These changes not only reduce the availability of clean water for irrigation but also pose risks to human health and ecosystems. Moreover, climate change is expected to exacerbate existing inequalities in water access. In many developing countries, smallholder farmers, who rely heavily on rainfed agriculture, are particularly vulnerable to changes in precipitation patterns and water availability [10]. Without adequate adaptation measures, these farmers face increased risks of crop failure, food insecurity, and poverty.

To address these challenges, a multi-faceted approach is needed, combining technological innovation, policy interventions, and community engagement. Technological solutions, such as precision irrigation, drought-resistant crop varieties, and remote sensing technologies, can enhance water use efficiency and reduce the vulnerability of agricultural systems to climate variability [11]. Policy measures, such as water pricing, subsidies for water-saving technologies, and integrated water resources management, can incentivize

sustainable water use and ensure equitable access to water resources. Community engagement and education are also critical for promoting sustainable water management practices and building resilience at the local level [12].

Looking ahead, there are several key areas where further research and innovation are needed to address the challenges of agricultural water management under climate change. First, there is a need for more accurate and localized climate projections to inform water management decisions. Second, research is needed to develop and scale up innovative technologies, such as smart irrigation systems, drought-tolerant crops, and water-efficient farming practices. Third, there is a need for more integrated approaches for water management that consider the interconnectedness of water, food, energy, and ecosystems. Finally, there is a need for greater collaboration and knowledge sharing among researchers, policymakers, farmers, and other stakeholders to ensure that adaptation strategies are effective, inclusive, and sustainable. By addressing these research gaps and fostering collaboration across sectors, we can build a more resilient and sustainable agricultural system that is capable of meeting the challenges of a changing climate and ensuring food security for all.

In conclusion, climate change poses significant challenges to agricultural water management, particularly in water-stressed regions. However, by adopting advanced irrigation technologies, implementing water-saving agronomic practices, and developing policies that promote sustainable water management, it is possible to enhance the resilience of agricultural systems and reduce their vulnerability to climate change. This Special Issue contributes to this goal by exploring historical and future trends in crop evapotranspiration and irrigation requirements, evaluating the effectiveness of various agronomic and policy measures, and proposing sustainable pathways for adaptation. By enhancing our understanding of the risks and opportunities associated with agricultural water management under climate change, we can develop more effective strategies to ensure food security and promote sustainable agricultural production in the face of a changing climate. Ultimately, the sustainable management of agricultural water resources is not only essential for ensuring food security but also for protecting ecosystems, supporting rural livelihoods, and promoting economic development. As the global community continues to grapple with the impacts of climate change, it is imperative that we prioritize the development and implementation of sustainable water management practices to safeguard this vital resource for future generations.

Conflicts of Interest: The authors declare no conflicts of interest.

List of Contributions

1. Zhang, Y.; Yang, P. A Simulation-Based Optimization Model for Control of Soil Salinization in the Hetao Irrigation District, Northwest China. *Sustainability* **2023**, *15*, 4467. https://doi.org/10.3390/su15054467
2. Li, P.; Yin, W.; Chen, G.; Guo, Y.; Fan, Z.; Hu, F.; Feng, F.; Fan, H.; He, W. Sustainable Analysis of Maize Production under Previous Wheat Straw Returning in Arid Irrigated Areas. *Sustainability* **2023**, *15*, 8935. https://doi.org/10.3390/su15118935
3. Zhang, X.; Zhang, J.; Xue, J.; Wang, G. Improving Wheat Yield and Water-Use Efficiency by Optimizing Irrigations in Northern China. *Sustainability* **2023**, *15*, 10503. https://doi.org/10.3390/su151310503
4. Phogat, V.; Šimůnek, J.; Petrie, P.; Pitt, T.; Filipović, V. Sustainability of a Rainfed Wheat Production System in Relation to Water and Nitrogen Dynamics in the Soil in the Eyre Peninsula, South Australia. *Sustainability* **2023**, *15*, 13370. https://doi.org/10.3390/su151813370
5. Abdelmoneim, A.A.; Khadra, R.; Elkamouh, A.; Derardja, B.; Dragonetti, G. Towards Affordable Precision Irrigation: An Experimental Comparison of Weather-Based and Soil Water Potential-Based Irrigation Using Low-Cost IoT-Tensiometers on Drip Irrigated Lettuce. *Sustainability* **2024**, *16*, 306. https://doi.org/10.3390/su16010306

6. Ahmed, W.; Ahmed, S.; Punthakey, J.F.; Dars, G.H.; Ejaz, M.S.; Qureshi, A.L.; Mitchell, M. Statistical Analysis of Climate Trends and Impacts on Groundwater Sustainability in the Lower Indus Basin. *Sustainability* **2024**, *16*, 441. https://doi.org/10.3390/su16010441
7. Julio, N.; Álvez, A.; Castillo, R.; Iglesias, K.; Rivera, D.; Ochoa, F.; Figueroa, R. The Role of River Vigilance Committees to Address New Socio-Climatic Conditions in Chile: Insights from Ostrom's Design Principles for Common-Pool Resource Institutions. *Sustainability* **2024**, *16*, 1027. https://doi.org/10.3390/su16031027
8. Kud, K.; Badora, A.; Woźniak, M. Sustainable Management in River Valleys, Promoting Water Retention—The Opinion of Residents of South-Eastern Poland. *Sustainability* **2024**, *16*, 4648. https://doi.org/10.3390/su16114648
9. Costa-Filho, E.; Chávez, J.L.; Zhang, H. Mapping Maize Evapotranspiration with Two-Source Land Surface Energy Balance Approaches and Multiscale Remote Sensing Imagery Pixel Sizes: Accuracy Determination toward a Sustainable Irrigated Agriculture. *Sustainability* **2024**, *16*, 4850. https://doi.org/10.3390/su16114850
10. Brandyk, A.; Oleszczuk, R.; Majewski, G.; Barszcz, M.; Rozbicka, K. Model-Supported Groundwater Table Control on the Vistula River Plain—Methodological Approach. *Sustainability* **2024**, *16*, 11190. https://doi.org/10.3390/su162411190

References

1. IPCC. *Climate Change 2021: The Physical Science Basis. Contribution of Working Group I to the Sixth Assessment Report of the Intergovernmental Panel on Climate Change*; Cambridge University Press: Cambridge, UK, 2021.
2. FAO. *The State of Food and Agriculture 2020: Overcoming Water Challenges in Agriculture*; Food and Agriculture Organization of the United Nations: Rome, Italy, 2020.
3. Javansalehi, M.; Shourian, M. Assessing the impacts of climate change on agriculture and water systems via coupled human-hydrological modeling. *Agr. Water Manag.* **2024**, *300*, 108919. [CrossRef]
4. Rosenzweig, C.E.; Elliott, J.; Deryng, D.; Ruane, A.C.; Mueller, C.; Arneth, A.; Boote, K.J.; Folberth, C.; Glotter, M.; Khabarov, N. Assessing agricultural risks of climate change in the 21st century in a global gridded crop model intercomparison. *Proc. Natl. Acad. Sci. USA* **2013**, *111*, 3268–3273. [PubMed]
5. Cramer, W.; Guiot, J.; Fader, M.; Garrabou, J.; Gattuso, J.P.; Iglesias, A.; Lange, M.A.; Lionello, P.; Llasat, M.C.; Paz, S. Climate change and interconnected risks to sustainable development in the Mediterranean. *Nat. Clim. Change* **2018**, *8*, 972–980. [CrossRef]
6. USDA. *U.S. Drought 2012: Farm and Food Impacts*; United States Department of Agriculture: Washington, DC, USA, 2013.
7. Barriopedro, D.; Fischer, E.M.; Luterbacher, J.; Trigo, R.M.; García-Herrera, R. The hot summer of 2010: Redrawing the temperature record map of Europe. *Science* **2011**, *332*, 220–224. [CrossRef] [PubMed]
8. Paerl, H.W.; Paul, V.J. Climate change: Links to global expansion of harmful cyanobacteria. *Water Res.* **2012**, *46*, 1349–1363. [CrossRef] [PubMed]
9. Ongley, E.D.; Zhang, X.L.; Tao, Y. Current status of agricultural and rural non-point source Pollution assessment in China. *Environ. Pollut.* **2010**, *158*, 1159–1168. [CrossRef] [PubMed]
10. IPCC. *Climate Change 2022: Impacts, Adaptation, and Vulnerability. Contribution of Working Group II to the Sixth Assessment Report of the Intergovernmental Panel on Climate Change*; IPCC: Geneva, Switzerland, 2022.
11. Rosegrant, M.W.; Ringler, C.; Zhu, T. Water for Agriculture: Maintaining Food Security under Growing Scarcity. *Annu. Rev. Environ. Resour.* **2010**, *34*, 205–222. [CrossRef]
12. Wutich, A.; Brewis, A.; Tsai, A. Water and mental health. *WIRES Water* **2016**, *3*, 145–165. [CrossRef]

sustainability

MDPI

Article

Model-Supported Groundwater Table Control on the Vistula River Plain—Methodological Approach

Andrzej Brandyk *, Ryszard Oleszczuk, Grzegorz Majewski, Mariusz Barszcz and Katarzyna Rozbicka

Institute of Environmental Engineering, Warsaw Univeristy of Life Sciences, Nowoursynowska St. 159, 02-776 Warsaw, Poland; ryszard_oleszczuk@sggw.edu.pl (R.O.); grzegorz_majewski@sggw.edu.pl (G.M.); mariusz_barszcz@sggw.edu.pl (M.B.); katarzyna_rozbicka@sggw.edu.pl (K.R.)

* Correspondence: andrzej_brandyk@sggw.edu.pl; Tel.: +48-22-5935377

Abstract: At present, a sustainable and wise management of water resources requires more insight into drainage/irrigation practices in river valleys. Since efficient sub-irrigation, based on reliable hydrometeorological forecasts, has been extensively considered with respect to water saving, the proper modeling tools were subsequently developed. An original, conceptual model for the management of drainage/irrigation systems was presented, taking into account the water inflow and storage in the soil profile. The aim was to propose a relatively simple procedure with parameters that relate to easily obtainable variables, e.g., groundwater table depth in the form of uncomplicated equations. The results of this tool were compared with the groundwater heads simulated using the recognized, common Modflow model. The comparisons proved a close match of the modeled variables and point at possibilities to calibrate it on polder areas.

Keywords: groundwater dynamics; drainage/irrigation plots; conceptual model; specific yield; drainage/irrigation time constant; calibration

Citation: Brandyk, A.; Oleszczuk, R.; Majewski, G.; Barszcz, M.; Rozbicka, K. Model-Supported Groundwater Table Control on the Vistula River Plain—Methodological Approach. *Sustainability* **2024**, *16*, 11190. https://doi.org/10.3390/su162411190

Academic Editors: Xiaolin Yang, Wenfeng Liu and Wen Yin

Received: 5 August 2024
Revised: 22 November 2024
Accepted: 13 December 2024
Published: 20 December 2024

1. Introduction

A proper description of river valley polder management at multiple scales and degrees of achievement has been established as one of the issues of modeling in environmental and hydrological sciences [1–5]. The existing models are based generally on analytical solutions of partial differential equations for well-defined soils and porous media or respective conceptual models dedicated to soil water management [6–8]. Still, the particular character and choice of those models and their parameters was the subject of controversy in terms of applicable conditions.

The main research field which still deserves insight and innovative solutions is drainage/irrigation scheduling, including the parameters that can effectively delineate the process [7–13]. For this purpose, this paper focuses on a conceptual model [13] based on the drainage/irrigation time constant, soil-specific yield and water fluxes in the soil profile related to the groundwater level position in the form of simple equations. The main novelty was to propose a relatively uncomplicated, analytical model for drainage/irrigation practices with the parameters related to easily measurable variables, e.g., groundwater table depth. Its suitability was proven at a polder in central Poland within a subirrigation system, based on the developed groundwater dynamics equation in ditch midspacing [13]. On the other hand, the results of the conceptual model were next compared with the common, numerical Modflow model, as the basic tool for groundwater table simulations over the valley areas.

2. Materials and Methods

2.1. Study Site

The model calibration was attempted within the sections of Troszyn Polder (with total area of 550 ha, 52.42–52.43 N, 19.83–19.835 E, and surface of research plots equal to

53 ha) located in the Valley of the Vistula River, central Poland, 15 km south of the city of Plock. This area was covered by a dense network of drainage/irrigation ditches (Figure 1) of design spacing equal to 120 m, and divided into basic subirrigation plots (S, A1, A2, C, B1, B2). They formed a complex hydraulic and hydrologic water distribution system, supplied by Gabinianka River (northern border), Dobrzykowski Channel (eastern border) and Słubicki Channel located in the center. The whole polder, situated parallel to the Vistula River at a distance of 2 km, is also characterized by nearly uniform terrain elevation (57.70 m above sea level) with subtle differences near the ditches (altitude in a close-to-ditch zone equals about 57.55 m asl.).

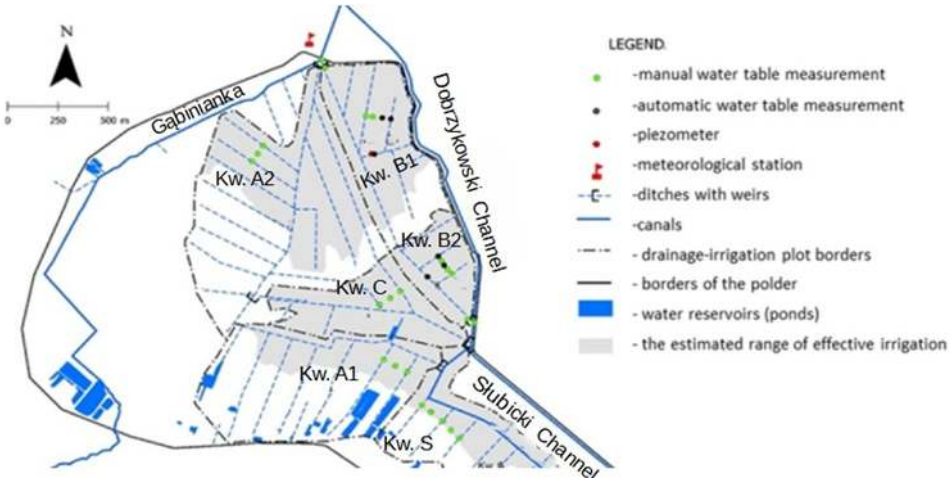

Figure 1. Troszyn Polder (the whole system of drainage/irrigation plots).

Considerable variability of soil types exists within the area as it was subject to a number of fluvial processes that finally shaped the structure of the Vistula Valley in this part of Poland [14]. The complexity of soil-forming processes was manifested through texture class fractions and variable organic matter content. The research site is covered by Fluvic Gleyic Phaeozems [15] based on 15 soil samples containing sand fraction—13% on average, standard deviation (SD)—7.7%; silt-averaging 56%, with SD of 6.0%; clay fraction equal to 20.5% on average, SD—7.5%; and organic matter content of 11.7% with SD that equaled 4.0%. A characteristic feature of the above-mentioned heavy soils is their high organic matter content, while their thickness ranges from 1.8 to 2.1 m and they are underlain by sandy aquifer. In such geomorphologic conditions, that area forms a typical polder, with terrain elevation that is approximately equal to mean water levels in the Vistula River. For those reasons, it needs proper water management to make its current use possible (3-swath meadows with an average hay yield of 10 t·ha^{-1}) and also provide protection against flooding phenomena [13].

The current stage of analyses focused only on the northern parts of the plots (A2, B1, Figure 2) in the elementary spaces between two parallel ditches (120 m wide by about 350 m long). Monitoring points were established within those plots: wells S2 and P2 in midspacing of the ditches for groundwater table recording; S1 and P1—water gauges for ditch water level observations; and S3—piezometer for aquifer head measurements.

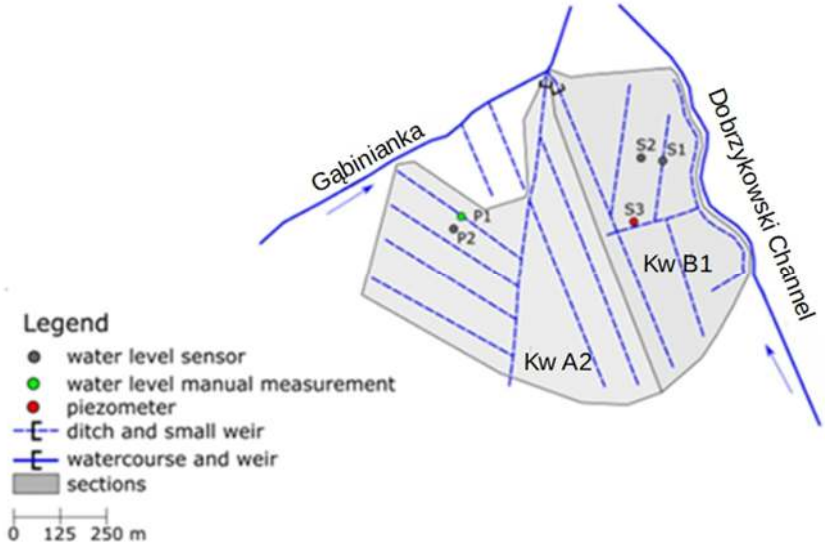

Figure 2. Analyzed plots of the polder.

Wells no. S2 and P2 as well as gauge no. S1 were equipped with automatic (Solinst Levelogger model 3001, Solinst Canada Ltd., Georgetown, ON, Canada) loggers for water table position recording, while at S3 (piezometer), the measurements were carried out manually. At well no. S2, the Adcon profile probe (SM1 Soil Moisture Sensor) was installed for soil moisture content recording with sensor spacing of 0.1 m (6 sensors in depth range 0.1–0.6 m) that was further utilized for rootzone moisture estimates in midspacing of the ditches. At well no. P2, rootzone volumetric moisture content was estimated through TDR measurements [16–19].

Based on the retention curve estimations for averaged 30 cm soil layer (rootzone), the value of θs reached 0.58 cm^3/cm^3, while θc was equal to 0.38 cm^3/cm^3, θ_{FC} to 0.47 cm^3/cm^3 and θ_{WP} equaled 0.25 cm^3/cm^3. The calculated, effective capillary range was equal to 1.0 m, hence the full range zp = za +1 m =1.3 m applied in the conceptual model (depth of root zone zp = 0.3 m). Additionally, the coefficient of effective precipitation (precipitation use efficiency) was assumed to be equal to 1 for the sake of modeling, and the values of crop coefficient for calculation of evapotranspiration were adopted for actual land use as a three-cut meadow of an average hay yield of 10 $t \cdot ha^{-1}$ [11,13].

Hydrogeological setting of the analyzed area involved one, unconfined sandy aquifer of an average thickness of 17 m, underlain by clay formations (Figure 3). This was essential to implement groundwater heads in the main horizon for the upward seepage representation in both conceptual and numerical model.

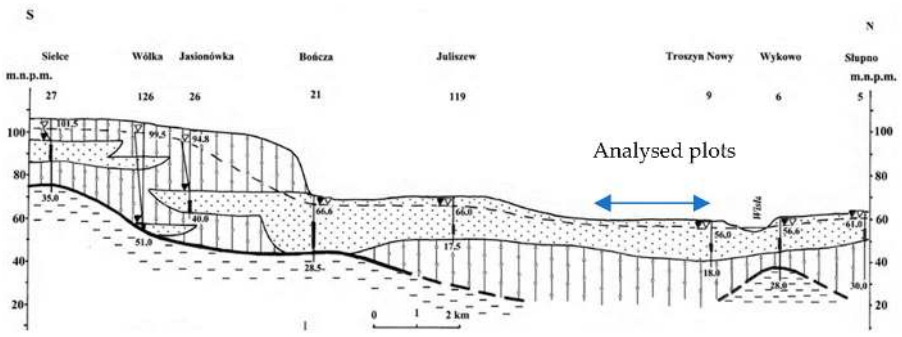

Figure 3. Hydrogeological cross-section through the Polder area: ▼—unconfined water table, ▽—confined water table.

2.2. Conceptual Modeling Procedures

The main part of the proposed model of drainage/irrigation (subirrigation) functioning, elaborated by Kaca [13], can be expressed as a conceptual equation of groundwater table dynamics in the following form:

$$h'_{2j+1} = h_{2j}\exp(A_T\Delta t) - \frac{1}{A_T T}\left(h_{1j+1-n} - h_{1j-n}\right) - \left[\frac{1}{A_T^2 T}\frac{h_{1j+1-n}-h_{1j-n}}{\Delta t} + \frac{1}{A_T}\left(\frac{1}{T}h_{1j-n} + \frac{B_z}{\mu}\right)\right][1-\exp(A_T\Delta t)]\ ; \quad (1)$$

$$n = 0,\ 1,\ 2, \ldots$$

$$A_T = \frac{A_z}{\mu_o} - \frac{1}{T}\ \mu_o > 0 \quad (2)$$

j = number of the current moment of calculation;
Δt = the computation interval of time, e.g., day $\left(\Delta t = t_{j+1-n} - t_{j-n} = t_{j+1} - t_j\right)$, [T];
n = natural number and zero;
$\tau = n \cdot \Delta t$ = time-lag of irrigation or drainage [T];
T = the time constant of drainage/irrigation [T];
A_z = vertical groundwater flux (from or to aquifer) [1/L];
B_z = infiltration or capillary rise equivalent of soil water [L/T];
μ_0 = the specific yield in soil profile [-];
h'_{2j+1} = groundwater level in midspacing of the ditches/drainpipes without taking into account deep percolation of soil water at the moment $j + 1$ [L];
h_{2j} = initial condition − groundwater level midspacing between the ditches/drain pipes after taking into account deep percolation of soil water, at the moment j [L];
h_{1j+1-n} and h_{1j-n} = inducing factors − the water table level in the ditches/in soil at the lines of the drainpipes in moment $j + 1 - n$ and $j - n$, respectively.

$$A_z = -S,\ B_z = S\left(z_p - z_s\right) - (ET - P_e) + q_n \quad \text{for } \left[\left(z_p - z_a\right) < \overline{h}' \le z_p\right] \wedge [(ET - P_e) > 0], \quad (3)$$

$$A_z = -S - (ET - P_e)\frac{1}{z_p - z_a},\ B_z = S\left(z_p - z_a\right) + q_n \quad \text{for } \left[0 < \overline{h}' \le (z_p - z_a)\right] \wedge [(ET - P_e) > 0], \quad (4)$$

$$A_z = -S,\ B_z = S\left(z_p - z_a\right) + q_n \quad \text{for } \left[\overline{h}' < 0\right] \vee [(ET - P_e) \le 0] \quad (5)$$

where
$\overline{h}' = \beta_1 h'_1 + (1 - \beta_1)h'_2$ = the average shallow level of groundwater at any given time without taking into account deep percolation of soil water [L];
$h'_1,\ h'_2$ = the water level in the ditches/in the line of the drainpipes and the shallow groundwater level midspacing between the ditches/drainpipes, respectively, at the cross-section without taking into account deep percolation of soil water [L];
β_1 = coefficient of the shape of the groundwater table curve between the ditches/drainpipes [-];
ET = flux density of evapotranspiration at the cross-section [L·T^{-1}];
P_e= flux density of effective precipitation and effective sprinkler irrigation rate (infiltration into the unsaturated zone) [L·T^{-1}];
z_p = depth beneath the land surface to the reference level (full capillary rise range) [L];
z_a = the depth of the root zone of plants in the soil profile [L];
z_s = actual depth to deep aquifer head (confined) [L];
m_1 = the thickness of the soil profile [L];
m_2 = the thickness of the aquitard over the aquifer[L];
S = water exchange coefficient between the aquifers [T^{-1}];

$q_n = q_i - q_0$ = the net lateral flux density of water in horizontal subsurface flow exchanged with adjacent areas (released from or taken into soil storage) [$L \cdot T^{-1}$].

At this stage of model description, we omitted a range of equations for water equivalent of transient porosity (water reserves in the soil profile). The relevant, fully developed equations are given in work [13], stressing a complex interdependence of water equivalent of transient porosity and the specific yield, evapotranspiration and precipitation rate, capillary rise range and water table position. A number of representative formulas may be also found for the relationships of the total specific yield and ground water table depth [13].

Since the conceptual model (Figures 4 and 5) requires the input of the water equivalent of transient porosity, of which starting values are relatively difficult to identify, the resultant average soil moisture of the soil root zone was incorporated into the model. This also generates possibility to simulate the soil moisture content or use it in the calibration process. The average soil moisture of the root layer with a thickness of z_a, along with the groundwater table level, h_{j+1}, is given by the following equation:

$$\theta = \theta_s - \frac{W_{j+1}^{corr} - \delta_{aj+1}}{z_a} \quad (6)$$

where

θ—average soil moisture of the root layer with thickness of z_a [L^3L^{-3}];

θ_s—average saturated soil moisture of the root layer with thickness of z_a [L^3L^{-3}];

δ_{aj+1}—transient porosity below the layer of the main mass of plants roots with thickness of z_a.

The above equation enabled flexibility in conceptual modeling, not by starting with estimated water equivalent (soil water reserves) of the transient porosity, but by launching the simulations using actually measured, volumetric soil water contents.

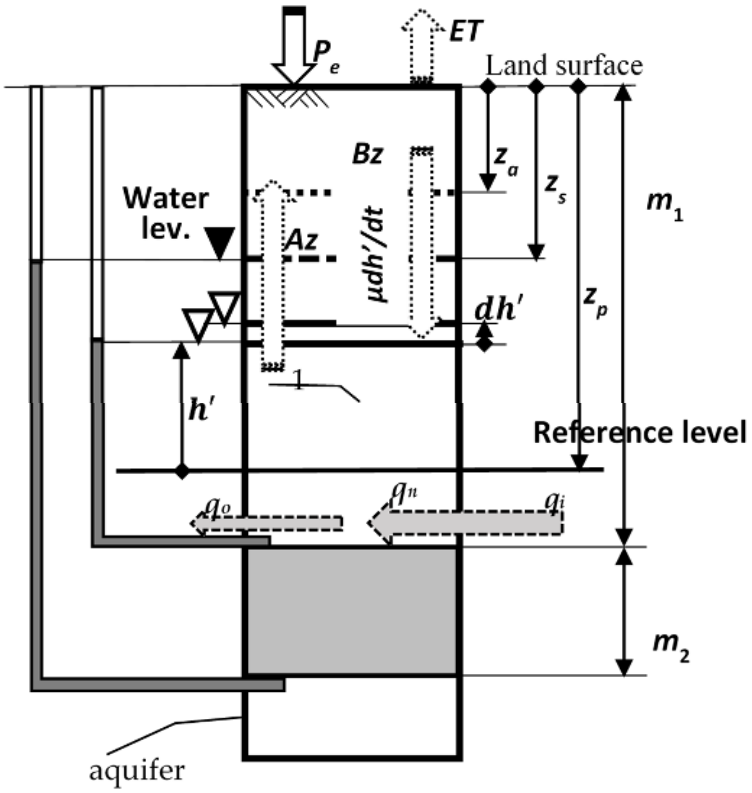

Figure 4. Model schematic of the soil profile. ▼—unconfined water table, ▽—confined water table.

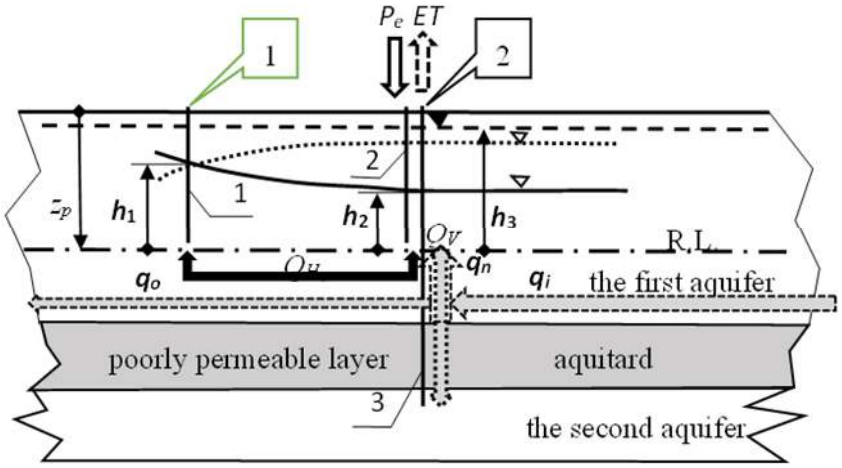

Figure 5. Schematic, model cross-section through the field perpendicular to two ditches: 1, 2—observation wells. ▼—unconfined water table, ▽—confined water table.

2.3. Numerical Modelling

A common groundwater flow model recognized world-wide, Modflow, was alternatively used to simulate groundwater table position in ditch midspacing within the analyzed plots. The following governing equation for a quasi-3-dimensional flow of groundwater in the saturated zone was utilized [19,20]:

$$\frac{d}{dx}\left(T_x\frac{dH}{dx}\right)+\frac{d}{dy}\left(T_y\frac{dH}{dy}\right)+\frac{d}{dz}\left(T_y\frac{dH}{dz}\right)-W=S\frac{dh}{dt} \quad (7)$$

where

T_x, T_y, T_z,—aquifer transmissivities in three directions, x, y, z [L^2T^{-1}], defined as follows:

$$T=\begin{cases} k{\cdot}m—for\ a\ confined\ aquifer \\ k(H-h)—for\ an\ unconfined\ aquifer; \end{cases} \quad (8)$$

k—saturated hydraulic conductivity [$L{\cdot}T^{-1}$];
m—aquifer thickness [L];
H—hydraulic head [L];
h—aquifer bottom elevation [L];
W—recharge from internal and external sources [$L{\cdot}T^{-1}$];
S—storage coefficient [-].

The differential equation is replaced in the Modlow code by a simplified form, based on mass conservation law. As a consequence, a continuous groundwater flow system is transformed into a discrete set of computational model grid cells (Figure 6), consisting of rows, columns and layers.

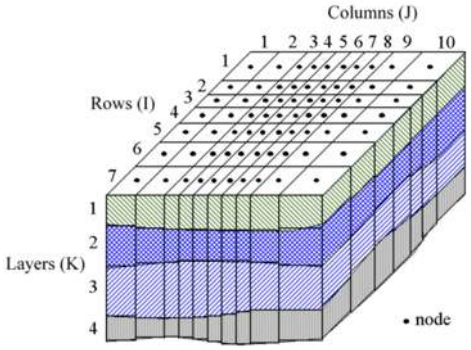

Figure 6. Sample numerical model grid, consisting of 10 columns, 7 rows and 4 layers.

Simulations involve mass balance conservation of all cells in the grid. Water table elevation in any individual cell depends on inflows from neighboring cells and external sources of water, such as precipitation, drain inflows or outflows, wells, pumping stations, irrigation rates or water reservoir leakage [21,22].

Rows and columns are defined in such a way to cover the whole modeled area in the plain view. The size of the rows and columns is related to the expected accuracy of the model but also occurring hydrogeological conditions, e.g., the spots of large hydraulic head gradients, such as wells, water intakes, flow barriers, etc. The number of model layers, on the other hand, is crucial to represent the setting of aquifers and aquitards. The layers are assigned to the main hydrostratigraphic units, with usual simplification of flow conditions; that is to say, one layer represents one aquifer. It is possible to assign computational layers to each geologic or stratigraphic formation individually, but it leads to multi-layer grids of a high complexity in terms of model calibration.

In the case analyzed herein, two model layers were used to represent the main aquifer, with the first one for shallow sandy layers and the second one used only to simulate vertical exchange of groundwater (vertical leakance) with the underlaying loamy deposits (Figure 3).

2.4. Model Assumptions Summary

The conceptual model of groundwater table dynamics (Section 2.2) needs calibration and validation on real, existing areas (plots), because it constitutes a newly developed tool (Equations (1)–(6)). The emerging need for testing that model is essential, because it offers potential to simulate a real water amount taken in or discharged in drainage/irrigation (subirrigation) conditions and further forecast impacts on soil management and crop yields. The possibilities are open to develop the conceptual model into operational planning tool for a number of interconnected plots, on condition that it is combined with water balance equation, considering the surface water exchange between the plots (connected by supplier canals) [13].

Detailed implications for water management over plots are the potential of the conceptual model, but the base is the modeling of the groundwater table and its variability using Modflow [17,19–21]. This has become the reason to possibly compare the groundwater level results of those models.

The advantage of the conceptual model (basically Equation (1)) is the link of

- Unsaturated and saturated zones. The model is capable of calculating the water reserves and transient leakage from the saturated zone to groundwater horizon. Modflow is pure saturated-zone model and needs calibration of the areal recharge (leakage) from vadose zone to groundwater table.
- The conceptual model considers only the groundwater table in midspacing of the ditches or drains. Modflow is capable of simulating it at every point of the plot (owing to spatial, numerical grid).
- The time of irrigation and groundwater inflow to the plot can be simulated by both the conceptual and the numerical model.
- The conceptual model takes into account one, main aquifer, which is usually enough to simulate the water management in drained or irrigated plots. Modflow, depending on the version, is able to consider dozens of aquifers or layers.
- Surface water inflow rates are considered by the conceptual model. Modflow alone does not, but since it can be integrated with known surface water models, it may then offer such possibility. For this reason, the presented conceptual model can be developed into a scheme of interconnected plots, including drainage/irrigation channels that connect them for water exchange estimation within the whole system. Modflow can account for groundwater exchange only, and in its original version is not capable of also being surface water distribution tool.

3. Results and Discussion

The simulations of groundwater tables in the midspacing of the ditches were attempted to gain initial insight into the possibilities of applying a conceptual model (Equations (1)–(6)) to valley area management. That model was subject to optimization [11,13] with the average approximation error as an estimator of the model quality and also visual comparisons of the modeled and observed groundwater tables.

$$Q_y = \sqrt{\frac{1}{N}\sum_{j=1}^{N}\left(y_j - \hat{y}_j\right)^2} \tag{9}$$

where

N = the number of results of the measurements and calculations taken for comparison;
y_j, $\widehat{y}_j$ = the calculated and measured values, respectively.

The y_j, $\widehat{y}_j$ values stand for the level of groundwater h_{2j} and $\widehat{h}_{2j}$ or alternatively the moisture content θ_{2j} and $\widehat{\theta}_{2j}$ in the root layer of the soil, in the middle of the ditches, calculated and measured, respectively. The criterion function (standard deviation of residual values) was minimized using the groundwater level data, providing the following resultant global parameter values: m_0—the specific yield (Equations (1) and (2)), T—the drainage/irrigation time constant (Equations (1) and (2)), S—the water exchange coefficient between the aquifers (Equations (3)–(5)) and additionally q_s—the saturated water content (Equation (6)). The optimization was based on assumptions of the Hooke–Jeeves algorithm [23] that introduced reasonable parameter value ranges, randomized their values within those ranges and defined the starting value of a parameter. Next, the ensemble of approximation errors was calculated and terminated when the minimum was reached. As given in Section 2.1, those parameters were optimized for two plots of the polder: B1 and A2 (Figures 7 and 8).

For both plots, similarities were found with respect to the parameter values. The specific yield m was equal to 0.13 [-] and the time constant T reached 10.5 days for two plots, while the S value was equal to 3.0×10^{-5} 1/d for the A2 plot and 1.5×10^{-3} 1/d for B1.

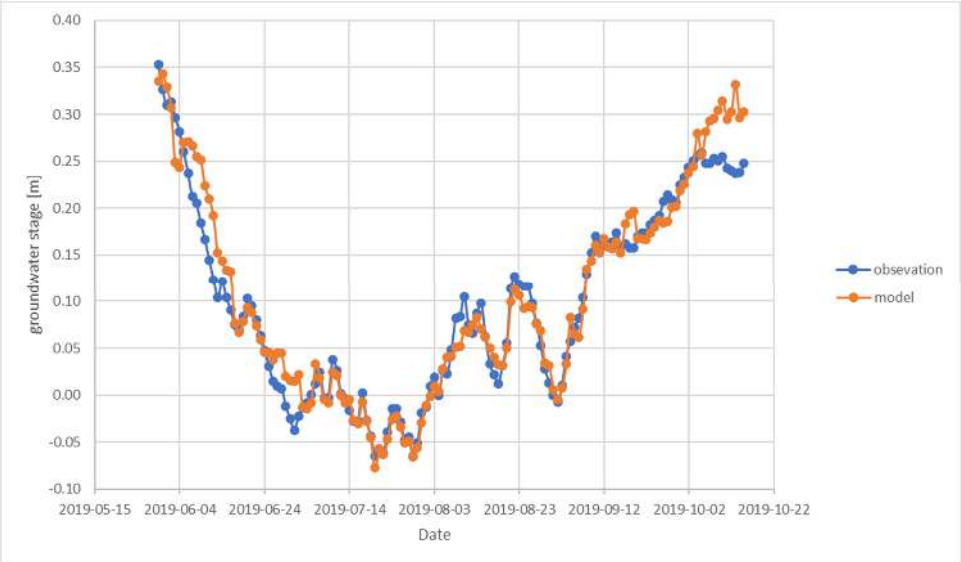

Figure 7. Comparison of modeled and observed groundwater stages at well S2, plot B1, conceptual model (calibration period).

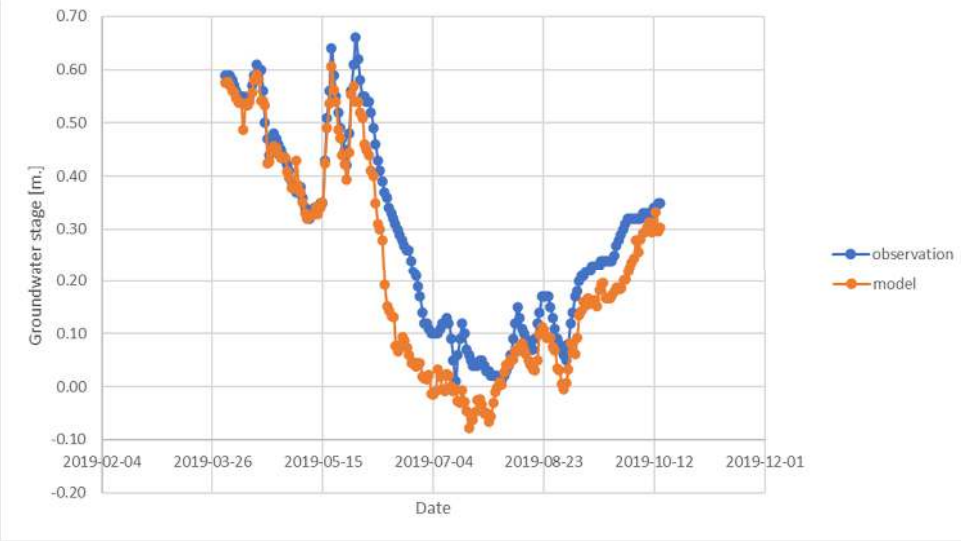

Figure 8. Comparison of modeled and observed groundwater stages at well P2, plot A2, conceptual model (calibration period).

The saturated water content q_s reached 0.77 for A2 and 0.68 for B1. The measurements of retention curve characteristics provided the q_s range: 0.57–0.64 for the B1 plot, which is fairly comparable with the calibrated values [13]. The approximation error (the deviation between the model and observations Qy) reached 0.044 m for the A2 plot (R^2 = 0.88) and 0.057 m for B1 (R^2 = 0.84), while the visual comparisons of the measured and simulated groundwater levels showed a close match.

Next, the results of the conceptual model and Modflow calibration were compared. The value of the specific yield m was also equal to 0.13, but the time constant T reached a longer time by Modflow calibration of about 30 days. S, the water exchange coefficient between the aquifers, showed similarity and equaled 3.2×10^{-5} 1/d. The approximation error Q_y amounted to 0.084 m for the Modflow model simulation.

The course of observations and Modflow model results for plot B1 also show agreement through visual comparisons (Figure 9). Taking into account that the trend of groundwater tables was preserved for both models and average simulation errors Qy were fairly comparable, the conceptual model has proven its reliability for groundwater dynamic simulations in ditch midspacing.

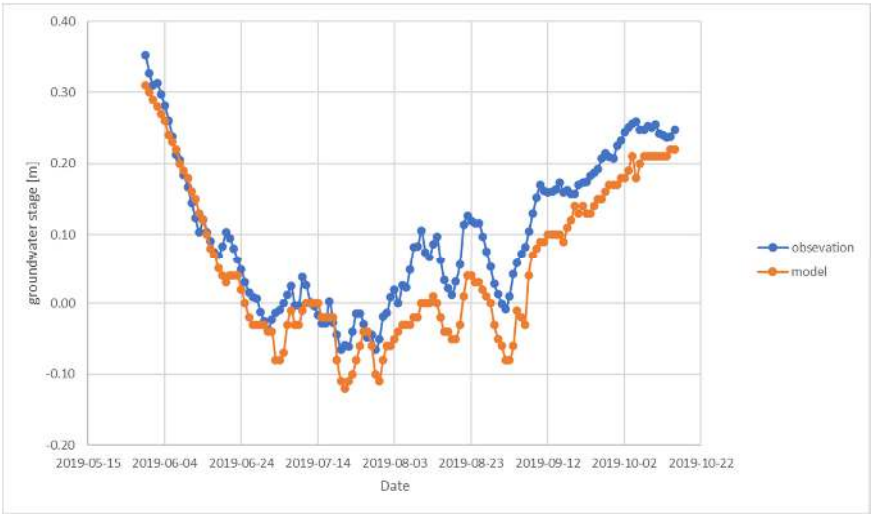

Figure 9. Comparison of modeled and observed groundwater stages for S2 well, plot B1, Modflow model (calibration period).

After the calibration stage, in order to complete the required model validation procedure, the course of independent groundwater table observations was gathered for both wells: S2 and P2. Those data encompassed the period 10 March 2020–22 August 2020 for the B1 plot (S2 well) and 10 March 2020–6 August 2020 for the A2 plot (P2 well). The model was run on the previously calibrated global parameter values, followed by the estimations of the match between the simulated and observed groundwater stages (Figures 10 and 11).

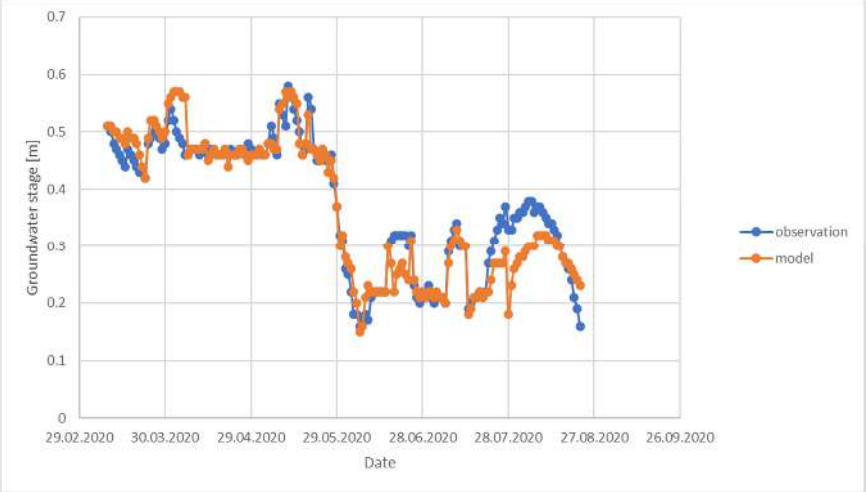

Figure 10. Comparison of modeled and observed groundwater stages at well S2, plot B1, conceptual model (validation period).

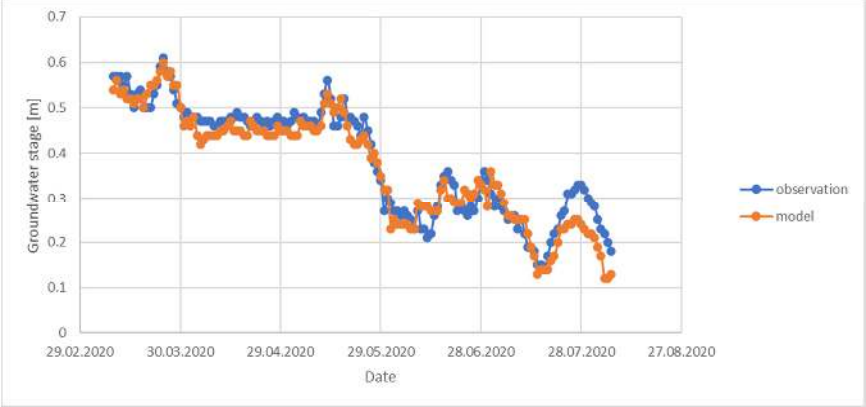

Figure 11. Comparison of modeled and observed groundwater stages at well P2, plot A2, conceptual model (validation period).

Again, the visual comparisons showed a close agreement of the modeled and observed variables. The approximation error (the deviation between the model and observations *Qy*) reached 0.09 m for the A2 plot (R^2 = 0.91) and 0.098 m for B1 (R^2 = 0.91) for the assumed validation period. The model exhibited satisfactory quality after validation to finally evidence the reliability of the whole modeling procedure, including the calibration stage followed by the verification of an independent set of observations.

Since the conceptual model is currently in its development and testing phase, Equations (1)–(6) were implemented as an Excel spreadsheet procedure to verify them under different conditions of the river valley areas (e.g., soil types, irrigated or drained plot size, precipitation end evaporation, position in the hydrographic system, etc.). Several test cases were assumed for groundwater and surface water level data collection, weather parameter recording and land and crop cover and topography measurements [13]. For the Solec object in central Poland, 30 km south of Warsaw [17], it was found that the parameters of the calibration reached the following values: m—a specific yield equal to 0.19, *T*—a time

constant of 47 days, *S*—a vertical exchange coefficient of 3.2 $\times$ 10^{-5} 1/d and *qs*—a saturated water content of 0.75 for peat soils within the subirrigation system. These were comparable to the previous studies on that area. For the northeastern areas of Poland, however, higher values of the drainage/irrigation time constant *T* (80 days) were found for Biebrza case studies of a subirrigation plot, along with a specific yield, *m*, of 0.16, a higher vertical exchange coefficient (0.014 1/d) and a *qs* equal to 0.82 for the peat–moorsh soil [13]. On the other hand, the Racot object, located in western Poland, revealed a specific yield, *m*, of 0.16, a time constant *T* of 1 day and a saturated water content, *qs*, equal to 0.90 for histic gley soils with two diverse moorshlayers, where the specific yield and saturated water content were different from the measured values by 16% [8]. It was noted that the main differences pertain to the drainage/irrigation time constant *T*, while other parameters manifested comparability between the research objects, characterized by similar soil types.

4. Conclusions

A conceptual model (Equations (1)–(6)), aimed to become a water management tool for polder areas, underwent the first attempts of calibration in terms of groundwater dynamic simulation. This is supposed to be the base for a fully applicable model for valley polders, on the condition that the fundamental, governing equation proves its calibration and validation quality. In this respect, we found a close match of the observed and modeled groundwater tables on two selected plots of the polder for the adopted calibration and validation periods. Moreover, similarities were reached for the course of groundwater tables simulated by the numerical, recognized Modflow model.

The calibration (optimization) revealed reasonable values of global parameters of the conceptual model for heavy soils (Fluvic Gleyic Phaeozems) underlain by sandy deposits (aquifers). Alternatives are open to also validate that model for rootzone soil water contents (Equation (6)). In terms of reproducibility, the calibration and validation found evidence for the correctness of the model assumptions. In a methodological sense, the proposed modeling procedure is one of the means of managing soil moisture on, e.g., riverside polders. It is meant to contribute to the existing state of knowledge, providing an alternative based on soil water equations (water reserves and water table positions), but it also needs sufficient comparisons with other, accepted models. A vital element, indispensable for building a complete water management tool for the polders, is the incorporation of the water balance equation and its on-site validation.

Author Contributions: Conceptualization, A.B.; methodology, A.B.; software, A.B. and R.O.; validation, R.O., G.M. and M.B.; formal analysis, A.B.; investigation, R.O.; resources, A.B. and K.R.; data curation, M.B.; writing—original draft preparation, A.B. and M.B.; writing—review and editing, K.R. and G.M.; visualization, A.B., R.O. and G.M.; supervision, M.B. All authors have read and agreed to the published version of the manuscript.

Funding: This research was funded by the project "Technological innovations and system of monitoring, forecasting and planning of irrigation and drainage for precise water management on the scale of drainage/irrigation system (INOMEL)" under the BIOSTRATEG3 program, funded by the Polish National Centre for Research and Development, contract number BIOSTRATEG3/347837/11/NCBR/2017.

Institutional Review Board Statement: Not applicable.

Informed Consent Statement: Not applicable.

Data Availability Statement: The data presented in this study are available on request from the corresponding author.

Acknowledgments: Administrative and technical support was provided by the BIOSTRATEG3 program.

Conflicts of Interest: The authors declare no conflicts of interest.

References

1. Van Keulen, H.; Van Beek, C.G. Water movement in layered soils—A simulation model. *Neth. J. Agric. Sci.* **1971**, *19*, 138–153. [CrossRef]
2. Wierenga, P.J.; De Wit, C.T. Simulation of heat transfer in soils. *Soil Sci. Soc. Am. Proc.* **1970**, *34*, 845–848. [CrossRef]
3. Gerke, H.H.; van Genuchten, M.T. A dual-porosity model for simulating the preferential movement of water and solutes in structured porous-media. *Water Resour. Res.* **1993**, *29*, 305–319. [CrossRef]
4. Cole, C.V.; Innis, G.S.; Stewart, J.W. Simulations of phosphorus cycling in semi arid grasslands. In *Grassland Simulation Model*; Innis, G.S., Ed.; Springer: Berlin/Heidelberg, Germany, 1978; Volume 26, pp. 205–230. [CrossRef]
5. Hunt, H.W.; Wall, D.H. Modelling the effects of loss of soil biodiversity on ecosystem function. *Glob. Change Biol.* **2002**, *8*, 33–50. [CrossRef]
6. Hopmans, J.W.; Bristow, K.L. Current capabilities and future needs of root water and nutrient uptake Modeling. *Adv. Agron.* **2002**, *77*, 103–183.
7. Raes, D.; Deproost, P. Model to assess water movement from a shallow water table to the root zone. *Agric. Water Manag.* **2003**, *62*, 79–91. [CrossRef]
8. Sojka, M.; Kozłowski, M.; Stasik, R.; Napierała, M.; Kęsicka, B.; Wróżyński, R.; Jaskuła, J.; Liberacki, D.; Bykowski, J. Sustainable Water Management in Agriculture—The Impact of Drainage Water Management on Groundwater Table Dynamics and Subsurface Outflow. *Sustainability* **2019**, *11*, 4201. [CrossRef]
9. Gurley Kahn, K.; Ge, S.; Saul Caine, J.; Manning, A. Characterization of the shallow groundwater system in an alpine watershed: Handcart Gulch, Colorado, USA. *Hydrogeol. J.* **2008**, *16*, 103–121. [CrossRef]
10. Vogel, H.J.; Roth, K. Moving through scales of flow and transport in soil. *J. Hydrol.* **2003**, *272*, 95–106. [CrossRef]
11. Brandyk, A.; Kaca, E.; Oleszczuk, R.; Urbański, J. Conceptual model of drainage—Subirrigation system functioning- first results from a case study of a lowland valley area in Central Poland. *Sustainability* **2021**, *13*, 107. [CrossRef]
12. Urbański, J.; Bajkowski, S.; Siwicki, P.; Oleszczuk, R.; Brandyk, A.; Popek, Z. Laboratory tests of water level regulators in ditches of irrigation systems. *Water* **2022**, *14*, 1259. [CrossRef]
13. Kaca, E. *Operational Planning of Subirrigation and Drainage-Computer Decision Support System with Case Studies*, 1st ed.; Bogucki Wydawnictwo Naukowe: Poznań, Poland, 2020; pp. 16–31, 81–86. (In Polish)
14. Wierzbicki, G.; Ostrowski, P.; Falkowski, T.; Mazgajski, M. Geological setting control of flood dynamics in lowland rivers (Poland). *Sci. Total Environ.* **2018**, *636*, 367–382. [CrossRef] [PubMed]
15. Agriculture Organization for the United Nations. *World Reference Base for Soil Resources*; World Soil Resources Report; FAO: Rome, Italy, 2014; update 2015.
16. Gnatowski, T.; Szatylowicz, J.; Pawluskiewicz, B.; Oleszczuk, R.; Janicka, M.; Papierowska, E.; Szejba, D. Field Calibration of TDR to Assess the Soil Moisture of Drained Peatland Surface Layers. *Water* **2018**, *10*, 1842. [CrossRef]
17. Oleszczuk, R.; Jadczyszyn, J.; Gnatowski, T.; Brandyk, A. Variation of moisture and soil water retention in a lowland area of Central Poland—Solec site case study. *Atmosphere* **2022**, *13*, 1372. [CrossRef]
18. Aliyari, F.; Bailey, R.; Tasdighi, A.; Dozier, A.; Arabi, M.; Zeiler, K. Coupled SWAT-MODFLOW model for large-scale mixed agro-urban river basins. *Environ. Model. Softw.* **2019**, *115*, 200–210. [CrossRef]
19. Sisay, B.M.; Nedaw, D.; Birhanu, B.; Gigar, A.G. Application of SWAT and MODFLOW models for characterization of surface–groundwater interaction in the Modjo River catchment, central Ethiopia. *Environ. Earth Sci.* **2023**, *82*, 341. [CrossRef]
20. Calderon-Palma, H.; Bentley, L. A regional scale groundwater flow model for the Leon- Chinandega aquifer, Nicaragua. *Hydrogeol. J.* **2007**, *15*, 1457–1472. [CrossRef]
21. Han, Q.; Xue, L.; Liu, Y.; Yang, M.; Chu, X.; Liu, S. Developing a multi-objective simulation-optimization model for ecological water conveyance in arid inland river basins. *J. Hydrol. Reg. Stud.* **2023**, *50*, 101551. [CrossRef]
22. Sunohara, M.D.; Gottschall, N.; Craiovan, E.; Wilkes, G.; Topp, E.; Frey, S.K.; Lapen, D.R. Controlling tile drainage during the growing season in Eastern Canada to reduce nitrogen, phosphorus, and bacteria loading to surface water. *Agric. Water Manag.* **2016**, *178*, 159–170. [CrossRef]
23. Kalyanmoy, D. *Optimization for Engineering Design*; Prentice Hall: New Delhi, India, 1988.

sustainability

MDPI

Article

Mapping Maize Evapotranspiration with Two-Source Land Surface Energy Balance Approaches and Multiscale Remote Sensing Imagery Pixel Sizes: Accuracy Determination toward a Sustainable Irrigated Agriculture

Edson Costa-Filho [1], José L. Chávez [1,*] and Huihui Zhang [2]

[1] Civil and Environmental Engineering Department, Colorado State University, Fort Collins, CO 80523, USA; edscos@colostate.edu
[2] Water Management and Systems Research Unit, United States Department of Agriculture, Agricultural Research Service, Fort Collins, CO 80526, USA; huihui.zhang@usda.gov
* Correspondence: jose.chavez@colostate.edu

Abstract: This study evaluated the performance of remote sensing (RS) algorithms for the estimation of actual maize evapotranspiration (ET_a) using different spaceborne, airborne, and proximal multispectral data in a semi-arid climate region to identify the optimal platform that provides the best ET_a estimates to improve irrigation water management and help make irrigated agriculture sustainable. The RS platforms used in the study included Landsat-8 (30 m pixel spatial resolution), Sentinel-2 (10 m), Planet CubeSat (3 m), multispectral radiometer or MSR (1 m), and a small uncrewed aerial system or sUAS (0.03 m). Two-source surface energy balance (TSEB) models, implementing the series and parallel surface resistance approaches, were used in this study to estimate hourly maize ET_a. The data used in this study were obtained from two maize research sites in Greeley and Fort Collins, CO, USA, in 2020 and 2021. Each research site had different irrigation systems. The Greeley site had a subsurface drip system, while the Fort Collins site had surface irrigation (furrow). Maize ET_a predictions were compared to observed maize ET_a data from an eddy covariance system installed at each research site. Results indicated that the MSR5 proximal platform (1 m) provided optimal RS data for the TSEB algorithms. The MSR5 "point-based" nadir-looking surface reflectance data and surface radiometric temperature combination resulted in the smallest error when predicting hourly (mm/h) maize ET_a. The mean bias and root mean square errors (MBE and RMSE, respectively), when predicting maize hourly ET_a using the MSR5 sensor data, were equal to −0.02 (−3%) ± 0.07 (11%) mm/h MBE ± RMSE and −0.02 (−3%) ± 0.09 (14%) mm/h for the TSEB parallel and series approaches, respectively. The poorest performance, when predicting hourly TSEB maize ET_a, was from Landsat-8 (30 m) multispectral data combined with its original thermal data, since the errors were −0.03 (−5%) ± 0.16 (29%) mm/h and −0.07 (−13%) ± 0.15 (29%) mm/h for the TSEB parallel and series approaches, respectively. These results indicate the need to develop methods to improve the quality of the RS data from sub-optimal platforms/sensors/scales/calibration to further advance sustainable irrigation water management.

Keywords: remote sensing; evapotranspiration; crop coefficient; surface energy balance; irrigation

Citation: Costa-Filho, E.; Chávez, J.L.; Zhang, H. Mapping Maize Evapotranspiration with Two-Source Land Surface Energy Balance Approaches and Multiscale Remote Sensing Imagery Pixel Sizes: Accuracy Determination toward a Sustainable Irrigated Agriculture. *Sustainability* **2024**, *16*, 4850. https://doi.org/10.3390/su16114850

Academic Editors: Wenfeng Liu, Xiaolin Yang and Wen Yin

Received: 8 January 2024
Revised: 8 May 2024
Accepted: 27 May 2024
Published: 6 June 2024

1. Introduction

To improve irrigation water management in agricultural fields and attain sustainability, it is critical to define the optimal irrigation time and irrigation amounts to replenish the soil vadose layers, where crop roots develop, to conserve water and soil resources. Irrigation water management practices are often based on the soil water balance (SWB) approach for irrigation scheduling development [1,2]. The SWB approach for irrigation provides a soil water volume balance that accounts for the inflow and outflow of water fluxes in the

crop root zone to define the temporal changes in the soil volumetric water content [3]. The simplified daily SWB approach is given by Equation (1):

$$D_{r,i} = D_{r,i-1} - (P - RO)_i - I_i - CR_i + ET_{c,i} + DP_i \quad (1)$$

where $D_{r,i}$ is the water depleted in the root zone at the end of day i^{th}; $D_{r,i-1}$ is the water in the root zone in the previous day $(i-1)^{th}$; P_i is the rainfall water depth; RO_i is the surface water runoff; I_i is the net irrigation water depth; CR_i is the capillary rise from shallow water table (groundwater); $ET_{c,i}$ is the daily crop evapotranspiration; DP_i is the deep percolation (vertical water loss beyond the root zone). All variables in Equation (1) are given as water depth units (e.g., mm or in).

Better irrigation strategies are often related to an SWB approach that accounts for an accurate ET_c estimate through the actual crop evapotranspiration (ET_a) rates determination. This is the correct amount of water depleted in the soil throughout the plant root zone that would be replenished with irrigation when ET_c (through ET_a) has been properly determined. In general, throughout this process, water and nutrient savings or conservation are achieved because common irrigation practices tend to over-irrigate, promoting water, soil, and agro-chemical losses through land surface runoff and deep percolation, potentially contaminating groundwater and/or surface water bodies. At the local farm scale, accurate crop ET_a estimation is critical to support quasi-real-time decision-making approaches for water allocation and optimization of irrigation water management [4,5].

Modeling advancements in remote sensing (RS) of the environment have facilitated the quasi-real-time mapping of crop water requirements or ET_a for irrigation on a spatio-temporal basis, using multispectral and thermal imagery from different sensor types [6,7] since the early 1970s. Remote sensing involves the scientific measurement of emitted and reflected light across various spectral ranges, including visible, invisible, and longwave infrared (LWIR), without direct contact with the target area [8]. Optical devices mounted on aerial platforms (e.g., small aircraft or automated aerial vehicles), spaceborne systems (e.g., satellites), and proximal instruments (e.g., handheld roaming or stationary radiometers) have generated data at different temporal, spectral, and spatial resolutions, benefiting applications like irrigation water management, soil nutrient monitoring, crop growth assessment, and yield mapping [9–11]. The use of RS techniques to support sustainability of irrigation scheduling practices has been investigated for more than 50 years [12,13].

Remote sensing of crop ET_a approaches that use multispectral and thermal data to map crop ET_a are fundamentally based on the land surface energy balance (SEB) concept. The SEB approach for estimating ET_a calculates the energy required for evaporating water (latent heat flux, LE) as the residual term of the simplified SEB (Equation (2)).

$$LE = R_n - G - H \quad (2)$$

where LE is the latent heat flux; R_n is the net radiation flux; G is the soil heat flux; and H is the sensible heat flux. All terms in Equation (2) are given in W/m^2. The SEB LE flux is then converted to instantaneous crop ET_a (e.g., mm/h) during the RS sensor overpass. There are two common methods to determine ET_a using the SEB approach: (a) the one-source SEB (henceforth, OSEB), which considers the combined contributions of soil and vegetation to ET_a rates [14–17], and (b) the two-source SEB (or TSEB) that partitions heat fluxes and the crop ET_a in a component related to the water transpired by the plants and another related to the evaporated water from the soil [18–21].

The TSEB is a robust SEB approach suitable for estimating spatial ET_a that was initially developed by [21]. The TSEB model has two different approaches for estimating the H flux in Equation (2): the parallel surface resistances TSEB (henceforth, $TSEB_{par}$) and the (in) series surface resistances TSEB (henceforth, $TSEB_{ser}$). The $TSEB_{par}$ model considers the processes of heat transfer among plants, soil, and the air above the canopy as independent of each other with two surface resistances for heat transfer. The $TSEB_{ser}$ method includes the concept of heat transfer interconnection in the soil–plant–atmosphere continuum through

an additional surface resistance term and a parametrization of the aerodynamic surface temperature (T_o) as a weighted-average temperature among soil, plant, and air temperatures with respective resistances as weights. Typical ET_a estimation errors, when using $TSEB_{par}$ or $TSEB_{ser}$, were reported to be within 7% to 25% for row crops [22–24]. In regard to the desired frequency of ET_a estimates, the study by [25] indicated that a four-day RS platform overpass frequency (of usable data) would be the minimum needed for current interpolation techniques to yield meaningful daily ET_a estimates between acquired RS data. However, with high RS data acquisition frequencies, more reliable and accurate daily ET_a estimations will be possible. Therefore, more timely and accurate irrigation water amounts would be delivered to surface and pressurized systems if accurate daily ET_a maps were produced.

Examining various RS platforms that offer multispectral images of cropland fields at diverse spectral and spatial resolutions is crucial for assessing the reliability of different ET_a prediction algorithms and their accuracy when predicting ET_a values in time and space [26]. Furthermore, accurate estimation of crop ET_a, when used to optimize the irrigation water amounts and timing of application, advances environmental sustainability by decreasing topsoil erosion in agricultural areas due to reduced field surface runoff and conserves water and soil nutrients within agricultural districts, protecting the environment by reducing groundwater withdrawn rates, maintaining ecological water table levels, and preserving adequate water quality of both aquifers and surface water bodies (e.g., lakes, artificial reservoirs, and rivers). However, there have been very few studies attempting to address the performance of the TSEB RS of ET_a algorithms across different spectral and spatial scales. In a recent study, Ref. [27] explored the accuracy of the TSEB model developed by [21] using different small uncrewed aerial system (sUAS or drone) imagery pixel sizes, ranging from 0.10 m to 0.60 m, in a vineyard field located in California. The drone-captured images were subsequently aggregated to produce lower-resolution imagery with pixel sizes spanning from 3.6 m to 30 m. The results from [27] demonstrated that errors in R_n and G were relatively consistent across various RS resolutions. In contrast, errors in H and LE fluxes exhibited a clear relationship with the spatial resolution of the RS data. Another study by [28] investigated the effect of pixel heterogeneity for tree–grass when predicting ET_a using hyperspectral airborne imagery (1.5 m to 1000 m spatial resolution) and Sentinel imagery products at 20 m and 1000 m using a TSEB RS algorithm in central Spain. They found that large uncertainty, when estimating ET_a, occurred for coarse spatial resolutions.

Even though these studies have contributed to science, there have not been comprehensive studies that evaluate the differences in accuracy of the TSEB RS of ET_a algorithms using multispectral images from multiscale RS platforms such as those from proximal, airborne, and spaceborne sensors. The published studies focused only on a few RS sensors or platforms, often resampling (upscaling) their images to generate different pixel spatial resolutions. Therefore, in this study, it is hypothesized that, depending on the source of a given RS image (e.g., spaceborne, airborne, proximal platforms, sensor type, and imagery post-processing corrections), the accuracy of ET_a mapping products will vary for a given RS of the ET_a algorithm. If the stated hypothesis is valid, determining the optimal RS spectral and spatial resolution becomes necessary (critical) to better sustain irrigated agriculture by improving the estimation of ET_a when sub-optimal RS platforms (data) are used with a given RS of the ET_a algorithm.

Therefore, the objectives of the study were to (a) assess the impact (errors) on hourly ET_a estimation associated with the use of different spectral and spatial resolution RS data from multispectral spaceborne, airborne, and proximal RS sensors and when using two different TSEB algorithms, and (b) identify the RS spectral and spatial data (resolution) that provides the most accurate TSEB-based maize ET_a predictions for a specific algorithm.

2. Materials and Methods

2.1. Description of the Research Sites

2.1.1. Limited Irrigation Research Farm (LIRF)

The Limited Irrigation Research Farm (LIRF) is located in Greeley, Colorado (CO), USA, and is under the management of the United States Department of Agriculture—Agricultural Research Service (USDA—ARS). The farm is geographically located at a latitude of 40.4463° N, a longitude of 104.6371° W, and an elevation of 1432 m above mean sea level (ASL). The study involved two adjacent rectangular maize fields, each measuring 190 m by 110 m (Figure 1), where field data were collected during the periods between July and September of 2020 and 2021.

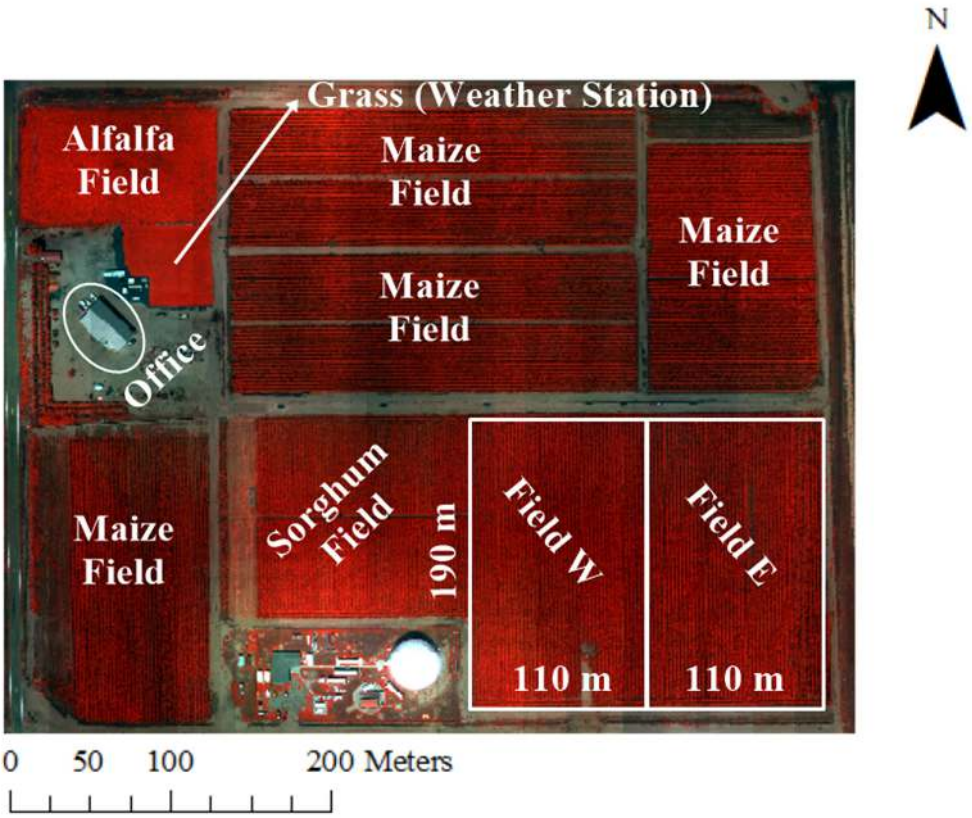

Figure 1. False-color image of the LIRF research site near Greeley, CO, USA. The study maize fields were Fields W and E located in the southeast corner of the research farm.

For each respective field crop growth season, each field was subjected to different irrigation water management strategies. In 2020, the West Field, hereafter referred to as Field W, was fully irrigated. In this context, "fully irrigated" represents the conditions in which frequent irrigation events were scheduled to maintain soil water content in the crop (maize) soil root zone at non-water-stress levels. Conversely, the East Field, designated as Field E, was managed as a deficit-irrigated field, resulting in crop/soil water stress conditions throughout the growing season. In 2021, the irrigation water management practices were switched between these treatment plots. Field W was transformed into the deficit-irrigated field, while Field E became the fully irrigated plot. A summary of soil wetting events, which includes irrigation and rainfall, for the years 2020 and 2021, is provided in Table 1.

Each maize field had the same irrigation system, a subsurface drip irrigation setup with laterals (pipes) buried at a depth of 0.23 m and emitters spaced every 0.30 m. The maize rows were north–south and were spaced 0.76 m apart. The distance between adjacent maize plants was 0.17 m. The planting density for maize remained consistent at 87,500 plants per hectare during both years. In 2020, the selected maize variety was drought

tolerant NK9227-5222A (Syngenta Inc., Basel, Switzerland). Planting took place on 6 May 2020, and the harvest occurred on 13 and 14 October 2020. In 2021, there was a change in maize varieties with the introduction of other drought-tolerant maize options, P9998Q and P0157AMXT (Pioneer Hi-Bred International, Inc., Johnston, IA, USA), along with CH 194-49 DG (Channel Bio Corporation, Saint Louis, MO, USA). Planting for this year was carried out on 13 May 2021, and the harvest took place on 11 and 12 October 2021. Fields W and E, each comprising approximately 83% of their respective plots, were planted with the maize variety P0157AMXT, as indicated in Figure 2. The experimental design and data collection stations at LIRF for the years 2020 and 2021 are shown in Figure 3. It is worth noting that the prevailing wind direction remained consistent: the wind was from the south (S) to southeast (SE) direction during both years of data collection.

2.1.2. Irrigation Innovation Consortium (IIC)

This study included data collected from the Colorado State University IIC site during 2020 and 2021. Two maize fields were selected as the primary locations for data collection (Figure 4). This site is located in Fort Collins, CO, USA, at a latitude of 40.5542° N, a longitude of 105.0038° W, and an elevation of 1486 m ASL. It has a local climate characterized as a subtropical steppe with cold semiarid tendencies.

Table 1. Cumulative soil wetting events (irrigation and rainfall) at LIRF Fields W and E in 2020 and 2021.

Irrigation Scheduling	Growing Season	Research Field	Irrigation Events	Cumulative Gross Irrigation (mm)	Cumulative Rainfall (mm)
Fully Irrigated	2020	W	5	472	36
	2021	E	4	330	98
Deficit Irrigated	2020	E	3	309	36
	2021	W	2	176	98

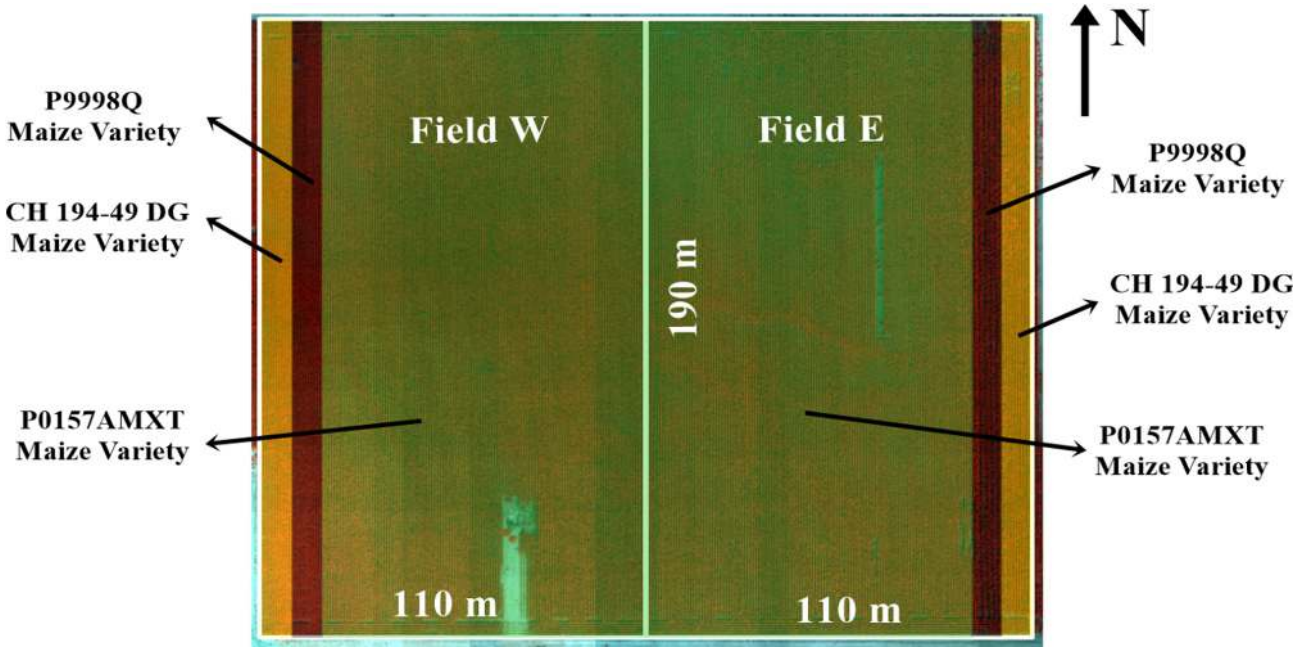

Figure 2. Plant variety map at LIRF (Fields W and E) in 2021. Most of the area was occupied by the P0157AMXT maize variety.

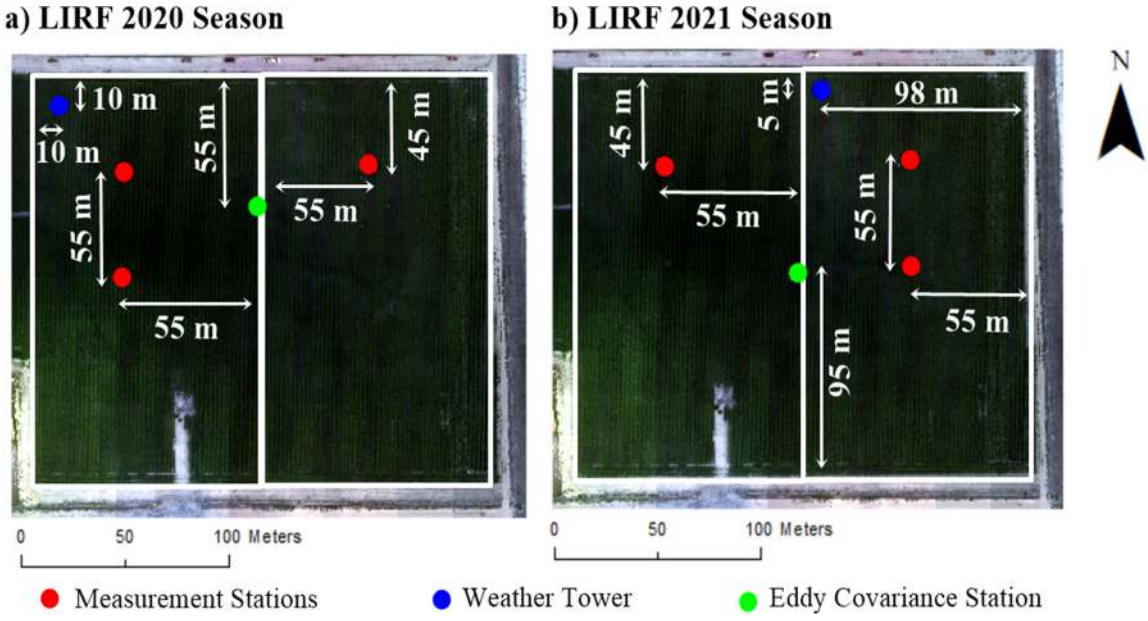

Figure 3. The 2020–2021 LIRF experiment design.

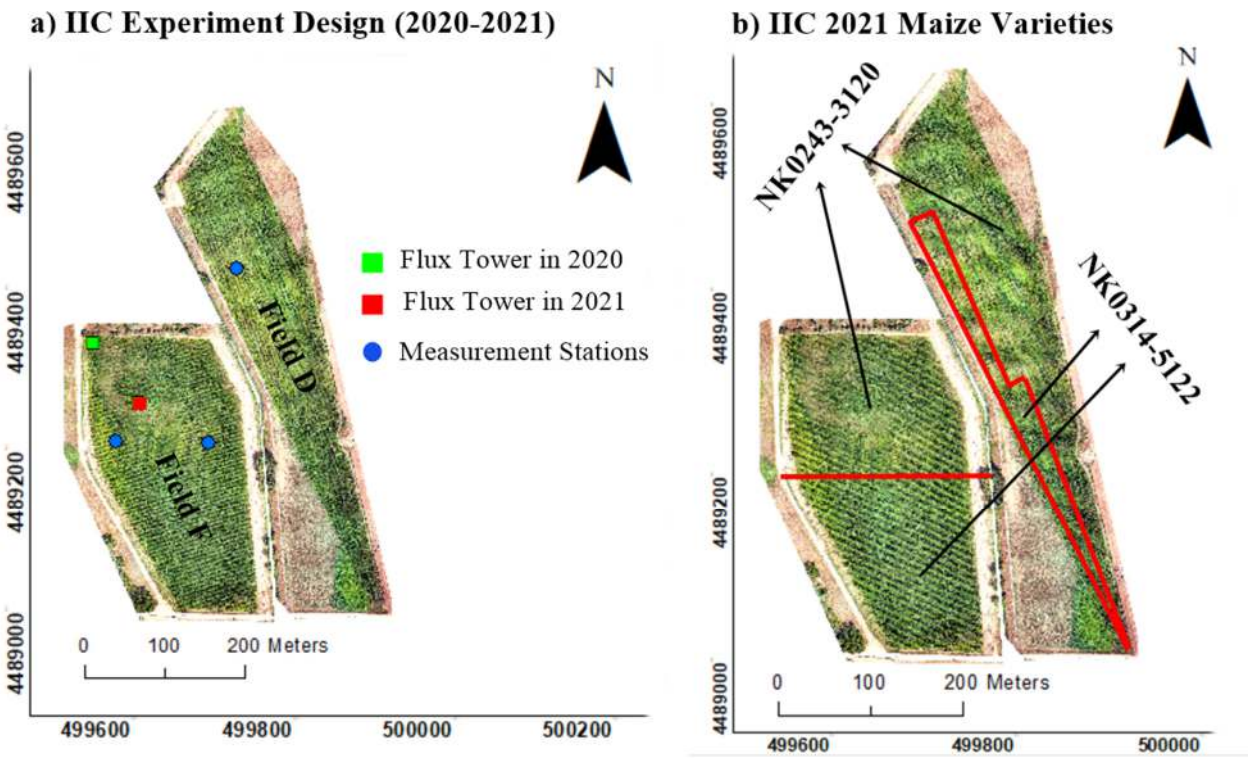

Figure 4. RGB (red–green–blue) map of the IIC research fields (**a**) and the maize varieties planted in 2021 (**b**). The study maize fields were Fields F and D. Areas in green are vegetation surfaces.

The data collection took place in two surface-irrigated (furrow) maize fields during July to September in both 2020 and 2021, as illustrated in Figure 4a. These two fields, designated as Fields F and D, had respective surface areas of 64,750 m^2 and 74,867 m^2. The crop-row orientation in Field F was east–west, while Field D had rows oriented in a north–southeast direction, with rows spaced approximately 0.17 m apart. The soil in both fields had a consistent sandy loam texture throughout the entire maize root zone system, with measured volumetric water content at field capacity (VWC_{FC}), permanent wilting

point (VWC_{PWP}), and saturation (VWC_{SAT}) of 0.189, 0.069, and 0.410 m^3/m^3, respectively. The surface irrigation system employed 40 mm diameter aluminum siphon tubes and delivered water to the fields from the main on-site irrigation canal located between the two research fields. The choice of maize varieties differed between 2020 and 2021. In 2020, G02K39-3120 (Golden Harvest, Minnetonka, MN, USA) was planted on May 13, at an approximate rate of 8 seeds per m^2. For 2021, the NK0243-3120 and NK0314-5122 varieties (Syngenta AG, Basel, Switzerland) were planted in both fields, as indicated in Figure 4b. The seeding date was 13 May 2021, and the planting rate was 8 seeds per m^2.

The direction of the irrigation water flow was from east to west in Field F. In the case of Field D, the irrigation water flowed in the furrows from north to southwest. The irrigation events usually took place two to three days after obtaining water from the Sand Dike Lateral Company in Fort Collins, CO, USA. Each irrigation event extended over a duration of 6 to 12 h. The irrigation scheduling was determined based on the FAO-56 methodology [2], which was an integral component of the Water Irrigation Scheduler for Efficient (WISE) Application [1]. The WISE application uses a water balance approach for determining irrigation amounts and timing based on a dual crop coefficient approach for ET_a estimation from tabularized crop coefficient (K_c) values, a water stress coefficient (K_s), and daily alfalfa reference ET (ET_r) rates.

The K_s value was set to 1 since the maize field was constantly irrigated during the data collection season, and root zone water depletion was assumed to have been kept below allowable water depletion levels.

Throughout both years of data collection, the prevailing wind direction was consistently from the southeast (SE) to the south (S). A summary of the data related to soil wetting events, encompassing both irrigation and rainfall events for the years 2020 and 2021, is given in Table 2.

Table 2. Cumulative soil wetting events (irrigation and rainfall) at IIC Fields F and D in 2020 and 2021.

Maize Growing Season	Research Field	Number of Irrigation Events	Cumulative Gross Irrigation (mm)	Cumulative Rainfall (mm)
2020	F	7	1620	34
	D	5	870	
2021	F	8	1081	104
	D	4	1064	

2.2. Crop Evapotranspiration Algorithm

2.2.1. Two-Source Surface Energy Balance (TSEB)

The TSEB estimates LE as follows (Equations (3)–(5)):

$$LE = LE_c + LE_{soil} \quad (3)$$

$$LE_c = Rn_c - H_c \quad (4)$$

$$LE_{soil} = Rn_{soil} - G - H_{soil} \quad (5)$$

where the subscripts "c" and "soil" refer to the "canopy" and "bare soil" conditions, respectively. All terms in Equations (3)–(5) have W/m^2 units.

The LE is converted from W/m^2 to hourly ET_a (mm/h) using Equation (6):

$$ET_{ah} = C_f \times d_f \times \frac{LE}{\lambda_v \rho_a} \quad (6)$$

where ET_{ah} is the hourly instantaneous actual crop ET_a (mm/h); d_f is a time-scale factor in seconds (e.g., 1 h = 3600 s); λ_v is the latent heat of water vaporization (J/kg); ρ_a is the air density (kg/m^3); C_f is a length scale conversion factor (e.g., 1000 mm/1 m).

The G model used was the soil heat flux (Equation (7)) approach recommended by [21], which is a fraction of the net radiation from the soil layer (Rn_{soil}) during midday conditions coinciding with most spaceborne RS platform overpass times.

$$G = 0.35 Rn_{soil} \tag{7}$$

The Rn_c and Rn_{soil} terms (appearing later in Equations (18) and (19)) are calculated following the approaches by [19,21] and indicated by Equations (8) and (9), respectively:

$$Rn_c = (1 - \Omega_{solar})(1 - \alpha_c)R_s + \exp(-0.95LAI)L_{sky} + [1 - \exp(-0.95LAI)]\epsilon_c \sigma T_{cK}^4 - \epsilon_{soil}\sigma T_{soilK}^4 \tag{8}$$

$$Rn_{soil} = \Omega_{solar}(1 - \alpha_{soil})R_s + [1 - \exp(-0.95LAI)]\left[\epsilon_a \sigma T_{aK}^4 + \epsilon_{soil}\sigma T_{soilK}^4 - 2\epsilon_c \sigma T_{cK}^4\right] \tag{9}$$

where Ω_{solar} is the solar atmospheric transmittance (dimensionless); α_c and α_{soil} are the canopy and bare soil albedo (dimensionless), respectively; ϵ_c is the canopy thermal emissivity (dimensionless); ϵ_{soil} is the bare soil thermal emissivity (dimensionless); ϵ_a is the air emissivity (dimensionless); T_{cK} is the canopy temperature (K); T_{soilK} is the soil temperature (K); T_{aK} is the air temperature (K); L_{sky} is the longwave radiation from the sky (W/m^2); σ is the Stefan–Boltzmann constant (5.67×10^{-8} $W/m^2/K^4$); LAI is the leaf area index (m^2/m^2); R_s is the incoming shortwave solar radiation (W/m^2).

The α_c and α_{soil} were calculated following the approaches by [29] and [30], respectively. The study by [29] gave an exponential model that relates maize albedo and green LAI for a semi-arid climate region. The study by [30] provided a multivariate model that relates α_{soil} and the visible surface reflectance bands of the light spectrum (RED, GREEN, and BLUE). The Ω_{solar} variable was calculated using the nonlinear model from [31], in which the Ω_{solar} is a function of LAI, surface absorptivity factor [32], light extinction coefficient, and the fraction of incident photosynthetically active radiation or PAR [33–35].

The T_{cK} and T_{soilK} are calculated through an iterative approach using Equation (10) below [21]:

$$T_{sK} \cong \left[f_c(\varphi)T_{cK}^4 + \left(1 - f_c(\varphi)T_{soilK}^4\right)\right]^{0.25} \tag{10}$$

where T_{sK} is the equivalent nadir-looking surface temperature calculated from plant and soil temperature composites (K); $f_c(\varphi)$ is the fractional green vegetation cover for a radiometric field-of-view angle φ [21].

The TSEB Series Approach for H Estimation

In the TSEB series algorithm ($TSEB_{ser}$), the heat exchange between soil, plant, and air is assumed to be interconnected [21]. The expressions for calculating H using the $TSEB_{ser}$ approach are given by Equations (11)–(13) below [21]:

$$H^{[ser]} = H_c^{[ser]} + H_{soil}^{[ser]} \tag{11}$$

$$H_c^{[ser]} = \rho_a C_{pa}\left(\frac{T_c - T_o^{[ser]}}{r_x}\right) \tag{12}$$

$$H_{soil}^{[ser]} = \rho_a C_{pa}\left(\frac{T_{soil} - T_o^{[ser]}}{r_{soil}}\right) \tag{13}$$

where T_c, T_{soil}, and $T_o{}^{[ser]}$ are the canopy, bare soil, and $TSEB_{ser}$ aerodynamic temperatures (K), respectively; r_x and r_{soil} are the total boundary layer resistance of canopy leaves (s/m) and the soil resistance (s/m), respectively. The superscript [ser] refers to the $TSEB_{ser}$ (series) algorithm. More details on how to calculate these resistance terms and other auxiliary variable inputs for the TSEB can be found in Appendices A and B.

The air parameters ρ_a and C_{pa} are calculated as indicated by Equations (14) and (15), respectively (as used in [36]):

$$\rho_a = \left(\frac{P}{R_d T_a}\right)\left(1 - \frac{0.378 e_a}{P}\right) \tag{14}$$

$$C_{pa} = 1004.7 \times \left(1 + \frac{0.522 e_a}{P}\right) \tag{15}$$

where P is the local atmospheric pressure (Pa); e_a is actual vapor pressure (Pa); R_d is the gas constant for dry air (≈287.04 J/kg/K). The air parameters ρ_a and C_{pa} are given in kg/m^3 and J/kg/K units, respectively.

The $T_o^{[ser]}$ (given in K) is calculated as indicated by Equation (16) [21]:

$$T_o^{[ser]} = \frac{T_a/r_{ah} + T_{soil}/r_{soil} T_c/r_x}{1/r_{ah} + 1/r_{soil} + 1/r_x} \tag{16}$$

In this study, we followed the improved $TSEB_{ser}$ approach from [18] and used the modified Penman–Monteith (PM) approach instead of the Priestley–Taylor (PT) modified model (as described in [21]) to calculate an initial T_c value to derive the surface temperature composites (T_c and T_{soil}). The modified PM approach for an initial T_c value is indicated by Equation (17):

$$T_{cO} = T_a + \frac{Rn_c r_{ah} \gamma (1 + r_c/r_{ah})}{\rho_a C_{pa} [\Delta + \gamma (1 + r_c/r_{ah})]} - \frac{e_s - e_a}{\Delta + \gamma (1 + r_c/r_{ah})} \tag{17}$$

where T_{cO} is the initial guess for canopy temperature (K); γ is the psychometric constant (kPa/°C); r_c is the bulk canopy resistance (s/m); Δ is the slope of the saturation vapor pressure curve (kPa/°C); e_s and e_a are the saturated and actual vapor pressures in kPa, respectively. The calculation of r_c is described in Appendix B.

The TSEB Parallel Approach for H Estimation

The TSEB parallel ($TSEB_{par}$) assumes that the processes that derive the heat transfer among plants, soil, and the air above are independent and can be modeled with two separate resistances for heat transfer [18,21]. The expressions for calculating H using the $TSEB_{par}$ approach are given by Equations (18)–(20) below [21]:

$$H^{[par]} = H_c^{[par]} + H_{soil}^{[par]} \tag{18}$$

$$H_c^{[par]} = \rho_a C_{pa} \left(\frac{T_c - T_a}{r_{ah}}\right) \tag{19}$$

$$H_{soil}^{[par]} = \rho_a C_{pa} \left(\frac{T_{soil} - T_a}{r_{ah} + r_{soil}}\right) \tag{20}$$

where the superscript [par] refers to the $TSEB_{par}$ (parallel) algorithm.

For the $TSEB_{par}$ algorithm, the initial assumption regarding the initial value for LE_c was based on the original work from [21] and indicated by Equation (21), as follows:

$$LE_{ci} = \left[1.3 f_g \left(\frac{\Delta}{\Delta + \gamma}\right)\right] [Rn_c + Rn_{soil} - (Rn_c + Rn_{soil}) \times \exp(0.90 \ln(1 - f_c))] \tag{21}$$

where LE_{ci} is the initial guess value for iterating T_c and T_{soil} (W/m^2), and f_g is the green fraction of LAI (dimensionless), calculated as indicated by [21].

2.3. Vegetation Indices Calculation

The normalized difference vegetation index (NDVI) and optimized soil-adjusted vegetation index (OSAVI) [37] were calculated by Equations (22) and (23), respectively:

$$\mathrm{NDVI} = \frac{\mathrm{NIR} - \mathrm{RED}}{\mathrm{NIR} + \mathrm{RED}} \tag{22}$$

$$\mathrm{OSAVI} = \frac{\mathrm{NIR} - \mathrm{RED}}{\mathrm{NIR} + \mathrm{RED} + 0.16} \times 1.16 \tag{23}$$

where NIR and RED are the surface reflectance values (decimals), for the near-infrared and red bands, provided by a given RS platform (dimensionless).

The f_c model used in the $TSEB_{ser}$ and $TSEB_{par}$ approaches is presented by Equations (24)–(28), as follows [21]:

$$f_{c,o} = 1 - \exp(-0.50\mathrm{LAI}) \tag{24}$$

$$\mathrm{LAI_L} = \mathrm{LAI}/f_{c,o} \tag{25}$$

$$f_s = 1 + f_{c,o} \times \exp(-0.50\mathrm{LAI_L}) - f_{c,o} \tag{26}$$

$$\mathrm{CF} = -\ln\left(\frac{f_s}{0.50\mathrm{LAI}}\right) \tag{27}$$

$$f_c = 1 - \exp(-0.50 \times \mathrm{CF} \times \mathrm{LAI}) \tag{28}$$

where $f_{c,o}$ is the initial f_c value before adjustments (dimensionless); $\mathrm{LAI_L}$ is the local LAI (m^2/m^2); f_s is the soil fractional cover (dimensionless); CF is the vegetation clumping factor (dimensionless).

The LAI is calculated using the model from [38], an exponential model calibrated for maize and sorghum and indicated by Equation (29) below:

$$\mathrm{LAI} = 0.263 \times \exp(3.813 \times \mathrm{OSAVI}) \tag{29}$$

Maize h_c was estimated through an exponential model for maize and soybeans and indicated by Equation (30) below [39]:

$$h_c = (1.86\mathrm{OSAVI} - 0.20) \times \left[1 + 4.82 \times 10^{-7}\exp(17.69\mathrm{OSAVI})\right] \tag{30}$$

2.4. Remote Sensing Platforms

2.4.1. Spaceborne

Landsat-8

Landsat-8 is a satellite-based RS platform jointly managed by the United States Geological Service (USGS) and the National Aeronautics and Space Administration (NASA). A Landsat-8 satellite is equipped with an operational land imager (OLI) and a thermal infrared sensor (TIRS). These instruments capture images of Earth's surface, with the OLI providing data at a spatial pixel resolution of 30 m and the TIRS at 100 m, resampled to 30 m [40]. These images are acquired every 16 days. The OLI sensor captures shortwave multispectral data, while the TIRS camera records longwave infrared (LWIR) thermal radiation images. The study sites, LIRF and IIC, are strategically located in the overlapping region of Landsat-8 scenes with path/row designations of 33/32 and 34/32, respectively. As a result, the temporal resolution for data acquisition for Landsat-8, in this study, was once every eight days depending on sky cloudiness conditions near noon time.

Landsat-8 follows a sun-synchronous orbit around Earth, orbiting at an altitude of 705 km, with equator crossings occurring at approximately 11:30 a.m. local time. The original radiometric resolution of Landsat-8 imagery is 12 bits, but this is enhanced to 16 bits after post-processing by USGS/NASA. To convert digital numbers (DN) into ground surface reflectance and nadir-looking temperature (Landsat-8 Level-2 imagery), linear calibration coefficients are provided in the metadata of the imagery file. Level-2 images un-

dergo rigorous calibration procedures, eliminating the need for additional post-processing once the final surface reflectance and temperature images are accurately derived from the original DN values, following the methods outlined by Roy et al. [40] in 2014. Further details regarding atmospheric corrections applied to Landsat-8 imagery can be found in [41]. Table 3 presents the spectral characteristics of the Landsat-8 bands considered in this research. The pixels that overlapped with the measurement stations at each research site were considered to be representative for the estimation of maize ET_a using the TSEB algorithm.

Table 3. Landsat-8 multispectral bands used in this study at both LIRF and IIC sites.

Bands	Central Wavelength (nm)	Bandwidth (nm)	Spatial Resolution (m)
BLUE	480	60	30
GREEN	560	60	30
RED	655	30	30
NIR	870	30	30
LWIR	1090	60	100 (Resampled to 30)

Sentinel-2

The Sentinel-2 satellites are under the care and operation of the European Space Agency (ESA), an intergovernmental organization representing 22 European countries. The management of the Sentinel satellite missions falls within the purview of the Copernicus Programme. This satellite constellation comprises two units, Sentinel-2A (S2A) and Sentinel-2B (S2B), taking Earth's landscape images at noon. Each of these satellites takes multispectral image scenes, covering an area of 290 km by 290 km. They orbit the Earth, providing imagery every 10 days for a single satellite device around the equator. When both satellites are combined, this interval shortens to 5 days. For areas located at mid-latitudes, such as the LIRF and IIC research facilities, the revisiting time is as frequent as every 2 to 3 days near local noon time. Additional details concerning the satellite's design, operation, and components can be found in the work of [42].

Both the S2A and S2B satellites follow sun-synchronous orbits, maintaining an average altitude of 786 km, with equator crossings occurring around noon local time (12 p.m.). It is important to note that Sentinel-2 satellites currently do not provide thermal imagery. The spatial resolution of Sentinel-2 images varies and depends on the specific multispectral bands in use, ranging from 10 m to 60 m. For this study, we have considered only Sentinel-2 bands 2, 3, 4, and 8, which offer a spatial resolution of 10 m, as these bands are provided at their original spatial resolution, as documented in Table 4.

Table 4. Sentinel-2 multispectral bands used in this study at LIRF and IIC research sites.

Bands	Central Wavelength (nm)	Bandwidth (nm)	Spatial Resolution (m)
BLUE	492	66	10
GREEN	560	36	10
RED	665	31	10
NIR	833	106	10

The original radiometric resolution of Sentinel-2 images is 12 bits. However, ESA enhances these images to a 16-bit radiometric resolution through post-processing. Sentinel-2 Level-2 images undergo calibration and pre-processing, aiming to provide ground-based surface reflectance. The surface reflectance images provided (downloaded) include a scaling factor of 10,000. To obtain surface reflectance decimal values, the Sentinel downloaded images are divided by 10,000. The atmospheric corrections are carried out using a radiative transfer algorithm developed by ESA, known as Sen2Cor. For details regarding the use

of Sen2Cor in atmospherically correcting S2A and S2B satellite images, refer to the work of [43]. The pixels that contained the stations of measurements for each research site were considered representative for the calculations of maize ET_a using the TSEB approaches.

Planet CubeSat

Planet CubeSat is a cost-effective commercial constellation of micro (Dove) satellites, managed by Planet Labs, Inc. in San Francisco, California, USA. Comprising over 130 CubeSat units, these satellites observe Earth's landscapes, providing high temporal (daily) and spatial resolutions (3 m). Planet CubeSat microsatellites capture multispectral imagery in the visible and near-infrared (NIR) portions of the light spectrum. The radiometric resolution of Planet CubeSat imagery starts at 12 bits during image acquisition but is enhanced to a 16-bit resolution through post-processing before it is made accessible for download. Planet CubeSat satellites are notably smaller and lighter (0.10 m × 0.10 m × 0.30 m and 4 kg, respectively) compared to their counterparts, like Landsat-8 and Sentinel-2. Operating in a sun-synchronous orbit with an altitude ranging from 450 km to 580 km, these satellites pass over the equator between 9:30 and 11:30 a.m. local time. We used imagery files from 11:30 a.m. since it was the closest to the other time of RS data acquisition regarding the other RS sensors in this study. Planet CubeSat's capabilities are exclusively limited to multispectral imagery, as detailed in Table 5. Unfortunately, thermal imagery is still not provided by these constellations of microsatellites.

Table 5. Planet CubeSat multispectral bands used in this study at LIRF and IIC research sites.

Bands	Central Wavelength (nm)	Bandwidth (nm)	Spatial Resolution (m)
BLUE	491	60	3
GREEN	566	90	3
RED	666	80	3
NIR	867	80	3

The surface reflectance images obtained by Planet CubeSat undergo pre-processing and calibration, also incorporating a scaling factor of 10,000. The imagery pre-processing and calibration process encompass adjustments for radiation scattering due to atmospheric gases, aerosol concentration, and their altitude-dependent variations between Earth's surface and the satellite's at-sensor camera in space. To enhance their calibration, data from MODIS (Moderate Resolution Imaging Spectroradiometer), such as water vapor, ozone, and aerosol quality control products, are utilized, along with the 6SV2.1 radiative transfer model. However, the atmospheric correction process is still evolving, primarily because Planet's imagery calibration does not currently address effects like stray light, haze, and the influence of thin cirrus clouds. The approach by Planet Labs assumes that Earth's landscapes behave as Lambertian surfaces, scattering light uniformly in all directions, and that all scenes are effectively at sea level. Following image acquisition, geometric corrections are meticulously executed using sensor telemetry, ground control points (GCP), and finely detailed digital elevation models (DEM). Furthermore, the Planet Team released a harmonized version of Planet imagery, including CubeSat data, aligning the quality of multispectral data with (calibration to) Sentinel-2 standards. For further details on the image harmonization processes, refer to the works of [44,45]. In this study, the primary data source used was the CubeSat harmonized images.

In our study using the data from the LIRF and IIC using all listed spaceborne RS sensors, we specifically focused on clear-sky images. This deliberate choice was made to ensure that cloud cover conditions did not interfere with the accuracy of ground-based surface reflectance and temperature values in our research fields. For Landsat-8, the evaluation of evapotranspiration (ET_a) included two different datasets. The first dataset involved the use of the original Landsat-8 platform, encompassing imagery data from OLIS

(multispectral) and TIRS (thermal). The second Landsat-8 dataset combined OLIS data with ground-based infrared temperature (IRT) data. The utilization of TIRS and ground-based T_s data was specific to the Landsat-8 spaceborne platform since Planet CubeSat and Sentinel-2 relied on ground-based nadir-looking IRT T_s data for input in the TSEB RS of the ET_a algorithms. This choice, in the case of the Landsat-8 imagery, was made due to the pivotal role of its TIRS data, albeit its original pixel size, in providing original spaceborne T_s information for maize ET_a estimation. The Planet Cubesat pixel data that had the measurement stations at LIRF and IIC were used for the estimation of maize ET_a using the TSEB algorithms.

2.4.2. Proximal

At the LIRF and IIC research sites, proximal surface reflectance and nadir-looking T_s data was obtained using a handheld multispectral radiometer (MSR5, CropScan Inc., Rochester, MN, USA). The MSR5 radiometer is a compact device consisting of a quasi-cubic radiometer measuring 0.80 × 0.80 × 0.10 m. It features an integrated IRT sensor from Exergen Corporation in Watertown, Massachusetts. The radiometer has a field of view (FOV) of 28 degrees and captures readings at an altitude of 2.2 m above ground level (AGS). This measurement setup covers an area on the ground equivalent to a 1-meter-diameter circle, with a 2V:1H aspect ratio (Table 6). The attached Exergen IRT, with a FOV ratio of 3V:1H, results in a spatial footprint of 0.80 m in diameter. The MSR5 is a passive sensor, relying on natural sunlight for data collection of surface temperature. It replicates the spectral characteristics of Landsat-5, obtaining data in the visible, NIR, and MIR (mid-infrared) light spectrum. For this study, we deployed MSR5 units at both the LIRF and IIC sites. The multispectral data from these MSR5 devices were sampled about once a week, with four readings at each measurement location across all research sites: more specifically, two readings within the crop rows and two readings in the maize inter-row spaces per site. These readings around solar noon (11:30 a.m. to 1:30 p.m.) were then averaged to obtain the final measurements per sampling location in each research site per field visit. The MSR5 measurements' locations were the reference for the selection of pixels from the different images/platforms or scales, considering areas with homogenous soil texture and canopy cover.

Table 6. The MSR5 multispectral bands used in this study at the LIRF and IIC research sites.

Bands	Central Wavelength (nm)	Bandwidth (nm)	Spatial Resolution (m)
BLUE	485	70	1
GREEN	560	80	1
RED	660	60	1
NIR	830	140	1

Airborne

The USDA-ARS Water Management and Systems Research Unit and the CSU Drone Center scheduled UAS missions for the research sites around local solar noon (11:30 a.m. to 1:30 p.m. MST). At the LIRF, the USDA-ARS team was responsible for conducting UAS missions, while the CSU Drone Center took charge of the UAS missions at the IIC site. These UAS images were acquired using a MicaSense RedEdge-MX multispectral camera (MicaSense Inc., Seattle, WA, USA), seamlessly integrated into the airborne platform. The RedEdge-MX detector captures data across the visible and invisible light spectrum, with bands including BLUE (475 nm, 32 nm bandwidth), GREEN (560 nm, 27 nm bandwidth), RED (668 nm, 14 nm bandwidth), and NIR (842 nm, 57 nm bandwidth).

The UAS's surface reflectance imagery data serve as another RS sensor for this study, and they were complemented by nadir-looking T_s data obtained from point-based measurements conducted at each of the research sites. This combined dataset is utilized as

input for estimating hourly maize ET_a using the TSEB approaches. For an overview of the UAS missions carried out in 2020 and 2021 at LIRF and IIC, refer to Table 7.

Table 7. The UAS mission summary for the USDA-ARS and CSU Drone Center at all sites.

	USD—ARS	**CSU Drone Center**
UAS Unit	DJI S900	DJI M600
Flight Altitude (m)	120	100
UAS Speed (m/s)	5	5
Temporal Resolution	Weekly	Weekly
Imagery Pixel Size (m)	0.03	0.08
Overlap/Sidelap Percentage (%)	88/70	80/70
Calibrated Reflectance Panel	Yes	Yes
Orthorectified Coordinate System	WGS84 UTM	WGS84 UTM
Post-processing Imagery Software	Agisoft Metashape	Pix4D v4.5.6

2.5. Field Data Collection

The experiment was replicated in both the LIRF and IIC sites to obtain similar datasets for the evaluation of the airborne, spaceborne, and proximal platforms' derived RS data when used in the prediction of ET_a using TSEB RS algorithms. A total of three field measurement stations provided the ground-based input data to estimate and evaluate maize ET_a. The following data were measured at each station: R_n, G, nadir-looking surface radiometric temperature (T_s), incoming shortwave solar radiation (R_s), shallow soil temperature, and volumetric water content. A flux tower provided measurements of H and LE in each research site (Figures 3 and 4a).

2.5.1. Surface Heat Fluxes

At the IIC site, a two-way NR-Lite and two four-way CNR1 net radiometers (Kipp and Zonen, Delft, The Netherlands) measured R_n at the height of 3.3 m AGS. At the LIRF site, each of the three net radiometers was a two-way NR-Lite in 2020 and 2021. The CNR1 radiometer was installed on Field F (west station). NR-Lite radiometers measure net shortwave and longwave radiation within a spectral range from 0.2 to 100 μm, temperature dependency of 0.12%/°C, and a directional error of less than 30 W/m^2 at, at least, 1000 W/m^2 [46]. The CNR1 radiometer provides data regarding all four terms of the net radiation budget, and it has a measurement uncertainty that is within 10 to 35 $\mu V/W/m^2$ and a directional error of 25 W/m^2 at 1000 W/m^2 [47].

Surface G data were determined using the soil heat flux plate method. At LIRF, two HFT3-L soil heat flux plates (Radiation and Energy Balance Inc., Bellevue, WA, USA) were buried at 0.08 m between and below maize rows at each measurement station. At the IIC site, the HFT3-L plates were placed between two consecutive maize rows due to the flooded furrow during irrigation events. One 5TE soil water content sensor (Decagon Devices Inc., Pullman, WA, USA) was buried at 0.04 m. Two T107 temperature probes (Campbell Scientific Inc., Logan, UT, USA) were installed at 0.02 and 0.06 m below ground surface (BGS) to determine average soil temperature and for the calculation of soil heat storage above the 0.08 m soil layer from the HFT3-L plates. The HFT3-L sensors have thicknesses and diameters equal to 3.91 and 38.2 mm, respectively. The measurement uncertainty of soil heat flux from the plates is 5% [48].

Measured LE and H data were produced from acquired high-frequency wind speed, air temperature, and water vapor measurements using an eddy covariance (EC) system installed at each research site. At the IIC (Figure 5a), the EC system consisted of an LI-7500A open-path CO_2/H_2O gas analyzer (LI-COR Biosciences, Lincoln, NE, USA) and a CSAT three-dimensional (3D) sonic anemometer (Campbell Scientific Inc., Logan, UT, USA). At

LIRF (Figure 5b), an LI-7500DS open-path gas analyzer (LI-COR Biosciences, Lincoln, NE, USA) and a Gill WindMaster three-dimensional (3D) sonic anemometer (Gill Instruments, Lymington, Hampshire, UK) provided measurements of LE and H, respectively. Both EC systems at LIRF and IIC were installed at 3.5 m AGS, positioned facing the prevailing wind direction at each site (135° azimuth angle), and set to a sampling frequency equal to 10 Hz. The EC turbulent fluxes and respective ancillary data were recorded as 15-min and half-hour averages at the IIC and LIRF sites, respectively. The EC system often provides imbalanced turbulent fluxes regarding SEB closure [49–51], with the closure SEB ratio "$(H + LE)/(R_n - G)$" ranging from 70 to 90% [52,53]. To improve the representativeness of H, LE, and ET_a measurements from the EC system, the residual-LE closure approach was chosen in this study to ensure the closure of the surface heat fluxes. The work of [54] indicated that the residual-LE method calculates measured LE as the difference among measured R_n, G, and H (from the EC system) and that most of the unresolved EC system closure issues are due to LE rather than H. Table 8 shows the corrections performed in the high-frequency EC data at LIRF and IIC in 2020 and 2021.

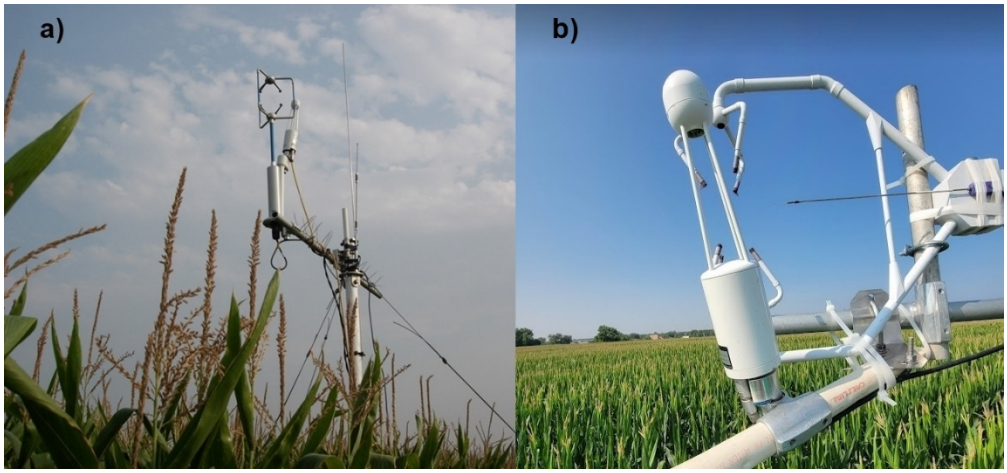

Figure 5. EC systems were installed at the LIRF (**a**) and IIC (**b**) sites in 2020 and 2021 at 3.5 m AGS. (**a**) courtesy of Jon Altenhofen.

Table 8. Correction methods applied to the EC data at LIRF and IIC.

Correction Method	Source	Research Site
Wind coordinate or tilt correction	[55,56]	LIRF and IIC
Air density fluctuation—the Webb–Pearman–Leuning (WPL) correction	[57]	LIRF and IIC
Humidity correction of sonic temperature	[58,59]	LIRF and IIC
Statistical analysis of data screening	[60]	LIRF
The angle of attack correction for 3D wind components	[61]	LIRF

A two-dimensional (2D) EC heat flux (source) footprint analysis was performed to filter the EC-derived heat flux data to consider only flux source areas contributing to H and LE fluxes coming strictly from the maize fields at both the LIRF and IIC sites (as described in [62]), which is an analytical heat-flux-source approach that provides 2D footprint extents based on turbulence characteristics of the air flow and surface, such as Monin–Obukhov atmospheric stability length (L_{MO}, m), friction velocity (u_*, m/s), the standard deviation of lateral velocity (σ_v), Z_u, Z_{om}, and the atmospheric boundary layer height (H_L). To compare the predictions of ET_a at each station of measurement with the hourly and daily EC ET_a data, it was assumed that the fixed measurement instrumentation stations that were within the 2D EC footprint were representative of observed ET_a data from the EC system during the RS platform overpass date and time (Figure 5). At the IIC site, the EC flux tower was

located at the northwest corner of the field in 2020. Since the west and east measurement stations (Field F on Figure 4a) were farther from the footprint area for H and LE fluxes, the data from the west station was assumed to represent a maize ET_a comparison between the EC data and the remote sensing of ET_a predictions since it was the closest station to the flux tower. Figures 6 and 7 show the 2D EC footprints that served as a reference to filter the EC data at the LIRF and IIC sites, respectively.

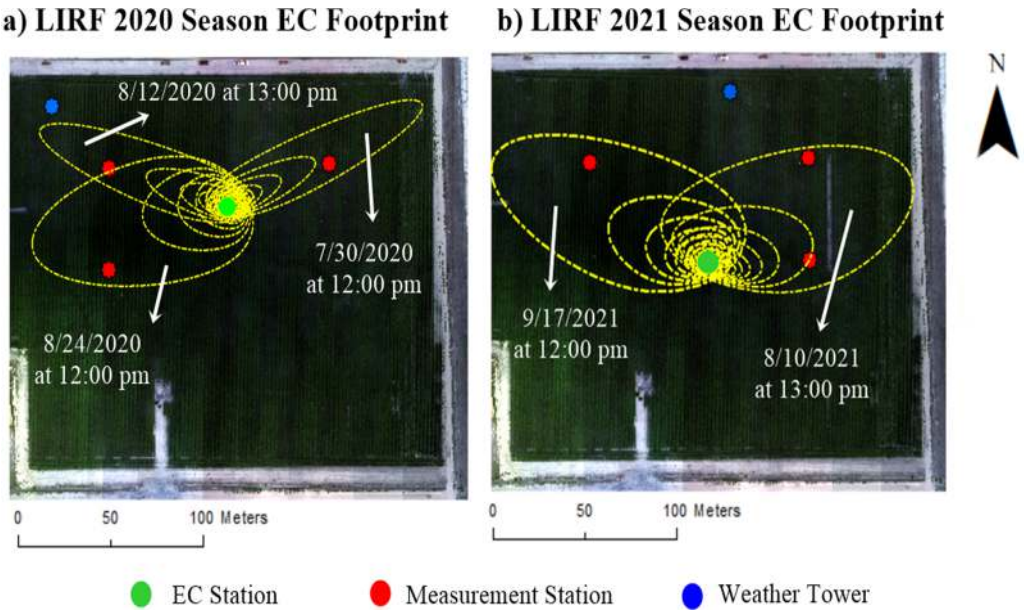

Figure 6. Two-dimensional EC footprint (yellow areas) at LIRF maize fields in 2020 (**a**) and 2021 (**b**).

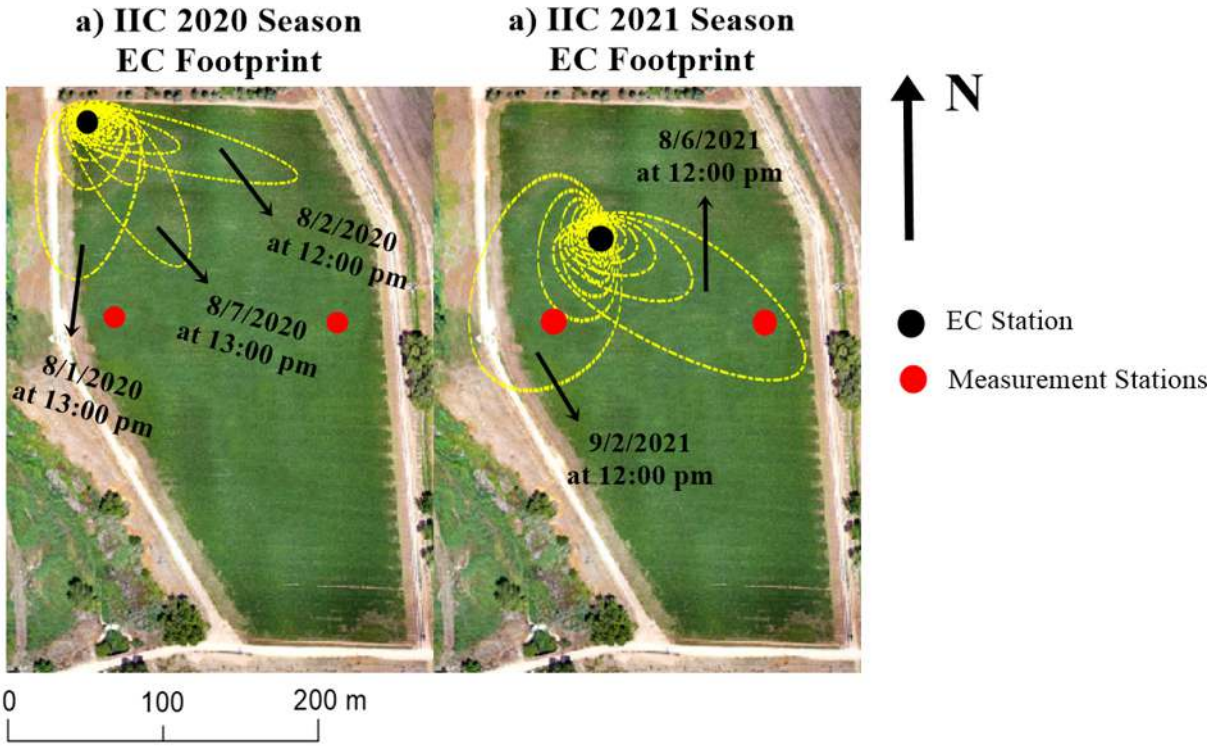

Figure 7. Two-dimensional EC footprint (yellow areas) at the IIC maize field F in 2020 (**a**) and 2021 (**b**).

2.5.2. Micrometeorological Data

Micrometeorological data were obtained at the EC heat flux or weather tower in each field. An HMP45C sensor probe (Vaisala, Helsinki, Finland) measured air temperature (T_a, °C) and relative humidity (RH, %) at 3.5 m AGS. The HMP45C probe has a 1000-ohm thermometer with measurement uncertainty within 0.20 to 0.30 °C at ambient temperatures varying from 20 to 40 °C. Within the HMP45C sensor, a HUMICAP H-chip measures RH with an uncertainty of approximately ±1% when T_a equals 20 °C [63]. Wind speed and direction were measured using a three-dimensional (3D) sonic anemometer installed at each research site, 3.5 m AGS. At IIC, the 3D sonic anemometer was a CSAT (Campbell Scientific Inc., Logan, UT, USA). In contrast, at LIRF, the 3D sonic anemometer was a Gill WindMaster 3D sonic anemometer (Gill Instruments, Lymington, Hampshire, UK). Incoming shortwave solar radiation was measured using an LI-200X pyranometer (LI-COR, Lincoln, NE, USA) at LIRF (3.3 m AGS) and the CNR01 net radiometer at the IIC site. The on-site weather data were recorded every minute and averaged every 15 min in CR1000 and CR3000 dataloggers (Campbell Scientific Inc., Logan, UT, USA) at the IIC and LIRF sites, respectively.

2.5.3. Surface Temperature Data

Nadir-looking T_s data were measured using SI-111 IRT sensors (Apogee Instruments, Logan, UT, USA). Each measurement station had one SI-111 IRT sensor installed 1 m above the canopy, nadir-looking, during the data collection campaign at IIC and LIRF. The IRT sensors were placed in a 4-meter-tall vertical post and raised to higher heights until the canopy reached maximum h_c, always keeping the 1-meter distance between the sensor and the top of the canopy. The FOV of SI-111 IRT sensors is a 22° half-angle. The sensors have a fast response time (<1 s) and a small uncertainty (±0.20 °C) when the target temperatures are between −20 °C and 65 °C. The ground-based area where most of the thermal radiation is sensed by the IRTs was equivalent to a 3-meter-diameter circumference. If we consider the upper part of the canopy, the footprint of the area sensed by the IRTs was about 1 m in diameter. The T_s data, alongside measured R_n and buried sensors to calculate surface G, were recorded every minute and averaged every 15 min in either a CR1000 or CR3000 datalogger (Campbell Scientific Inc., Logan, UT, USA) in each measurement station at LIRF and IIC. The SI-111 IRT sensors provided the input data to run the TSEB approaches in this study considering all RS sensors but the MSR.

2.6. Statistical Data Analysis

The following statistical variables have been considered to compare the performance of the different ET_a models across the spaceborne and airborne RS platforms: mean bias error (MBE), root mean square error (RMSE), normalized MBE (NMBE), normalized RMSE (NRMSE), and the coefficient of determination (R^2). Equations (31)–(34) indicate MBE, NMBE, RMSE, and NRMSE, respectively:

$$MBE = \left(\frac{1}{n}\right)\sum_{i=1}^{n}(E_i - O_i) \tag{31}$$

$$NMBE = \left(\frac{MBE}{\overline{O}}\right) \times 100\% \tag{32}$$

$$RMSE = \sqrt{\left(\frac{1}{n}\right)\sum_{i=1}^{n}(E_i - O_i)^2} \tag{33}$$

$$NRMSE = \left(\frac{RMSE}{\overline{O}}\right) \times 100\% \tag{34}$$

where $\overline{O}$ is the mean of the observed data; n is the sample size; E_i and O_i are the estimated and observed values, respectively. NMBE and NRMSE are given in percentages, while

Equations (32) and (34) provide statistical indicators with the same units of the primary variables. Based on the guidelines in [64], the performances of the ET_a models have been classified into one of the following categories: excellent (NRMSE $\leq$ 10%), good (10% < NRMSE $\leq$ 20%), fair (20% < NRMSE $\leq$ 30%), and poor (NRMSE > 30%).

The R^2, in the context of model performance assessment, informs about the degree of variability in the observed data explained by the modeling approach. Equation (35) gives the mathematical expression for R^2:

$$R^2 = \frac{\sum (E_i - \overline{E})(O_i - \overline{O})}{\sqrt{\left[\sum (E_i - \overline{E})^2\right]\left[\sum (O_i - \overline{O})^2\right]}} \quad (35)$$

where $\overline{E}$ is the mean value of the predictions. This study defines the optimal remote sensing platform as the source of multispectral data with the smallest NRMSE. In case two or more platforms have identical NRMSE, the highest d_r index between the two platforms is considered the optimal data for a given remote sensing of the ET_a algorithm. The modified index of agreement (d_r) was calculated to assess model performance by comparing the sum of the residuals to the total difference between observed values and the respective mean of the measured data. Higher d_r values indicate that the predicted values have more statistical agreement with the observed data, showing better model performance [65].

Outliers have been excluded from the analysis based on the median absolute deviation approach (MADA). The MADA method for filtering extreme values in a dataset uses the median instead of the mean as a central tendency measure. The median allows for flagging points that do not conform with the sampled data's trends [66]. The MADA index is defined by Equation (36) when a Gaussian distribution assumption is considered for the data without the influence of extreme values [67].

$$\text{MADA} = 1.4826 \times \text{Median}[|x_i - Median(x)|] \quad (36)$$

where x_i is the value of a given variable at a specified timestep; Median(x) is the median of the variable's sample size. In this study, the criteria for filtering the data for potential outliers was the recommendation by [66]. The median $\pm$ 2.5 times the MADA index is the cutoff value expected in each sampled dataset.

3. Results

3.1. Error Analysis from the TSEB Algorithms

3.1.1. TSEB Data Analysis Combined (LIRF and IIC 2020–2021)

The results from $TSEB_{par}$ and $TSEB_{ser}$ of the ET_a algorithms indicated that data used from the MSR5 (1 m) RS sensor resulted in the best performance when estimating hourly maize ET_a compared to the use of other RS platforms' data, since the smallest NRMSE was 11% and 14%, respectively, for both TSEB algorithms used. The overall errors in predicting hourly maize ET_a using MSR5 (1 m) data were -0.02 (-3%) $\pm$ 0.07 (11%) mm/h and -0.02 (-4%) $\pm$ 0.09 (14%) mm/h for the $TSEB_{par}$ and $TSEB_{ser}$, respectively. The errors associated with Landsat-8 (30 m) TIRS data used in the RS of ET_a estimation were -0.03 (-5%) $\pm$ 0.16 (29%) mm/h and -0.07 (-13%) $\pm$ 0.15 (29%) mm/h, while reductions of 31% and 34% in NRMSE were observed when the TIRS was replaced by the ground-based IRT data for the $TSEB_{par}$ and $TSEB_{ser}$, respectively (Figures 8 and 9).

The NRMSE errors in estimating H using Landsat-8 multispectral visible and NIR and TIRS data were greater than 30% for the $TSEB_{par}$ and $TSEB_{ser}$, while the NRMSE from the remaining spaceborne, airborne, and proximal platforms were within 20 to 30% (Figures 10 and 11). Using proximal IRT data to estimate maize ET_a with Landsat-8 (30 m), surface reflectance improved the estimation of hourly maize ET_a, with reduced model performance errors of 0.02 (4%) $\pm$ 0.10 (19%) mm/h and -0.04 (-8%) $\pm$ 0.11 (20%) mm/h for the $TSEB_{par}$ and $TSEB_{ser}$, respectively. Most of the improvements in hourly maize ET_a using $TSEB_{par}$ and $TSEB_{ser}$ were due to better H predictions than the accuracy

on the estimation of R_n and G fluxes. For the $TSEB_{par}$, the performance of the R_n model did not significantly change when using TIRS and IRT data since the NRMSE was 13% and 14%, respectively. The TSEB G model NRMSE ranged from 20 to 45% across all the RS platforms in this study, which had a fair to poor performance since NRMSE > 20%. However, since the magnitude of G is much smaller than R_n and H, the error propagation in LE estimates due to G is also smaller than the other two SEB input fluxes. Furthermore, the original TSEB G model assumes that G varies linearly with the R_n flux associated with bare soil. However, the work of [18] indicated that G and bare soil R_n have a time-phased difference between the two fluxes that requires a specific local calibration.

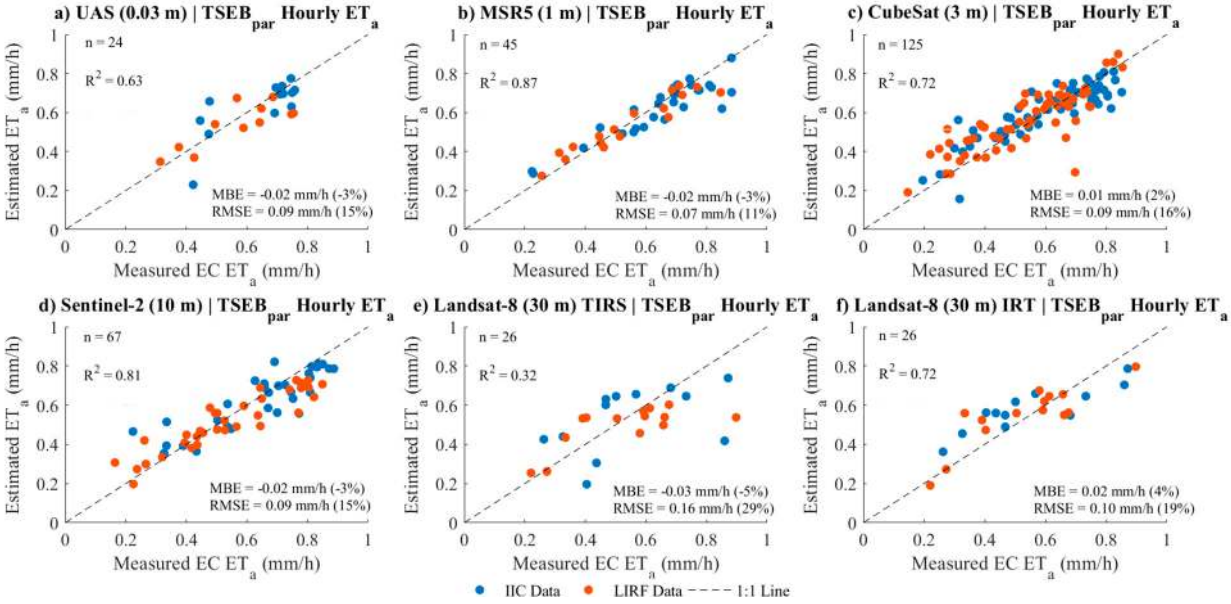

Figure 8. Scatter plots (1:1 line) and error analysis results regarding the TSEB parallel ($TSEB_{par}$) maize hourly ET_a modeling results for the combined LIRF and IIC 2020–2021 data. The sample size (*n*) of each platform is indicated in the figure.

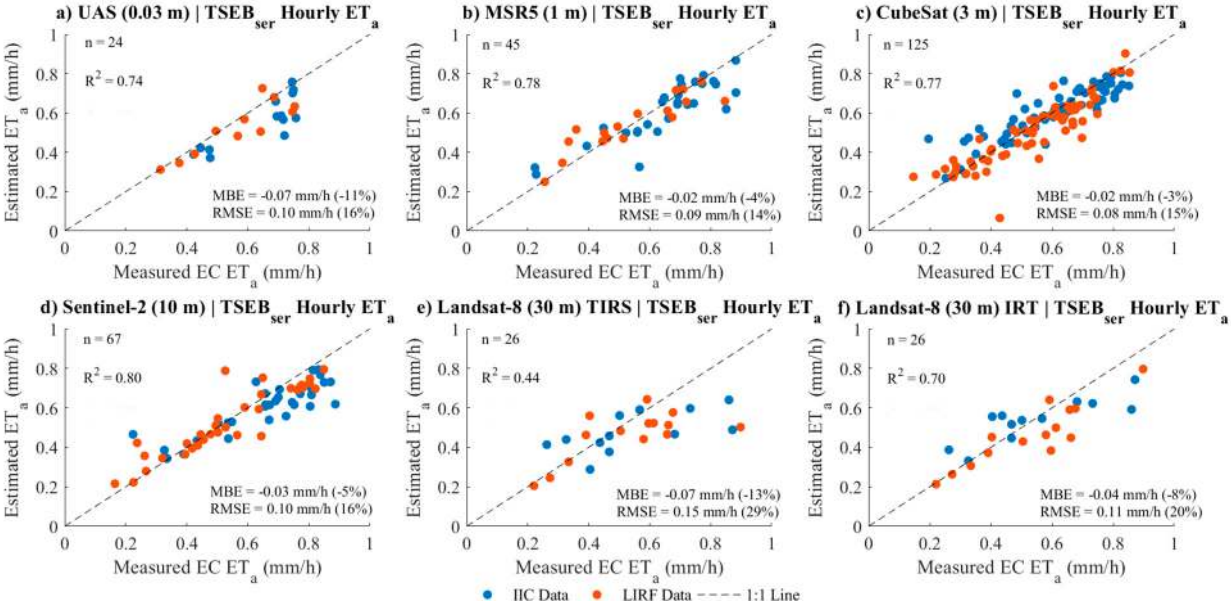

Figure 9. Scatter plots (1:1 line) and error analysis results regarding the TSEB series ($TSEB_{ser}$) maize hourly ET_a modeling results for the combined LIRF and IIC 2020–2021 data. The sample size (*n*) of each platform is indicated in the figure.

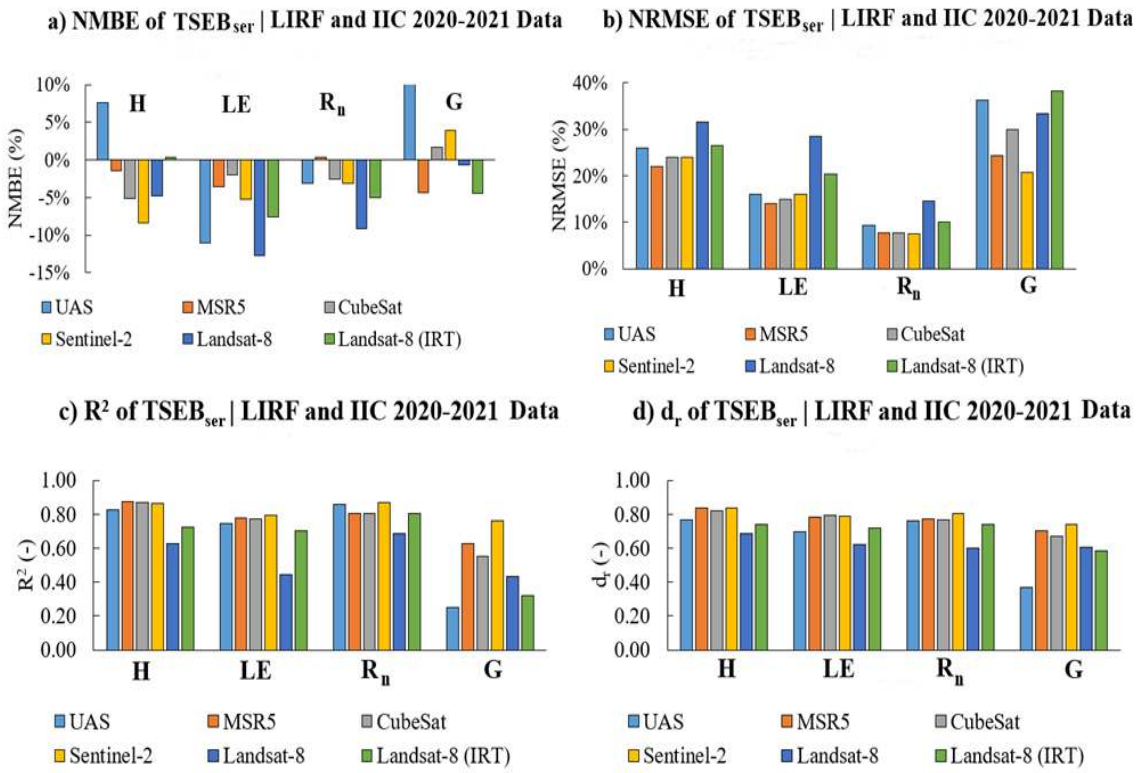

Figure 10. Error analysis of the SEB fluxes using the TSEB series (TSEB$_{ser}$) algorithm and LIRF and IIC 2020–2021 data combined.

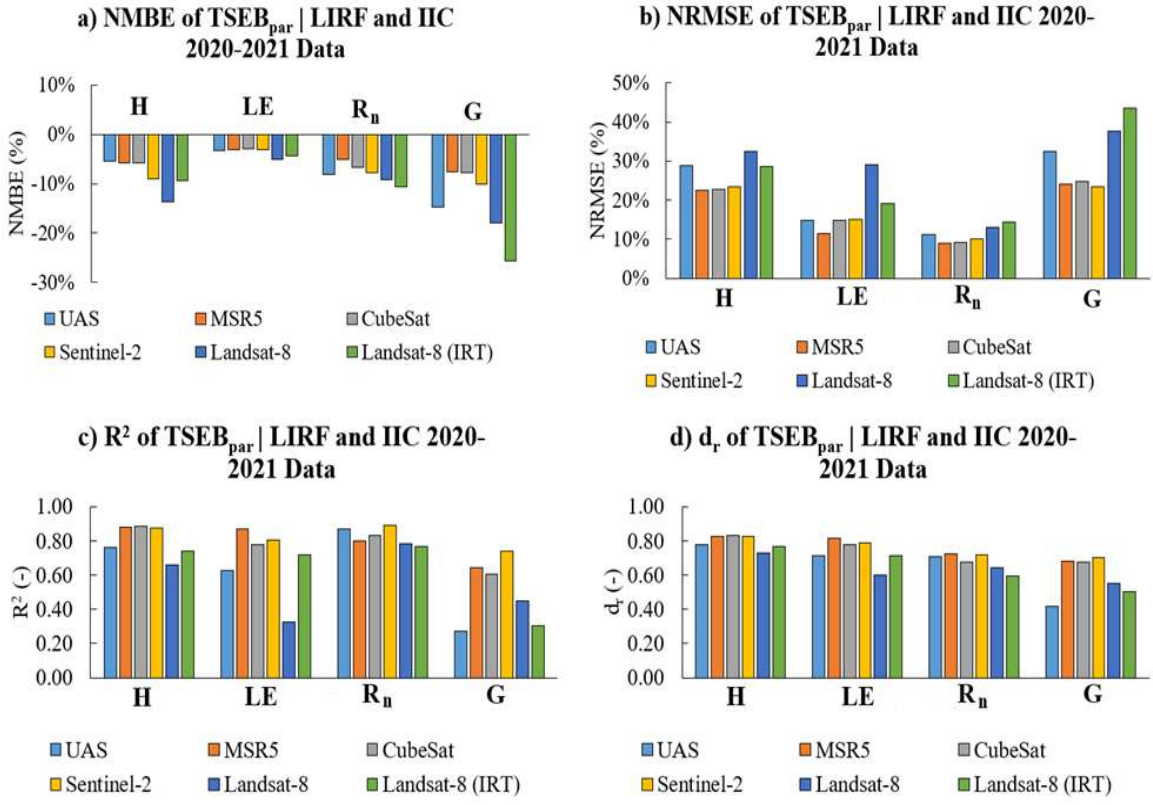

Figure 11. Error analysis of the SEB fluxes using the TSEB parallel (TSEB$_{par}$) algorithm and LIRF and IIC 2020–2021 data combined.

A consistent trend of maize ET_a underestimation was present for all spaceborne platforms/sensors (data) when considering the $TSEB_{ser}$ RS of the ET_a algorithm. The $TSEB_{ser}$ hourly maize ET_a underestimation range was within −3% (CubeSat) to −13% (Landsat-8 TIRS). When considering the $TSEB_{par}$ algorithm, there was an underestimation of hourly maize ET_a when using UAS (−3%), MSR5 (−3%), Sentinel-2 (−3%), and Landsat-8 TIRS (−5%). The slight overestimations of hourly maize ET_a for CubeSat (3 m) and Landsat-8 IRT (30 m) were 2% and 4%, respectively. Sentinel-2 (10 m) and Planet CubeSat (3 m) had similar performances since the NRMSE for $TSEB_{par}$ and $TSEB_{ser}$ had a 6% difference between the two high-resolution spaceborne platforms.

The underestimation trend shows a concurrent bias in the $TSEB_{ser}$ algorithm's ability to predict actual ET_a rates across various platforms. The largest underestimation by Landsat-8 TIRS could be attributed to its thermal infrared sensor's spatial resolution and spectral characteristics, which may not fully capture the heterogeneous surface temperature and moisture conditions within agricultural fields. This result suggests that there are limitations, inherent to this sensor, in accurately detecting surface temperatures for relatively small maize fields displaying some surface heterogeneity. The slight overestimations noted with CubeSat and Landsat-8 IRT suggest that these sensors, at their respective resolutions, might capture more of the variance in surface temperatures and moisture levels than the TIRS sensor. These discrepancies underscore the importance of the spectral and spatial resolution's role in capturing field heterogeneity.

The comparative performance of Sentinel-2 and Planet CubeSat, with a minimal difference in NRMSE for both TSEB algorithms, indicates that high-resolution spaceborne platforms are capable of providing reliable ET_a estimates, as compared to Landsat-8. The similar performance of these two sensors, despite their different operational designs and data characteristics, suggests that high-spatial-resolution spaceborne sensors have better results for small agricultural fields, compared to coarse satellite pixel resolutions. It also highlights the critical role of spatial resolution in capturing the detailed variability of agricultural landscapes, which is essential for promoting conditions to enhance sustainable irrigation water management in cropland fields.

In addition, the trend of underestimation observed with the $TSEB_{par}$ algorithm across UAS, MSR5, Sentinel-2, and Landsat-8 TIRS (with relatively minor variations) suggests the need for algorithmic adjustments or enhancements to further improve ET_a estimates. The TSEB RS of the ET_a models were originally developed and validated using airborne data at a 5 m spatial resolution. Given the large number of input parameters in the TSEB RS of ET_a, some of the uncertainty in the final maize ET_a estimation might be due to sub-models that do not have locally calibrated parameters for the semi-arid region across different climate conditions. Nevertheless, the performance of the ET_a algorithm is acceptable.

In our study, the range of accuracy of both TSEB approaches for maize ET_a (10–30%) was consistent with previously reported values in the current existing literature for other row crops such as vineyards when using sUAS imagery aggregated to different local spatial scales (e.g., 4 m, 7 m, 14 m, and 30 m) [27] and soybeans and maize when using Landsat-7 (30 m) and UAS (6 m) imagery spatial scales [68]. The similar results obtained between maize ET_a observed and estimated values from previous studies using different spatial and spectral resolution RS sensors reinforces the reliability of selecting finer RS spatial resolution sensors to use as input for predicting crop ET_a with a TSEB RS of the ET_a algorithm to advance sustainable agricultural water management. Both Ref. [27] and Ref. [68] indicated that the smallest errors observed when predicting LE and crop ET_a occurred at spatial resolutions less than 15 m.

The comparative analysis of multiple RS sensors presented a relevant understanding of their data quality as input for predicting maize ET_a using the TSEB RS of the ET_a algorithms evaluated in the study. Despite the overall agreement in ET_a accuracy observed in the existing literature, it is important to consider factors such as spectral resolution, revisit frequency, and sensor-specific limitations when deciding which RS sensor (data) is better, given the site-specific conditions and sustainable irrigation needs. Since the

MSR5 (proximal RS sensor) has limitations regarding the spatial coverage of large fields in a timely manner, operational costs, and data processing, its use could be hindered throughout different stages of the growing season. Given that the high-spatial-resolution spaceborne platforms (e.g., Sentinel-2 and Planet CubeSat) had similar accuracy performances (NMBE and NRMSE) compared to the MSR5 (Figures 10 and 11), their use could be justified when proximal RS devices are not ideal for collecting data over large agriculture fields with significant areas of canopy heterogeneity that make on-site data acquisition challenging and unrealistic.

3.1.2. TSEB Data Analysis Separately for LIRF and IIC 2020–2021 Data

When evaluating the LIRF 2020–2021 data alone, the results were also consistent with the previous combined data from LIRF and IIC regarding both the $TSEB_{ser}$ and $TSEB_{par}$ algorithms. The proximal platform MSR5 (1 m) outperformed all other platforms since it had the smallest NRMSE equal to 10% ($TSEB_{par}$) and 14% ($TSEB_{ser}$) see Tables 9 and 10. Underestimation (NMBE) of $TSEB_{par}$ hourly maize ET_a predictions ranged from −1 to −7% for the Landsat-8 TIRS (30 m), Sentinel-2 (10 m), MSR5 (1 m), and UAS (0.03 m). Overestimation of $TSEB_{par}$ maize ET_a was observed in the case of RS data used from the Planet CubeSat (3 m) and Landsat-8 IRT platforms, with respective NMBE equal to 4% and 3%. Regarding the $TSEB_{ser}$ RS of the ET_a algorithm, similar trends of underestimation and overestimation of hourly maize ET_a were observed compared to the $TSEB_{par}$ algorithm. There were 28% and 26% reductions in NRMSE, respectively, for the $TSEB_{par}$ and $TSEB_{ser}$ RS of ET_a results when Landsat-8 surface reflectance and IRT T_s data were used to estimate hourly maize ET_a. When evaluating the IIC 2020–2021 data alone, the results were again consistent with the previous analysis regarding LIRF and the combined LIRF-IIC data. Similarly, the MSR5 (1 m) outperformed the spaceborne and airborne platforms/sensors, with an overall error equal to −0.03 (−4%) ± 0.08 (12%) mm/h and −0.04 (−6%) ± 0.09 (14%) for the $TSEB_{par}$ and $TSEB_{ser}$, respectively.

Table 9. Error analysis from the $TSEB_{par}$ hourly maize ET_a evaluation for the LIRF and IIC 2020–2021 data.

Site	Platform	Spatial Resolution (m)	*n*	MBE (mm/d)	NMBE (%)	RMSE (mm/d)	NRMSE (%)	R^2
LIRF	Landsat-8 TIRS	30	14	−0.04	−7%	0.13	25%	0.51
	Landsat-8 IRT	30	14	0.02	3%	0.09	18%	0.73
	Sentinel-2	10	35	−0.02	−4%	0.09	16%	0.85
	CubeSat	3	63	0.02	4%	0.10	18%	0.69
	MSR5	1	17	−0.01	−1%	0.06	10%	0.91
	UAS	0.03	11	−0.03	−5%	0.09	15%	0.67
IIC	Landsat-8 TIRS	30	12	−0.02	−3%	0.18	33%	0.24
	Landsat-8 IRT	30	12	0.03	5%	0.11	21%	0.76
	Sentinel-2	10	32	−0.01	−2%	0.09	15%	0.73
	CubeSat	3	62	0	0%	0.08	14%	0.76
	MSR5	1	28	−0.03	−4%	0.08	12%	0.82
	UAS	0.03	13	−0.01	−2%	0.09	14%	0.58

Table 10. Error analysis from the $TSEB_{ser}$ hourly maize ET_a evaluation for the LIRF and IIC 2020–2021 data.

Site	Platform	Spatial Resolution (m)	*n*	MBE (mm/d)	NMBE (%)	RMSE (mm/d)	NRMSE (%)	R^2
LIRF	Landsat-8 TIRS	30	14	−0.07	−13%	0.14	27%	0.48
	Landsat-8 IRT	30	14	−0.07	−13%	0.10	20%	0.81
	Sentinel-2	10	35	−0.01	−2%	0.08	15%	0.83
	CubeSat	3	63	−0.03	−6%	0.09	16%	0.79
	MSR5	1	17	0	0%	0.08	14%	0.82
	UAS	0.03	11	−0.04	−8%	0.08	14%	0.78
IIC	Landsat-8 TIRS	30	12	−0.07	−13%	0.16	30%	0.41
	Landsat-8 IRT	30	12	−0.01	−2%	0.12	21%	0.71
	Sentinel-2	10	32	−0.05	−8%	0.11	17%	0.75
	CubeSat	3	62	0.01	1%	0.08	13%	0.78
	MSR5	1	28	−0.04	−6%	0.09	14%	0.75
	UAS	0.03	13	−0.09	−13%	0.11	17%	0.72

4. Discussion

The observed results were related to differences in RS sensor types, the assumptions of the TSEB ET_a model and inherent uncertainty, and the complex physical processes that derive the heat and water vapor transfer between the surface and atmosphere. Regarding the RS data characteristics, the spatial resolution significantly impacts the accuracy of the hourly maize ET_a.

The RS platforms with higher spatial resolution (<10 m) capture finer surface feature details within agricultural fields. These high-spatial-resolution data have the potential to better characterize spatial variability in soil and vegetation conditions, which is essential for accurate crop ET_a estimation using the TSEB RS of ET_a algorithm. The RS sensors with coarse spatial resolution, such as Landsat-8 (30 m), have limitations in providing relevant multispectral data that represents well local variations of the Ts and surface reflectance values for smaller agricultural fields. These limitations can lead to increased uncertainty in ETa estimates, particularly in row crop fields.

The integration of ground-based measurements, such as IRT nadir-looking Ts data, has been shown to significantly improve the accuracy of RS-based ET_a estimates, especially when coarse Ts spatial-resolution data are not representative of local field conditions. The observed underestimation of the ET_a estimation, when using the proximal, airborne, and spaceborne RS surface reflectance data, may be related to uncertainties in the TSEB model parameters and the simplifications of the surface energy balance equations. Another challenge regarding the use of different RS sensors is the temporal resolution. Limited revisit frequencies and local atmospheric effects (e.g., aerosols) can introduce uncertainty in data acquisition and quality, ultimately impacting ET_a estimates.

Accurate, spatio-temporal ET_a predictions are essential for increasing crop yields while mitigating water scarcity issues, a critical factor in securing water sustainability within a diverse range of water stakeholders. While remote sensing data, particularly through the TSEB model, has significantly advanced our understanding of crop ET_a, challenges persist in implementing sustainable solutions within agricultural settings.

Despite the potential of RS to advance sustainable water management in irrigated fields, limitations exist. Spaceborne data such as those from Landsat-8, Sentinel-2, and Planet CubeSat often lack consistent daily imagery acquisition for ideal ET_a modeling conditions, and this inconsistency can create challenges in implementing daily irrigation scheduling based on RS data inputs. To overcome the limitations, we propose an approach

that integrates multiscale RS imagery from different platforms to generate RS data on a daily basis with similar radiometric quality to be readily available for water stakeholders (e.g., water management authorities, engineers, and agronomists). This integrated multiscale approach can provide consistent daily RS data for calculating crop ET_a and supporting water management decisions at local and large scales in agricultural settings.

Beyond the RS platforms' spectral resolution, revisit frequency, and sensor-specific limitations and calibration, other factors merit consideration for a comprehensive understanding and effective adoption of RS technologies in agriculture. Atmospheric variables such as humidity, temperature, concentration of gases, dust, and wind speed can significantly affect the accuracy of RS data, particularly for spaceborne sensors. Nonetheless, a multi-source RS data analysis can compensate for the limitations of individual RS sensors/platforms, offering an expanded perspective of crop water requirements that can lead to more sustainable irrigation practices in cropland.

5. Conclusions

This research was conducted in a semi-arid climate area, in maize fields irrigated with sub-surface drip and furrow irrigation systems, at two research sites in northern Colorado, USA. We aim to investigate the performance of two TSEB remote sensing of ET_a algorithms when using input data from different (multiscale) remote sensing sensors/platforms. The hypothesis was that the accuracy of RS of ET_a estimation depended on both the pixel spatial and spectral/radiometric resolutions of the multispectral data used and on the specific parameters within the RS of the ET_a algorithms. The primary conclusion is that, for both TSEB approaches evaluated ($TSEB_{par}$ and $TSEB_{ser}$), the best remote-sensing-based surface reflectance and temperature data for predicting maize hourly ET_a were those from the handheld MSR5 radiometer. The second-best RS data were multispectral surface reflectance images from the UAS, Planet, and Sentinel-2 RS platforms (plus surface temperature from stationary IRT sensors). However, using RS data from Landsat (optical and TIRS) resulted in larger ET_a estimation errors.

While it is possible to estimate crop ET_a using various remote sensing platforms, selecting the most suitable RS data for a given ET_a algorithm has the potential to significantly enhance irrigation water management by using more accurate ET_a estimates. In this study, it was found that the accuracy of the ET_a predictions was not the same across the different remote sensing sensors.

The use of the appropriate remote sensing data (i.e., MSR5) with the TSEB remote sensing of ET_a algorithms, to optimize maize irrigation scheduling, presents a significant contribution toward advancing sustainability in irrigated agriculture. The combination of MSR5 multispectral and thermal data to determine the contributions of soil and vegetation components to ET_a can offer a more accurate understanding of water consumption in cropland ecosystems, compared to the most common Landsat data use.

To improve the effectiveness of sustainable solutions using remote sensing data, future research in sustainability should focus on refining the TSEB algorithms, integrating diverse datasets within the same data analysis context, and addressing challenges associated with scaling from local (e.g., farms) to regional (e.g., irrigation districts and watersheds) levels.

This study highlights the need for further research aimed at improving the data quality of sub-optimal remote sensing platforms/sensors when only those data are available. It is critical to develop imagery calibration protocols to improve the quality of the remote sensing data needed for the prediction of crop ET_a under different surface and climate conditions. This would help enable the use of the most desirable remote sensing data with high accuracy for effective irrigation water management. Also, we recognize the need for more research including a wider range of commercial crops to strengthen the analysis of how the TSEB approaches perform when estimating crop ET_a for other crop types.

Additionally, the role of advanced spatial data analysis and machine learning algorithms in processing and interpreting RS data could be an alternative to explore to improve the quality of the RS data for the sensors that did not perform better than the MSR5. These

technologies can provide a possible framework to address complex patterns and relationships within large imagery datasets, facilitating more applied and predictive approaches to crop water use and stress levels. By leveraging the computational capabilities of these artificial intelligence models, researchers and practitioners can refine the application of TSEB RS algorithms and determine irrigation scheduling practices to meet the water requirements of specific crops under local field conditions.

Author Contributions: E.C.-F. processed the data, conducted the statistical analysis, and wrote the bulk of the manuscript. J.L.C. developed the research proposals, guided the study, supervised field/lab work and data processing, and edited the manuscript, and H.Z. was involved in fieldwork planning, manuscript formatting, and writing adjustments. All authors have read and agreed to the published version of the manuscript.

Funding: This research was mainly funded by the Colorado Agricultural Experiment Station (CAES)—and the United Stated Department of Agriculture—National Institute of Food and Agriculture (USDA NIFA) through project grant number COL00796.

Institutional Review Board Statement: Not applicable.

Informed Consent Statement: Not applicable.

Data Availability Statement: The data presented in this study are available on request from the corresponding author.

Acknowledgments: The authors are grateful to the Colorado Agricultural Experiment Station (CAES)—USDA NIFA research project award COL00796, to Northern Colorado Water Conservancy District, and to the Irrigation Innovation Consortium (IIC) for funding this research effort. Furthermore, we would like to thank Cole Lucero, Rustin Jensen, Mia Morones, Kelsey Walker, Jon Altenhofen, Katie Ascough, Brianna Trotter, Alex Olsen, Kevin Yemoto, Ross Steward, Garrett Banks, and Luke Stark for their participation and field efforts to collect data, install instrumentation, and manage farm management activities. We also thank Allan Andales and Ansley Brown for the collaborative efforts provided during the data collection seasons at the IIC research site in 2020 and 2021.

Conflicts of Interest: The authors declare that they do not have any conflicts of interest, nor any competing financial interests or personal relationships that could have appeared to influence the contents of this study.

Appendix A. Calculation of Auxiliary Variables for the TSEB Algorithm

The r_{ah} term is calculated using Equation (A1) as follows (as in [69]):

$$r_{ah} = \frac{\ln\left(\frac{z_u - d}{z_{oh}}\right) - \psi_h}{u_* k} \tag{A1}$$

where z_u is the height of wind speed measurement (m); d is the zero-plane displacement height (m); z_{oh} is the roughness length for heat transfer (m); ψ_h is the atmospheric stability correction function for heat transfer (dimensionless); k is the von Kármán constant and is set to 0.41 [70,71].

The shear or friction velocity (Equation (A2)) is calculated as follows (as in [69]):

$$u_* = \frac{Uk}{\ln\left(\frac{z_u - d}{z_{om}}\right) - \psi_m} \tag{A2}$$

where u_* is the mean shear velocity (m/s), ψ_m is the atmospheric stability correction function for momentum transfer (dimensionless); z_{om} is the roughness length for momentum transfer (m); and U is the mean horizontal wind speed (m/s).

The ψ_h and ψ_m are equal to zero for quasi-neutral atmospheric conditions. When thermal stratification exists, the Monin–Obukhov stability length (L_{MO}) and theory is considered to correct the estimations of momentum and heat transfer [72]. For unstable

($L_{MO} < 0$) and stable ($L_{MO} > 0$) atmospheric conditions, Equations (A3) and (A4) present the models for the atmospheric stability corrections for heat transfer [73–75]:

$$\psi_h = \begin{cases} 2 \times ln\left(\frac{1+x_1^2}{2}\right) - 2 \times \ln\left(\frac{1+x_1^2}{2}\right), \ L_{MO} < 0 \\ -5 \times \left(\frac{z_u - d}{L_{MO}}\right), \ L_{MO} > 0 \end{cases} \quad \text{(A3)}$$

$$x_1 = \left[1 - 16\left(\frac{z_u - d}{L_{MO}}\right)\right]^{0.25} \quad \text{(A4)}$$

where L_{MO} is the Monin–Obukhov stability length (m) and is calculated as indicated by Equation (A5) below:

$$L_{MO} = -\frac{u_*^3 \ T_a \ \rho_a \ C_{pa}}{g \ k \ H} \quad \text{(A5)}$$

where g is the gravitational acceleration (≈9.81 m/s^2).

For unstable and stable atmospheric conditions, Equation (A6) indicates the models for the atmospheric stability corrections for momentum transfer [73–75]:

$$\psi_m = \begin{cases} 2 \ ln\left(\frac{1+x_1}{2}\right) + ln\left(\frac{1+x_1^2}{2}\right) - 2\arctan(x_1) + \frac{\pi}{2}, \ L_{MO} < 0 \\ -5 \times \left(\frac{z_u - d}{L_{MO}}\right), \ L_{MO} > 0 \end{cases} \quad \text{(A6)}$$

The roughness elements d, z_{om}, and z_{oh} are calculated as indicated by Equations (A7)–(A9), respectively [76]:

$$z_{om} = \begin{cases} z'_o + 0.28 \ h_c \ \sqrt{J}, \ 0 \le J \le 0.20 \\ 0.3 \ h_c\left(1 - \frac{d}{h_c}\right), \ 0.20 < J \le 2 \end{cases} \quad \text{(A7)}$$

$$d = h_c \left[ln\left(1 + J^{\frac{1}{6}}\right) + 0.03 \ ln\left(1 + J^6\right)\right] \quad \text{(A8)}$$

$$z_{oh} = 0.10 \times z_{om} \quad \text{(A9)}$$

where z'_o is the roughness length of the soil surface ($z'_o \approx 0.01$ m), and J is equal to 20% of LAI (m^2/m^2).

Appendix B. Calculation of TSEB Soil and Canopy Resistances When Estimating H

The r_{soil} (s/m) is calculated using Equations (A10)–(A13) [21]:

$$r_{soil} = \frac{1}{0.004 + 0.012 \ U_{soil}} \quad \text{(A10)}$$

$$U_{soil} = U_{canopy} \times \exp\left(-a_{ext} \times \left[1 - \frac{0.05}{h_c}\right]\right) \quad \text{(A11)}$$

$$U_{canopy} = \frac{u_*}{k} \times \ln\left(\frac{h_c - d}{z_{om}}\right) \quad \text{(A12)}$$

$$a_{ext} = 0.28 \times (CF \times LAI)^{\frac{2}{3}} \times h_c^{\frac{1}{3}} \times w_c^{-\frac{1}{3}} \quad \text{(A13)}$$

where U_{soil} is the mean horizontal wind speed at the ground surface (m/s); U_{canopy} is the mean horizontal wind speed at the top of the canopy (m/s); w_c is the mean leaf width (for maize, 0.09 m); a_{ext} is the wind factor (dimensionless).

The r_x term (s/m) is calculated using Equations (A14) and (A15) below [21]:

$$r_x = \frac{C'}{LAI}\left(\frac{\Delta}{U_{d+z_{om}}}\right)^{\frac{1}{2}} \tag{A14}$$

$$U_{d+z_{om}} = U_{canopy} \times exp\left[-a_{ext} \times \left(1 - \frac{d + z_{om}}{h_c}\right)\right] \tag{A15}$$

where C′ is a weighing coefficient (set to 90 as indicated by [77]) and U_{d+zom} is the mean horizontal wind speed at the height equal to d + z_{om} (m/s).

The r_c term is calculated using Equations (A16) and (A17) [78]:

$$\frac{r_c}{r_{ah}} = \begin{cases} 3.09 \times \frac{r_*}{r_{ah}} + 2.41 \times \sqrt{\frac{r_*}{r_{ah}}} + 0.62, & LAI < 2 \\ 2.74 \times \frac{r_*}{r_{ah}} - 5.90 \times \sqrt{\frac{r_*}{r_{ah}}} + 7.04, & LAI \geq 2 \end{cases} \tag{A16}$$

$$r_* = \rho_a C_{pa}\left[\frac{e_s - e_a}{\gamma(R_n - G)}\right] \tag{A17}$$

where r_* is the climatic resistance (s/m).

References

1. Andales, A.A.; Bauder, T.A.; Arabi, M. A Mobile Irrigation Water Management System Using a Collaborative GIS and Weather Station Networks. In *Practical Applications of Agricultural System Models to Optimize the Use of Limited Water*; Ahuja, L.R., Ma, L., Lascano, R., Eds.; Advances in Agricultural Systems Modeling; ASA-CSSA-SSSA: Madison, WI, USA; Volume 5, 2014; pp. 53–84.
2. Allen, R.G.; Pereira, L.S.; Raes, D.; Smith, M. *Crop Evapotranspiration-Guidelines for Computing Crop Water Requirements-FAO Irrigation and Drainage Paper 56*; FAO: Rome, Italy, 1998; 300p.
3. Han, M.; Zhang, H.; Chávez, J.L.; Ma, L.; Trout, T.J.; DeJonge, K.C. Improved Soil Water Deficit Estimation through the Integration of Canopy Temperature Measurements into a Soil Water Balance Model. *Irrig. Sci.* **2018**, *36*, 187–201. [CrossRef]
4. Anderson, R.G.; French, A.N. Crop Evapotranspiration. *Agronomy* **2019**, *9*, 614. [CrossRef]
5. Gowda, P.H.; Chávez, J.L.; Colaizzi, P.D.; Evett, S.R.; Howell, T.A.; Tolk, J.A. Remote Sensing Based Energy Balance Algorithms for Mapping ET: Current Status and Future Challenges. *Trans. ASABE* **2007**, *50*, 1639–1644. [CrossRef]
6. Atzberger, C. Advances in Remote Sensing of Agriculture: Context Description, Existing Operational Monitoring Systems and Major Information Needs. *Remote Sens.* **2013**, *5*, 949–981. [CrossRef]
7. Shanmugapriya, P.; Rathika, S.; Ramesh, T.; Janaki, P. Applications of Remote Sensing in Agriculture-A Review. *Int. J. Curr. Microbiol. Appl. Sci.* **2019**, *8*, 2270–2283. [CrossRef]
8. Rott, H. Physical Principles and Technical Aspects of Remote Sensing. In *Remote Sensing in Hydrology and Water Management*; Springer: Berlin/Heidelberg, Germany, 2000; pp. 15–39. [CrossRef]
9. Maes, W.H.; Steppe, K. Perspectives for Remote Sensing with Unmanned Aerial Vehicles in Precision Agriculture. *Trends Plant Sci.* **2019**, *24*, 152–164. [CrossRef] [PubMed]
10. Pinter, P.J.; Hatfield, J.L.; Schepers, J.S.; Barnes, E.M.; Moran, M.S.; Daughtry, C.S.T.; Upchurch, D.R. Remote Sensing for Crop Management. *Photogramm. Eng. Remote Sens.* **2003**, *69*, 647–664. [CrossRef]
11. Zhang, B.Z.; Kang, S.Z.; Zhang, L.; Du, T.S.; Li, S.E.; Yang, X.Y. Estimation of Seasonal Crop Water Consumption in a Vineyard Using Bowen Ratio-Energy Balance Method. *Hydrol. Process.* **2007**, *21*, 3635–3641. [CrossRef]
12. Nieuwenhuis, G.J.A.; Klaassen, W. *Estimation of the Regional Evapotranspiration from Remotely Sensed Crop Surface Temperatures*; Arable Land ICW No. 1057; ICW: Wageningen, The Netherlands, 1978.
13. Stone, L.R.; Horton, M.L. Estimating Evapotranspiration Using Canopy Temperatures: Field Evaluation. *Agron. J.* **1974**, *66*, 450–454. [CrossRef]
14. Boulet, G.; Olioso, A.; Ceschia, E.; Marloie, O.; Coudert, B.; Rivalland, V.; Chirouze, J.; Chehbouni, G. An Empirical Expression to Relate Aerodynamic and Surface Temperatures for Use within Single-Source Energy Balance Models. *Agric. For. Meteorol.* **2012**, *161*, 148–155. [CrossRef]
15. Lafleur, P.M. Energy Balance and Evapotranspiration from a Subarctic Forest. *Agric. For. Meteorol.* **1992**, *58*, 163–175. [CrossRef]
16. Moran, M.S.; Jackson, R.D.; Raymond, L.H.; Gay, L.W.; Slater, P.N. Mapping Surface Energy Balance Components by Combining Landsat Thematic Mapper and Ground-Based Meteorological Data. *Remote Sens. Environ.* **1989**, *30*, 77–87. [CrossRef]
17. Tang, R.; Li, Z.-L.; Jia, Y.; Li, C.; Chen, K.-S.; Sun, X.; Lou, J. Evaluating One- and Two-Source Energy Balance Models in Estimating Surface Evapotranspiration from Landsat-Derived Surface Temperature and Field Measurements. *Int. J. Remote Sens.* **2013**, *34*, 3299–3313. [CrossRef]

18. Colaizzi, P.D.; Kustas, W.P.; Anderson, M.C.; Agam, N.; Tolk, J.A.; Evett, S.R.; Howell, T.A.; Gowda, P.H.; O'Shaughnessy, S.A. Two-Source Energy Balance Model Estimates of Evapotranspiration Using Component and Composite Surface Temperatures. *Adv. Water Resour.* **2012**, *50*, 134–151. [CrossRef]
19. Kustas, W.P.; Norman, J.M. A Two-Source Energy Balance Approach Using Directional Radiometric Temperature Observations for Sparse Canopy Covered Surfaces. *Agron. J.* **2000**, *92*, 847–854. [CrossRef]
20. Massman, W.-W.R. A Surface Energy Balance Method for Partitioning Evapotranspiration Data into Plant and Soil Components for a Surface with Partial Canopy Cover. *Wiley Online Libr.* **1992**, *28*, 1723–1732. [CrossRef]
21. Norman, J.M.; Kustas, W.P.; Humes, K.S. A Source Approach for Estimating Soil and Vegetation Energy Fluxes in Observations of Directional Radiometric Surface Temperature. *Agric. For. Meteorol.* **1995**, *77*, 263–293. [CrossRef]
22. French, A.N.; Hunsaker, D.J.; Sanchez, C.A.; Saber, M.; Gonzalez, J.R.; Anderson, R. Satellite-Based NDVI Crop Coefficients and Evapotranspiration with Eddy Covariance Validation for Multiple Durum Wheat Fields in the US Southwest. *Agric. Water Manag.* **2020**, *239*, 106266. [CrossRef]
23. Sánchez, J.M.; López-Urrea, R.; Valentín, F.; Caselles, V.; Galve, J.M. Lysimeter Assessment of the Simplified Two-Source Energy Balance Model and Eddy Covariance System to Estimate Vineyard Evapotranspiration. *Agric. For. Meteorol.* **2019**, *274*, 172–183. [CrossRef]
24. Sánchez, J.M.; Simón, L.; González-Piqueras, J.; Montoya, F.; López-Urrea, R. Monitoring Crop Evapotranspiration and Transpiration/Evaporation Partitioning in a Drip-Irrigated Young Almond Orchard Applying a Two-Source Surface Energy Balance Model. *Water* **2021**, *13*, 2073. [CrossRef]
25. Trezza, R.; Allen, R.G.; Kilic, A.; Ratcliffe, I.; Tasumi, M. Influence of Landsat Revisit Frequency on Time-Integration of Evapotranspiration for Agricultural Water Management. In *Advanced Evapotranspiration Methods and Applications*; Daniel, B., Ed.; IntechOpen: Rijeka, Croatia, 2018; Chapter 3. [CrossRef]
26. Aragon, B.; Ziliani, M.G.; McCabe, M.F. Revisiting the Spatial Scale Effects on Remotely Sensed Evaporation. In Proceedings of the International Geoscience and Remote Sensing Symposium (IGARSS), Brussels, Belgium, 12–16 July 2021; pp. 6579–6582. [CrossRef]
27. Nassar, A.; Torres-Rua, A.; Kustas, W.; Nieto, H.; McKee, M.; Hipps, L.; Stevens, D.; Alfieri, J.; Prueger, J.; Alsina, M.M.; et al. Influence of Model Grid Size on the Estimation of Surface Fluxes Using the Two Source Energy Balance Model and sUAS Imagery in Vineyards. *Remote Sens.* **2020**, *12*, 342. [CrossRef]
28. Burchard-Levine, V.; Nieto, H.; Riaño, D.; Migliavacca, M.; El-Madany, T.S.; Guzinski, R.; Martín, M.P. The Effect of Pixel Heterogeneity for Remote Sensing Based Retrievals of Evapotranspiration in a Semi-Arid Tree-Grass Ecosystem. *Remote Sens. Environ.* **2021**, *260*, 112440. [CrossRef]
29. Costa-Filho, E.; Chávez, J.L.; Comas, L. Determining Maize Water Stress Through a Remote Sensing-Based Surface Energy Balance Approach. *Irrig. Sci.* **2020**, *38*, 501–518. [CrossRef]
30. Post, D.F.; Fimbres, A.; Matthias, A.D.; Sano, E.E.; Accioly, L.; Batchily, A.K.; Ferreira, L.G. Predicting Soil Albedo from Soil Color and Spectral Reflectance Data. *Soil Sci. Soc. Am. J.* **2000**, *64*, 1027–1034. [CrossRef]
31. Norman, J.M.; Jarvis, P.G. Photosynthesis in Sitka Spruce (*Picea sitchensis* (Bong.) Carr.): V. Radiation Penetration Theory and a Test Case. *J. Appl. Ecol.* **1975**, *12*, 839. [CrossRef]
32. Norman, J.M. Modelling the Complete Crop Canopy. In *Modification of the Aerial Environment of Plants*; ASAE Monograph: St. Joseph, MI, USA, 1979; Volume 2, pp. 249–277.
33. Goudriaan, J. *Crop Micrometeorology: A Simulation Study*; Pudoc: Wageningen, The Netherlands, 1977.
34. Nikolov, N.T.; Zeller, K.F. A Solar Radiation Algorithm for Ecosystem Dynamic Models. *Ecol. Modell.* **1992**, *61*, 149–168. [CrossRef]
35. Spokas, K.; Forcella, F. Estimating Hourly Incoming Solar Radiation from Limited Meteorological Data. *Weed Sci.* **2006**, *54*, 182–189. [CrossRef]
36. Ham, J.M. Useful Equations and Tables in Micrometeorology. In *Micrometeorology in Agricultural Systems*; Agronomy Monographs; American Society of Agronomy, Crop Science Society of America, and Soil Science Society of America: Madison, WI, USA, 2015; pp. 533–560. [CrossRef]
37. Rondeaux, G.; Steven, M.; Baret, F. Optimization of Soil-Adjusted Vegetation Indices. *Remote Sens. Environ.* **1996**, *55*, 95–107. [CrossRef]
38. Chávez, J.L.; Neale, C.M.U.; Prueger, J.H.; Kustas, W.P. Daily Evapotranspiration Estimates from Extrapolating Instantaneous Airborne Remote Sensing ET Values. *Irrig. Sci.* **2008**, *27*, 67–81. [CrossRef]
39. Anderson, M.C.; Neale, C.M.U.; Li, F.; Norman, J.M.; Kustas, W.P.; Jayanthi, H.; Chavez, J.O.S.E. Upscaling Ground Observations of Vegetation Water Content, Canopy Height, and Leaf Area Index during SMEX02 Using Aircraft and Landsat Imagery. *Remote Sens. Environ.* **2004**, *92*, 447–464. [CrossRef]
40. Roy, D.P.; Wulder, M.A.; Loveland, T.R.; Woodcock, C.E.; Allen, R.G.; Anderson, M.C.; Helder, D.; Irons, J.R.; Johnson, D.M.; Kennedy, R.; et al. Landsat-8: Science and Product Vision for Terrestrial Global Change Research. *Remote Sens. Environ.* **2014**, *145*, 154–172. [CrossRef]
41. Vermote, E.; Justice, C.; Claverie, M.; Franch, B. Preliminary Analysis of the Performance of the Landsat 8/OLI Land Surface Reflectance Product. *Remote Sens. Environ.* **2016**, *185*, 46–56. [CrossRef] [PubMed]

42. Drusch, M.; del Bello, U.; Carlier, S.; Colin, O.; Fernandez, V.; Gascon, F.; Hoersch, B.; Isola, C.; Laberinti, P.; Martimort, P.; et al. Sentinel-2: ESA's Optical High-Resolution Mission for GMES Operational Services. *Remote Sens. Environ.* **2012**, *120*, 25–36. [CrossRef]
43. Main-Knorn, M.; Pflug, B.; Louis, J.; Debaecker, V.; Müller-Wilm, U.; Gascon, F. Sen2Cor for Sentinel-2. *SPIE* **2017**, *10427*, 37–48. [CrossRef]
44. Csillik, O.; Belgiu, M.; Asner, G.P.; Kelly, M. Object-Based Time-Constrained Dynamic Time Warping Classification of Crops Using Sentinel-2. *Remote Sens.* **2019**, *11*, 1257. [CrossRef]
45. Kington, J.D., IV; Jordahl, K.A.; Kanwar, A.N.; Kapadia, A.; Schönert, M.; Wurster, K. Spatially and Temporally Consistent Smallsat-Derived Basemaps for Analytic Applications. In *AGU Fall Meeting Abstracts*; American Geophysical Union: Washington, DC, USA, 2019; IN13B-0716. Available online: https://ui.adsabs.harvard.edu/abs/2019AGUFMIN13B0716K/abstract (accessed on 7 January 2024).
46. Campbell Scientific. *NR-Lite Net Radiometer: Instruction Manual*; Campbell Scientific Inc.: Logan, UT, USA, 2001.
47. Kipp & Zonen. *Instruction Manual CNR1 Net-Radiometer*; Kipp & Zonen: Delft, The Netherlands, 2002.
48. Campbell Scientific. *HFT3 Soil Heat Flux Plate Instruction Manual*; Campbell Scientific Inc.: Logan, UT, USA, 2003.
49. Foken, T. The Energy Balance Closure Problem: An Overview. *Ecol. Appl.* **2008**, *18*, 1351–1367. [CrossRef] [PubMed]
50. Liu, H.; Gao, Z.; Katul, G.G. Non-Closure of Surface Energy Balance Linked to Asymmetric Turbulent Transport of Scalars by Large Eddies. *J. Geophys. Res. Atmos.* **2021**, *126*, e2020JD034474. [CrossRef]
51. Oncley, S.P.; Foken, T.; Vogt, R.; Kohsiek, W.; DeBruin, H.A.R.; Bernhofer, C.; Christen, A.; van Gorsel, E.; Grantz, D.; Feigenwinter, C.; et al. The Energy Balance Experiment EBEX-2000. Part I: Overview and Energy Balance. *Bound.-Layer Meteorol.* **2007**, *123*, 1–28. [CrossRef]
52. Goulden, M.L.; Daube, B.C.; Fan, S.M.; Sutton, D.J.; Bazzaz, A.; Munger, J.W.; Wofsy, S.C. Physiological Responses of a Black Spruce Forest to Weather. *J. Geophys. Res. Atmos.* **1997**, *102*, 28987–28996. [CrossRef]
53. Liu, S.M.; Xu, Z.W.; Wang, W.Z.; Jia, Z.Z.; Zhu, M.J.; Bai, J.; Wang, J.M. A Comparison of Eddy-Covariance and Large Aperture Scintillometer Measurements with Respect to the Energy Balance Closure Problem. *Hydrol. Earth Syst. Sci.* **2011**, *15*, 1291–1306. [CrossRef]
54. Twine, T.E.; Kustas, W.P.; Norman, J.M.; Cook, D.R.; Houser, P.R.; Meyers, T.P.; Prueger, J.H.; Starks, P.J.; Wesely, M.L. Correcting Eddy-Covariance Flux Underestimates over a Grassland. *Agric. For. Meteorol.* **2000**, *103*, 279–300. [CrossRef]
55. Kaimal, J.C.; Finnigan, J.J. *Atmospheric Boundary Layer Flows: Their Structure and Measurement*; Oxford University Press: New York, NY, USA, 1994.
56. Tanner, C.B.; Thurtell, G.W. Anemoclinometer Measurements of Reynolds Stress and Heat Transport in the Atmospheric Surface Layer. In *Theory, Practice and Description of the ECPACK Library*; Meteorology and Air Quality Group: Wageningen, The Netherlands, 1969.
57. Webb, E.K.; Pearman, G.I.; Leuning, R. Correction of Flux Measurements for Density Effects Due to Heat and Water Vapour Transfer. *Q. J. R. Meteorol. Soc.* **1980**, *106*, 85–100. [CrossRef]
58. Schotanus, P.; Nieuwstadt, F.T.M.; de Bruin, H.A.R. Temperature Measurement with a Sonic Anemometer and Its Application to Heat and Moisture Fluxes. *Bound.-Layer Meteorol.* **1983**, *26*, 81–93. [CrossRef]
59. Van Dijk, A.; Moene, A.F.; De Bruin, H.A.R. *The Principles of Surface Flux Physics: Theory, Practice and Description of the ECPACK Library*; Internal Report 2004/1; Meteorology and Air Quality Group, Wageningen University: Wageningen, The Netherlands, 2004; 99p.
60. Vickers, D.; Mahrt, L. Quality Control and Flux Sampling Problems for Tower and Aircraft Data. *J. Atmos. Oceanic Technol.* **1997**, *14*, 512–526. [CrossRef]
61. Nakai, T.; Shimoyama, K. Ultrasonic Anemometer Angle of Attack Errors under Turbulent Conditions. *Agric. For. Meteorol.* **2012**, *162–163*, 14–26. [CrossRef]
62. Kljun, N.; Calanca, P.; Rotach, M.W.; Schmid, H.P. A simple two-dimensional parameterisation for Flux Footprint Prediction (FFP). *Geosci. Model Dev.* **2015**, *8*, 3695–3713. [CrossRef]
63. Campbell Scientific. *Model HMP45C Temperature and Relative Humidity Probe: Instruction Manual*; Campbell Scientific Inc.: Logan, UT, USA, 2004.
64. Jamieson, P.D.; Porter, J.R.; Wilson, D.R. A Test of the Computer Simulation Model ARCWHEAT1 on Wheat Crops Grown in New Zealand. *Field Crops Res.* **1991**, *27*, 337–350. [CrossRef]
65. Willmott, C.J.; Robeson, S.M.; Matsuura, K. A Refined Index of Model Performance. *Int. J. Climatol.* **2012**, *32*, 2088–2094. [CrossRef]
66. Leys, C.; Ley, C.; Klein, O.; Bernard, P.; Licata, L. Detecting Outliers: Do Not Use Standard Deviation Around the Mean, Use Absolute Deviation Around the Median. *J. Exp. Soc. Psychol.* **2013**, *49*, 764–766. [CrossRef]
67. Rousseeuw, P.J.; Croux, C. Alternatives to the Median Absolute Deviation. *J. Am. Stat. Assoc.* **1993**, *88*, 1273–1283. [CrossRef]
68. Li, F.; Kustas, W.P.; Prueger, J.H.; Neale, C.M.; Jackson, T.J. Utility of Remote Sensing–Based Two-Source Energy Balance Model Under Low- and High-Vegetation Cover Conditions. *J. Hydrometeorol.* **2005**, *6*, 878–891. [CrossRef]
69. Verma, S.B. Aerodynamic Resistances to Transfers of Heat, Mass, and Momentum. In *Estimation of Areal Evapotranspiration*; International Association of Scientific Hydrology: Goring Reading, UK, 1989; pp. 13–20.
70. Dyer, A.J. A Review of Flux-Profile Relationships. *Bound.-Layer Meteorol.* **1974**, *7*, 363–372. [CrossRef]
71. Dyer, A.J.; Hicks, B.B. Flux-Gradient Relationships in the Constant Flux Layer. *Q. J. R. Meteorol. Soc.* **1970**, *96*, 715–721. [CrossRef]

72. Monin, A.S.; Obukhov, A.M. Basic Laws of Turbulent Mixing in the Surface Layer of the Atmosphere. *Contrib. Geophys. Inst. Acad. Sci. USSR* **1954**, *151*, e187.
73. Businger, J.A.; Wyngaard, J.C.; Izumi, Y.; Bradley, E.F. Flux-Profile Relationships in the Atmospheric Surface Layer. *J. Atmos. Sci.* **1971**, *28*, 181–189. [CrossRef]
74. Paulson, C.A. The Mathematical Representation of Wind Speed and Temperature Profiles in the Unstable Atmospheric Surface Layer. *J. Appl. Meteorol.* **1970**, *9*, 857–861. [CrossRef]
75. Webb, E.K. Profile Relationships: The Log-Linear Range, and Extension to Strong Stability. *Q. J. R. Meteorol. Soc.* **1970**, *96*, 67–90. [CrossRef]
76. Choudhury, B.J.; Monteith, J.L. A Four-Layer Model for the Heat Budget of Homogeneous Land Surfaces. *Q. J. R. Meteorol. Soc.* **1988**, *114*, 373–398.
77. Grace, J. Some Effects of Wind on Plants. In *Plants and Their Atmospheric Environment*; Grace, J., Ford, E.D., Jarvis, P.G., Eds.; Blackwell Scientific: London, UK, 1981; pp. 31–56.
78. Yan, H.; Shi, H.; Hiroki, O.; Zhang, C.; Xue, Z.; Cai, B.; Wang, G. Modeling Bulk Canopy Resistance from Climatic Variables for Predicting Hourly Evapotranspiration of Maize and Buckwheat. *Meteorol. Atmos. Phys.* **2015**, *127*, 305–312. [CrossRef]

sustainability

MDPI

Article

Sustainable Management in River Valleys, Promoting Water Retention—The Opinion of Residents of South-Eastern Poland

Krzysztof Kud [1,*], Aleksandra Badora [2] and Marian Woźniak [1]

[1] Department of Enterprise, Management and Ecoinnovation, The Faculty of Management, Rzeszów University of Technology, 12 Powstanców Warszawy Street, 35-959 Rzeszów, Poland; mwozniak@prz.edu.pl
[2] Department of Agricultural and Environmental Chemistry, University of Life Sciences in Lublin, 15 Akademicka Street, 20-950 Lublin, Poland; aleksandra.badora@up.lublin.pl
* Correspondence: kkud@prz.edu.pl

Abstract: Sustainable development is implemented not only at the global level, but primarily in local environments. Shaping the space of river valleys becomes particularly important in the face of climate change and growing water deficit. The article therefore addresses the issue of the social perception of water management in the context of climate change. The aim was to answer the questions: what is the social awareness of water management in the face of climate change, and what sustainable solutions are socially accepted? The research was carried out in the south-eastern part of Poland, in the Podkarpackie and Lublin voivodeships. The diagnostic survey method, an original survey form, and the CAWI technique were used. The study group analyzed the perception of global, negative megatrends, and challenges related to water retention in the context of climate change. The task was to identify respondents' awareness of new sustainable management methods in river valleys. Due to the fact that the studied area is largely agricultural, differences in the perception of the studied items were sought, depending on the place of residence. It was assumed that inhabitants of rural areas have greater contact with nature, which may change their perception, and differences were looked for depending on the region of residence. Differences in the perceptions of the studied phenomena were also searched for, depending on the respondent's sex. The calculations show that the place of residence (urban–rural) and the regions (Podkarpackie–Lublin voivodeships) do not differentiate the perceptions of most of the examined items. However, sex primarily affects the perception of global megatrends and the perception of climate change. The results indicate the respondents' lack of awareness about natural forms of water retention. Respondents expected the implementation of outdated technical forms of flood protection. Expectations focused mainly on flood embankments and large dam reservoirs. There was strong belief among respondents regarding global megatrends and their impacts on social and economic life. A knowledge deficit was identified in relation to sustainable management methods in river valleys that favor water retention.

Keywords: water management and retention; climate change; sustainable development of river valleys; economics and public goods; south-eastern Poland

Citation: Kud, K.; Badora, A.; Woźniak, M. Sustainable Management in River Valleys, Promoting Water Retention—The Opinion of Residents of South-Eastern Poland. *Sustainability* **2024**, *16*, 4648. https://doi.org/10.3390/su16114648

Academic Editors: Wenfeng Liu, Xiaolin Yang and Wen Yin

Received: 27 March 2024
Revised: 29 April 2024
Accepted: 25 May 2024
Published: 30 May 2024

1. Introduction

Water security can be defined as the adaptive capacity to ensure the sustainable availability and safe use of adequate, reliable, and resilient water quantity and quality for health, livelihoods, ecosystems, and a productive economy, and for disaster risk reduction [1]. Ensuring water security involves managing too much or too little water and its quality. Water security refers to the growing importance of the sustainable management of water resources in a way that protects against any water-related disasters. Water security concerns both ecosystem health and economic development [2]. In environmental–ecological terms, water security shows the amount of water needed to maintain or improve environmental quality [3]. Available water resources are under pressure from many sectors, such as

agriculture, industry, tourism, transport, and energy. The issue of water security is also the subject of activities of the European Union [4]. The EU pays particular attention to the allocation and use of water resources, in particular, in sensitive economic sectors [5]. Currently, it is equally important to reduce the risk of floods, but also to limit the effects of drought.

All investment decisions, regarding flood protection, are mainly based on the results of a cost benefit analysis. This analysis can answer the questions related to economic efficiency, investment outlays, replacement costs of operation, and maintenance of technical infrastructure, as well as social and environmental costs related to changes in the conditions of natural ecosystems, biodiversity, and landscape [6]. Expenditures on flood protection measures in EU countries were estimated at a total of EUR 2.5 billion per year. In turn, expenditure under the European Regional Development Fund and the Cohesion Fund, in 2014–2020, intended for adaptation to climate change, and the prevention and management of climate-related risks, including floods and droughts, amounted to approximately EUR 6.3 billion. This presents an average of approximately EUR 0.9 billion per year [7]. In light of the presented challenges, the sustainable management of river valleys, with particular emphasis on natural water retention mechanisms, becomes of great importance [8].

1.1. The Impact of the Economy on Strategies to Ensure Water Security

Proper water management is becoming increasingly important, especially in the context of observed climate changes. Modern climate change includes an increase in air temperature on Earth, which, in turn, may affect other elements that shape the climate. According to some authors [9], in the years 2011–2020, the average temperature of the Earth was 1.09 °C higher, compared to the pre-industrial period, i.e., in the years 1850–1900. A change in one factor can, in turn, create a new set of conditions, which, in turn, can secondarily drive changes in the weather and climate elements. Currently, for example, there are intense droughts, water shortages, and serious fires on the one hand, and on the other hand, there are melting glaciers, rising sea levels, floods, catastrophic storms, and similar weather phenomena. The abovementioned phenomena have an impact on the environmental economy and are perceived differently, socially, in different regions of the world [10–12]. Changes in water resources and the biodiversity of water and land reservoirs are just some of the effects of violent weather phenomena. However, they imply a negative impact on agriculture and forestry [13], and on human health [14].

According to [15], an author who used 12 climate models for quantitative analysis, describing the impact of climate effects on global water resources; there will be an increase in the impact of climate effects on water resources in eastern Equatorial Africa, North America, and Eurasia, and in the La Plata Basin in South America. This increase will be in the range of 10–40% in 2050. In turn, the described dependence will decrease by 10–30% in Southern Europe, the Middle East, the western part of North America, and the Republic of South Africa [16]. Some authors [17] conducted research aimed at linking climate change and the chemical composition of groundwater. The research shows that seasonal floods, caused by extreme precipitation, are responsible for biochemical and geochemical redox processes, which result in groundwater contamination in post-flood areas. However, another author [18] concluded that the sustainable development of river valleys has a retention function and ensures safety both during floods and droughts. Riparian meadows can also be a source of biomass for fodder, or an energy carrier. Moreover, flood meadows can be an ecological buffer, capturing excess nutrients from surface runoff [18]. In turn, other authors [19] conducted a case study to show how to solve water scarcity problems resulting from climate change. These authors presented a hydro-economic model that combines elements of hydrology, economics, and the environment. This model was applied to arid and semi-arid regions in Spain. The research results indicate that the occurring drought phenomena have a significant impact on social wellbeing, and in the conditions examined by the abovementioned authors, there was a reduction in net agricultural production. Agriculture is the sector that consumes the most water in the world and needs it to feed

humanity [20]. Energy is also highly dependent on water, making electricity production one of the main drivers of global water scarcity [21]. In fact, it is difficult to imagine any human activity that is independent of water [22,23].

Hydrological droughts and forecasts of their occurrence in the future are becoming a serious challenge due to the complex interactions between climate, hydrology, and humans [24]. In many parts of the world, there are heated discussions about expanding reservoirs to counteract droughts and water shortages. However, contrary to popular belief, in some cases, the construction of reservoirs increases the risk of susceptibility to drought threats, and this, in turn, increases the potential damage associated with the construction of such water storage facilities [25]. Dam reservoirs operate mainly at points, which leads to an increase in the groundwater level, only in a limited area around the reservoir. At the same time, the groundwater level lowers downstream. As a result, this leads to local droughts. Still water retained in a reservoir evaporates faster, compared to water moved by a river current or retained in a wetland. Paradoxically, dam reservoirs contribute to a faster loss of water that should be retained in the environment. It is also often associated with the need to relocate entire settlements. Areas with high historical, cultural, agricultural, and natural values are therefore irretrievably lost. The construction of dam reservoirs is not a solution to the water deficit because, most often, it does not solve the problem of drought, but only transfers its effects to the lower sections of the river. The construction of water stages and dam reservoirs also disrupts the ecological continuity of a river, i.e., the transport of trailing debris, and interrupts the movement routes of fish and other animal species. In this situation, the properties of water, its temperature, oxygenation, and fertility also change, contributing to the threat and elimination of the lives of typical river organisms [26,27]. On the other hand, projections of the impact of climate change on flood characteristics are very sensitive to the detailed nature of these changes. The hydrological cycle is expected to be intensified by global warming, which is likely to increase the intensity of extreme rainfall events and the risk of flooding. It is also estimated that extreme rainfall and flooding may occur in all climatic regions. These phenomena may result in an excessive supply of various nutrients and pollutants to wetlands [28,29].

There are examples of synergies and antagonisms between the risk of floods and droughts and the actions limiting their impacts on the environment [30]. The very concept of a multifunctional dam reservoir illustrates just such a conflict. In order to reduce the risk of flooding, a given empty volume of the warehouse must be maintained, and thus, a possible flood wave is taken into account. However, the flood control measures described above mean the loss of the ability to store larger amounts of water, which may be very valuable in the event of a hydrological drought [31]. Therefore, to prevent drought, a "wet" reservoir would be preferred, while, to reduce flood risk, a "dry" reservoir (polder) would be preferred, collecting a larger amount of flood water. Therefore, what is better for reducing flood risk may not be good for reducing drought risk.

To ensure sustainable management in river valleys, the restoration of catchment areas is important. It involves restoring the flooding of coastal areas by moving flood embankments away. Activities of this type are also important for flood protection by slowing down water outflow. On the scale of the entire catchment area, it is important to protect wetlands in the water management system. The basis for ensuring proper water conditions in wetlands is to maintain the natural hydrological regime of the river, including periods of elevated water levels. It should be emphasized that drainage is one of the main causes of the destruction of wetlands. It is therefore necessary to limit water runoff as the primary method of protecting them. Natural riparian meadows are a very important element of sustainable management in river valleys. An important element of natural valleys of large rivers are ecosystems shaped by floodplains, complexes of rushes, thickets, and riparian forests. These ecosystems, now often cut off from the river by flood embankments, are subject to degradation and evolving into distorted land systems [32,33].

Hence, river restoration techniques, such as moving embankments by increasing their span and creating polders, may be beneficial in both cases [34].

Water retention—storing water when it is abundant and releasing it when it is scarce—is an essential measure to reduce the risks of floods and droughts [35,36]. The effectiveness of different types of flood storage systems should be considered in the context of their impact on reducing the volume of flood runoff. Created forests and other green areas, as well as small reservoirs or polders, can serve as integrated solutions and reduce the risk of flooding for many years. In turn, reducing the risk of long-term floods (e.g., by protecting against 100-year floods) requires the renaturalization of river spaces (i.e., "space for the river") and ensuring a large retention capacity in reservoirs [37]. To reduce the risk of floods and droughts, it is necessary to increase the capacity of various types of storage facilities, both natural and artificial [38]. These plans should also take into account water retention in the river valley landscape or soil retention, which is based on the assumption that an increase in the content of organic matter in the soil results in an increase in water storage [39]. The storage capacity of aquifers and the possibility of their recharge by abundant floodwaters should also be taken into account [40]. The appropriate connection of retention activities must be adapted to the actual hydrological, geological, and environmental conditions, as well as the existing and planned infrastructure in the river basin [41]. It also requires monitoring the effectiveness of such activities within local and regional systems, and adapting them to spatial development plans [42].

Public awareness that water management is a political issue is growing. Therefore, there is currently a tendency to talk about tasks related to water management as water resources management [43]. Water management, in particular, rainwater management in urbanized areas, seems to be the main challenge in the era of climate transformation [44]. Despite imprecise legal regulations, many Polish cities—especially those exposed to the effects of river floods or, in general, to the effects of flash floods—have started implementing organizational and legal changes to find and create an appropriate model for rainwater management in their area. This is a model that is intended to reduce the risk of floods and minimize the effects of drought, while enabling the cofinancing of their occurrence [45].

Polish legal regulations specify that flood protection is achieved, in particular, by: "(1) shaping the spatial development of river valleys or flood areas, mainly areas of particular flood risk; (2) rational water retention and use of flood protection structures, as well as control of water flows; (3) ensuring the functioning of the early warning system against dangerous phenomena, occurring in the atmosphere and hydrosphere, and flood forecasting; (4) preservation, creation and restoration of water retention systems; (5) construction, reconstruction and maintenance of flood protection structures; (6) conducting icebreaking campaigns and (7) conducting information policy, regarding flood protection and limiting its effects" [46]. Polish legal conditions are consistent with the European Union Directive [47].

Growing concerns related to climate change have focused spatial management in cities on mainly flood protection. As a consequence of such actions, cities are often not prepared for water shortages [48]. There are also studies on the maximization of water resources, but they are less concerned with the control and management of its demand. Achieving synergies and benefits in urban agglomerations, in the case of rainwater collection and reuse systems, are presented as topics requiring development, not only from the point of view of design, but also from the points of view of the management, decision making, and preparation of the final consumer for the "new water" that can be used in the context of the circular economy [49]. According to some authors [50], the implementation of green and blue urban infrastructure (GBI) is a positive undertaking because it ensures carbon dioxide sequestration, water retention, regulation, thermal comfort, and the improvement of biodiversity in the built environment, as well as around urban settlements [51]. Other studies have found that water quality in cities has improved significantly, as it has decreased, the number of waterborne diseases [52,53]. Moreover, the quality and availability of recreational facilities in urban surroundings have also increased [54].

Ecologists and landscape historians, as well as flood managers, attach more and more importance to the protection of flood meadows. They are valued as heritage, have ecological potential, and provide opportunities for local flood management [55]. According to some authors [56], flood meadows are characterized by specific flora and fauna that have settled and flourished, partly due to the humid environment and partly due to specific management practices. Some other authors [57] found that vegetation succession is controlled by water table configuration. The proper management of flood meadows therefore allows for more sustainable hay yields [58]. According to the report [59], an important task is to increase the availability of water in small river valleys through traditional irrigation. This type of treatment should also be treated as a proecological factor.

Most studies also indicate a positive relationship between species diversity and biomass production in flood meadows [60–62]. However, some studies have shown that managing grasslands to maintain high biodiversity is often incompatible with managing them to obtain maximum economic profit [63]. Therefore, even if the production conditions and quality of biomass are limited, the benefits for biodiversity and potentially for other ecosystem services fully justify the use and appropriate management of grasslands. It is also important that, in these areas, there are diversified subsidy systems, developed in accordance with European programs and subsidies to maintain the high value of natural grasslands [64]. Moreover, economic aspects are always important when investing in new irrigation networks or the modernization of existing irrigation systems [65]. On the one hand, the costs of investment, maintenance of the irrigation system, management expenses, and water prices should be taken into account, and on the other hand, the benefits resulting from increasing or stabilizing biomass yields [66].

1.2. Management in River Valleys to Promote Water Retention

Human settlements and the development of a country's economy are closely dependent on rivers. An example of such a relationship is ancient Egypt, or the cultures of Mesopotamia. Nowadays, especially in the context of climate change, the proper management of river valleys is becoming more and more important. Water retention solutions concern water supply for residents, industry, flood safety, and limiting the effects of drought. The use of various forms of retention, including natural (protection of water resources and the restoration or maintenance of natural ecosystems), significantly contribute to reducing the sensitivity of society, the environment, and the country's economy to the effects of climate change. Providing an appropriate amount of water in conditions of high climatic uncertainty, through its rational use, will allow the water needs of all users to be met. Water retention activities are aimed at limiting and slowing down the outflow of water from the catchment area [67]. Water retention solutions existing in Poland, but also in other European Union countries, require a transformation and adaptation to new challenges [68].

Poland's water resources are much smaller, compared to other European countries. The average amount of rainfall in our country is approximately 630 mm [44]; therefore, among other things, the country's spatial development should take into account increased water retention. The most well-known division of retention includes the distinction of whether water is stored in natural or manmade forms. This is how a distinction is made between natural and artificial retention [63]. Water retention capacity is an important element of the landscape in river valleys. In turn, the thickness of the humus layer has a significant impact on the soil's retention capacity [69]. Therefore, the proper development of agriculture is an element of increasing the retention capacity of the area.

The development of urbanization and technical transformation of river valleys contributed to the reduction in the water retention capacity [70]. The unfavorable environmental effects of river transformations have become an impulse to modify river management methods and search for more effective solutions. Among these activities, the restoration of rivers deserves attention [71] and, where possible, preserving their natural character. Restoring rivers to their natural state helps reduce the speed of water flow, which is slowed down by aquatic vegetation as well, as the diversified course of the riverbed.

However, technical flood protection methods do not provide the expected safety and are very expensive. Additionally, they often accelerate the outflow of water from the catchment area. High flood embankments cause water to accumulate, and the narrow area between the embankments increases the risk of catastrophic floods because there is no room to store a large mass of water in a small volume. The embankments limit the alluvial process, which reduces the fertility of alluvial soils in the river valley. The consequences are the accumulation of sediments in the embankment area and the aggradation of the bed. Additionally, it increases the risk of flooding because, sometimes, the river flows higher than the bottom of its valley [72].

In order to increase water retention, flood areas are to be excluded from intensive agricultural production and are to be allocated to extensive meadows or areas excluded from use, left to recreate the natural plant community's characteristic of a given area [73]. Technical flood management strategies that produce unsatisfactory results find an alternative in natural flood management. Strategies of this type are implemented, by leaving space for rivers and increasing the retention capacity of the river valley [32].

Therefore, the development of valleys should be adapted to current environmental conditions [72], for example, giving up the construction of groans and embankments that limit the free shaping of the riverbed, then natural riverbed systems will be reconstructed. Moreover, the area between the embankments can be significantly expanded by moving flood embankments or eliminating them altogether in areas that may experience local flooding. This will allow the river to freely shape its bed (returning to the meandering, braided, or ridged nature of the river), and will slow down the water outflow [71]. It is also possible to expand the area between embankments in the mouth sections of tributaries to enable the deposition of carried material in their valleys. A good way is to create polders for the periodic retention of flood waters. The removal of trees and shrubs from the area between the embankments should also be abandoned to enable the regeneration of natural riverside ecosystems. In addition, drainage should be improved so that fields and meadows can be irrigated when there is a lack of moisture in the soil. It is also necessary to withdraw settlements and infrastructure from the flood terrace [59]. Revitalization and restoration make it possible to manage flood risk and reduce the risk of flooding caused by too deeply incised riverbeds and the inability to dissipate the energy of flood waters, and reduce flood loss caused by accelerated water runoff, due to a lack of retention in flood areas. Restoration reduces the threat of drought, resulting from accelerated runoff, and the lack of resistance of regulated rivers to low flows resulting from the lack of differentiation in hydromorphological conditions. As a result, restored rivers do not require maintenance activities and their valleys constitute an important element of water retention [74].

It should be emphasized that restoration activities are expensive, so wherever the river has a nature close to natural, it is necessary to preserve this character. Local communities should be made aware of this because they decide what local space development looks like. Spatial management is shaped according to the principles established at the national level, but is implemented at the lowest level of administration, i.e., in municipalities. Moreover, spatial development plans are subject to public consultations, so the way the space is shaped largely depends on society's expectations. However, social expectations depend on the level of public awareness; therefore, the research problem presented in this scientific article can be formulated as a general question: "what is society's awareness of water management in the situation of climate change, and what solutions are socially accepted?".

2. Materials and Methods

Based on the main question, presented at the end of the previous chapter, detailed research questions were asked:

- How do respondents perceive water deficit amid negative megatrends?
- Do respondents understand the need to increase water retention?
- How do respondents imagine the proper management of river valleys to ensure water security?

- Is the free flow of flood waters perceived by respondents as an element of proper water management?
- Do the respondents' sex and place of residence influence the perception of water resources management?

Table 1 presents the research items that were posed to respondents in the survey questionnaire. These items were divided into three groups: (i) regarding megatrends; (ii) relating to water management; and (iii) regarding climate change. In the respondents' answers, attempts were made to find correlations within each group and between the mentioned groups of items.

Table 1. List of studied items.

Items Related to Megatrends
1. The most important global problem is environmental pollution;
2. The most important global problem is poverty and misery;
3. The most important global problem is hunger;
4. The most important global problem is water deficit;
5. The most important global problem is lifestyle diseases;
6. The most important global problem is climate change;
7. The most important global problem is the depletion of non-renewable energy sources;
8. The most important global problem is the growing world population;
Items Related to Water Management
9. Poland is facing a deep water deficit;
10. here is a need to increase small water retention;
11. Several large dams need to be built on major rivers;
12. Cities lack water retention infrastructure;
13. Developed riverside areas should be embanked;
14. Riverside areas used for agriculture should be embanked;
15. Undeveloped riverside areas should allow flood waters to flow freely;
16. Rivers need regulation;
17. Agricultural development of flood areas favoring water retention should be co-financed from the state budget;
18. Flood embankments in agricultural areas should be limited;
19. Development of flood plains should be prohibited;
Items Related to Climate Change
20. Climate change is currently one of the greatest threats to modern civilization;
21. Climate change has a direct impact on people's lives;
22. There are many issues more important than climate change and they require action first;
23. Climate change is a natural phenomenon, therefore it does not require our intervention;
24. Climate change is now virtually unstoppable;
25. Climate change causes fear and anxiety;
26. Humanity is transforming the landscape and consuming natural resources at a rate that makes their natural reproduction impossible;
27. The average temperature on our planet depends on the amount of solar radiation, absorbed by the Earth's surface and atmosphere, and on the amount and type of greenhouse gases in the atmosphere;
28. Current human activity significantly changes the state of the climate system, and the functioning of natural processes;
29. The increase in greenhouse gas emissions is closely related to the development of human civilization

The CAWI (Computer-Assisted Web Interview) technique was used in the diagnostic examination. Respondents were invited by sending them a link to the survey form. There were several dozen people in both voivodeships (Lubelskie and Podkarpackie). At the same

time, an invitation to participate in the study was posted on social media, and a survey was sent to enterprises and institutions cooperating with the authors of this publication. Then, the respondents also invited their friends who met the conditions regarding place of residence in one, or another voivodeship, to participate in the study. The survey was partial, nonprobabilistic, each participation was voluntary, and anonymous, and each respondent could stop filling out the form at any time. Therefore, it is not possible, to locate each respondent in a specific place on the map of each voivodeship (Scheme 1). Of the 825 collected questionnaires, 732 were accepted by the authors, because they were completely reliably and met the requirements of the respondent's place of residence in the surveyed voivodeships.

Scheme 1. Research area—marking the number of respondents in voivodeships [75].

The target group was adults aged ≥18 years old. They were residents of south-eastern Poland, from the voivodeships mentioned in the previous paragraph of the description. The study area was selected due to the agricultural and natural environmental values in both regions [76]. Moreover, both voivodeships are located in the temperate climate zone, with elements of maritime and continental climates [77,78]. However, according to the Köppen–Geiger classification [79,80], some regions in eastern Poland were classified as Dfb (snow climate). In both studied voivodeships, average winter temperatures range from −2 to −3 °C, and in summer the average temperature is about 18 °C, while average annual rainfall is 500–650 mm in the Lublin region, and 750–800 mm in Podkarpacie [81]. When characterizing the research regions, it should be emphasized that, despite many environmental similarities, we observed some differences. In the context of this research, the fact that there is a greater number and frequency of floods and flooding in the Podkarpackie voivodeship, compared to the Lublin voivodeship, may be significant. However, in the Lublin voivodeship, we experience droughts more often [82,83]. This assumption was taken into account by the authors of this publication, which is why a different number of surveys was deliberately collected in individual regions (Scheme 1). Therefore, the last detailed research question, included at the beginning of this chapter, concerns the place of residence, not only in the urban–rural context, but also in the context of the region from which the respondent came. The authors of this publication also assumed that respondents from rural areas, regardless of the voivodeship, have a slightly different view of the existence of floods and flooding in agricultural areas than respondents from cities. Farmers, from both voivodeships, have closer contact with nature and can be included in programs regarding subsidies for retention systems in flood areas, which in turn may be important in the perception of water management issues [84]. Moreover, the studied area of Poland is a

microscale, referring to a broader, nationwide problem, because it is known that water in agriculture is crucial in every region.

The survey questionnaire was subjected to reliability analysis using the Cronbach's alpha test. The test result was 0.709491, which is a satisfactory level [85,86]. The study was correlational in nature as it looked for relationships between individual groups of items, as well as between items in each group, without the possibility of influencing the level of individual variables. Since the study was not probabilistic in nature, the conclusions apply only to the surveyed group of respondents. To evaluate individual items, a five-point Likert scale, with a neutral value, was used [87]. The values on the scale are marked as follows: 1—definitely not; 2—probably not; 3—neither yes nor no; 4—probably yes; and 5—definitely yes. The structure of the response scores was calculated and analyzed. A simple Pearson correlation (r) between the examined items was also calculated, with a significance level of 0.05. In order to verify the answers to the research questions regarding the differences between qualitative variables, such as sex and place of residence (urban–rural), regardless of the voivodeship, and in the context of residence in a given voivodeship (Lubelskie–Podkarpackie), regardless of origin from an urban or rural area, a chi-squared test of independence was performed [88,89]. Categorized charts of the average scores of the tested items were also prepared. The results are presented in the tables and figures in the next section.

3. Results

The research group consisted of 732 people. Women constituted 67% of the respondents and men 33%. A total of 48% of all respondents lived in cities and 52% in rural areas; these percentages were the same by sex. Figures 1–3 present the structure of item ratings and the cumulative percentage of positive and negative ratings.

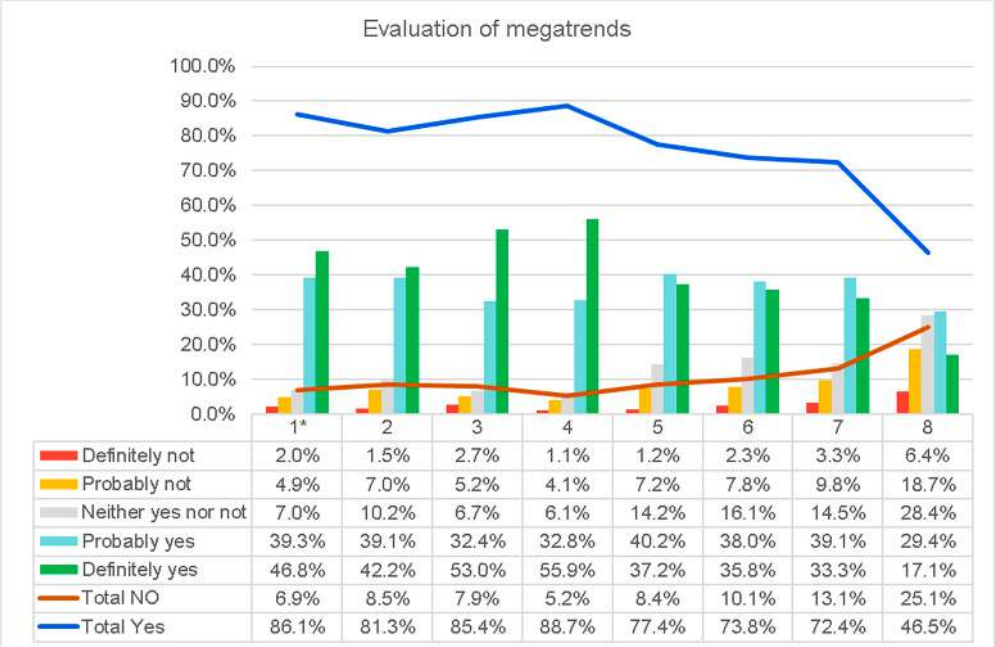

	1*	2	3	4	5	6	7	8
Definitely not	2.0%	1.5%	2.7%	1.1%	1.2%	2.3%	3.3%	6.4%
Probably not	4.9%	7.0%	5.2%	4.1%	7.2%	7.8%	9.8%	18.7%
Neither yes nor not	7.0%	10.2%	6.7%	6.1%	14.2%	16.1%	14.5%	28.4%
Probably yes	39.3%	39.1%	32.4%	32.8%	40.2%	38.0%	39.1%	29.4%
Definitely yes	46.8%	42.2%	53.0%	55.9%	37.2%	35.8%	33.3%	17.1%
Total NO	6.9%	8.5%	7.9%	5.2%	8.4%	10.1%	13.1%	25.1%
Total Yes	86.1%	81.3%	85.4%	88.7%	77.4%	73.8%	72.4%	46.5%

Figure 1. Structure of assessments of diagnostic items regarding megatrends. *—The names of the items are included in Table 1.

All, of the abovementioned negative megatrends were appreciated by the respondents (Figure 1). Water deficit (item 4; 88.7% of responses), hunger (item 3; 85.4%), and environmental pollution (item 1; 86.1%) were considered the most important on a global scale. It is worth emphasizing that all global problems were clearly noticed by the respondents, except for the issue of the overpopulation of the planet (item 8). In this case, the answers were more diverse than in the case of the other megatrends. These results indicate that the study

group was highly aware of water shortages on a global scale. However, we assessed the same phenomenon differently on a national scale. The problem of water deficit in Poland (item 9) was noticed by 47.7% of the respondents, most of whom assessed this fact with some uncertainty, while 29.8% of people adopted a neutral, undecided attitude.

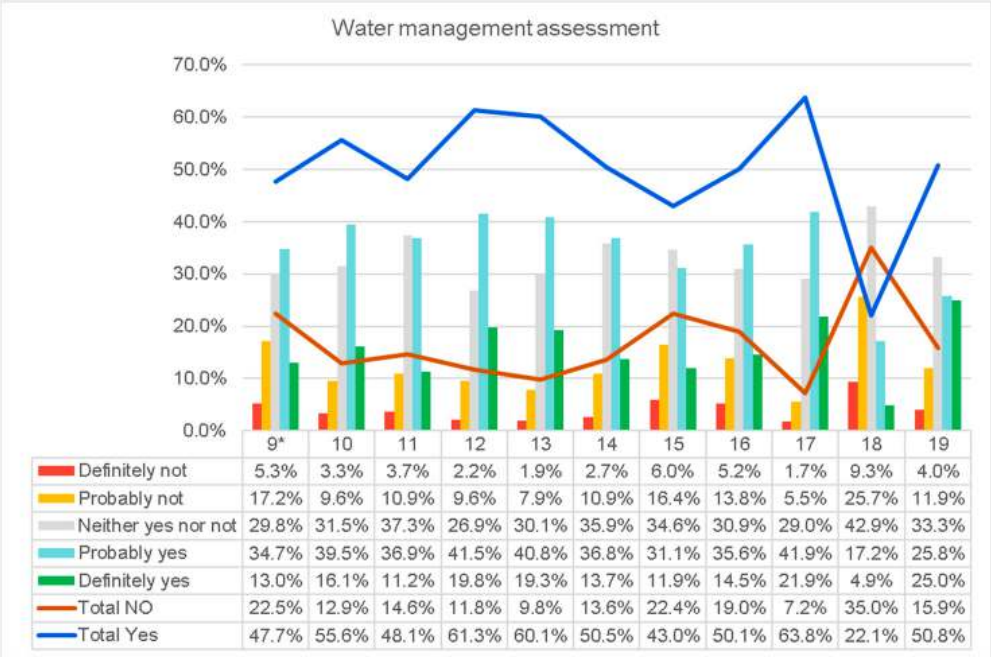

	9*	10	11	12	13	14	15	16	17	18	19
Definitely not	5.3%	3.3%	3.7%	2.2%	1.9%	2.7%	6.0%	5.2%	1.7%	9.3%	4.0%
Probably not	17.2%	9.6%	10.9%	9.6%	7.9%	10.9%	16.4%	13.8%	5.5%	25.7%	11.9%
Neither yes nor not	29.8%	31.5%	37.3%	26.9%	30.1%	35.9%	34.6%	30.9%	29.0%	42.9%	33.3%
Probably yes	34.7%	39.5%	36.9%	41.5%	40.8%	36.8%	31.1%	35.6%	41.9%	17.2%	25.8%
Definitely yes	13.0%	16.1%	11.2%	19.8%	19.3%	13.7%	11.9%	14.5%	21.9%	4.9%	25.0%
Total NO	22.5%	12.9%	14.6%	11.8%	9.8%	13.6%	22.4%	19.0%	7.2%	35.0%	15.9%
Total Yes	47.7%	55.6%	48.1%	61.3%	60.1%	50.5%	43.0%	50.1%	63.8%	22.1%	50.8%

Figure 2. Structure of ratings for items relating to water management in Poland. *—The names of the items are included in Table 1.

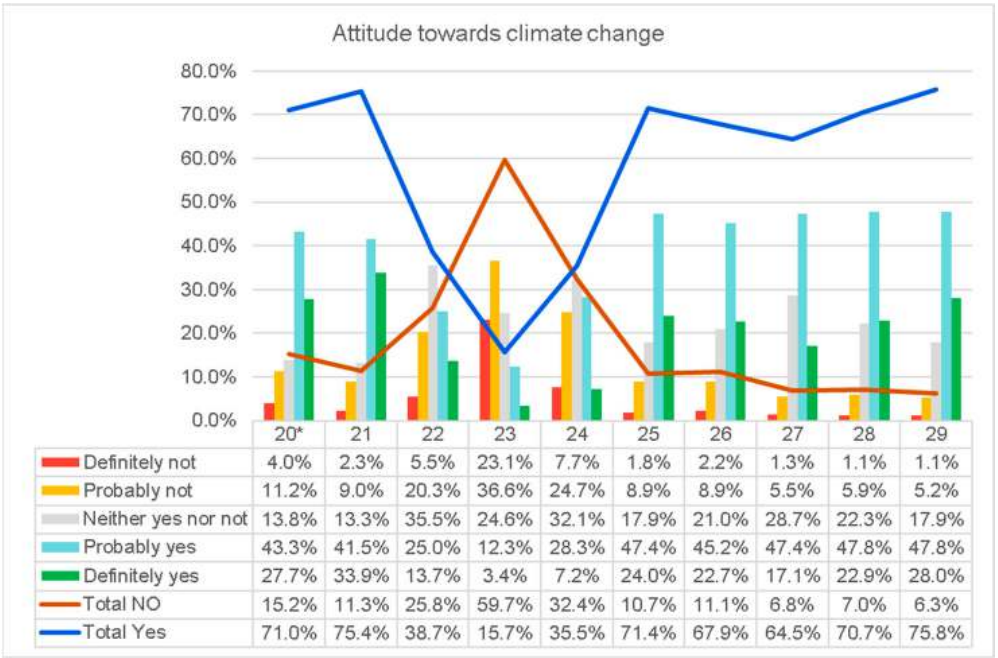

	20*	21	22	23	24	25	26	27	28	29
Definitely not	4.0%	2.3%	5.5%	23.1%	7.7%	1.8%	2.2%	1.3%	1.1%	1.1%
Probably not	11.2%	9.0%	20.3%	36.6%	24.7%	8.9%	8.9%	5.5%	5.9%	5.2%
Neither yes nor not	13.8%	13.3%	35.5%	24.6%	32.1%	17.9%	21.0%	28.7%	22.3%	17.9%
Probably yes	43.3%	41.5%	25.0%	12.3%	28.3%	47.4%	45.2%	47.4%	47.8%	47.8%
Definitely yes	27.7%	33.9%	13.7%	3.4%	7.2%	24.0%	22.7%	17.1%	22.9%	28.0%
Total NO	15.2%	11.3%	25.8%	59.7%	32.4%	10.7%	11.1%	6.8%	7.0%	6.3%
Total Yes	71.0%	75.4%	38.7%	15.7%	35.5%	71.4%	67.9%	64.5%	70.7%	75.8%

Figure 3. Structure of ratings for items relating to climate change. *—The names of the items are included in Table 1.

In the assessment of water management (Figure 2), the highest support was received for agricultural co-financing for the development of flood areas that favors retention (63.8% of support, item 17). This means that respondents expect state intervention in activities that

increase water retention. However, 35% of the respondents are against the liquidation of flood embankments in agricultural areas (item 18), which contradicts the implementation of the decision of including riverside areas used for agriculture into the organized small retention system. It is worth emphasizing that the respondents expect the construction of flood embankments to protect built up areas (60.1% of responses; item 15), which could indicate a lack of the respondents' sense of security. It should be emphasized that the respondents' belief in the effectiveness of flood embankments in ensuring safety contradicts the actions that increase water retention and slow down its outflow. On this basis, it can be concluded that the studied community still expects the implementation of a negatively verified strategy to withdraw people's access to water.

It is worth emphasizing that, in the assessment of item 15, relating to the free flow of flood waters in undeveloped riparian areas, 43% of respondents assessed such solutions positively, however over 1/3 of the respondents (34.6%) showed a neutral attitude. "Neither yes nor not". Such results indicate the need to conduct educational activities that increase the level of knowledge about the benefits resulting from the alluvial process in meadows and pastures, and from slowing down the outflow of water from river catchments. At the same time, an important aspect of shaping the development of river valleys, favoring water retention, are economic incentives encouraging farmers to change the form of land use.

More than half of the respondents (61.3%) also noted the lack of retention infrastructure in cities (item 12). This opens up another area of research related to green–blue urban infrastructure, which is important, not only for aesthetic reasons, but, above all, for limiting the formation of heat islands in cities.

In the part of the study regarding the perception of climate change, the vast majority of respondents (75.8%; item 29) expressed a belief in the anthropogenic causes of this phenomenon. At the same time, opinions were expressed about the direct impact of climate change on people's lives (75.4%; item 21), and it was indicated that climate change causes fear and anxiety (71.4% of affirmative answers; item 25).

Item 23, relating to the natural causes of climate change, was opposed by the respondents (59.7% of respondents). However, the vast majority of respondents were convinced that human activity changes the state of the climate system (70.7%; item 28), and that the increase in greenhouse gas emissions is closely related to the development of human civilization (75.8%; item 29). These data indicate the respondents' strong belief in the anthropogenic causes of climate change (Figure 3).

The respondents' belief regarding the causative role of humans in shaping natural phenomena may also concern flood safety. The trust of respondents in the technical flood protection measures discussed above makes it difficult to implement the strategy of leaving space for rivers. This is related to the development of the technical expansion of rivers, maintaining a false sense of security, and maintaining a vicious circle of flood protection.

A simple Pearson correlation analysis was performed in the collected research material. Its aim was to identify the relationships between the ratings of individual items. Tables 2–5 use a color scale to indicate the strength of correlation, according to the scale, presented by some authors [89]. Table 2 shows the correlation coefficients between item ratings regarding negative megatrends. A strong, positive correlation was found between respondents' perception of water deficit (item 4) and the perceptions of environmental pollution problems (item 1), poverty (item 2), hunger (item 3), and lifestyle diseases (item 5). A strong correlation was also found between the perception of climate change (item 12) and the depletion of non-renewable energy sources (item 13). The above correlation coefficients were positive, which proves the high level of ecological sensitivity of the respondents. This is also confirmed by the results presented in Figure 1.

Table 2. Correlation coefficients (r) between items, regarding threats resulting from civilization development *.

Rated Items	1 *	2	3	4	5	6	7
2	0.318 $p = 0.000$						
3	0.311 $p = 0.000$	0.731 $p = 0.000$					
4	0.461 $p = 0.000$	0.465 $p = 0.000$	0.559 $p = 0.000$				
5	0.306 $p = 0.000$	0.326 $p = 0.000$	0.312 $p = 0.000$	0.408 $p = 0.000$			
6	0.534 $p = 0.000$	0.148 $p = 0.000$	0.170 $p = 0.000$	0.358 $p = 0.000$	0.348 $p = 0.000$		
7	0.340 $p = 0.000$	0.249 $p = 0.000$	0.182 $p = 0.000$	0.348 $p = 0.000$	0.356 $p = 0.000$	0.504 $p = 0.000$	
8	0.211 $p = 0.000$	0.065 $p = 0.079$	0.074 $p = 0.046$	0.193 $p = 0.000$	0.132 $p = 0.000$	0.282 $p = 0.000$	0.335 $p = 0.000$

Explanation of the color scale

None	Negligible	Weak	Moderate	Strong	Very Strong	Perfect	Statistically significant coefficient
<0.1	0.1–0.2	0.2–0.3	0.3–0.4	0.4–0.7	0.7–0.9	0.9–1	$p \leq 0.05$

*—The names of the items are included in Table 1.

Table 3. Correlation coefficients (r) between issues related to the assessment of Poland's water management.

Rated Items	9	10	11	12	13	14	15	16	17	18
10	0.515 $p = 0.000$									
11	0.371 $p = 0.000$	0.443 $p = 0.000$								
12	0.357 $p = 0.000$	0.462 $p = 0.000$	0.361 $p = 0.000$							
13	0.189 $p = 0.000$	0.216 $p = 0.000$	0.317 $p = 0.000$	0.407 $p = 0.000$						
14	0.091 $p = 0.014$	0.201 $p = 0.000$	0.267 $p = 0.000$	0.261 $p = 0.000$	0.550 $p = 0.000$					
15	0.119 $p = 0.001$	0.128 $p = 0.001$	0.069 $p = 0.064$	0.154 $p = 0.000$	0.182 $p = 0.000$	0.073 $p = 0.050$				
16	0.064 $p = 0.084$	0.114 $p = 0.002$	0.328 $p = 0.000$	0.159 $p = 0.000$	0.258 $p = 0.000$	0.280 $p = 0.000$	−0.010 $p = 0.781$			
17	0.179 $p = 0.000$	0.267 $p = 0.000$	0.181 $p = 0.000$	0.258 $p = 0.000$	0.286 $p = 0.000$	0.305 $p = 0.000$	0.163 $p = 0.000$	0.269 $p = 0.000$		
18	0.084 $p = 0.024$	0.082 $p = 0.026$	0.046 $p = 0.212$	0.111 $p = 0.003$	−0.046 $p = 0.217$	−0.112 $p = 0.002$	0.183 $p = 0.000$	0.014 $p = 0.698$	0.015 $p = 0.694$	
19	0.164 $p = 0.000$	0.224 $p = 0.000$	0.122 $p = 0.001$	0.214 $p = 0.000$	0.210 $p = 0.000$	0.094 $p = 0.011$	0.138 $p = 0.000$	0.032 $p = 0.390$	0.194 $p = 0.000$	0.160 $p = 0.000$

Explanation of the color scale

None	Negligible	Weak	Moderate	Strong	Very Strong	Perfect	Statistically significant coefficient
<0.1	0.1–0.2	0.2–0.3	0.3–0.4	0.4–0.7	0.7–0.9	0.9–1	$p \leq 0.05$

*—The names of the items are included in Table 1.

Table 4. Correlation coefficients (r) between issues related to climate change.

Rated Items	20	21	22	23	24	25	26	27	28
21	0.6203								
	$p = 0.000$								
22	−0.2853	−0.1945							
	$p = 0.000$	$p = 0.000$							
23	−0.3693	−0.3300	0.3454						
	$p = 0.000$	$p = 0.000$	$p = 0.000$						
24	−0.0664	−0.0836	0.1697	0.3754					
	$p = 0.073$	$p = 0.024$	$p = 0.000$	$p = 0.000$					
25	0.4559	0.4543	−0.1800	−0.2442	0.0073				
	$p = 0.000$	$p = 0.000$	$p = 0.000$	$p = 0.000$	$p = 0.844$				
26	0.3291	0.2848	−0.0808	−0.0998	0.0952	0.3956			
	$p = 0.000$	$p = 0.000$	$p = 0.029$	$p = 0.007$	$p = 0.010$	$p = 0.000$			
27	0.1951	0.2709	0.0577	−0.0137	0.0594	0.2455	0.3468		
	$p = 0.000$	$p = 0.000$	$p = 0.119$	$p = 0.712$	$p = 0.109$	$p = 0.000$	$p = 0.000$		
28	0.3750	0.3577	−0.1296	−0.2407	−0.0532	0.3286	0.3423	0.3094	
	$p = 0.000$	$p = 0.000$	$p = 0.000$	$p = 0.000$	$p = 0.150$	$p = 0.000$	$p = 0.000$	$p = 0.000$	
29	0.2904	0.2804	−0.0036	−0.1820	0.0202	0.2441	0.3392	0.3628	0.5116
	$p = 0.000$	$p = 0.000$	$p = 0.921$	$p = 0.000$	$p = 0.585$	$p = 0.000$	$p = 0.000$	$p = 0.000$	$p = 0.000$

Explanation of the color scale

None	Negligible	Weak	Moderate	Strong	Very Strong	Perfect	Statistically significant coefficient
<0.1	0.1–0.2	0.2–0.3	0.3–0.4	0.4–0.7	0.7–0.9	0.9–1	$p \leq 0.05$

*—The names of the items are included in Table 1.

Table 5. Correlation coefficients (r) between the assessment of water management and the perception of the problem of climate change.

Rated Items	20	21	22	23	24	25	26	27	28	29
9	0.320	0.240	−0.104	−0.164	−0.067	0.185	0.151	0.120	0.183	0.157
	$p = 0.000$	$p = 0.000$	$p = 0.005$	$p = 0.000$	$p = 0.070$	$p = 0.000$	$p = 0.000$	$p = 0.001$	$p = 0.000$	$p = 0.000$
10	0.292	0.307	−0.077	−0.189	−0.059	0.200	0.132	0.115	0.243	0.178
	$p = 0.000$	$p = 0.000$	$p = 0.038$	$p = 0.000$	$p = 0.108$	$p = 0.000$	$p = 0.000$	$p = 0.002$	$p = 0.000$	$p = 0.000$
11	0.230	0.213	−0.074	−0.118	0.011	0.197	0.114	0.050	0.187	0.137
	$p = 0.000$	$p = 0.000$	$p = 0.044$	$p = 0.001$	$p = 0.775$	$p = 0.000$	$p = 0.002$	$p = 0.174$	$p = 0.000$	$p = 0.000$
12	0.255	0.269	−0.074	−0.124	−0.011	0.233	0.145	0.048	0.199	0.161
	$p = 0.000$	$p = 0.000$	$p = 0.047$	$p = 0.001$	$p = 0.762$	$p = 0.000$	$p = 0.000$	$p = 0.194$	$p = 0.000$	$p = 0.000$
13	0.200	0.236	0.052	−0.057	−0.013	0.190	0.163	0.143	0.172	0.128
	$p = 0.000$	$p = 0.000$	$p = 0.157$	$p = 0.123$	$p = 0.724$	$p = 0.000$	$p = 0.000$	$p = 0.000$	$p = 0.000$	$p = 0.001$
14	0.183	0.185	−0.022	−0.114	−0.040	0.230	0.131	0.086	0.191	0.117
	$p = 0.000$	$p = 0.000$	$p = 0.557$	$p = 0.002$	$p = 0.280$	$p = 0.000$	$p = 0.000$	$p = 0.020$	$p = 0.000$	$p = 0.001$
15	0.058	0.104	0.086	0.056	0.024	0.055	0.097	0.131	0.026	−0.005
	$p = 0.119$	$p = 0.005$	$p = 0.020$	$p = 0.129$	$p = 0.517$	$p = 0.134$	$p = 0.008$	$p = 0.000$	$p = 0.477$	$p = 0.901$
16	0.180	0.148	0.028	−0.085	−0.038	0.148	0.098	0.023	0.100	0.054
	$p = 0.000$	$p = 0.000$	$p = 0.445$	$p = 0.021$	$p = 0.306$	$p = 0.000$	$p = 0.008$	$p = 0.544$	$p = 0.007$	$p = 0.145$
17	0.170	0.226	−0.021	−0.075	0.017	0.206	0.149	0.183	0.165	0.228
	$p = 0.000$	$p = 0.000$	$p = 0.575$	$p = 0.041$	$p = 0.656$	$p = 0.000$	$p = 0.000$	$p = 0.000$	$p = 0.000$	$p = 0.000$
18	−0.002	0.012	0.069	0.097	0.133	−0.031	−0.047	−0.019	−0.073	0.010
	$p = 0.955$	$p = 0.755$	$p = 0.064$	$p = 0.009$	$p = 0.000$	$p = 0.400$	$p = 0.207$	$p = 0.611$	$p = 0.048$	$p = 0.779$
19	0.096	0.103	0.034	−0.082	−0.027	0.084	0.107	0.093	0.079	0.104
	$p = 0.009$	$p = 0.005$	$p = 0.359$	$p = 0.026$	$p = 0.465$	$p = 0.024$	$p = 0.004$	$p = 0.012$	$p = 0.033$	$p = 0.005$

Explanation of the color scale

None	Negligible	Weak	Moderate	Strong	Very Strong	Perfect	Statistically significant coefficient
<0.1	0.1–0.2	0.2–0.3	0.3–0.4	0.4–0.7	0.7–0.9	0.9–1	$p \leq 0.05$

*—The names of the items are included in Table 1.

Table 3 presents the results of a simple correlation, calculated between items, regarding water management in Poland. A strong positive correlation was found between the respondents' perception of the need to increase low retention (item 10), the awareness of water deficit (item 9), and the belief in the lack of reference infrastructure in cities (item 12). It is worth emphasizing that there was a strong correlation between the belief in the need to increase small retention (item 10) and the belief in the need to build large dam reservoirs (item 11). These results indicate a certain dissonance, because modern space development, which favors water retention, is moving away from the construction of large dam reservoirs to the development of all forms of small retention. The obtained results may indicate that the level of awareness of the surveyed society is too low. This observation is also confirmed by the results of a strong correlation between expectations regarding the construction of flood embankments to protect built up areas (item 13) and agricultural areas (item 14). This proves that respondents believe that flood embankments provide effective protection. In this context, however, it is worth emphasizing the existence of a medium-degree correlation between respondents' expectations regarding river regulation (item 16) and the belief in the need to build large dams (item 11).

It is worth emphasizing that no significant correlations were found between the assessment of the possibility of flood waters spreading freely in coastal areas (item 15) and other elements of the water management assessment. In the light of the results presented in Table 3 and Figure 2, it can be concluded that respondents expect the introduction of rational management in river valleys, but based on river regulation, the construction of flood embankments and large retention reservoirs.

Table 4 contains the results of a simple correlation analysis between the ratings of items regarding the issue of climate change. The data in the Table 4 show that respondents who considered climate change to be one of the most important threats to modern civilization (item 20) also admitted that these changes have a direct impact on people's lives (item 21) and are the reasons for anxiety and even fear (item 25). These people also believe that we are currently dealing with excessive consumption (item 26), and they see human activity as the cause of changes in the climate system (item 28). A significant number of respondents (see Chart 3) were convinced that human activities are causing climate change and that it is possible to stop this change. Some respondents (less than 16%; Figure 3), however, believe that climate change is a natural phenomenon and does not require human intervention.

It is worth emphasizing that there was a correlation between the assessments of the anthropogenic impact on climate change (item 28) and the recognition of these changes as the main problem concerning civilization (item 20). This was confirmed by the respondents' recognition of the direct impact of climate change on humans (item 21) and other items (25, 26, 27, and 29) regarding the threats resulting from these changes.

The analysis of correlations between items relating to the assessment of water management and the assessment of negative megatrends did not indicate any strong dependencies. A weak correlation was found between the assessment of water deficit on a global scale (item 4) and water deficit in Poland (item 9), r = 0.2042. A similar relationship was determined in relation to the perception of climate change (item 6) and the need to increase low retention (item 10), r = 0.2297. There was also a weak correlation between the items regarding the lack of infrastructure to retain water in the city (item 12) and environmental pollution (item 1), r = 0.02158, and the perception of climate change (item 6), r = 0.2007. All correlation coefficients listed here were statistically significant.

Table 5 shows the results of a simple correlation between the items on water management and the items on the perception of climate change. A weak and moderate correlation was found between the perception of climate change, as the main civilization problem (item 20) and the belief in the direct impact of climate change on people's lives (item 21), as well as between the awareness of water deficit (item 9), the need for development small retention (item 10), the belief in the need to build large dams (item 11), or awareness of the lack of water retention in cities (item 12).

This research showed that the majority of respondents believed in the anthropogenic causes of climate change pointing to the negative effects of human activity. However, with regard to water management, there is no such reflection. Simple correlation coefficients calculated between the assessment of the need to limit flood embankments (item 18), the assessment of the need to exclude flood areas from development (item 19) and issues related to climate change (items 20 to 29) indicated no or insignificant correlations. Therefore, it can be assumed that the respondents are not aware of the negative effects of improper land use in flood areas. However, in relation to climate, there is an awareness of human errors. Therefore, the conclusion is that intensive educational work is needed in the field of proper management in river valleys.

At the conceptualization stage, it was assumed that the respondents' sex and place of residence were determinants of the perception of the surveyed items. Place of residence was defined in two ways. First of all, the calculations were carried out in relation to cities and villages, and secondly in relation to the region from which the respondents came. Therefore, the null hypothesis (H0) of no relationship and the alternative hypothesis (H1) were formulated, according to which the variables are explained under the influence of determinants. In order to verify the H0 hypothesis, the chi-squared test of independence was calculated, and categorized charts were prepared. The results are presented in Table 6 and Figures 4–7.

Table 6. Results of the chi-squared test regarding the independence of the influence of respondents' sex and place of residence on the obtained results (N = 732).

Item **	Sex			Place of Residence Town/Village			Region of Residence		
	χ^2	df	p	χ^2	df	p	χ^2	df	p
Items related to megatrends									
1	38.899	df = 4	p = 0.00000 *	4.980	df = 4	p = 0.28938	0.6210	df = 4	p = 0.96070
2	36.267	df = 4	p = 0.00000 *	0.334	df = 4	p = 0.98754	3.749	df = 4	p = 0.44110
3	24.249	df = 4	p = 0.00007 *	7.154	df = 4	p = 0.12799	1.405	df = 4	p = 0.84339
4	30.439	df = 4	p = 0.00000 *	8.393	df = 4	p = 0.07819	3.093	df = 4	p = 0.54242
5	26.367	df = 4	p = 0.00003 *	3.042	df = 4	p = 0.55082	2.269	df = 4	p = 0.68638
6	16.409	df = 4	p = 0.00252 *	6.821	df = 4	p = 0.14564	11.344	df = 4	p = 0.02295 *
7	20.426	df = 4	p = 0.00041 *	2.992	df = 4	p = 0.55924	2.997	df = 4	p = 0.55840
8	1.082	df = 4	p = 0.89709	1.670	df = 4	p = 0.79619	1.630	df = 4	p = 0.80339
Items related to water management									
9	4.274	df = 4	p = 0.37013	2.275	df = 4	p = 0.68533	8.693	df = 4	p = 0.06926
10	4.654	df = 4	p = 0.32471	4.852	df = 4	p = 0.30278	1.568	df = 4	p = 0.81450
11	5.688	df = 4	p = 0.22366	3.624	df = 4	p = 0.45926	10.273	df = 4	p = 0.03607 *
12	4.401	df = 4	p = 0.35442	3.355	df = 4	p = 0.50032	4.507	df = 4	p = 0.34167
13	3.194	df = 4	p = 0.52593	0.399	df = 4	p = 0.98258	3.659	df = 4	p = 0.45414
14	13.642	df = 4	p = 0.00853 *	0.921	df = 4	p = 0.92159	12.876	df = 4	p = 0.01190 *
15	1.656	df = 4	p = 0.79863	4.846	df = 4	p = 0.30348	1.759	df = 4	p = 0.77990
16	1.577	df = 4	p = 0.81291	6.831	df = 4	p = 0.14511	10.387	df = 4	p = 0.03438 *
17	3.295	df = 4	p = 0.50977	4.289	df = 4	p = 0.36828	5.3485	df = 4	p = 0.25337
18	2.000	df = 4	p = 0.73567	18.304	df = 4	p = 0.00108 *	7.612	df = 4	p = 0.10686
19	4.157	df = 4	p = 0.38521	2.486	df = 4	p = 0.64710	0.7387	df = 4	p = 0.94647
Items related to climate change									
20	27.478	df = 4	p = 0.00002 *	2.147	df = 4	p = 0.70867	1.963	df = 4	p = 0.74261
21	18.000	df = 4	p = 0.00123 *	4.474	df = 4	p = 0.34562	8.654	df = 4	p = 0.07037
22	10.884	df = 4	p = 0.02790 *	2.511	df = 4	p = 0.64269	7.512	df = 4	p = 0.11118
23	24.071	df = 4	p = 0.00008 *	1.750	df = 4	p = 0.78170	0.934	df = 4	p = 0.91969
24	3.700	df = 4	p = 0.44808	0.598	df = 4	p = 0.96330	3.867	df = 4	p = 0.42425
25	22.517	df = 4	p = 0.00016 *	3.793	df = 4	p = 0.43479	1.976	df = 4	p = 0.74025
26	9.532	df = 4	p = 0.04909 *	3.438	df = 4	p = 0.48729	1.560	df = 4	p = 0.81606
27	3.852	df = 4	p = 0.42635	6.095	df = 4	p = 0.19218	8.336	df = 4	p = 0.08003
28	7.219	df = 4	p = 0.12478	6.056	df = 4	p = 0.19497	7.692	df = 4	p = 0.10354
29	13.480	df = 4	p = 0.00915 *	0.483	df = 4	p = 0.97511	3.727	df = 4	p = 0.44414

*—Statistically significant coefficient. **—The names of the items are included in Table 1.

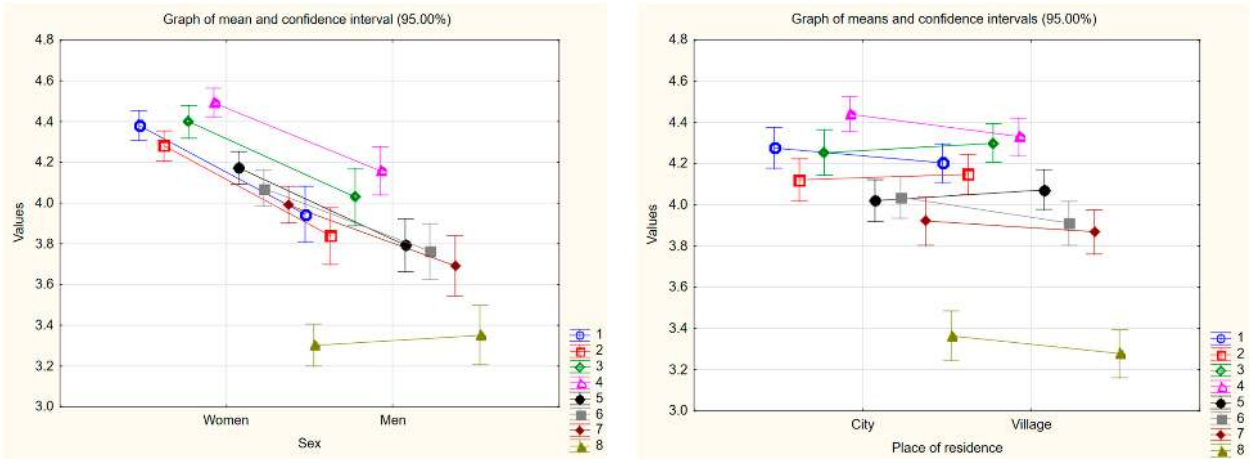

(**a**) (**b**)

Figure 4. Average ratings for megatrend items. Chart divided by (**a**) sex and (**b**) place of residence of respondents (urban–rural). The names of the items are listed in Table 1.

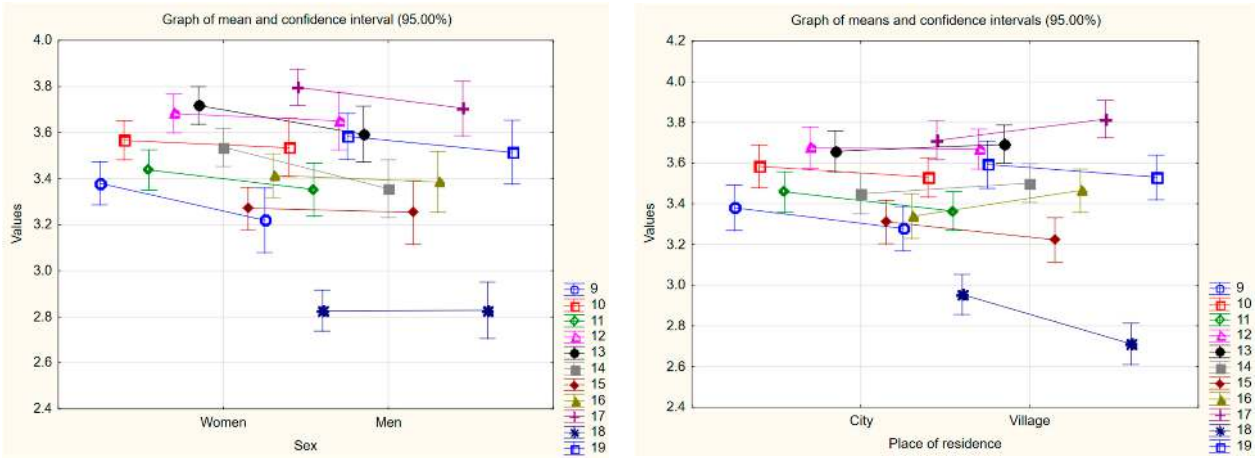

(**a**) (**b**)

Figure 5. Average ratings for water management items. Chart divided by (**a**) sex and (**b**) place of residence of respondents (urban–rural). The names of the items are listed in Table 1.

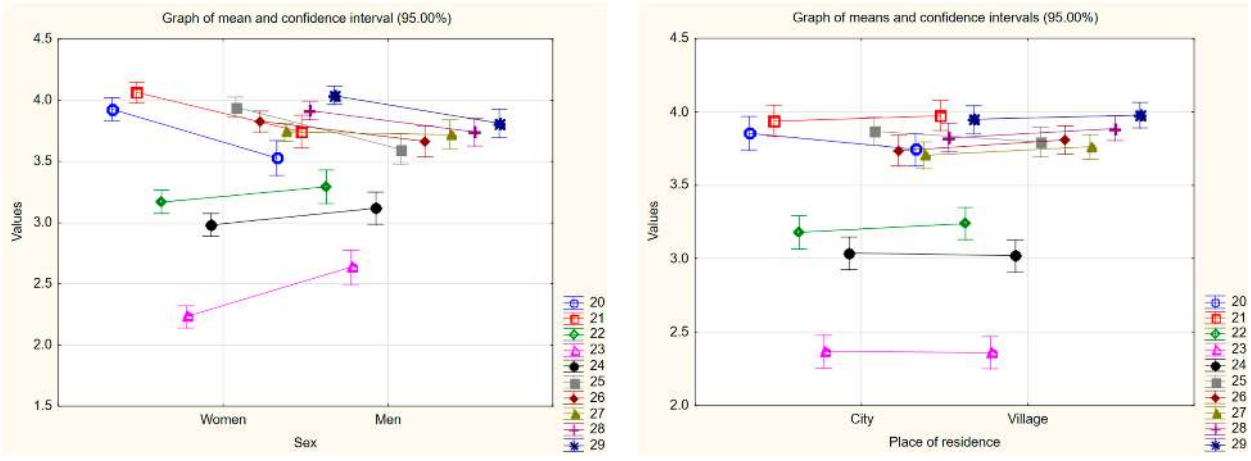

(**a**) (**b**)

Figure 6. Average ratings for climate change items. Chart divided by (**a**) sex and (**b**) place of residence of respondents (urban–rural). The names of the items are listed in Table 1.

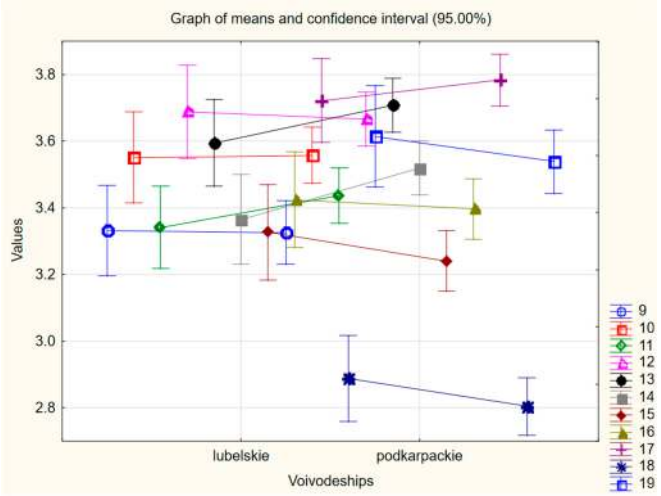

Figure 7. Average ratings for items regarding water management. Chart categorized by respondents' regions of residence (Lublin–Podkarpackie voivodeships). The names of the items are listed in Table 1.

The calculations show that the sex of the respondents differentiates the perception of negative megatrends (Table 6). Women had a higher level of sensitivity to negative phenomena on a global scale, which is confirmed by the data in Figure 4a. In the scale used, the value of 3.0 was a neutral position, so it is worth emphasizing that all average ratings indicate a confirmation of the existence of a given problem. The lowest averages related to the issue of planet overpopulation (item 8). In this case, no differences were found between the respondent's sex and opinions on this subject.

In the conducted research, the perception of negative megatrends was not determined by the respondents' place of residence. Although the average ratings differed slightly between rural and urban residents, these differences were not statistically significant (Table 6 and Figure 4b).

Among the items relating to water management, sex did not generally determine the perception of the examined issues. Only in relation to the construction of flood embankments to protect agricultural land (item 14) was there a difference between the assessments of women and men. In this case, women showed greater acceptance of such investments (Figure 5a). Therefore, when planning educational campaigns aimed at promoting a security strategy that involves leaving space for rivers, it should be considered that it should be addressed primarily to women.

The respondents' place of residence was not a factor differentiating the perception of water management in Poland (Table 6 and Figure 5b). Only in relation to the limitation of flood embankments in agricultural areas, statistically significant differences were found between urban and rural inhabitants. It should be emphasized that the average ratings for this item were lower than 3.0, which means that such activities are not accepted. In this case, rural residents expressed a more determined opposition to the liquidation of flood embankments in agricultural areas.

When looking for differences in the assessment of water management, depending on the region where the respondents lived, the chi-squared test in most cases confirmed the null hypothesis (H0) of no differences (Table 6). This means that the perception of most of the studied water management items was similar in both regions. Statistically significant differences were noted only for three items (Figure 7). The data presented in Figure 7 show that respondents living in the Podkarpackie voivodeship assessed the need to build large dam reservoirs on main rivers (item 11) and the need to embank the riverside areas used for agriculture more highly than respondents from the Lublin region. However, respondents living in the Lublin voivodeship assessed the need to regulate rivers more highly (item 16). It is worth emphasizing that the cases discussed concerned the implementation of an outdated strategy for ensuring water security. The differences indicated here concern

average ratings that were above the neutral value and, therefore, were positive assessments of ineffective actions.

In the group of items regarding climate change, most of the ratings varied, depending on the sex of the respondents (Table 6 and Figure 6a). Comparing the average ratings of the examined items categorized by sex, it can be concluded that women expressed greater concerns about climate change (items 20 and 21) and a greater belief that human actions will influence the observed changes (item 23). However, the respondents' place of residence did not determine their perception of the issue of climate change (Table 6 and Figure 6b). This may mean that the perception of global phenomena, such as climate change, was shaped by more than local factors. This can be treated as a guideline for creating educational campaigns regarding strategies to increase water retention. Popularization of this issue, and reliable and easily accessible knowledge on this subject, would create a positive social climate, conducive to activities that increase low water retention.

4. Discussion

4.1. Perception of Sustainable Management in River Valleys

The third decade of the 21st century is characterized by tensions and difficulties of a social, military, and natural nature. The observed climate changes are characterized by an increasingly frequent occurrence of extreme phenomena, such as floods, droughts, hurricane winds, and long periods of high temperatures [28,63,78,81]. Per capita water availability is decreasing around the world. This decline varies across regions of the world, with Europe having the lowest one [90]. Since this is a relative measure for demographic reasons in European countries, this coefficient is decreasing more slowly than, for example, in Africa. Therefore, an important issue is to determine social perceptions of issues related to water management.

Nearly a quarter of a century ago, in 2000, the World Commission on Dams Report was published, in which the authors point out the need to change the strategy for ensuring water safety [27]. This report drew attention to the growing flood losses resulting from increased technical development in flood areas. The negatively verified strategy of moving water away from people, consisting of building large dams, regulating rivers, and building flood embankments, must gradually be replaced by a strategy of increasing water retention, by leaving space for rivers [64]. The research was intended to identify society's awareness of water management.

The area of research conducted is specific for two reasons. Firstly, in Poland, during the period of communism and a centrally controlled economy, spatial development was carried out, aimed at limiting wetlands. Flood prevention activities primarily focused on accelerating water outflow [37,40]. Secondly, the south-eastern part of Poland is agricultural in nature, with a fragmented spatial structure of arable fields [76,91], which can be used to increase soil and landscape retention. Knowledge of the social perceptions of negative megatrends, climate change, and water management is a cognitive gap that this study aims to fill, at least partially.

Water security covers not only the availability of water, but also situations of its excess, i.e., floods [92]. Research by other authors [27,93,94] indicates that dams create a false sense of security among the local community. Therefore, it is important not only to learn about the social perception of water safety, but also to provide education addressed to both residents and decision makers. At the same time, the hydrological effects of large dams vary. It sometimes happens that negative consequences occur in the part of the river located below the dam [95]. It should also be emphasized that large dams have a negative impact on fishing and agriculture, and often have negative social effects [96]. Our research identified respondents' attitudes regarding their trust in dams as a means of ensuring safety.

It is worth emphasizing that, in the study area, there is a complex of large dams in the towns of Solina and Myczkowce. Therefore, some respondents live in areas that are protected against flooding by infrastructure measures. Research conducted in Switzerland [94] shows that the best security effects are achieved by combining infrastructure measures

with non-structural measures, such as spatial planning and river restoration, focused on natural security mechanisms. The authors of these studies emphasize the role of the social perception of flood risk in shaping an appropriate safety policy. The analysis of our research shows that respondents underestimate non-structural measures.

In the research conducted in neighboring countries (Germany, the Czech Republic, and Slovakia) [97], the authors pointed out the important role of natural landscapes in shaping water retention. Natural remedies have been shown to retain water in the soil, increasing crop productivity and helping to cool the landscape. However, in our research, landscape retention measures were not appreciated by the respondents. The research shows that the construction of large retention reservoirs was expected.

The perception of many phenomena, e.g., climate change, depends, on the place of residence and profession [98]. Farmers who, while performing their work, are in close contact with nature on a daily basis, have a good understanding of the human–environment relationship [99].

4.2. Factors Differentiating the Perception of Sustainable Management in River Valleys

Adaptation activities that improve water security, especially in the context of climate change, include traditional activities. They involve proper agricultural management and space management in a way that increases water retention. Even though these activities are traditional methods, they are treated as innovative [8].

The research area of south-eastern Poland included two voivodeships that share many similarities [76,81]. However, there are differences in terms of hydrology and flood risk. The Podkarpackie voivodeship is at greater risk of flooding than the Lublin voivodeship [82]. Therefore, one might expect differences in the approach to water management, depending on the region of residence of the respondents. A statistical confirmation of these differences was noted in this research, only in relation to methods of ensuring flood safety. The surveyed inhabitants of the Podkarpackie voivodeship expected the construction of large retention reservoirs and embankments of agricultural land in flood areas to a greater extent than the inhabitants of the Lublin voivodeship. The inhabitants of the Lublin voivodeship expected river regulation, to a greater extent.

Differences in the perception of water management, depending on the place of residence, have not been confirmed. Residents of both rural and urban areas perceived the studied items in a similar way. However, differences were found in the perceptions of negative megatrends and climate change, depending on the sex of the respondents. In this case, women showed a level of concern about global problems and the state of the Earth's climate. The obtained results confirm the research of other authors [100,101]. However, in relation to the perception of water management, the sex of the respondents did not play a significant role.

In the light of these results, it can be concluded that the message regarding climate change effectively shapes the public's perception of this phenomenon. However, with regard to effective methods of ensuring flood safety and mitigating the effects of drought, a gap in the public's awareness was identified. Therefore, knowledge should be disseminated regarding the possibility of increasing retention through the proper management of river valleys. This is a task for government and local government authorities, as well as scientific associations and communities of practice [42].

Economic mechanisms used by state authorities could contribute to increasing retention in rivers, thanks to permanent grasslands cultivated in riparian areas. Recognizing meadows and pastures in riparian areas, increasing water retention as public goods co-financed from the state budget, could encourage farmers to change the way, they use riverside areas [39]. For this to happen, first of all, it is necessary to change the perception of water management and popularize the strategy of ensuring flood safety, which involves leaving space for rivers.

5. Summary and Conclusions

In terms of the first two research questions regarding water deficit and the need to increase water retention based on the conducted research, it can be concluded that the respondents are well informed about global, negative megatrends. These phenomena also include water deficit. The people surveyed were aware of the growing water deficit, both on a global and national scale. Women have shown greater sensitivity to global issues. Similar conclusions can be drawn regarding the perception of climate change. The surveyed people were convinced that climate change is one of the most important problems of the modern world. At the same time, they had a strong belief in the anthropogenic causes of these changes and the possibility of limiting them. Items containing information about the natural causes of climate change, and the impossibility of stopping it, were met with fierce opposition. This means that activities shaping the perception of climate issues and social sensitivity to major, negative, global megatrends have effectively shaped the perception of these topics.

The respondents' perception of water management varied, but most of them were views and expectations that were part of the strategy of moving water away from people. The respondents noticed the water deficit in Poland and were aware of the lack of water retention infrastructure in cities. However, they associated the issue of water retention mainly with the construction of large retention reservoirs. The respondents widely expected the construction of flood embankments. Measures to slow down water runoff by allowing rivers to flow freely have met with a lack of acceptance. Yes, the respondents expected financial support from the state authorities, but the allocation of riparian areas to meadows and pastures was not understood by them. These type of meadows can constitute an element of water retention, only if they are not embanked and the river can flow freely. Meanwhile, the respondents proposed the construction of flood embankments along agricultural areas.

Based on the collected data, the following conclusions were formulated:

1. The surveyed community noticed the problem of growing water deficit.
2. The study group was aware of the need to increase water retention, but the knowledge regarding the methods of implementing this task was outdated and limited.
3. Respondents expected government support in activities increasing water retention, but they also expected activities to accelerate the rate of water outflow.
4. A cognitive gap was identified in the study group regarding the benefits of the free flow of flood waters in riparian areas.
5. An extensive information campaign is necessary, increasing the public's awareness of the need to develop small retention and eco-innovative developments of river valleys.
6. The research showed that the place of residence (urban–rural) and the regions (Podkarpackie–Lublin voivodeship) do not differentiate the perception of most of the examined items. However, sex primarily affected the perception of global megatrends and the perception of climate change.

6. Contributions and Limitations

The contribution of this study to the development of science is to fill the gap in identifying the perception of proper water management by the inhabitants of one of the poorest regions in Poland. The contribution of the research to the development of science is also the identification of the lack of awareness of respondents regarding new sustainable management methods in river valleys. The research results can be a source of information for decision makers, as they can be used to shape public perception of the challenges related to spatial management, which promotes increased water retention, and social education to reduce the negative effects of floods and droughts. Greater attention should also be paid to education related to the ecological and buffer roles of flood meadows.

The limitations of this study are that all the variables were measured simultaneously, so the study is cross-sectional, and greater attention may be needed concerning other causes of the phenomena under study. Further research in this direction would provide a clearer

picture. Moreover, the exploratory nature of the study provides important insights, but these should be interpreted as general results.

We propose repeating this study several times in the future. This would provide an image of changes, over time, in the perception of sustainable management in river valleys. To continue this work, we suggest that future studies be carried out in a larger area covering the entire country and take into account the nature of river valleys. We also propose probabilistic sampling, which will better reflect the demographics of the study area.

Author Contributions: Conceptualization: K.K., A.B. and M.W.; methodology: K.K. and A.B.; software: K.K. and A.B; validation: K.K., A.B. and M.W.; formal analysis: K.K. and A.B.; compiled by A.B. and K.K.; resources: A.B., K.K. and M.W.; data processing: K.K. and A.B.; writing—original project preparation: K.K., A.B. and M.W.; writing—review and editing: A.B. and K.K.; visualization: K.K. and A.B. All authors have read and agreed to the published version of the manuscript.

Funding: Rzeszow University of Technology, Poland, and University of Life Sciences in Lublin, Poland.

Institutional Review Board Statement: Not applicable.

Informed Consent Statement: Not applicable.

Data Availability Statement: The research results were obtained from questionnaires constructed by the authors of this publication.

Conflicts of Interest: The authors declare no conflicts of interest.

References

1. What Is Water Security? Available online: https://www.globalwaters.org/resources/blogs/swp/what-water-security (accessed on 4 April 2024).
2. Marcal, J.; Antizar-Ladislao, B.; Hofman, J. Addressing Water Security: An Overview. *Sustainability* **2021**, *13*, 13702. [CrossRef]
3. Li, B.; Zhang, W.; Long, J.; Chen, M.; Nie, J.; Liu, P. Regional water resources security assessment and optimization path analysis in karst areas based on emergy ecological footprint. *Appl. Water Sci.* **2023**, *13*, 142. [CrossRef]
4. Noty Tematyczne o Unii Europejskiej. Parlament Europejski. Ochrona wód I Gospodarka Wodna. Available online: https://www.europarl.europa.eu/factsheets/pl/sheet/74/protection-et-gestion-des-eaux (accessed on 4 April 2024).
5. Komunikat Komisji do Parlamentu Europejskiego, Rady, Europejskiego Komitetu Ekonomiczno-Społecznego i Komitetu Regionów Plan Ochrony Zasobów Wodnych Europ/* COM/2012/0673 Final */Document 52012DC0673. Available online: https://eur-lex.europa.eu/legal-content/PL/TXT/?uri=CELEX:52012DC0673 (accessed on 4 April 2024).
6. Godyn, I. Ocena efektywności ekonomicznej inwestycji przeciwpowodziowych December 2015. *Gospod. Prakt. Teor.* **2015**, *38*, 5–22. [CrossRef]
7. Dyrektywa Powodziowa—Nastąpiły Postępy w Ocenie Ryzyka, Jednak Wymagana Jest Poprawa Planowania i Wdrażania. Available online: https://op.europa.eu/webpub/eca/special-reports/floods-directive-25-2018/pl/ (accessed on 4 April 2024).
8. AL-Falahi, A.H.; Barry, S.; Gebrechorkos, S.H.; Spank, U.; Bernhofer, C. Potential of Traditional Adaptation Measures in Mitigating the Impact of Climate Change. *Sustainability* **2023**, *15*, 15442. [CrossRef]
9. IPCC. *2021: Climate Change 2021: The Physical Science Basis*; Contribution of Working Group I to the Sixth Assessment Report of the Intergovernmental Panel on Climate Change; Masson-Delmotte, V., Zhai, P., Pirani, A., Connors, S.L., Péan, C., Berger, S., Caud, N., Chen, Y., Goldfarb, L., Gomis, M.I., et al., Eds.; Cambridge University Press: Cambridge, UK; New York, NY, USA, 2021; p. 2391. [CrossRef]
10. Abeysingha, N.S.; Singh, M.; Islam, A.; Sehgal, V.K. Climate change impacts on irrigated rice and wheat production in Gomti River basin of India: A case study. *Springerplus* **2016**, *5*, 1250. [CrossRef]
11. Bhattarai, D.P.; Shakya, N.M. Conjunctive use of water resources in sustainable development of agriculture in Terai Nepal. *J. Inst. Eng.* **2019**, *15*, 210–217. [CrossRef]
12. Chen, T.C.; Hsieh, T.S.; Shichiyakh, R.A. Sustainable operation of surface-groundwater conjunctive use systems in the agricultural sector. *J. Water Land Dev.* **2021**, *51*, 25–29. [CrossRef]
13. Bhattacharyya, A.; Rahman, M.L. Mandatory CSR Expenditure and Firm Performance. *J. Contemp. Account. Econ.* **2019**, *15*, 100163. [CrossRef]
14. Flores, L.; Bailey, R.T.; Kraeger-Rovey, C. Analyzing the effects of groundwater pumping on an urban stream-aquifer system. *J. Am. Water Resour. Assoc.* **2020**, *56*, 310–322. [CrossRef]
15. Milly, P.; Dunne, K.; Vecchia, A. Global pattern of trends in streamflow and water availability in a changing climate. *Nature* **2005**, *438*, 347–350. [CrossRef]
16. Sabale, R.; Venkatesh, B.; Jose, M. Sustainable water resource management through conjunctive use of groundwater and surface water: A review. *Innov. Infrastruct. Solut.* **2023**, *8*, 17. [CrossRef]

17. Aladejana, J.A.; Kalin, R.M.; Sentenac, P.; Hassan, I. Assessing the impact of climate change on groundwater quality of the shallow coastal aquifer of eastern dahomey basin, Southwestern Nigeria. *Water* **2020**, *12*, 224. [CrossRef]
18. Kud, K. Biomass of riparian meadows as an integrator of energy policy, spatial and water. *Stud. I Mater.* **2018**, *28*, 80–89. [CrossRef]
19. Kahil, M.T.; Dinar, A.; Albiac, J. Modeling water scarcity and droughts for policy adaptation to climate change in arid and semiarid regions. *J. Hydrol.* **2015**, *522*, 95–109. [CrossRef]
20. Pissarra, T.C.T.; Fernandes, L.F.S.; Pacheco, F.A.L. Production of clean water in agriculture headwater catchments: A model based on the payment for environmental services. *Sci. Total Environ.* **2021**, *785*, 147331. [CrossRef] [PubMed]
21. Shijian, J.; Jing, T.; Kwabi, D.G.; Ji, Y.; Tong, L.; De Porcellinis, D.; Goulet, M.-A.; Pollack, D.A.; Gordon, R.G.; Aziz, M.J. A Water-Miscible Quinone Flow Battery with High Volumetric Capacity and Energy Density. *ACS Energy Lett.* **2019**, *4*, 1342–1348. Available online: https://nrs.harvard.edu/URN-3:HUL.INSTREPOS:37366505 (accessed on 24 May 2024).
22. Savenije, H.H.G. Why Water Is Not an Ordinary Economic Good, or Why the Girl Is Special. *Phys. Chem. Earth* **2002**, *27*, 741–744. [CrossRef]
23. Bai, Y.; Ochuodho, T.O.; Yang, J. Impact of land use and climate change on water-related ecosystem services in Kentucky. *Ecol. Indic.* **2019**, *102*, 51–64. [CrossRef]
24. Yuan, X.; Jiao, Y.; Yang, D.; Lei, H. Reconciling the attribution of changes in streamflow extremes from a hydroclimate perspective. *Water Resour. Res.* **2018**, *54*, 3886–3895. [CrossRef]
25. Baldassarre, D.; Wanders, G.N.; AghaKouchak, A.; Kuil, L.; Rangecroft, S.; Veldkamp, T.I.E.; Garcia, M.; van Oel, P.R.; Breinl, K.; Van Loon, A.F. Water shortages worsened by reservoir effects. *Nat. Sustain.* **2018**, *1*, 617–622. [CrossRef]
26. Dlaczego Zbiorniki Zaporowe nie są Dobrym Narzędziem w Walce z Suszą? Available online: https://straznicy.wwf.pl/wp-content/uploads/2020/07/dlaczego-zbiorniki-zaporowe-nie-s%C4%85-dobrym-narz%C4%99dziem-w-walce-z-susz%C4%85.pdf (accessed on 23 March 2024).
27. The Report of the World Commission on Dams. *Dams and Development: A New Framework for Decision-Making*; London VAEARTHSCAN Earthscan Publications Ltd.: London, UK, 2000. [CrossRef]
28. Tabari, H. Climate Change Impact on Flood and Extreme Precipitation Increases with Water Availability. *Sci. Rep.* **2020**, *10*, 13768. [CrossRef] [PubMed]
29. Bochenek, W.; Wiejaczka, Ł. Current and future variability of water supply to a mountain reservoir (Polish Carpathians). *Stoch. Environ. Res. Risk Assess* **2023**, *37*, 5051–5069. [CrossRef]
30. Ward, P.J.; de Ruiter, M.C.; Mård, J.; Schröter, K.; Van Loon, A.; Veldkamp, T.; von Uexkull, N.; Wanders, N.; AghaKouchak, A.; Arnbjerg-Nielsen, K. The need to integrate flood and drought disaster risk reduction strategies. *Water Secur.* **2020**, *11*, 100070. [CrossRef]
31. McGrane, S.J. Impacts of urbanisation on hydrological and water quality dynamics, and urban water management: A review. *Hydrol. Sci. J.* **2016**, *61*, 2295–2311. [CrossRef]
32. Ellis, N.; Anderson, K.; Brazier, R. Mainstreaming natural flood management: A proposed research framework derived from a critical evaluation of current knowledge. *Prog. Phys. Geogr. Earth Environ.* **2021**, *45*, 819–841. [CrossRef]
33. Informacyjny Serwis Mokradłowy. Available online: https://www.bagna.pl/zglebiaj-wiedze/ochrona-mokradel/mom/122-obom (accessed on 4 April 2024).
34. Secretariat of the Convention on Biological Diversity. *Voluntary Guidelines for the Design and Effective Implementation of Ecosystem-Based Approaches to Climate Change Adaptation and Disaster Risk Reduction and Supplementary Information*; Technical Series No. 93; Secretariat of the Convention on Biological Diversity: Montreal, QC, Canada, 2019; pp. 1–156. Available online: https://www.cbd.int/doc/publications/cbd-ts-93-en.pdf (accessed on 24 May 2024).
35. Aerenson, T.; Tebaldi, C.; Sanderson, B.; Lamarque, J. Changes in a suite of indicators of extreme temperature and precipitation under 1.5 and 2.0 degrees warming. *Environtal Res. Lett.* **2018**, *13*, 035009. [CrossRef]
36. Kundzewicz, Z.W.; Pinskwar, I. Are Pluvial and Fluvial Floods on the Rise? *Water* **2022**, *14*, 2612. [CrossRef]
37. Piniewski, M.; Marcinkowski, P.; Kundzewicz, Z.W. Trend detection in river flow indices in Poland. *Acta Geophys.* **2018**, *66*, 347–360. [CrossRef]
38. Konieczny, R.; Pińskwar, I.; Kundzewicz, Z.W. The September 2017 flood in Elbląg (Poland) in perspective. *Meteorol. Hydrol. Water Manag.* **2018**, *6*, 67–78. [CrossRef]
39. Abdallah, A.M.; Jat, H.S.; Choudhary, M.; Abdelaty, E.F.; Sharma, P.C.; Jat, M.L. Conservation Agriculture Effects on Soil Water Holding Capacity and Water-Saving Varied with Management Practices and Agroecological Conditions: A Review. *J. Agron.* **2021**, *11*, 1681. [CrossRef]
40. Zalewski, M.; Kiedrzyńska, E.; Mankiewicz-Boczek, J.; Izydorczyk, K.; Jurczak, T.; Jarosiewicz, P. Zatrzymać wodę, opóźnić odpływ. *Academia* **2020**, *2*, 58–61. Available online: https://journals.pan.pl/Content/117643?format_id=1 (accessed on 14 January 2024).
41. Mizia, M. Przyszłość w nowoczesnym projektowaniu miast (The future in modern city design). *PUA Przestrz. Urban. Archit.* **2020**, *1*, 39–54. [CrossRef]
42. Kundzewicz, Z.W.; Januchta-Szostak, A.; Nachlik, E.; Pińskwar, I.; Zaleski, J. Challenges for Flood Risk Reduction in Poland's Changing Climate. *Water* **2023**, *15*, 2912. [CrossRef]
43. Hjorth, P.; Madani, K.; Adaptive, K. Water Management: On the Need for Using the Post-WWII Science in Water Governance. *Water Resour. Manag.* **2023**, *37*, 2247–2270. [CrossRef]

44. Ziernicka-Wojtaszek, A.; Kopcińska, J. Variation in atmospheric precipitation in Poland in the years 2001–2018. *Atmosphere* **2020**, *11*, 794. [CrossRef]
45. Rosiek, K. Analysis of operator models for rainwater management in Poland—Towards the integrated management model. *Econ. Environ.* **2023**, *85*, 110–139. [CrossRef]
46. Dz. U. 2023 poz. 1478. Obwieszczenie Marszałka Sejmu Rzeczypospolitej Polskiej z Dnia 16 Czerwca 2023 r. w Sprawie Ogłoszenia Jednolitego Tekstu Ustawy—Prawo Wodne. Available online: https://isap.sejm.gov.pl/isap.Nsf/download.xsp/WDU20230001478/T/D20231478L.pdf (accessed on 22 April 2024).
47. DYREKTYWA 2007/60/WE Parlamentu Europejskiego i Rady z dnia 23 października 2007 r. w Sprawie Oceny Ryzyka Powodziowego i Zarządzania nim. Available online: https://sip.lex.pl/akty-prawne/dzienniki-UE/dyrektywa-2007-60-we-w-sprawie-oceny-ryzyka-powodziowego-i-zarzadzania-nim-67719456 (accessed on 22 April 2024).
48. Guthrie, L.; Furlong, C.; De Silva, S. Capturing different perspectives on integrated urban water management issues. *Water Policy* **2020**, *22*, 252–275. [CrossRef]
49. Vinagre, V.; Fidélis, T.; How, L.A. Can We Adapt Together? Bridging Water Management and City Planning Approaches to Climate Change. *Water* **2023**, *15*, 715. [CrossRef]
50. He, C.; Liu, Z.; Wu, J.; Pan, X.; Fang, Z.; Li, J.; Bryan, B.A. Future global urban water scarcity and potential solutions. *Nat. Commun.* **2021**, *12*, 4667. [CrossRef] [PubMed]
51. de Groot, B.; Leendertse, W.; Arts, J. Co-Evolution of Organizations in Infrastructure Planning: The Role of Communities of Practice as Windows for Collective Learning Across Project-Oriented Organizations. *Adm. Soc.* **2022**, *54*, 1328–1356. [CrossRef]
52. Haase, D. Reflections about blue ecosystem services in cities. *Sustain. Water Qual. Ecol.* **2015**, *5*, 77–83. [CrossRef]
53. Krauze, K.; Wagner, I. From classical water-ecosystem theories to nature-based solutions—Contextualizing nature-based solutions for sustainable city. *Sci. Total Environ.* **2019**, *655*, 697–706. [CrossRef] [PubMed]
54. Jose, A.; de Oliveira, P.; Bellezoni, R.A.; Shih, W.; Bayulken, B. Innovations in Urban Green and Blue Infrastructure: Tackling local and global challenges in cities. *J. Clean. Prod.* **2022**, *362*, 132355. [CrossRef]
55. Szpikowski, J.; Szpikowska, G.; Domańska, M. Old melioration systems: The influence onto functioning of geoecosystems of river valleys in the Parsęta basin (NW Poland). *Quaest. Geogr.* **2015**, *34*, 129–140. [CrossRef]
56. Boulton, A.M.; Davies, K.F.; Ward, P.S. Species richness, abundance, and composition of ground-dwelling ants in northern California grasslands: Role of plants, soil, and grazing. *Environ. Entomol.* **2005**, *34*, 96–104. [CrossRef]
57. Murray, B.R.; Zeppel, M.; Hose, G.C.; Eamus, D. Groundwater dependent ecosystems in Australia: It's more than just water for rivers. *Ecol. Manag. Restor.* **2023**, *4*, 110–113. [CrossRef]
58. Kirwan, L.; Luescher, A.; Sebastia, M.T.; Finn, J.A.; Collins, R.P.; Porqueddu, C.; Helgadottir, A.; Baadshaug, O.H.; Brophy, C.; Coran, C.; et al. Evenness drives consistent diversity effects in intensive grassland systems across 28 European sites. *J. Ecol.* **2007**, *95*, 530–539. [CrossRef]
59. Borek, Ł.; Drymajło, K. The role and importance of irrigation system for increasing the water resources: The case of the Nida river valley. *Acta Sci. Pol. Form. Circumiectus* **2019**, *18*, 19–30. [CrossRef]
60. Guo, Q.F.; Shaffer, T.; Buhl, T. Community maturity. species saturation and the variant diversityproductivity relationships ingrasslands. *Ecol. Lett.* **2006**, *9*, 1284–1292. [CrossRef]
61. Grace, J.B.; Anderson, T.M.; Smith, M.D.; Seabloom, E.; Andelman, S.J.; Meche, G.; Weiher, E.; Allain, L.K.; Jutila, H.; Sankaran, M.; et al. Does species diversity limit productivity in natural grassland communities? *Ecol. Lett.* **2007**, *10*, 680–689. [CrossRef]
62. De Boeck, H.J.; Lemmens, C.M.H.M.; Zavalloni, C.; Gielen, B.; Malchair, S.; Carnol, M.; Merckx, R.; Van den Berge, J.; Ceulemans, R.; Nijs, I. Biomass production in experimental grasslands of different species richness during three years of climate warming. *Biogeosciences* **2008**, *5*, 585–594. [CrossRef]
63. Grygoruk, M.; Mirosław-Świątek, D.; Chrzanowska, W.; Ignar, S. How Much for Water? Economic Assessment and Mapping of Floodplain Water Storage as a Catchment-Scale Ecosystem Service of Wetlands. *Water* **2013**, *5*, 1760–1779. [CrossRef]
64. Müller, I.B. *The Influence of Traditional Flood Irrigation on Biodiversity—Plant Functional Composition and Plant Nutrient Availability in Central European Grassland*; Universität Koblenz-Landau: Koblenz, Germany; Landau, Germany, 2017; Available online: https://d-nb.info/1138981672/34 (accessed on 15 February 2024).
65. Phillips-Mao, L.; Refsland, J.M.; Galatowitsch, S.M. Cost-Estimation for Landscape-Scale Restoration Planning in the Upper Midwest, U.S. *Ecol. Restor.* **2015**, *33*, 135–146. [CrossRef]
66. Napierała, M.; Sojka, M.; Jaskuła, J. Impact of Water Meadow Restoration on Forage Hay Production in Different Hydro-Meteorological Conditions: A Case Study of Racot, Central Poland. *Sustainability* **2023**, *15*, 2959. [CrossRef]
67. Monitor Polski, Dziennik Urzędowy Rzeczypospolitej Polskiej, Warszawa, dnia 4 Października 2019 r., Poz. 941, UCHWAŁA NR 92 RADY MINISTRÓW z dnia 10 Września 2019 r. w Sprawie przyjęcia "Założeń do Programu Przeciwdziałania Niedoborowi Wody na lata 2021–2027 z perspektywą do roku 2030". Available online: https://isap.sejm.gov.pl/isap.nsf/download.xsp/WMP20190000941/O/M20190941.pdf (accessed on 17 February 2024).
68. Gryz, J.; Gromadzki, S. *Przeciwdziałanie Suszy. Retencja Wody w Systemie Zarządzania Kryzysowego Polski*; Warszawa Wydawnictwo PWN: Warszawa, Poland, 2021; ISBN 9788301216153.
69. Krnáčová, Z.; Kenderessy, P.; Hreško, J.; Kubínsky, D.; Dobrovodská, M. Assessment of Landscape Retention Water Capacity and Hydrological Balance in Traditional Agricultural Landscape (Model Area Liptovská Teplička Settlements, Slovakia). *Water* **2020**, *12*, 3591. [CrossRef]

70. Stecher, G.; Hohensinner, S.; Herrnegger, M. Changes in the water retention of mountainous landscapes since the 1820s in the Austrian Alps. *Front. Environ. Scente* **2023**, *11*, 1219030. [CrossRef]
71. Johnson, M.F.; Thorne, C.R.; Castro, J.M.G.; Kondolf, N.; Mazzacano, C.S.; Rood, S.B.; Westbrook, C. Biomic river restoration: A new focus for river management. *River Res. Applic.* **2020**, *36*, 3–12. [CrossRef]
72. Plit, J. Zarządzanie krajobrazem dolin rzecznych. *Zarządzanie Kraj. Kult. Pr. Kom. Kraj. Kult.* **2008**, *10*, 230–240. Available online: https://krajobrazkulturowy.us.edu.pl/publikacje.artykuly/zarzadzanie/plit.pdf (accessed on 15 February 2024).
73. Uchwała nr 152 Rady Ministrów z dnia 22 Sierpnia 2023 r w Sprawie Przyjęcia "Programu Przeciwdziałania Niedoborowi Wody na lata 2023–2027 z Perspektywą do Roku 2030". Available online: https://monitorpolski.gov.pl/M2023000111901.pdf (accessed on 14 February 2024).
74. Łapuszek, M. *Podstawy Rewitalizacji Dolin Rzecznych*; Politechnika Krakowska: Kraków, Poland, 2023; Available online: https://repozytorium.biblos.pk.edu.pl/redo/resources/46548/file/resourceFiles/LapuszekM_PodstawyRewitalizacji.pdf (accessed on 15 February 2024).
75. Wykaz Jednostek NUTS 2021 w Polsce (as at 1 January 2021). Available online: https://stat.gov.pl/statystyka-regionalna/jednostki-terytorialne/klasyfikacja-nuts/klasyfikacja-nuts-w-polsce/ (accessed on 5 March 2023).
76. Databases Statistics Poland (GUS). GUS Warszawa, 2021. Available online: https://stat.gov.pl/banki-i-bazy-danych/ (accessed on 17 January 2024).
77. Tomczyk, A.M.; Bednorz, E. (Eds.) *Atlas Klimatu Polski (1991–2020)*; Bogucki Wydawnictwo Naukowe: Poznań, Poland, 2022; ISBN 978-83-7986-415-7. Available online: https://repozytorium.amu.edu.pl/items/089ee5e3-37b2-4bc8-b8c6-163e15456a1c (accessed on 17 January 2024).
78. Woś, A. *Klimat Polski w Drugiej Połowie XX Wieku*; Wydawnictwo Naukowe UAM: Poznań, Poland, 2010; pp. 1–489, ISBN 978-83-232-2180-7.
79. Beck, C.; Grieser, J.; Rudolf, B. *A New Monthly Precipitation Climatology for the Global Land Areas for the Period 1951 to 2000*; Climate Status Report 2004; German Weather Service: Offenbach, Germany, 2005; pp. 181–190. Available online: https://opendata.dwd.de/climate_environment/GPCC/PDF/pdf_28_precipitation.pdf (accessed on 19 January 2024).
80. Kottek, M.; Grieser, J.; Beck, C.; Rudolf, B.; Rubel, F. World map of the Köppen-Geiger climate classification updated. *Meteorol. Z.* **2006**, *15*, 259–263. [CrossRef] [PubMed]
81. Raport IMGW-PIB: Klimat Polski 2022 (Poland's Climate 2022). METEO IMGW-PIB, 2023. Available online: https://www.imgw.pl/badania-nauka/klimat (accessed on 17 February 2024).
82. Siwiec, E. (Ed.) *Atlas Skutków Zjawisk Ekstremalnych w Polsce*; Instytut Ochrony Środowiska—Państwowy Instytut Badawczy: Warszawa, Poland, 2022. Available online: https://klimada2.ios.gov.pl/files/2023/Atlas_skutkow_zjawisk_ekstremalnych_w_Polsce.pdf (accessed on 10 April 2024).
83. Mioduszewski, W. Zjawiska Ekstremalne w Przyrodzie—Susze i Powodzie. Rozdział 3. W: (Lachacz, A. eds.) Wybrane Problemy Ochrony Mokradeł. Współczesne Problemy Kształtowania i Ochrony Środowiska, Monografie nr 3p, 2012. Available online: http://www.uwm.edu.pl/environ/vol03p/vol_03p_tytul.pdf (accessed on 24 May 2024).
84. Borowska-Stefańska, M. Zagospodarowanie terenów zagrożonych powodziami w gminach województwa łódzkiego. *Przegląd Geogr.* **2015**, *87*, 535–553. Available online: https://rcin.org.pl/igipz/Content/56855/PDF/WA51_77386_r2015-t87-z3_Przeg-Geogr-Borowska.pdf (accessed on 24 May 2024).
85. Agboola, S.; Joel, M.B.M. Classification of Some Seasonal Diseases: A Hierarchical Clustering Approach. *Biomed. Stat. Inform.* **2017**, *2*, 122–127. Available online: https://1library.net/document/q0grg13z-classification-seasonal-diseases-hierarchical-clustering-approach.html (accessed on 22 February 2024).
86. StatSoft Electronic Statistics Textbook. Available online: https://www.statsoft.pl/textbook/stathome.html (accessed on 17 February 2024).
87. Bielecka, A. *Statystyka dla Menedzerów. Teoria i Praktyka (Statistics for Managers. Theory and Practice)*; Warszawa Wolters Kluwer: Warsaw, Poland, 2021; pp. 1–506.
88. Aczel, A.D. *Statystyka w Zarzadzaniu (Statistics in Management)*; Warszawa Wydawnictwo Naukowe PWN: Warsaw, Poland, 2018; ISBN 978-83-01-19537-3.
89. Akoglu, H. User's guide to correlation coefficients. *Turk. J. Emerg. Med.* **2018**, *18*, 91–93. [CrossRef] [PubMed]
90. United Nations. *The United Nations World Water Development Report 2023: Partnerships and Cooperation for Water*; UNESCO: Paris, France, 2023; Available online: https://reliefweb.int/report/world/united-nations-world-water-development-report-2023-partnerships-and-cooperation-water-enit (accessed on 17 February 2024).
91. Kundzewicz, Z.W.; Kanae, S.; Seneviratne, S.I.; Handmer, J.; Nicholls, N.; Peduzzi, P.; Mechler, R.; Bouwer, L.M.; Arnell, N.; Mach, K.; et al. Flood risk and climate change: Global and regional perspectives. *Hydrol. Sci. J.* **2013**, *59*, 1–28. [CrossRef]
92. Octavianti, T. Rethinking water security: How does flooding fit into the concept? *Environ. Sci. Policy* **2020**, *106*, 145–156. [CrossRef]
93. Fu, X.; Bell, R.; Junqueira, J.R.; White, I.; Serrao-Neumann, S. Managing rising residual flood risk: A national survey of Aotearoa-New Zealand. *J Flood Risk Manag.* **2023**, *16*, e12944. [CrossRef]
94. Glaus, A.; Mosimann, M.; Röthlisberger, V.; Ingold, K. How flood risks shape policies: Flood exposure and risk perception in Swiss municipalities. *Reg. Environ. Chang.* **2020**, *20*, 120. [CrossRef] [PubMed]
95. Villablanca, L.; Batalla, R.J.; Piqué, G.; Iroumé, A. Hydrological effects of large dams in Chilean rivers. *J. Hydrol. Reg. Stud.* **2022**, *41*, 101060. [CrossRef]

96. Yoshida, Y.; Lee, H.S.; Trung, B.H.; Tran, H.-D.; Lall, M.K.; Kakar, K.; Xuan, T.D. Impacts of Mainstream Hydropower Dams on Fisheries and Agriculture in Lower Mekong Basin. *Sustainability* **2020**, *12*, 2408. [CrossRef]
97. Sušnik, J.; Masia, S.; Kravčík, M.; Pokorný, J.; Hesslerová, P. Costs and benefits of landscape-based water retention measures as nature-based solutions to mitigating climate impacts in eastern Germany, Czech Republic, and Slovakia. *Land Degrad. Dev.* **2022**, *33*, 3074–3087. [CrossRef]
98. Zeleke, T.; Beyene, F.; Deressa, T.; Yousuf, J.; Kebede, T. Vulnerability of Smallholder Farmers to Climate Change-Induced Shocks in East Hararghe Zone, Ethiopia. *Sustainability* **2021**, *13*, 2162. [CrossRef]
99. Tran, D.D.; Quang, C.N.X.; Tien, P.D.; Tran, P.G.; Kim Long, P.; Van Hoa, H.; Ngoc Hoang Giang, N.; Thi Thu Ha, L. Livelihood Vulnerability and Adaptation Capacity of Rice Farmers under Climate Change and Environmental Pressure on the Vietnam Mekong Delta Floodplains. *Water* **2020**, *12*, 3282. [CrossRef]
100. Kret, M.E.; De Gelder, B. A review on sex differences in processing emotional signals. *Neuropsychologia* **2012**, *50*, 1211–1221. [CrossRef] [PubMed]
101. Donner, N.C.; Lowry, C.A. Sex differences in anxiety and emotional behavior. *Pflügers Arch.-Eur. J. Physiol.* **2013**, *465*, 601–626. [CrossRef] [PubMed]

sustainability

MDPI

Article

The Role of River Vigilance Committees to Address New Socio-Climatic Conditions in Chile: Insights from Ostrom's Design Principles for Common-Pool Resource Institutions

Natalia Julio [1,2,*], Amaya Álvez [2,3], Rodrigo Castillo [2,4], Kimberly Iglesias [5], Diego Rivera [2,6], Fernando Ochoa [7] and Ricardo Figueroa [1,2]

1 Departamento de Sistemas Acuáticos, Facultad de Ciencias Ambientales y Centro EULA, Universidad de Concepción, Concepción 4070386, Chile; rfiguero@udec.cl
2 Centro de Recursos Hídricos para la Agricultura y la Minería (CRHIAM), Concepción 4070411, Chile; aalvez@udec.cl (A.Á.); rodrigo.castillo@uach.cl (R.C.); diegorivera@udd.cl (D.R.)
3 Departamento de Derecho Público, Facultad de Ciencias Jurídicas y Sociales, Universidad de Concepción, Concepción 4070386, Chile
4 Facultad de Ciencias Jurídicas y Sociales, Universidad Austral de Chile, Puerto Montt 5489001, Chile
5 Independent Researcher, Arcangel 1218, Santiago 8900000, Chile; kimberly.iglesias@gmail.com
6 Facultad de Ingeniería, Universidad del Desarrollo, Santiago 7610658, Chile
7 Faculty of Geography, Ruprecht-Karls-Universität Heidelberg, 69120 Heidelberg, Germany; fernando.ochoa.udec@gmail.com
* Correspondence: natijulio@gmail.com

Abstract: Chile is currently facing a mega-drought, which is expected to lead to a significant increase in the water stress level. Social conflicts related to water use are linked to the effects of climate change and a governance system marked by the privatization of the natural resources of public interest. This study aims to analyze whether the current Chilean water governance scheme can adapt to the effects of climate change through a critical observation of the role of the River Vigilance Committees (RVCs; private user organizations exercising the public function of water management), from the perspective of Ostrom's design principles for long-enduring Common-pool Resource (CPR) institutions. We analyze legal approaches, management mechanisms, and decision-making processes under the socio-climatic conditions that the country is currently facing. The results indicate that, with a few exceptions, the Chilean governance system does not allow RVCs to effectively incorporate the design principles—and, therefore, to achieve adaptation—due to dispersed functions, the exclusion of water users, and a lack of planning at different levels. We propose that water governance should consider the creation of River Basin Boards with broader planning powers, as well as the incorporation of different relevant stakeholders.

Keywords: adaptive governance; climate change; Elinor Ostrom; river vigilance committees; water governance

Citation: Julio, N.; Álvez, A.; Castillo, R.; Iglesias, K.; Rivera, D.; Ochoa, F.; Figueroa, R. The Role of River Vigilance Committees to Address New Socio-Climatic Conditions in Chile: Insights from Ostrom's Design Principles for Common-Pool Resource Institutions. *Sustainability* **2024**, *16*, 1027. https://doi.org/10.3390/su16031027

Academic Editors: Wenfeng Liu, Xiao Lin Yang and Wen Yin

Received: 5 September 2023
Revised: 16 November 2023
Accepted: 7 December 2023
Published: 25 January 2024

1. Introduction

Water is regarded as a scarce resource, and it is becoming scarcer. Global freshwater use accounts for 3895.5 billion cubic meters per year [1], and approximately 2 billion people live in water-scarce countries [2]. Among the uses of freshwater, agriculture currently accounts for 69% of total water withdrawals [3], having been reported as 82% in the case of Chile (for agricultural and livestock activities) [4].

Chile has based its economic growth on the exploitation of natural resources, meaning that water is a fundamental element for the agricultural sector. Unfortunately, Chile has been experiencing a water crisis, influenced in part by a mega-drought that has extended over the past 14 years due to (among other factors) climate change [5]. Water scarcity poses problems not only for social and economic development, but also for environmental conservation [6].

The decrease in rainfall has intensified throughout the country over the past three decades, and significant deficits have been observed at almost all precipitation gauging stations [7]. Moreover, the World Resources Institute [8] indicated that Chile could face significantly increased water stress levels by 2040, classifying this risk as "extremely high".

Disputes over the use of water have significantly marked the history of social conflicts in Chile over the last three decades. The National Institute of Human Rights has indicated that 44% of the socio-environmental conflicts in the country are directly related to water [9], initially linked to droughts and the depletion of aquifers [10], but are now also related to inadequate water management and governance [11]. Considering a scenario of uncertainty regarding the effects of climate change, the World Bank [12,13] issued a series of recommendations to Chile concerning these matters; however, they still need to be implemented. Furthermore, water governance in the country has received multiple criticisms related to social inequality and the negative impacts on aquatic ecosystems [14–17].

The current Water Code (enacted in 1981) is Chile's most important legal body regulating water management, introducing water as a private good through Water Use Rights (WUR). The development of this model has occurred through three key principles: (i) the use of water markets for the management of water demand and supply; (ii) the right to exploit water as a private good protected by the State; and (iii) the delegation of water allocation management to private users [18–20].

The latter is regarded as a 'self-management' approach [21], meaning that private WUR holders become the most relevant actors involved in water use, management, and control within a specific territorial extent. They are generally grouped into Water Users Organizations (WUOs), described as private institutions exercising public functions in accordance with the Water Code. We distinguish two types of WUOs, based on the purpose of their administration: (i) WUOs extracting water from private artificial irrigation channels; and (ii) WUOs extracting water directly from rivers (natural flows). Within this second group, the River Vigilance Committees (RVCs) gather special attention, given that they are conceived as private institutions managing a public good (river basins or river sections). In this sense, managing water as a national asset for public use implies an important responsibility for RVCs, not only for having a coordinating role but also for taking care for the adequate allocation and conservation of water resources [22].

The political regime implemented during the military dictatorship in Chile set the context for the privatization of natural resources (and services of public interest) in the 1970s, 1980s, and 1990s [23], a process theoretically supported by the statements of Hardin's Tragedy of the Commons [24]. Years later, one of its most powerful critiques was proposed by Ostrom [25]—in her work titled Governing the Commons—where, in opposition to the dualistic classification of public and private goods, she invites us to take a third approach: the collective governance of common-pool resources [26].

Ostrom's theoretical approach has significantly guided Common-Pool Resource (CPR) institutions, and her eight design principles have been prominent across different disciplines [27]. Moreover, considering the climate change scenario, experienced not only in Chile but also worldwide, some studies have proposed Ostrom's principles as an alternative to achieve an adaptive water governance system that is sustainable, resilient to change and uncertainty, and which can address existing and upcoming conflicts involving water [28,29]. For instance, Heikkila et al. [30] analyzed fourteen interstate river basin compacts (agreements among states for managing interstate rivers) varying in terms of supply and demand settings. They analyzed the types of linkages established by each compact through a documentary analysis of their constitution agreements, official meeting minutes, and annual reports, which were coded according to Ostrom´s design principles. They concluded that there exists a direct correlation between the quality of the linkages and the socio-climatic conditions and management issues the states faced when signing those agreements, noting that the linkages which had been signed in times of scarcity and conflict had a broader diversity of principles involved. In addition, Quinn et al. [31] performed a qualitative assessment (through semi-structured interviews) of the extent to which each

design principle seemed to function in the administration of forest, pasture, and water resources in twelve villages in semi-arid Tanzania. They concluded that boundary-related issues and conflict-negotiation mechanisms were key in semi-arid zones, and that the need to adapt to address ecological uncertainty implied that numerous management organizations would be viewed as lacking or non-existent when evaluated through the lens of the design principle methodology, suggesting that the design principles should not be used as an imposed blueprint for water resource management systems; rather, they offer a framework for analysis. In this sense, Huntjens et al. [28] studied the applicability of eight refined and extended institutional design propositions based on Ostrom's principles, performing a documentary analysis of water management policies in the Netherlands, South Africa (river basins), and Western Australia (groundwater systems), and proposed a "management of learning" approach to deal with complexity and uncertainty, according to context-specific socio-climatic conditions.

Taking this into consideration, we agree that Ostrom's design principles comprise adaptive management processes, regarding adaptive governance as a social dimension in a sustainable ecosystem management (including freshwater systems) [32]. Therefore, we consider it important to analyze the applicability of Ostrom's design principles for CPR institutions within the context of the Chilean water governance system under the current socio-climatic conditions that the country is currently facing, within a scenario of increasing conflicts over access to water and uncertainty about the effects of climate change.

In Chile, Ostrom's Theory of the Commons has been applied within the legal framework, both in studies on the economic development model [33] and the communal property regime [34]. In addition, it has inspired a review of natural common property management structures [35], and their design principles for CPR institutions were partially used in the analysis of the Chilean legal groundwater regulation [17] and water management schemes [36]. In turn, the distinction among different methods for configuring property has been quoted by Vergara [37], justifying water markets (supply and demand relationships for the allocation of water resources) and creating distance from the conception of water as a public good of state concern.

Although Ostrom's precepts have already been used in the general analysis of water management in Chile, we find it interesting to evaluate whether the country´s unique water management model can promote adaptation to climate change, regarding the RVCs as an object of analysis. Given the significant influence that the self-management approach of the RVCs has in the water sector, it is important to analyze their role in addressing social and environmental conflicts within the current Chilean water governance framework. Therefore, this study aims to understand the performance of RVCs in adapting to the current climate change scenario, taking Ostrom's eight design principles as a baseline for analysis. For this, we examine RVCs as long-enduring Common-Pool Resource organizations, focusing on their integration mechanisms, decision-making processes, and socio-environmental responsibilities.

2. The Socio-Climatic Scenario: The Current State of Water Resources and Water Management in Chile

2.1. Hydrological and Climatic Conditions

The Chilean continental territory spans from 18° S to 55° S (4300 km) and is surrounded by the Pacific Ocean and the Andes mountains, encompassing a large latitudinal and longitudinal diversity of geographical, hydrogeological, and climate settings.

The climatic characteristics are highly variable across the country. In the northern part (18–33° S), arid and semi-arid conditions are observed, varying to a Mediterranean climate in central Chile (33–42° S) and temperate-wet climates in the southern area (42–55° S). Rainfall displays great intra-seasonal, inter-annual, and decadal variability, controlled by both frontal systems hitting the coast and large-scale climate processes such as the El Niño Southern Oscillation [38]. The average annual rainfall varies from 0 mm/y in the northernmost part of the country to 200–1000 mm/y in central Chile, while in the area extending from 35° S to the south, precipitation increases to over 1000 mm per year [39].

Regarding the seasonal variability in central Chile, the winter months (May to August) concentrate 85% of the total annual rainfall while, during the summer months (December to March), the average annual rainfall is less than 5%.

Regarding surface water, the average runoff values in the northern region have been observed in the range of 1 to 20 m^3/s, those in the central zone vary from 100 to 4000 m^3/s, and those in southern Chile may reach over 10,000 m^3/s [40]. Groundwater in the north is made up of fossil waters, as rainfall is extremely low, while central Chile has alluvial aquifers of very high transmissivity, so water users are prone to use groundwater both as a backup and a primary choice for use. Snowpacks and glaciers are critical components of the water supply in Chile, and snowmelt is the main streamflow source during the dry season [41].

Just as rainfall and runoff rates vary across the country, the same can be observed for water availability, which is territorially unequal. From central Chile to the north, the average water availability per inhabitant is less than 800 m^3/year while, in the south, this average exceeds 10,000 m^3/year [42]. Likewise, nearly 60% of the population is concentrated in a territory that is considered arid, where more than 70% of the national GDP is produced [43]. Traditionally, Chile has concentrated its irrigated agricultural production in the central zone for internal consumption and exportation based on fruit trees and cereal crops. Irrigation is key for producing high-quality crops and orchards, as rainfall is less than 15% of average annual values in the middle of the agricultural season [40].

However, climate change has posed an increasing risk to water supply. Chile is currently experiencing a situation of water scarcity, as reflected by a decrease in rainfall that has been intensifying [7]. If these conditions continue, the agricultural sector will be significantly affected. Due to climate change effects such as global warming, the main export-earning crops are expected to move south (resulting in land-use changes), and agricultural employment may decrease over the next few decades [44].

2.2. Chilean Water Management and Governance

In Chile, it is difficult to specify the functions related to entities managing water due to institutional dispersion in the matter. According to an assessment carried out by the World Bank in 2013, more than 40 public and private organizations are involved in water management in the country, revealing a system that presents overlaps and a lack of clarity in the performed functions [13].

In its original version presented in 1981, the Chilean Water Code allowed water regulation as a private good through WURs, expressed in units of volume per unit of time (i.e., cubic meters per hour; liters per second). WURs were given in perpetuity and free of charge. They are conceived as private property and, therefore, could be sold or mortgaged. Furthermore, a WUR was not subject to a specific use, and the holder could change its use without justification. The State grants a WUR to anyone who requests it, if it is available, and the Water Code allows for the use of water markets for re-allocation. In this sense, in the case of irrigated agriculture, for instance, WUR owners can use a transaction system to re-allocate the resource to those users who need more water to satisfy their production.

This situation was recently changed by a legal reform in 2022 (Law 21.435), in which important environmental and human rights aspects were incorporated into the regulations of the Chilean Water Code. Although the structure of the water market is maintained in the regulation, obligations to report the use of water to individuals are incorporated, the period for the constitution of WURs is limited, and a hierarchy of uses has been incorporated for the first time, prioritizing human consumption and ecosystem preservation [45,46].

Regarding management aspects, the Water Code allowed for the establishment of a dual institutional system: a centralized administration exercised by the state administrative institutions, within which the General Water Directorate (DGA, in its Spanish acronym) plays a very important role, and a decentralized administration, corresponding to the WUR holders organized in different sections of the same river basin—the River Vigilance Committees (RVCs).

At present, the bodies that manage water at the basin level are the RVCs. Currently, there are 57 RVCs legally constituted throughout the country [47]. Despite recognizing and promoting the importance of self-management, the RVCs do not ensure that all those affected by water management can participate in decision-making or resolve conflicts, as the RVCs are composed exclusively of WURs holders. The RVCs are mainly located in sectors related to agricultural activities in water-scarce areas, where the current Chilean water management system has been regarded as ineffective and insufficient to deal with the water crisis [14,15].

3. Materials and Methods

This study used a qualitative strategy, which allowed us to collect data to obtain more robust evidence to achieve our research aim [48], based on three steps: (i) descriptive legal analysis, (ii) documentary analysis, and (iii) semi-structured interviews.

The descriptive legal analysis involved a review of the legal norms applicable to water governance in Chile, as they are applied at the national level, regardless of geography- or climate-specific characteristics. The descriptive legal analysis was useful to determine the nature of the legal bodies involved in water management, the type of institutions involved, and the modifications that this normative scheme has undergone over the past few decades. The main legal bodies reviewed were the Political Constitution of Chile of 1980, the Water Code of 1981, and Law 21.435, which modified the Water Code [49]. This method allowed us to analyze the relationship among the normative configuration of the Chilean legal scheme and the practical consequences observed when exercising the functions of RVCs in Chile.

The second step involved analyzing the theoretical approaches of Ostrom's eight principles for long-enduring CPR institutions applicable to the RVCs, regarding the eco-social reality in which the RVCs carry out their functions (Table 1). For this, we performed a documentary analysis, which included government reports and the scientific literature on the functioning of river management in Chile and its socio-climatic conditions. The public sources of these reports were the Chilean General Water Directorate (DGA), the National Irrigation Commission (CNR), the National Institute of Human Rights (INDH), the Chilean Ministry of Environment and the Chilean Ministry of Agriculture. The main sources among the private organizations were the Chilean Institute of Engineers and Fundación Chile.

Finally, after the documentary analysis, we conducted five semi-structured interviews (year 2022) with one government employee, two academic experts on the management carried out by the RVCs, and two members of two RVCs that were considered pioneers in carrying out activities that go beyond what is merely established by the law, which therefore deserved to be particularly analyzed as, according to our knowledge, they could involve a greater diversity of principles than other RVCs at the national level. These RVCs covered the Biobío River Basin and the first section of the Cachapoal River and its tributaries. These five interviewees were asked questions about the functioning, organizational forms, and management schemes of these RVCs.

In this sense, documents and transcripts of interviews were critically analyzed in relation to their compliance to Ostrom's design principles for long-enduring CPR institutions in the following manner: (i) the legal and documentary analysis allowed us to identify the degree to which norms and the general management context governing the operation of RVCs in Chile complies with Ostrom´s principles, and (ii) the semi-structured interviews allowed us to identify which of Ostrom´s design principles were particularly followed by the two selected RVCs, in relation to the legal context in which they were embedded.

Table 1. Ostrom's design principles for long-enduring Common-Pool Resource (CPR) institutions [25].

Number	Principle	Content
1	Clearly defined boundaries	Individuals or households who have rights to withdraw resource units from the CPR must be clearly defined, as must the boundaries of the CPR itself
2	Congruence between appropriation and provision rules and local conditions	Appropriation rules restricting time, place, technology, and/or quantity of resource units are related to local conditions and to provision rules requiring labor, materials, and/or money
3	Collective Choice Arrangements	Most individuals affected by the operational rules can participate in modifying the operational rules.
4	Monitoring	Monitors, who actively audit CPR conditions and appropriator behavior, are accountable for the appropriators or are appropriators
5	Graduated sanctions	Appropriators who violate operational rules are likely to be assessed by graduated sanctions (depending on the seriousness and context of the offense) by other appropriators, by officials accountable to these appropriators, or by both
6	Conflict resolution mechanisms	Appropriators and their officials have rapid access to low-cost local arenas to resolve conflicts among appropriators or between appropriators and officials
7	Minimal recognition of rights to organize	The rights of appropriators to devise their own institutions are not challenged by external governmental authorities.
8	For CPRs that are parts of larger systems: Nested enterprises	Appropriation, provision, monitoring, enforcement, conflict resolution, and governance activities are organized in multiple layers of nested enterprises

Study Areas

Figure 1 shows the jurisdiction of the RVC of the first section of the Cachapoal River and its tributaries and the RVC of the Biobío River Basin, which operate in the river basin of the same names, located in central and south-central Chile, respectively. The Cachapoal River sub-basin (34° S 70° W) runs for 170 km and is characterized by a temperate Mediterranean climate. Its population is 584,000 inhabitants, 30% of whom work in agricultural activities, and it originates from the Andes Mountains and ends in the Rapel Reservoir [50]. Three different RVCs operate on the territories of this sub-basin; namely, the first, second, and third sections, with the RVC of the first section of the Cachapoal River and its tributaries (from now on, the 'RVC of the first section of the Cachapoal River') being located at the headwaters of the river.

The Biobío River basin (36° S 73° W) originates from the Icalma and Galletué lakes in the Andes mountains and flows to enter the Pacific Ocean near Concepción city after following a course of 380 km. The basin has a population of about 1,206,070 inhabitants [51]. Its climate is a transition zone between a warm temperate Mediterranean climate and a humid temperate or rainy climate. Productive sectors in the basin are related to forestry, agriculture, industry (pulp and paper, metallurgic, chemical and oil refinery industries), and the hydroelectric sector, being the main source of energy supply in the country [52]. Land-uses in this region are mainly allocated to forest plantations, at 2.2 million hectares (about 60% of the total area) [53].

Figure 2 illustrates time-series for the first section of the Cachapoal River and the Biobío River basin, based on data obtained from Alvarez-Garreton et al. [54]. Available time-series are representative for each region, providing homogenized data on precipitation, temperatures, potential evapotranspiration, and streamflow at the basin scale.

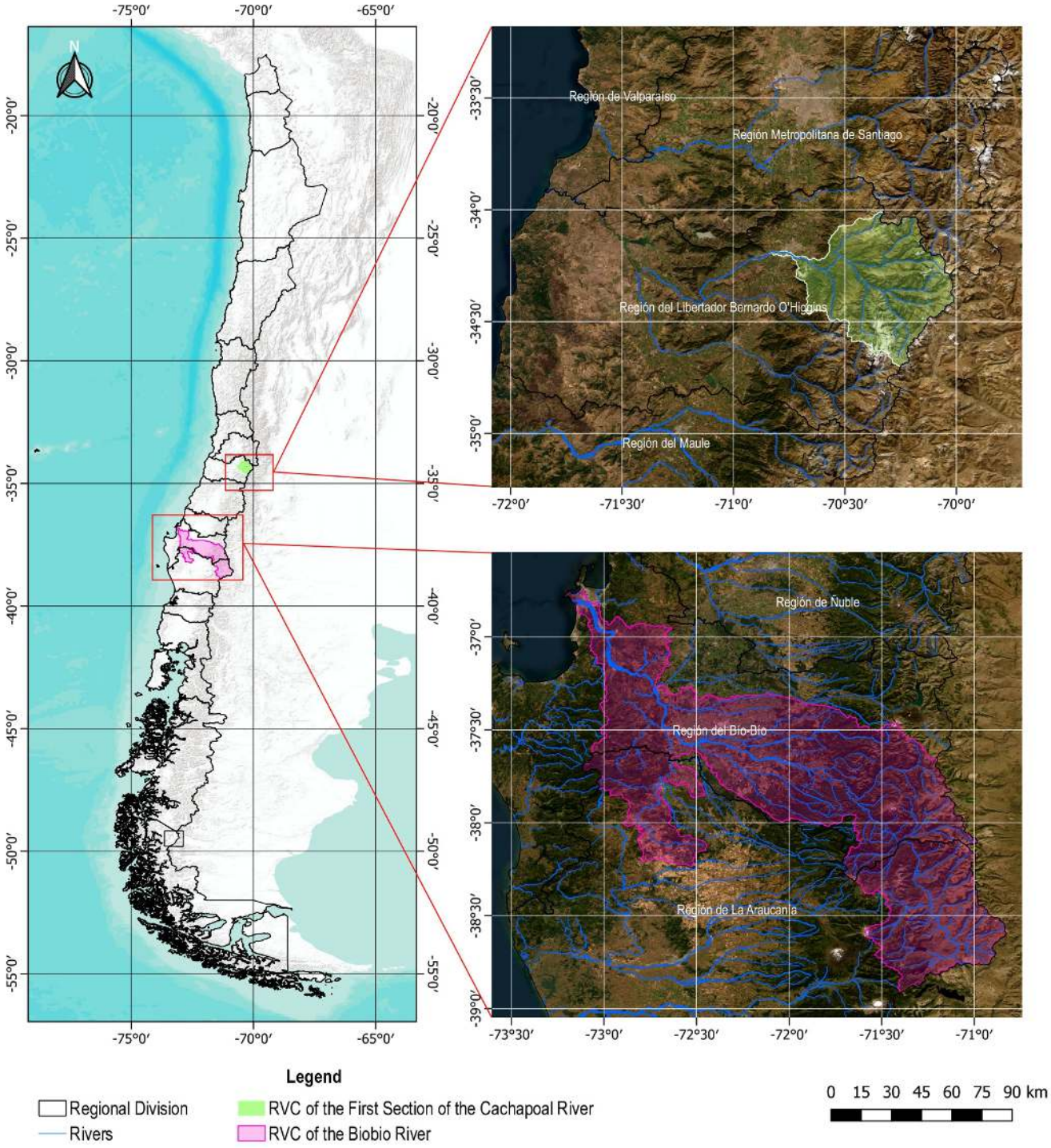

Figure 1. The jurisdiction of the RVCs of the first section of the Cachapoal River and The Biobío River Basin.

The study areas have different hydrological situations, even though the same climate regime forces both. Figure 2 highlights water scarcity, climate change, and variability conditions, showing the records for two main hydroclimatic variables that affect the water balance: precipitation and streamflow at the outlet. On one hand, precipitation is the only water input to the systems, while streamflow mimics water availability. It is worth noting that topography, geomorphology, hydrogeological setting, size, land-use, and land-cover control rainfall–runoff processes. Overall, since 2010, there has been a decreasing trend in rainfall and streamflow for both sites, while granted water rights show negligible increases,

conforming to a scarcity scenario worsened by the current drought. The first section of the Cachapoal River encompasses 2400 km^2 with a maximum elevation of 5150 masl. The mean annual precipitation is 1328 mm with a strong seasonality that peaks in winter (May to September). Since 2008, the 48-month Standardized Precipitation Index has been in the drought band, from marginal values in 2010 to extreme drought in 2020, as precipitation has declined significantly. The seasonal, inter-annual, and decadal variability is related to a substantial decrease in stream flow (ca. 30 m^3/s per decade). Annual mean flows are less than 20 m^3/s, with peaks during winter from runoff and spring from snowmelt, while surface water rights account for ca. 5 m^3/s.

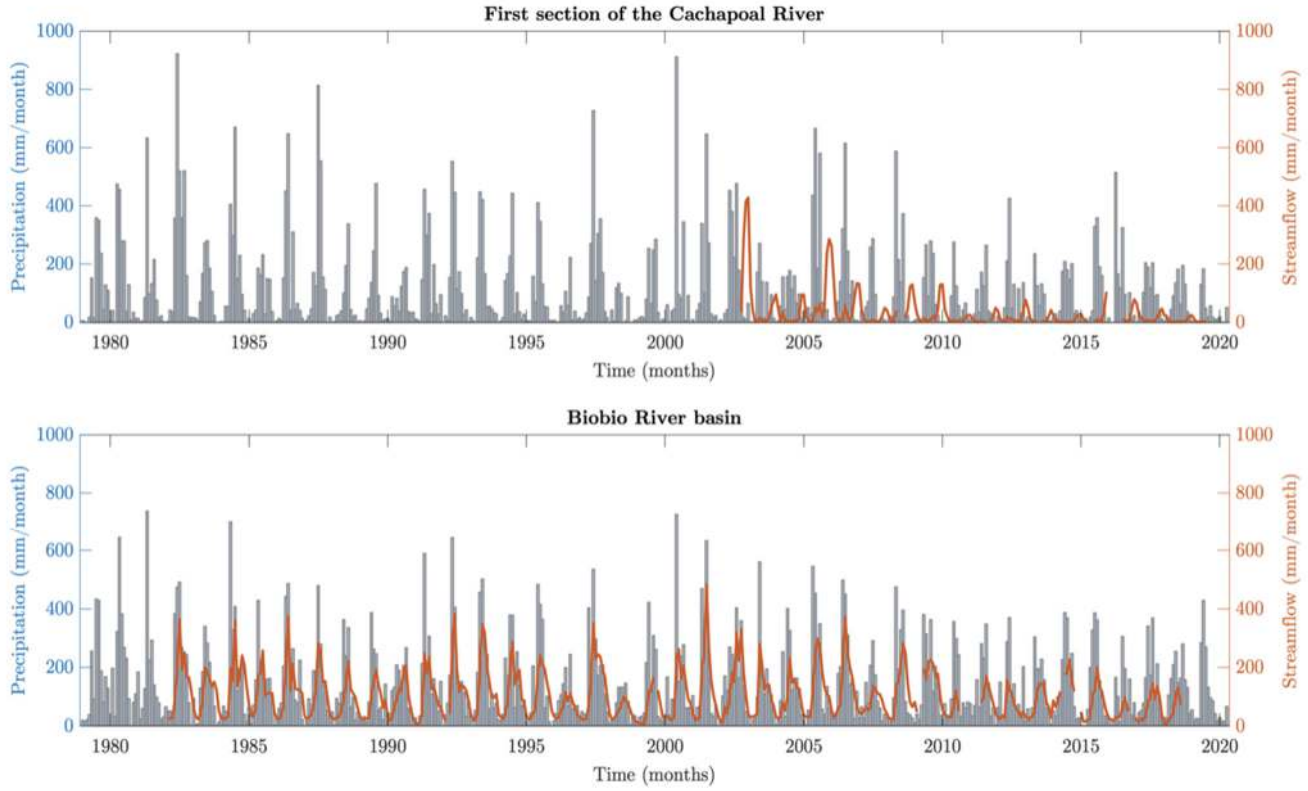

Figure 2. Time-series of precipitation and streamflow at the outlet for both study areas. Both variables are in mm for comparison. Data from Alvarez-Garreton et al. [54].

The Biobio River encompasses 24,270 km^2 with a maximum elevation of 3509 masl, which discharges into the Pacific Ocean after 380 km. The mean annual precipitation is 840 mm, with a strong seasonality that peaks in winter (May to September). As the drainage area is ten times that of the first section of the Cachapoal River, stream flows are less sensitive to rainfall. However, the annual precipitation in headwater watersheds is close to 3000 mm. Since 2008, the 48-month Standardized Precipitation Index has been in the drought band, from marginal values in 2010 to strong drought in 2020, as precipitation has declined significantly. The decrease in streamflow has been ca. 55 m^3/s per decade. Annual mean flows are less than 1000 m^3/s, with peaks during winter. Since 2010, the summer streamflow has been less than 200 m^3/s, while surface water rights account for ca. 149 m^3/s.

Both sites are under increasing pressure, facing decreasing precipitation, and rising seasonal and inter-annual variability. However, the Biobio River basin appears to be in a better position, as its size allows it to buffer upstream changes in rainfall and snowfall. For instance, water from the Andes re-circulates in the central valley through natural groundwater recharge, percolation from irrigation land, and discharge from industries. The Cachapoal River heavily depends on rainfall and snowmelt in a smaller area, with a much lower chance of water re-circulation within the system.

4. Results

4.1. Ostrom's Design Principles for Long-Enduring CPR Institutions Applied to RVCs

Ostrom provided several examples of long-lasting CPR institutions, arguing that institutions maintained over a prolonged period are signals of success [27]. She explored the favorable and unfavorable conditions for developing long-lasting CPR institutions, and identified the eight design principles which are essential for success [25]. Below, we critically apply Ostrom's design principles of CPR Institutions to the internal decision-making mechanisms of RVCs, including the processes of participation, collective action, and learning.

4.1.1. Clearly Defined Boundaries

Defining the boundaries of a CPR and specifying who is authorized to use it is the first step in organizing a collective action. It is essential to determine the scale of the processes and to recognize the actors involved in terms of defining who is responsible for the management, construction of the rules of use, and the development of the mechanisms to exclude others in order to prevent over-exploitation. Additionally, it is important to determine the carrying capacity of the system to sustain the extraction by the individuals of the collective and to understand the regenerative capacity of the natural system [25].

The current Chilean water management model has been criticized for a lack of updated information (which is also deeply centralized) regarding the current availability of water, the effects of climate change on surface water and groundwater, and the hydrogeological behavior of the aquifers [11], which is the responsibility of government organizations. For this reason, collecting adequate data about the CPR's boundaries, the carrying capacity of the system, and the number of actors involved is usually performed by the RVCs, which generally use their resources to obtain such data. However, economic and professional resources differ among the RVCs in the country, and some cannot afford data-monitoring systems.

Another issue regarding CPR boundaries is related to determining an adequate spatial unit for water management. Globally, the river basin is generally considered the most accepted territorial unit for water resource management [55–57]; however, although the Water Code specifies that RVCs have jurisdiction on a river basin, in practice, these institutions have been historically organized on river sections (articles 263 and 264 of the Water Code).

In this sense, multiple RVCs can co-exist in a single river basin, as is the case for the RVC of the first section of the Cachapoal River (located at the headwaters of the Cachapoal River) with respect to the RVCs of the second and third sections (located downstream, in the same river). The fact that the same river stream is shared by three institutions that have independent forms of self-management inevitably causes some conflict and communication problems among them, which have arisen due to the mega-drought conditions that the country is currently experiencing.

The latter does not seem to be a problem for the Biobío basin, as it is the only basin that has a RVC with a jurisdiction extending from the source of the river to its river's mouth. This implies an advantage when it comes to resolving conflicts and managing the river basin according to its complete hydrological condition.

4.1.2. Congruence between Appropriation and Provision Rules and Local Conditions

The rules for using, managing, and protecting water must be clearly defined. Community decision-making requires adopting a collective agreement that considers the perspective of local cultural and social values, thus considering the collective capacities and ecological characteristics of the CPR. In this sense, the rules of use must be defined in accordance with the environmental, social, and economic conditions within the boundaries of the CPR [25].

This principle is linked to the first one, in terms of the coherence among the norms and local conditions that respond to the need to react to the specific management challenges of the CPR. In the case of water management, this specificity connects to a 'territorialization' of WURs (i.e., a process that is a consequence of geographical and climatic diversity).

This process forces—especially in conditions of scarcity—the performance of different practices to precisely address the resolution of problems regarding governance and resource allocation [58].

General legal and management factors in the Chilean case, however, encounter two obstacles: on one hand, national standards that homogenize the management of radically different water realities are used [17], while on the other hand, the artificial sectioning of river basins (two or more RVCs can manage different river sections) has been carried out, thus reducing the capacity for internal coordination. In addition, territorial planning instruments are currently only obliged to include urban areas (communal, inter-communal, and metropolitan), and not rural areas, which can encompass important zones of the river basin that are not adequately regulated.

In this regard, RVCs have shown an unequal performance when facing the various issues that may occur in their areas of action, involving the contamination of irrigation channels, coordination between different uses, and the need to increase efficiency when facing conditions of scarcity [59]. Some of these organizations, such as the RVC of the first section of the Cachapoal River, have been able to address such issues, assuming roles that go beyond the conventional duty of water distribution. This RVC participates in the river quality monitoring program organized by state and private agencies, actively engaging with scientists and other RVCs. As an example, one of its members stated the following:

> *"I insist that cooperation agreements work as long as people want them to work. Therefore, people are more important than documents. We have been involved in different water boards, such as environmental certification boards for agricultural schools, and we are free to do so. Others have told us not to get involved in things that are not written (Water Code). But not here. Here, in everything related to the water problem, we say: let's do it!"* Member of the RVC of the first section of the Cachapoal River

In addition, the RVC of the Biobío River Basin aims to incorporate an Integrated River Basin Management, considering the protection of water quality, ecosystems, and groundwater availability [60]. As one of its members declared,

> *"I arranged a second meeting, a few months later, in the same place with the same actors [. . .]. I asked them to make other decisions, for example, the characteristics that our RVC was going to have. I suggested that the characteristics of this RVC should not be the standard characteristics of all the RVCs, but rather that we should aspire to something more, that we should aspire to a basin organization that would really allow us to carry out integrated management. And I believe that this got a lot of people excited. I asked the universities to explain to us what the training process was like [. . .] which were the limitations and problems for this [. . .]. One of the characteristics we defined was that we were going to cover the entire basin [. . .] from the source of the river in the lagoons to its estuary"* Member of the RVC of the Biobío River Basin

4.1.3. Collective Choice Arrangements

This principle enables CPR institutions to adapt their rules to local circumstances, as individuals interacting directly with each other and the physical environment can modify these rules over time to better adapt them to changing environmental conditions. The rules of use may be flexible under critical disturbances; however, with the return of standard conditions, the community should review the rules and their compliance [25].

When reviewing the basic conditions that allow agents to jointly manage an economic good, Ostrom has pointed out that most individuals affected by the operating rules should participate in their modification. This possibility is manifested not only in the foundation of these rules, but also in their permanent revision and adaptation following the social-environmental changes observed at the local level. Water regulation requires feedback, as the current environmental crisis scenarios force the need for a dynamic perspective [61].

Taking these factors into consideration, the Chilean management model presents some particularities in relation to what it considers to be the "most affected individuals".

According to Ostrom, this concept clarifies that those affected by a certain condition (i.e., water scarcity) suffer—in one way or another—the consequences of changes in the allocation or administration of the CPR [25]. According to the Chilean legislation, RVCs can only be composed by WUR holders and, in practice, most of the country's RVCs are composed of agricultural irrigators [62]. However, there are other water uses that could be affected by the changing socio-climatic conditions of the river basin, such as cultural and recreational activities that do not operate under the WUR system. In this regard, there are individuals who use water for several different purposes and do not have the opportunity to participate in the RVC's decision-making processes.

Although the RVCs were traditionally mostly composed of farmers who used water for irrigation and industrial purposes, since the beginning of the 2000s, several RVCs have changed their statutes to incorporate sanitary and hydroelectric companies. The RVC of the first section of the Cachapoal River initiated this process, including actors such as mining, sanitation, and hydroelectric power generation companies. Some RVCs have considered incorporating different users since the beginning of their foundation process, as is the case of the RVC of the Biobío River Basin. Moreover, it is important to highlight that some agricultural irrigators have recently incorporated hydroelectric generation systems within their irrigation channels.

4.1.4. Monitoring

CPR institutions have monitoring mechanisms relevant to the conservation of natural resources. In this sense, safeguarding natural resources through adequate management entails a greater community commitment to observing and recording processes, events and, in some cases, physical and environmental variables. This community-based monitoring system does not necessarily have to be valued by external agencies. The collective institution carries out the mechanisms to supervise the proper use of the resource. When the state or an external agent must sanction or validate a community monitoring mechanism, it is an indicator of the weakness and fragility of the community [25].

The factors subject to monitoring by the management institution vary. In the specific case of water management, this includes—among other aspects—the evaluation of compliance and decisions on extraction quotas, the proper use of extraction systems, the maintenance of minimum flows, and the environmental quality of the waters subject to administration.

In the Chilean management system, the Water Code provides the RVCs with the structure for their administrative bodies for exercising control and monitoring functions. In this matter, the Board of Directors of the RVC is empowered to ensure that water is collected by adequate structures (Water Code, article 274.1). In addition, this body may appoint a water distributor who reports to the RVC, in order to ensure that water is not subtracted or used by those without WURs (Water Code, article 278.2).

Monitoring water extraction is also carried out by public agencies, particularly by the DGA. Since the legal reforms implemented in 2018 and 2022, the State has expanded the DGA's attributions, incorporating the monitoring of the quality and quantity of the water in attention to its conservation and protection.

In the case of the first section of the Cachapoal River and the Biobío River Basin, both RVCs benefit from water quality monitoring programs at the river basin level, which are carried out thanks to the coordination of government agencies and private companies. The former RVC participates in the Cachapoal River Board of Directors which, together with other environmental committees, has collaborated with other RVCs, government agencies, and private companies to obtain water quality monitoring data in the sub-basins that composed the Rapel River basin for approximately 12 years. Although it does not participate directly, the RVC of the Biobío River Basin makes its decisions based on a program called the Biobío River quality monitoring program. The PMBB (in its Spanish acronym) was created in 1994, and has been monitoring the water quality of the Biobío river basin in a joint effort between the University of Concepción and private companies.

4.1.5. Graduated Sanctions

In solid CPR institutions, supervision and penalization are not carried out by external authorities but rather by the participants. The CPR appropriators create an internal compliance system to discourage those who are tempted to break the rules. Supervision costs are low in many long-term CPR institutions due to the rules in use, as there are usually both economic and moral sanctions. In collective action institutions, being repeatedly recognized as an infringer puts not only an individual at risk, but also the reputation of the collective unit (e.g., family) to which they belong [25].

Within the Chilean management context, it is important to highlight that RVCs follow the precepts of the Water Code with respect to the application of sanctions to its members. In this case, the supervisory duty carried out by the DGA as a governmental body is imperative. The DGA's resolution Number 185 established the Control and Enforcement Department, the main objective of which is to provide guidance, direct norms, and contribute to the "water watching and supervision" function exercised by the DGA in accordance with article 299 letters c and d [63].

Control and enforcement are administrative procedures defined in the Water Code, encompassing sanctions (if applicable), mainly of an economic nature (such as fines), and the ordering of certain administrative actions (i.e., shutting down illegal water extraction infrastructure). In the case of an infringement of the Water Code regulations, fines may be applied for tax benefits, which are graduated on a scale from the first to the fifth degree, depending on the nature of the infringement (articles 173 and 173ter of the Water Code). For the determination of the amount of the fine, the Water Code states that certain circumstances must be taken into consideration, such as the affected flow rate, surface waters or groundwater, whether the rights of third parties are affected, the number of harmed users, the degree to which the aquifer is affected, and the zone in which the infringement takes place, among others. For instance, obtaining a double registration of a WUR in the Public Water Registry, either intentionally for personal benefit or to the detriment of third parties, is one of the most serious punishable behaviors.

In addition to the rules that the RVCs must comply with according to the Water Code, some RVCs have additional graduated sanctions, such as the RVC of the first section of the Cachapoal River, which are related to moral sanctions. As one of its members detailed, it is possible to observe that this RCV has a monitoring system that involves sanctions if rules are not followed:

> *"One of our functions is to monitor extractions. We check the extractions all day and every day. We have a person who is assigned to do that. We have an operator who goes around and checks and telemetry systems that report. And now we are developing a software with a 'traffic lights' system that indicates that when is red, you are behaving badly or, if is green, you are doing well. It is that simple, with colors, because nobody has time to read a lot of numbers. But if you look at the website and somebody is green, and you are red, and everybody knows you are red, you are going to worry. Regardless of whether you are red or orange. Period. Nobody wants to be orange or red".* Member of the RVC of the First Section of the Cachapoal River

4.1.6. Conflict Resolution Mechanisms

In theory, in models of rule-governed behavior, rules are enforced by external agents and are usually indisputable. However, this is not often observed in practice, as rules can be interpreted differently by diverse appropriators. If individuals must follow specific rules for a long period of time, when infractions occur, there must be a mechanism through which the problem can be discussed and resolved [25].

In the case of RVCs, Rojas [22] has distinguished three ways of resolving conflicts arising from the use and management of water: (i) conflicts related to the exercise of WURs (in situations of faults or abuses committed in water allocation, or in their economic management) can be solved by the RVC's Board of Directors as an arbitrator (without the formalities of a court), and subsequently claimed in the courts of justice; (ii) requesting

external arbitration for the resolution of conflicts regarding the exercise of WURs through an administrative procedure initiated by the DGA; and (iii) directly resolving conflicts regarding the exercise and loss of WURs and all other water-related issues (article 181 to 185 of the Water Code) through a claim for protection that has a single objective—the immediate re-establishment of water use—ending with the interferences that disturb the exercise of the WUR [64]. Regarding the internal conflict resolution mechanism of the Board of Directors, fines and sanctions such as cutting off the water supply can be applied.

Other types of conflicts related to water use in river basins can be solved through administrative and legal means external to the RVCs (as they are not part of their legal attributions). A frequently used legal means to resolve conflicts is the "protection action" to safeguard certain fundamental rights contemplated by the Political Constitution (1980); for instance, to resolve conflicts involving the exercise of the human right to water [65]. However, this kind of action has not yet generated significant modifications to the water management system.

In the case of the RVC of the first section of the Cachapoal River and the RVC of the Biobío River basin, both entities do not have registered internal conflicts. This is particularity due, in our opinion, to the fact that the former has an advantage as it receives water in the highest section of the river, where there is generally greater control of the river flow distribution, while the latter has hydrological conditions that still allow it to have adequate availability for its members, who formed this RVC under a preventive principle in the face of negative projections of water availability in the future.

4.1.7. Minimal Recognition of Rights to Organize

Appropriators often design their own rules without developing formal governmental supervision systems. If external government agents control the development and compliance of the internal community's rules, this compliance system will not be sustained over time.

In this case, the RVC is considered to have a high level of autonomy in decision-making within the limits of its jurisdiction. Although the RCVs must be governed minimally by what is specified in the Water Code, the State does not intervene in internal water allocation systems or the mechanisms for re-allocating WURs (water markets usually govern the latter).

Under this level of autonomy, the RVCs can elaborate their statutes, conflict resolution mechanisms (through private arbitration), sanctions, and the composition of their management bodies, all within the legal framework. Within the Chilean water governance system, this situation—far from generating a consensus on the exercise of these functions as an adequate exercise of autonomy—has been criticized due to the differences between the public administrative role (i.e., performed by the DGA) and the role carried out by the RVCs, the former presenting severe defects in terms of its supervisory capacity, support in conflict resolution, and maintenance of an adequate information system [36]. However, regarding the organizations, some interviewees recognized that maintaining a good relationship with government agencies and other RCVs is beneficial for water management.

4.1.8. Nested Enterprises

Complex and enduring CPR institutions are organized in various layers at the local, regional, and national levels. In this sense, the management of the CPR must be performed within a network of coordination, congruence, and effective communication between these levels [25].

The RVCs in Chile do not comply (or, at least, not fully) with this principle, considering the lack of mechanisms for linking local to larger-scale management plans. The only connection/correlation that could occur at different levels can be observed in the case of the RVCs regarding the other WUOs that compose them (Irrigation Channels Associations, Water Communities, and Drainage Communities). However, as they are goods (resources) of a different nature (a common good on one hand, and already-extracted private water on the other), it would not exactly imply a case of "nested enterprises".

In the case of a basin management organization being sub-divided to perform its functions under the supervision of a higher authority, or when sections of the same river coordinate their functions, shared management could occur at different levels, allowing the generation of management plans and general norms regarding the whole river basin in a binding manner. In Chile, the discussion about who could fulfil such a role has been settled either at the political or the legislative level, with relevant developments in the reform of the Water Code in the year 2022 and the Climate Change Law in 2022, both of which consider the future existence of strategic water resource plans at the basin level, elaborated within the framework of a national water resource policy.

Considering the principle of nested enterprises, two cases were observed in which the RVC of the first section of the Cachapoal River has associated with other public and private administrative entities: the Board of Directors of the Cachapoal River and the Colchagua´s Clean Water Board, both of which are coordinated by the regional ministerial secretary of the Environment (in a representation of the Ministry of the Environment at the regional level). These boards, which have operated since 2001, manage issues related to financing and monitoring the Cachapoal River's water quality, and are collaborative bodies in developing environmental education initiatives.

Before its formation, the RVC of the Biobío Basin attempted to conform a River Basin Council, aiming to link with other institutions at other levels. According to one of its members:

> *"(Given the uncertainty caused by Climate Change and other threats, such as the future Hydric Highway project) I organized a meeting in a very nice restaurant by the Biobio River, and I invited as many people as I could have access to, in order to discuss this issue. On that occasion, I took the precaution of also inviting users from the hydroelectric world, the industrial world and, of course, all the WUOs. I invited representatives of civil society, such as some people who also represented other uses, such as tourism, fishing [. . .]. I also included the academia [. . .] and I also included people from the government. I did a presentation about how I think resources should me managed [. . .] and, finally, I asked them a question: if after having learned about this, they thought it was necessary to organize a RVC. This was done in a very well-documented way, notes were taken, very orderly. And the response was unanimous [...] all those who attended were motivated and said: yes, let's organize it".* Member of the RVC of the Biobio River Basin

5. Discussion

In Ostrom's Theory of the Commons, the regulation of natural resources and property avoids the strict and traditional conception of state–private separation and, instead, constitutes a fertile mix of private and public institutions, recognizing the importance of local actors in the conservation or degradation of the commons. According to Singleton [27], Ostrom´s Theory of the Commons is prevalent, in part, as it becomes an alternative to the pessimistic approaches of a homo economicus that cannot cooperate effectively around natural resources. She responds to Hardin's Tragedy of the Commons, which points out that a group of individuals pursuing their interests in the administration of goods will tend to exploit the resource until its total depletion. In contrast to Hardin, Ostrom indicates that resources will not necessarily be depleted, as she analyzed certain cases in which resources were managed sustainably, rationally, and better than in a system based on individual private property [25].

This review of Ostrom's management principles in relation to the structure and functioning of RVCs provided some elements for discussion: the geographical framework of action, the concept of 'user', and issues regarding collective choice arrangements.

5.1. The Geographical Framework: Moving from Sectioning to an Integrated Management of the Commons

Regarding spatial (geographical) scale, some critiques have arisen around Ostrom's design principles. Singleton [27] has argued that, besides individual self-interest as a barrier

to successful CPR institutions, socio-economic forces outside the CPR institution could be important with respect to its likely success. However, the same author stated that this is partly valid because some design principles are aware that local institutions do not exist in isolation. In addition, Araral [66] has stated that Ostrom's critique of Hardin is useful in the case of small-scale, locally governed commons, while Hardin´s theory seems to remain valid for large-scale and global commons. This occurs as trust and reciprocity—two core factors to achieve cooperation in the commons [67]—can be observed due to face-to-face communication [66]. Thus, even though they are largely accepted, Ostrom's principles are continuously challenged under new theoretical developments and new observational information. In fact, trust and reciprocity were mentioned by interviewees when asked about the relationship that the RVC of the first section of the Cachapoal River had with other RVCs and public entities. The exchange of knowledge regarding how to respond to new environmental conditions has involved a learning process to move towards adaptation.

An important element of discussion is the definition of a range of actions for the management body, which must be determined in the geographical dimension. In the case of the RVCs, although initially determined by the river basin (defined in Article 3 of the Water Code), the law admits the possibility of sectioning a single river basin. This fragmentation generally exacerbates conflicts between upstream and downstream boards. To the best to our knowledge, the RVC of the Biobío River Basin is the only RVC in Chile whose jurisdiction covers the river from its source to its mouth. This has brought advantages in terms of resolving possible conflicts and is a positive step toward Integrated River Basin Management, which has been promoted to adapt to the effects of climate change [68].

Another issue that impacts the separation of the ranges of action corresponds to the separation that Chilean legislation makes for water management regarding the territory and its physical characteristics. Territorial planning instruments mainly concentrate on urban areas, not including the situation of watersheds that are not located in the urban context, with little possibility of regulating activities that cause direct and indirect effects on water availability and quality. In addition, the exclusion of WUR holders who extract water from the ground through wells [17] also affects the determination of the action ratio in geographical terms, due to a separation (in terms of management) between surface and underground water.

The proposal to strengthen the management of common goods in the case of water, by supporting the attributions and intervention of the RCVs or the creation of basin boards, should consider an extension of the territorial scope that effectively integrates the entire river basin, in both its urban and rural dimensions, and consider the capacity to influence and provide feedback to those institutions in charge of territorial planning. In addition, the legal territorial framework should allow enough flexibility to grant local management that adapts to the conditions of each river basin throughout the territory, according to different socio-climatic characteristics and the development of nested enterprises.

We argue that Ostrom's design principles are suitable for analyzing the community administration of river basins as common goods through a self-management approach. At the river basin scale, this mechanism adapts to territorial characteristics and the social traditions of those who benefit from CPR use. These principles applied to the RVCs emphasize integrating different types of stakeholders and their forms of participation, the relationship between these institutions and non-extractive uses, and their role in environmental conservation and the maintenance of water availability.

5.2. The RVCs and the Concept of 'User'

In Governing the Commons, Ostrom [25] refers to the concept of 'user for purposes of participation' which, in the Chilean case, applies to the RVCs as the entities in charge of managing WURs in rivers and/or river sections. According to Ostrom's perspective, this concept is geared towards considering users as individuals affected by the operating rules. In our opinion, in the case of water, this might not be so clear due to specific needs related

to advances in technology, population growth, and the effects of climate change, affecting its availability for ecosystem functions. In our understanding, this determines an unclear definition of the category of 'users'.

In the Chilean legislation, water management involves a restricted conception of users when establishing WUOs in the Water Code, particularly the RVCs. Such participation is restricted to WUR holders, represented by the Board of Directors. In this way, the user concept—which includes self-management organizations—is linked to the owner of the actual private right of exploitation. This situation, which is allowed by the Water Code, is detrimental with respect to the process of participation within the RVCs and, therefore, in conceiving an adaptive governance system.

The RVCs recognize the safeguarding of public interest [18], as their functions affect the conservation of a national good for public use, such as river basins. The conception of users, understood as only those with a direct economic interest in water extraction (consumptive or not), moves away from the configuration of a community regime such as the Theory of the Commons, as it does not incorporate all those affected by the decisions of the management body. Instead, it is concerned with generating mechanisms to protect the property rights of WUR holders. The Water Code does not distinguish geographical or cultural spaces in determining individuals or groups affected by decisions and rules. However, RVCs have made efforts to assume the functions that their context requires, even if they are not provided by law, as noted in Section 4.

The duality that RVCs face in terms of being a body constituted by private actors fulfilling the functions of a public body affects the incorporation of key users. The legislation does not distinguish the type of rights in question; therefore, the ancestral rights of native people and groundwater rights are not usually incorporated into RVCs. Indeed, groundwater users are allowed to conform to a different entity, different from surface water uses, even being part of the same basin. The problems caused by this lack of incorporation not only relate to an impairment of the right of some stakeholders to participate in the decision-making process within the RVC, but also to an impact on the public interest in trying—at least in part—to carry out a harmonious management of water allocation.

The described situation has been reversed in some cases by incorporating these types of users, but within the frameworks prescribed by the Water Code [69]. This is the case of the RVC of the first section of the Cachapoal River, into which legal entities such as ESSBIO (water sanitation company), the state company CODELCO (mining), and hydroelectric companies have been incorporated, which are WUR holders that have been excluded in the past. However, this is an exceptional situation in most RVCs, which has been driven by conflicts, some even reaching the Chilean courts. In this matter, the expansion of the concept of a Water User emerges as a necessary objective to be achieved to comply with real participation, which is a principle of adaptive governance of the commons.

It is essential to highlight that the modification of water governance in Chile does not necessarily imply a direct integration of other stakeholders into the RVCs. Rather, it is also important to re-think their role within a larger context, such as the already mentioned River Basin Councils.

5.3. Issues about Collective Choice Arrangements: The Water Shares

The existence of collective choice arrangements is one of the principles that Ostrom established in the configuration of permanent models for the management of a CPR. The possibility that the decisions are made by the majority of those affected corresponds to an important contribution of the author in the notion of democracy in the management of natural resources.

The application of the voting mechanism to RVC members based on shares, which are distributed according to the number of WURs held by each member (Water Code, article 268), is similar in this matter to the system of administration of a Joint-Stock Company [18]. Equating these shares to decision-making power is a sort of internal governance system, especially in the case of those profit-seeking legal entities, as could be the case of

business companies and corporations. The rationale is that the greater the investment (or economic interest involved), the greater the right to decide regarding the CPR. Although this could be understandable in a business company, we believe that, in managing the common interest, it does not adequately consider the special characteristics of water as a national good for public use.

The eventual inclusion of new stakeholders for whom the use of water goes beyond economic interest (subsistence farming communities, citizens and native peoples, among others) into management bodies necessarily implies re-consideration of the current decision-making mechanisms. In fact, the formal incorporation of other stakeholders in the use of water has been proposed for more than a decade. Documents such as the World Bank report [13] or the one prepared by the Chilean Institute of Engineers on Integrated Water Resources Management [70] have included several technical proposals to improve water management, incorporating the concept of integration into the Chilean water governance system. One proposal is to create new institutions (i.e., River Basin Boards) with the power to include different social and economic actors in the use of water resources, or the joint development of basin management plans that include RVCs and other WUOs. This could be a solution to the restricted power in decision-making that the current legislation provides for RVCs. However, the formal extension of the decision-making power of RVCs implies the inclusion of new actors besides WUR holders. Although this option regards the characteristics of a CPR institution (according to Ostrom's conception), it is currently doubtful whether RVCs will fulfill functions for which they are not mandated by law or for which they do not have financial aid. In this sense, transforming into an adaptive decision-making model requires major legal changes, including amendments to the current Chilean Constitution.

In this sense, the RVC of the first section of the Cachapoal River and the RVC of the Biobío River Basin go beyond some of the functions and boundaries stated by the Water Code. Although these RVCs participate in educational stances, collaborate with other entities, are worried about water quality issues, and are willing to consider the opinions of other relevant water users in the future, they do not fully comply with all eight of Ostrom's design principles for long-enduring CPR institutions.

6. Conclusions

From an analysis of the general characteristics of the water management and governance situation in Chile, it was determined that, although the RVCs recognize and promote the importance of self-management, they do not ensure that all those affected by water management can participate in decision-making or resolve conflicts, as they are composed exclusively of WUR holders. Contrasting with the obtained legal research results with Ostrom's design principles for long-enduring CPR institutions, there is an important exclusion of some critical water users (especially non-extractive users with no recognized or constituted water rights), an unequal decision-making process based on the number of water shares (in some cases linked to economic power), and a lack of integrated planning at different levels. Furthermore, as mentioned above, RVCs usually cover a specific section of a river basin, not the whole river basin. These characteristics, added to the current water crisis in Chile, seem worrisome when considering how to move towards an adaptive governance system.

The maintenance of the current water model in Chile contributes to the deepening of a governance and availability crisis, to social conflicts associated with water access and allocation, and to the imbalance in its different uses and functions to the detriment of those that are outside of the extractive economic categories.

The recent reform to the Chilean water legislation seems to be insufficient to correct these inequalities and inadequate in the face of the challenges posed by climate change and governance of the CPR. Chilean water governance should consider the existence of River Basin Boards with broader planning powers, incorporating water users in the various dimensions that such management affects.

A new form of governance that goes beyond these management mechanisms must take on these challenges to increase integration, enabling fair decision-making and coordination between different levels. To this end, the principles of the governance of the commons can provide not only a prism of analysis—as in this work—but also a basis for projection, adapted to the water and social realities in the Chilean case and worldwide.

Author Contributions: Conceptualization and formal analysis, N.J., A.Á. and R.C.; methodology, N.J., A.Á. and D.R.; investigation: N.J., R.C., K.I. and F.O.; writing—original draft preparation, N.J., A.Á., R.C., K.I. and F.O.; resources: N.J. and D.R.; writing—review and editing, N.J., A.Á., R.C. and R.F.; supervision, A.Á. and R.F.; funding acquisition, N.J., A.Á., D.R. and R.F. All authors have read and agreed to the published version of the manuscript.

Funding: This research was funded by project Fondecyt Regular 1230520 (D.R.).

Institutional Review Board Statement: Not applicable.

Informed Consent Statement: Not applicable.

Data Availability Statement: The data presented in this study are available on request from the corresponding author. The data are not publicly available due to privacy restrictions.

Acknowledgments: Water Resources Center for Agriculture and Mining (CRHIAM): project ANID/FONDAP/15130015 and ANID/FONDAP/1523A0001 and the National Agency for Research and Development ANID/Subdirección de capital humano/doctorado nacional/folio N°21221448.

Conflicts of Interest: The authors declare no conflict of interest.

References

1. The World Bank. Annual Freshwater Withdrawals, Total (Billion Cubic Meters). Available online: https://data.worldbank.org/indicator/ER.H2O.FWTL.K3 (accessed on 5 July 2023).
2. UN-Water. *The United Nations World Water Development Report 2020: Water and Climate Change*; UNESCO: Paris, France, 2020.
3. UN-Water. *The United Nations World Water Development Report 2021: Valuing Water*; UNESCO: Paris, France, 2021.
4. Olivares, M. *Agua y Recursos Hídricos: Agenda del Ministerio de Agricultura en el Marco del Desarrollo Sustentable del Sector Agropecuario [Water and Water Resources: Agenda of the Ministry of Agriculture within the Framework of Sustainable Development of the Agricultural Sector]*; ODEPA: Santiago, Chile, 2022.
5. MMA. Cambio Climático: Chile Sumará 14 años Consecutivos de Sequía y Proyectan Aumentos en Olas de Calor [Climate Change: Chile Will Have 14 Consecutive Years of Drought and Projected Increases in Heat Waves]. Available online: https://mma.gob.cl/cambio-climatico-chile-sumara-14-anos-consecutivos-de-sequia-y-proyectan-aumento-en-olas-de-calor/#:~:text=%E2%80%9CNo%20solo%20es%20un%20a%C3%B1o,otros%20meses%20fueron%20bastante%20secos (accessed on 5 July 2023).
6. GWP. *Ecosystem Services and Water Security*; Global Water Partnership: Stockholm, Sweden, 2014.
7. DGA. Informe Hidrometereológico Semanal (03 de Julio de 2023) [Weekly Hydrometeorological Report (July 3, 2023)]. Available online: https://dga.mop.gob.cl/productosyservicios/informacionhidrologica/Informe%20HidroMeteorolgico%20Semanal/Informe_semanal_03_07_2023.pdf (accessed on 5 July 2023).
8. The World Resources Institute. Ranking the World's Most Water-Stressed Countries in 2040. Available online: https://www.wri.org/insights/ranking-worlds-most-water-stressed-countries-2040 (accessed on 6 July 2023).
9. INDH. Mapa de Conflictos Socio Ambientales en Chile [Map of Socioenvironmental Conflicts in Chile]. Available online: https://mapaconflictos.indh.cl/#/ (accessed on 25 August 2023).
10. Siebert, S.; Burke, J.; Faures, J.M.; Frenken, K.; Hoogeveen, J.; Döll, P.; Portmann, F.T. Groundwater use for irrigation: A global inventory. *J. Hydrol. Earth Syst. Sci.* **2010**, *14*, 1863–1880. [CrossRef]
11. Escenarios Hídricos 2030. *Resumen Estratégico: Transición Hídrica, el Futuro del Agua en Chile [Strategic Summary: Water Transition, the Future of Water in Chile]*; Fundación Chile: Santiago, Chile, 2019.
12. The World Bank. *Chile: Diagnóstico de la Gestión de los Recursos Hídricos [Chile: Diagnosis of Water Resources Management]*; DGA MOP: Santiago, Chile, 2011.
13. The World Bank. *Estudio para el Mejoramiento del Marco Institucional para la Gestión del Agua [Study for the Improvement of the Institutional Framework for Water Management]*; DGA MOP: Santiago, Chile, 2013.
14. Bauer, C. *Canto de Sirenas: El Derecho de Aguas Chileno Como Modelo para Reformas Internacionales [Siren Song: Chilean Water Law as a Model for International Reform]*, 2nd ed.; Ediciones El Desconcierto: Santiago, Chile, 2015.
15. Budds, J. Securing the market: Water security and the internal contradictions of Chile's Water Code. *Geoforum* **2020**, *113*, 165–175. [CrossRef]
16. Guiloff, M. A pragmatic approach to multiple water use coordination in Chile. *Water Int.* **2012**, *37*, 121–130. [CrossRef]

17. Rivera, D.; Godoy-Faúndez, A.; Lillo, M.; Alvez, A.; Delgado, V.; Gonzalo-Martín, C.; Menasalvas, E.; Costumero, R.; García-Pedrero, Á. Legal disputes as a proxy for regional conflicts over water rights in Chile. *J. Hydrol.* **2016**, *535*, 36–45. [CrossRef]
18. Rojas, C. La categoría jurídica de los servicios privados de interés público: El caso de las Juntas de Vigilancia de los Ríos [The legal status of private services in the public interest: The case of the River Vigilance Committees]. *Rev. Chil. Derecho* **2014**, *41*, 171–204. [CrossRef]
19. Budds, J. Governance of water and development within the market: The social relations of control over water in the framework of Chile's Water Code. *Investig. Geográficas* **2020**, *59*, 16–27. [CrossRef]
20. Valdés-Pineda, R.; Pizarro, R.; García-Chevesich, P.; Valdés, J.B.; Olivares, C.; Vera, M.; Balocchi, F.; Pérez, F.; Vallejos, C.; Fuentes, R.; et al. Water governance in Chile: Availability, management and climate change. *J. Hydrol.* **2014**, *519*, 2538–2567. [CrossRef]
21. Vergara, A. Sistema y autonomía del Derecho de Aguas [System and autonomy of water law]. In *Derecho de Aguas*; Universidad Externado de Colombia: Bogotá, Colombia, 2012; Volume 5, pp. 255–281.
22. Rojas, C. Autogestión y autorregulación regulada de las aguas: Organizaciones de Usuarios de Aguas (OUA) y juntas de vigilancia de ríos [Self-management and self-regulation: Water users' organizations (OUA) and River Vigilance Committees]. *Rev. Ius Praxis* **2014**, *20*, 123–162. [CrossRef]
23. Locher, F. Cold War Pastures: Garrett Hardin and the Tragedy of the Commons. *Rev. Hist. Mod. Contemp.* **2012**, *60*, 7–36.
24. Hardin, G. The Tragedy of the Commons. *Science* **1968**, *162*, 1243–1248. [CrossRef]
25. Ostrom, E. *Governing the Commons: The Evolution of Institutions for Collective Action*; Cambridge University Press: Cambridge, UK, 1990.
26. Rodríguez, L. Reseña del gobierno de los bienes comunes: La evolución de las instituciones de acción colectiva de Ostrom, Elinor [Review of Ostrom's Governance of the Commons: The Evolution of Collective Action Institutions]. *Rev. Pueblos Front. Digit.* **2010**, *6*, 363–375. [CrossRef]
27. Singleton, B.E. What's missing from Ostrom? Combining design principles with the theory of sociocultural viability. *Environ. Polit.* **2017**, *26*, 994–1014. [CrossRef]
28. Huntjens, P.; Lebel, L.; Pahl-Wostl, C.; Camkin, J.; Schulze, R.; Kranz, N. Institutional Design Propositions for the Governance of Adaptation to Climate Change in the Water Sector. *Glob. Environ. Chang.* **2012**, *22*, 67–81. [CrossRef]
29. Robertson, J. The Common Pool Resource Heatmap: A Tool to Drive Changes in Water Law and Governance. *Water* **2021**, *13*, 3110. [CrossRef]
30. Heikkila, T.; Schlager, E.; Davis, W. The role of cross-scale institutional linkages in common pool resource management: Assessing interstate river compacts. *Policy Stud. J.* **2011**, *39*, 121–145. [CrossRef]
31. Quinn, C.; Huby, M.; Kiwasila, H.; Lovett, J. Design principles and common pool resource management: An institutional approach to evaluating community management in semi-arid Tanzania. *J. Environ. Manag.* **2007**, *84*, 110–113. [CrossRef]
32. Folke, C.; Hahn, T.; Olsson, P.; Norberg, J. Adaptive Governance of Social-Ecological Systems. *Annu. Rev. Environ. Resour.* **2005**, *30*, 441–473. [CrossRef]
33. Greve, G. Institucionalidad e Innovación: Un Cambio de Foco al Modelo de Desarrollo [Institutionality and Innovation: A Change of Focus to the Development Model]. [Tesis Universidad de Chile] Santiago. 2015. Available online: https://repositorio.uchile.cl/bitstream/handle/2250/130820/Institucionalidad-e-innovaci%C3%B3n-un-cambio-de-foco-al-modelo-de-desarrollo-actual.pdf?sequence=1&isAllowed=y (accessed on 25 August 2023).
34. Míguez, M. De las cosas comunes a todos los hombres: Notas para un debate [Of things common to all men: Notes for a discussion]. *Rev. Chil. Derecho* **2014**, *41*, 7–36. [CrossRef]
35. Correa, H.; Blanco-Wells, G.; Barrena, J.; Tacón, A. Self-organizing processes in urban green commons. The case of the Angachilla wetland, Valdivia-Chile. *Int. J. Commons* **2018**, *12*, 573–595. [CrossRef]
36. Costa, E. Diagnóstico para un cambio: Los dilemas de la regulación de las aguas en Chile [Diagnosis for a change: The dilemmas of water regulation in Chile]. *Rev. Chil. Derecho* **2016**, *43*, 335–354. [CrossRef]
37. Vergara, A. *Crisis Institucional del Agua: Descripción del Modelo Jurídico, Crítica a la Burocracia y Necesidad de Tribunales Especiales [Water Institutional Crisis: Description of the Legal Model, Criticism of Bureaucracy and the Need for Special Tribunals]*; Ediciones Universidad Católica de Chile: Santiago, Chile, 2015.
38. Aceituno, P.; Boisier, J.; Garreaud, R.; Rondanelli, R.; Rutllant, J.A. Climate and Weather in Chile. In *Water Resources of Chile*; Fernández, B., Gironás, J., Eds.; Springer: Cham, Switzerland, 2021; Volume 8.
39. Aitken, D.; Rivera, D.; Godoy-Faúndez, A.; Holzapfel, E. Water Scarcity and the Impact of the Mining and Agricultural Sectors in Chile. *Sustainability* **2016**, *8*, 128. [CrossRef]
40. Villamar, C.; Vera-Puerto, I.; Rivera, D.; De la Hoz, F. Reuse and Recycling of Livestock and Municipal Wastewater in Chilean Agriculture: A Preliminary Assessment. *Water* **2018**, *10*, 817. [CrossRef]
41. McPhee, J.; MacDonell, S.; Casassa, G. Snow Cover and Glaciers. In *Water Resources of Chile*; Fernández, B., Gironás, J., Eds.; Springer: Cham, Switzerland, 2021; Volume 8.
42. Jiménez, S.; Wainer, J. *Serie Informe Económico 263: Realidad del Agua en Chile: ¿escasez o Falta de Infraestructura? [The Reality of Water in Chile: Scarcity or Lack of Infrastructure?]*; Libertad y Desarrollo: Santiago, Chile, 2017.
43. Centro de Análisis de Políticas Públicas. *Informe País: Estado del Medio Ambiente en Chile 2018 [Country Report: State of the Environment in Chile 2018]*; Instituto de Asuntos Públicos Universidad de Chile: Santiago, Chile, 2019.
44. Melo, O.; Foster, W. Agricultural and Forestry Land and Labor Use under Long-Term Climate Change in Chile. *Atmosphere* **2021**, *12*, 305. [CrossRef]

45. Castillo, R.; Gómez, G.; Vidal, G. Ley 21.435 de Reforma al Código de Aguas [Law 21.435 to reform the Water Code]. *AIDIS CHILE* **2022**, *61*, 22–30.
46. Celume, T. Reconocimiento legal del derecho humano al agua y sus implicancias en los principios que informan el Código de Aguas [Legal recognition of the human right to water and its implications in the principles that inform the Water Code]. *Rev. Derecho Ambient.* **2022**, *18*, 35–61. [CrossRef]
47. DGA. Registro Público de Organizaciones de Usuarios [Public Registry of Water User Organizations]. Available online: https://dga.mop.gob.cl/administracionrecursoshidricos/OU/Paginas/default.aspx (accessed on 20 October 2023).
48. Bryman, A. *Social Research Methods*, 4th ed.; Oxford University Press: New York, NY, USA, 2012.
49. Manrique, M.L.; Navarro, P.; Peralta, J. Criminal law and legal dogmatics. *Dogmatics Const. Interpret.* **2017**, *31*, 3806. [CrossRef]
50. Novoa, V.; Ahumada-Rudolph, R.; Rojas, O.; Munizaga, J.; Sáez, K.; Arumí, J.L. Sustainability Assessment of the Agricultural Water Footprint in the Cachapoal River Basin, Chile. *Ecol. Indic.* **2019**, *98*, 19–28. [CrossRef]
51. DGA. *Atlas del Agua [Water Atklas]*; Gobierno de Chile: Santiago, Chile, 2016.
52. Parra, O.; Figueroa, R.; Valdovinos, C.; Habit, E.; Díaz, M.E. *Programa de Monitoreo de la Calidad del Agua del Sistema Río Biobío 1994–2012: Aplicación del Anteproyecto de Norma Secundaria de la Calidad Ambiental (NSCA) del Río Biobío [Water Quality Monitoring Program for the Biobío River System 1994–2012: Application of the Draft Secondary Environmental Quality Standard (NSCA) for the Biobío River]*; Universidad de Concepción: Concepción, Chile, 2013.
53. INFOR. *Anuario Forestal Ministerio de Agricultura [Forestry Yearbook of the Ministry of Agriculture]*; Gobierno de Chile: Santiago, Chile, 2017.
54. Alvarez-Garreton, C.; Mendoza, P.A.; Boisier, J.P.; Addor, N.; Galleguillos, M.; Zambrano-Bigiarini, M.; Lara, A.; Puelma, C.; Cortes, G.; Garreaud, R.; et al. The CAMELS-CL dataset: Catchment attributes and meteorology for large sample studies–Chile dataset. *Hydrol. Earth Syst. Sci.* **2018**, *22*, 5817–5846. [CrossRef]
55. GWP. *TAC Background Papers No. 4: Integrated Water Resources Management*; Global Water Partnership: Stockholm, Sweden, 2000.
56. Wang, G.; Mang, S.; Cai, H.; Liu, S.; Zhang, Z.; Wang, L.; Innes, J.L. Integrated watershed management: Evolution, development and emerging trends. *J. For. Res.* **2016**, *27*, 967–994. [CrossRef]
57. Kaval, P. Integrated catchment management and ecosystem services: A twenty-five-year overview. *Ecosyst. Serv.* **2019**, *37*, 100912. [CrossRef]
58. Embid, A. El derecho de aguas del siglo XXI [Water law in the 21st century]. *Actas Derecho Aguas* **2012**, *2*, 79–104.
59. Arumi, J. *Gestión Integrada de Recursos Hídricos [Integrated Water Resources Management]*; Mesa de Agua y Medio Ambiente [Water and Environment Committee]: Santiago, Chile, 2015.
60. Melo, O. Experiencias de integración de la gestión de las aguas superficiales y subterráneas [Experiences in the management integration of surface water and groundwater]. *Rev. Asoc. Chil. Riego Drenaje* **2019**, *30*, 22–24.
61. Retamal, R.; Andreoli, A.; Arumi, J.L.; Rojas, J.; Parra, O. Gobernanza del agua y cambio climático: Fortalezas y debilidades del actual sistema de gestión del agua en Chile [Water governance and climate change: Strengths and weaknesses of the current water management system in Chile. Internal análisis]. Análisis interno. *Interciencia* **2013**, *38*, 8–16.
62. CNR–National Commission of Irrigation Chile. *Gestión Integrada de los Recursos Hídricos y Algunas Experiencias de Organizaciones de Usuarios del Agua [Chile. Integrated Water Resources Management and Some Experiences of Water Users' Organizations]*; Gobierno de Chile: Santiago, Chile, 2005.
63. Castro-Portales, D.; Moraga-Navarro, M.P. Resolución de conflictos al interior de las organizaciones de usuarios de aguas en Chile: ¿Judicialización o arbitraje? [Conflict resolution within water users' organizations in Chile: Judicialization or arbitration?]. *Agric. Soc. Desarro.* **2015**, *12*, 319–347. [CrossRef]
64. Delgado, V.; Álvez, A.; Ochoa, F.; Sandoval, M.I. El amparo de aguas en la jurisprudencia chilena (2013–2015) [El amparo de aguas en la jurisprudencia chilena (2013–2015)]. *Rev. Derecho Estado* **2018**, *41*, 197–225. [CrossRef]
65. García, B. La compatibilidad del derecho humano al agua con la legislación chilena: El reconocimiento latinoamericano de este derecho [The compatibility of the human right to water with Chilean legislation: Latin American recognition of this right]. *Rev. Ius Praxis* **2020**, *26*, 172–194. [CrossRef]
66. Araral, E. Ostrom, Hardin and the commons: A critical appreciation and a revisionist view. *Environ. Sci. Policy* **2014**, *36*, 11–23. [CrossRef]
67. Dietz, T.; Ostrom, E.; Stern, P. The Struggle to Govern the Commons. *Science* **2003**, *302*, 1907–1912. [CrossRef]
68. Julio, N.; Figueroa, R.; Ponce-Oliva, R.D. Advancing toward water security: Addressing governances failures through a metagovernance of modes approach. *Sustain. Sci.* **2022**, *17*, 1911–1920. [CrossRef]
69. Delgado, V.; Arumi, J.L.; Reicher, O. Lessons from Spanish and US Law for adequate regulation of groundwater protection areas in Chile, especially drinking water deposits. *J. Water Resour. Manag.* **2017**, *31*, 4699–4713. [CrossRef]
70. Instituto de Ingenieros de Chile. *Hacia una Gestión Integrada de Recursos Hídricos: Una Propuesta [Towards Integrated Water Resources Management: A Proposal for an Integrated Water Resources Management System]*; Instituto de Ingenieros de Chile: Santiago, Chile, 2012.

sustainability

MDPI

Article

Statistical Analysis of Climate Trends and Impacts on Groundwater Sustainability in the Lower Indus Basin

Waqas Ahmed [1,2], Suhail Ahmed [1], Jehangir F. Punthakey [3,4], Ghulam Hussain Dars [1], Muhammad Shafqat Ejaz [5], Abdul Latif Qureshi [1] and Michael Mitchell [3,*]

[1] US Pakistan Center for Advanced Studies in Water, Mehran University of Engineering and Technology, Jamshoro 76062, Sindh, Pakistan; wapathan.uspcasw@faculty.muet.edu.pk (W.A.); engrsam1306@gmail.com (S.A.); ghdars.uspcasw@faculty.muet.edu.pk (G.H.D.); alqureshi.uspcasw@faculty.muet.edu.pk (A.L.Q.)
[2] Department of Stochastic Simulation and Safety Research for Hydrosystems, University of Stuttgart, 70569 Stuttgart, Germany
[3] Gulbali Institute, Charles Sturt University, Albury, NSW 2640, Australia; eco@ecoseal.com
[4] Ecoseal Developments Pty Ltd., Roseville, NSW 2069, Australia
[5] Department of Civil Engineering, NED University of Engineering and Technology, Karachi 75270, Sindh, Pakistan; msejaz@hotmail.com
* Correspondence: mimitchell@csu.edu.au

Abstract: Agricultural intensification is increasing global demand for water, with groundwater especially susceptible given its year-round reliability. Climate change impacts on groundwater recharge exacerbate uncertainties for future access and use, especially for large aquifers across alluvial plains such as the Indus Basin of Pakistan. To generate better understanding of climate change impacts on groundwater balances in such contexts, we used MODFLOW 2005 to quantify the groundwater budget of the Northern Rohri Canal Command Area under RCP 4.5 and 8.5 climatic scenarios, while also taking climatic regionalisation into account. Under a baseline scenario, total annual pumping in the northern Rohri command was estimated to be 3.619 billion cubic metres (BCM), and the total net loss in storage over the simulation period from October 2010 to April 2014 was estimated at 1.244 BCM per year. By 2047, net decline in storage is projected to more than double to 2.185 per year under RCP 4.5 scenario and 2.214 under RCP 8.5. Our estimates suggest that a sustainable yield across the command area should be managed at approximately 3 ± 0.3 BCM per year to ensure sufficient adaptive reserves of groundwater for access during times of drought and inadequate surface supply, while also reducing waterlogging impacts from high watertables. This first-time estimate of sustainable yield provides irrigation system managers with an overall guide from which divisional-scale measures to achieve the goal can be identified through stakeholder engagement.

Keywords: groundwater; climate change; Mann–Kendall; Sen's slope; RCPs

Citation: Ahmed, W.; Ahmed, S.; Punthakey, J.F.; Dars, G.H.; Ejaz, M.S.; Qureshi, A.L.; Mitchell, M. Statistical Analysis of Climate Trends and Impacts on Groundwater Sustainability in the Lower Indus Basin. *Sustainability* **2024**, *16*, 441. https://doi.org/10.3390/su16010441

Academic Editors: Xiao Lin Yang, Wenfeng Liu and Wen Yin

Received: 27 October 2023
Revised: 17 December 2023
Accepted: 20 December 2023
Published: 4 January 2024

1. Introduction

Groundwater is an essential source of water for irrigation, industry, and human consumption. Across the Indus Basin Irrigation System (IBIS) of Pakistan, access to groundwater allows farmers to irrigate crops on demand, compensating for temporal and spatial shortages in IBIS canal water supplies. Farmers thus use groundwater as a dependable supplemental supply to irrigate their crops according to requirements [1,2]. Recent estimates suggest that groundwater provides up to 60% of Pakistan's irrigation supply [3], with Pakistan now the third-largest user of groundwater for irrigation in the world [4]. However, access to groundwater also varies from year to year, depending on climatic conditions and river flows. In some parts of the IBIS, increased use of groundwater is enabled by the accumulation of fresh groundwater due to seepage from canals and irrigation return

flows, allowing farmers in such areas to increase cropping intensity, thus helping address the nation's food security needs. During dry years and times of low canal supply, groundwater supply is critical. This can also be observed from the increasing rate of tubewells in Pakistan, with an estimated 1.39 million in operation in 2019, and broad consensus that rates of groundwater pumping exceed recharge [5]. Such imbalances not only mean that groundwater levels are in decline [6], but there is also increasing risk of saline intrusion [7], reduced groundwater quality [8], and higher pumping costs borne by farmers [9]. In the irrigated and coastal regions of Sindh province, these problems are more severe because of seawater intrusion, poor irrigation practices, and industrial effluents that further worsen groundwater quality. A total of 75% of groundwater in Sindh is saline and 70% of tubewells pump saline water [10]. Managing the use of marginal and brackish groundwater will require farmers to adopt improved conjunctive management strategies.

Climate change is already changing the functioning of natural ecosystems, including groundwater. Pakistan is especially susceptible, ranked seventh most affected country by climate change in the Global Climate Risk Index [11]. Most of the country is arid or semi-arid with temporal and spatial variability in climatic parameters, making it crucial to understand the impacts of climate change on water availability and management. Yet one IPCC report noted a global dearth of research on the potential impacts of climate change on groundwater [12], even though its share in the use of water worldwide has increased, especially in arid and semi-arid regions. The effects of climate change on groundwater are not straightforward. There is a substantial uncertainty in the estimation of magnitude and trends of climate change in terms of rainfall, temperature, evapotranspiration, and vapour pressure [13]. While it might be assumed that greater rainfall leads to increased recharge, there are exceptions. Such a link can be affected by rainfall seasonality, intensity, humidity, air temperature, and crop evapotranspiration under changing climatic conditions. While projections of increased rainfall variability may increase groundwater recharge due to intense rainfall that eventually infiltrates to become part of the watertable, projected higher temperatures under climate change mean higher rates of crop evapotranspiration, resulting in less net recharge of groundwater.

Groundwater flow modelling provides a simulation environment to assess the impact of climatic stress on the groundwater system. Several studies in the Central Indus Basin used groundwater modelling to assess the impact of external stresses (e.g., [14,15]). In the Lower Indus Basin, groundwater modelling studies have been conducted at small spatial scales to study groundwater hydraulics and hydro salinity behaviour (e.g., [16–18]). Studies related to the impacts of climatic change on groundwater in the Lower Indus Basin are limited, especially at the regional scale.

Given the lack of research and considerable uncertainty, a practical way forward is to pursue more local-focused research so that the particular combination of parameters that may be influenced by climate change in particular places can be determined, which can then offer suggestions for management and planning relevant to those places. The current study was therefore designed to evaluate groundwater resources for the Northern Rohri Canal Command Area, a component of the IBIS located in the Sindh province of Pakistan, where irrigation with marginal quality groundwater and a changing climate are resulting in increased risk to agricultural production. The possible parameters of interest include rainfall and crop evapotranspiration, and increased groundwater extractions for irrigated regions, as these parameters may behave differently under a changing climate. The primary objectives of the study were to: (1) delineate zones with similar characteristics based on long-term trends of rainfall and evapotranspiration datasets; (2) identify the statistically significant trends in different zones for rainfall or evapotranspiration based on future trends; and (3) quantify and assess groundwater sustainability with respect to water levels and water balance.

2. Hydrogeology of the Lower Indus Basin

The Lower Indus Basin (LIB) lies in the Himalayan foredeep—a region of subsidence in front of the Himalayan belt. The alluvial complex of the LIB forms a highly permeable unconfined aquifer. The thickness of the alluvium is not known accurately but it exceeds 182 metres over large parts of the basin [19]. Hydraulic conductivity varies between 10 and 20 metres/day (m/d) with anisotropy kh:kv between 100 and 500, and specific yield ranges from 5 to 15% [20,21].

The pattern of the regional flow follows the direction of the river quite closely though some of the flow drains towards the desert in the east and the hills in the west. The groundwater has its origin in the river system which has been flowing through the valley since late Tertiary times in contrast to the central and upper Indus plains where rainfall contributes significantly to recharge [22]. Historically, the watertable has remained shallow. A generally rising watertable trend (moving upward) has prevailed in recent times [23], with 32% of the canal command area under shallow watertables (1.6 to 3 m), and approximately 60% considered waterlogged (in the range of 0.25 to 1.5 m) [24].

Major recharge in the region can be attributed to the river system, canal leakages, and infiltration from irrigation return flows. In recent years (i.e., 2010, 2011, and 2022), short-duration high-rainfall events have occurred across the region, which would be a significant contribution to recharging the aquifer and requires further investigation. Due to shallow watertables, direct evapotranspiration from the groundwater is also significant in the LIB. Groundwater use in the LIB is moderate and mostly concentrated in freshwater zones. The reason for this is the constraint on the useable volume in some areas due to the presence of salinity and high arsenic contamination [25,26].

3. Materials and Methods

3.1. Study Area

The study area chosen is the Northern Rohri Canal Command Area (CCA), supplied from the left bank of Sukkur Barrage, which covers an intensively cultivated area across the districts of Sukkur, Khairpur, Naushero Feroze, and Shaheed Benazirabad (Figure 1). The study area has four major canals and is divided into five irrigation divisions, i.e., Khaipur West, Khairpur East, Rohri, Dad, and Nasrat divisions. Surface irrigation is the main source and groundwater is secondary but significant, especially between the Indus River and Rohri Canal. The geographical region of the study area is mostly arid and semi-arid, with low annual rainfall and higher evapotranspiration rates, and where temperature increments are expected to be greater than average. May and June have maximum temperatures which can exceed 45 °C, while January is considered the coldest month when temperatures can go below 10 °C. Most rainfall occurs in the months of July, August, and September, with mean annual rainfall ranging between 100 mm to 200 mm. An increasing shortage of surface water has led to a dramatic increase in groundwater use. The groundwater in the area ranges from fresh along the Indus River to marginally fresh and saline across the CCA, dictating where groundwater is likely to be used for irrigation.

3.2. Input Data

Table 1 shows the input dataset used in the study, and a description of the preprocessing of the raw dataset is provided below for acquiring the final data used to model the groundwater system.

3.2.1. Aquifer Properties

A database of 163 bores with logs was compiled from sources provided by Sindh Irrigation Department (SID), WAPDA's SCARP Monitoring Organization (SMO), and from various previous field studies. These logs were scanned, georeferenced, and compiled in a lithology database. The borelogs, including additional logs from drilling undertaken in our case study sites, were used to estimate hydraulic conductivity, specific yield, specific storage, and porosity.

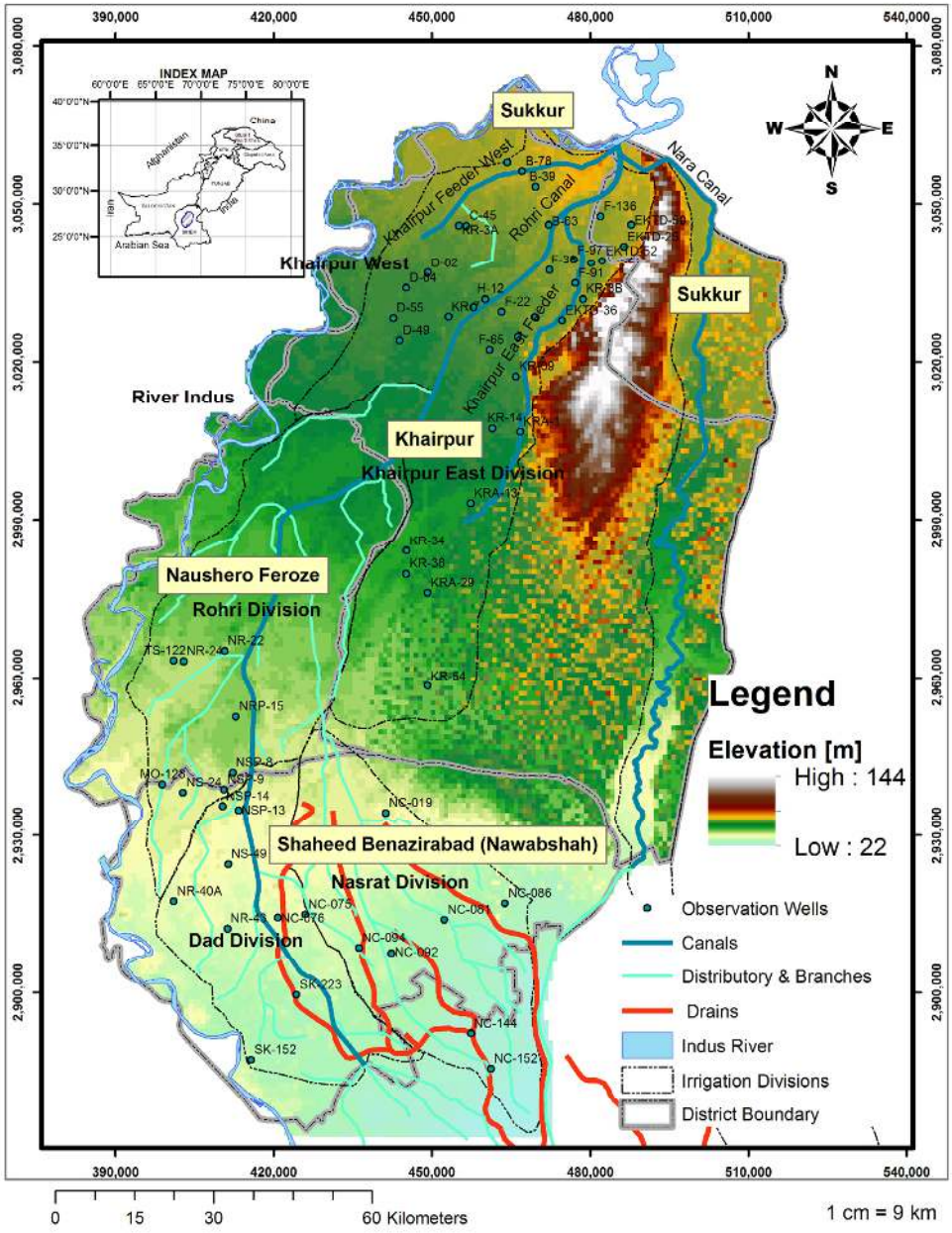

Figure 1. Location of the study area and its features (topography, rivers, canals, branches, drainage system, and observation wells).

3.2.2. Precipitation and Temperature

Average monthly temperature and precipitation data over ninety years (2010–2099) for Sindh were acquired from the Numerical Modelling Group of Research and Development Division, Pakistan Metrological Department (PMD). In the current study, RCP4.5, and RCP8.5, both medium and high-end scenario were used. Details for processing methods of the climate dataset can be found in [27].

3.2.3. Evapotranspiration

The number of weather stations with long-term or multi-parameter data records in the Indus Basin is limited and the climate data in much of the region are limited to maximum and minimum temperatures, and rainfall. For our study, we therefore used the Blaney–Criddle Equation (1) to calculate potential evapotranspiration (ETo) using temperature estimated for RC 4.5 and RCP 8.5 scenarios. This is a temperature-based method and can be calculated from the mean temperature as a function of latitude and longitude (see

Equation (1)). These data were re-gridded on the groundwater model grid of 1000 m by 1000 m using kriging interpolation.

$$ET_o = p * (0.46 * T(mean) + 8) \quad (1)$$

where *ETo* is the reference crop evapotranspiration (mm/d); $T(mean)$ is the mean daily temperature (°C); and p is the mean daily percentage of annual daytime hours.

Table 1. Summary of datasets, their resolution, and sources used in the study.

Method	Data	Spatial and Temporal Resolution	Source
Climatic Regionalisation and trend analysis	Precipitation	Monthly, 25 km × 25 km	https://www.pmd.gov.pk/rnd/rndweb/rnd_new/climchange_ar5.php (accessed on 3 January 2024)
	Temperature	Monthly, 25 km × 25 km	https://www.pmd.gov.pk/rnd/rndweb/rnd_new/climchange_ar5.php (accessed on 3 January 2024)
	Potential Evapotranspiration	Monthly, 25 km × 25 km	Derived from Temperature datasets using Blaney-Criddle approach
Groundwater model	Topography	90 m × 90 m	https://csidotinfo.wordpress.com/data/srtm-90m-digital-elevation-database-v4-1/ (accessed on 3 January 2024)
	Aquifer properties	163 borelogs spatially spread in the study area	https://doi.org/10.4225/08/5a3b567bc9004 (accessed on 3 January 2024)
	River, canal, and drainage hydraulic properties	Properties at main regulators. Interpolated at every kilometre.	Sindh Irrigation Department and Sindh Irrigation and Drainage Authority
	Initial water levels	Bi-annually from 2010 to 2014, 59 spatial points observed	SCARP Monitoring Organization, WAPDA
	Surface water supplies	Monthly	Sindh Irrigation Department and Sindh Irrigation and Drainage Authority
	Pumping	Extraction per unit square km	Estimated through survey.

3.2.4. River and Drainage Properties

The river, canal, and drainage aquifer interaction can be represented by the conductance such that the seepage from/to the river is proportional to the head in the river stage and head in the aquifer cell. In order to define the conductance, river, canal, and drainage hydraulic properties at the main regulators and control sections were collected from SID. These were digitised and interpolated for model cells.

3.2.5. Groundwater Pumping

In order to estimate the pumping, a survey was conducted to estimate a density of 5 wells per square kilometre. Most of the private tube wells have a capacity of 1–2 cusecs and pump for an average of 8 h per day. At the tail reaches, groundwater was the sole source of irrigation, and at the mid reaches, farmers used groundwater during periods of surface water shortages.

3.3. Methods

Figure 2 shows the flow chart of the overall methodology. In the first step, climatic regionalisation was carried out for Sindh using Spatial K'luster Analysis using the Tree Edge Removal (SKATER) algorithm [28]. In the second step, trend analysis was performed using Mann–Kendall and Sen's slope statistics on datasets of precipitation and potential evapotranspiration (PET) for 2010–2099 [29,30]. In the third step, a groundwater flow model using MODFLOW 2005 [31] was calibrated for the study area from October 2010 to

April 2014 and simulated until 2047 for generating future water level and budget timeseries. Then, a detail groundwater sustainability assessment was performed using these simulated timeseries of water level and water budget.

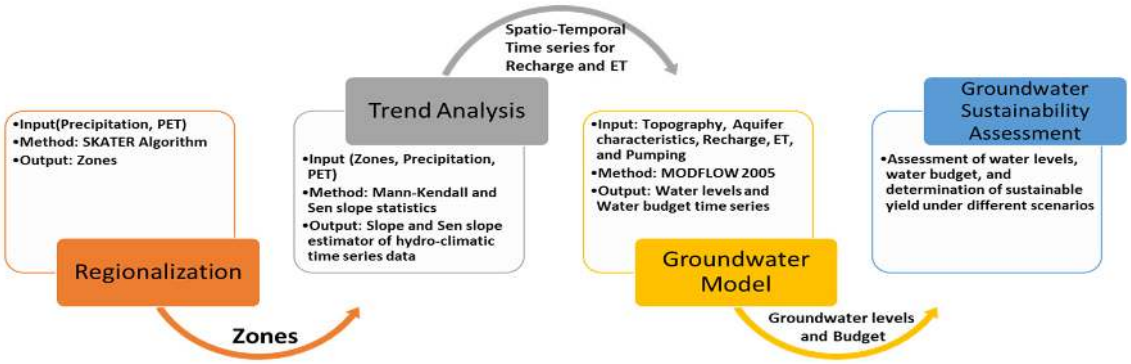

Figure 2. Flow chart for overall methodology.

3.3.1. Climate Regionalisation

Regionalising is a valuable technique used frequently in disciplines dealing with large spatial datasets. The goal is to preserve the patterns in the dataset and produce homogeneous and contiguous clusters. The SKATER method [28] was chosen to regionalise Sindh based on projected annual average precipitation and potential evapotranspiration. Its efficiency for regionalisation is because it "combines the use of a minimum spanning tree with combinational optimisation techniques" [28] (p. 809). SKATER represents the objects as graphs that captures adjacency relationships among objects as connections.

3.3.2. Trend Analysis

The Mann–Kendall trend [29] was used to detect any statistically significant trends in precipitation, potential evapotranspiration, and droughts in the future due to climate change. This is a non-parametric test and suitable for those data series where the trend is assumed to be monotonic (i.e., the trend is continuously increasing or continuously decreasing). The test was conducted on a significant level α: 0.05, meaning that there is a 5% probability that the values are from a random distribution, and with that probability, it would be erroneous to reject the null hypothesis (Ho) of no trend. For prediction of the magnitude of the true slope of hydro-climatic time series data, a non-parametric Sen's slope estimator [30] method was used.

3.3.3. Groundwater Flow Model Development

Water balance assessment was performed via calibration of the groundwater flow model (i.e., MODFLOW 2005 [31]) from October 2010 to April 2014. A monthly water balance was quantified. MODFLOW 2005 uses a continuity equation for water balance (Equation (2)) and a finite difference scheme to solve it numerically:

$$\frac{\partial}{\partial \mathrm{x}}\left(k_{fx}\frac{\partial \mathrm{h}}{\partial \mathrm{x}}\right)+\frac{\partial}{\partial \mathrm{y}}\left(k_{fy}\frac{\partial \mathrm{h}}{\partial \mathrm{y}}\right)+\frac{\partial}{\partial \mathrm{z}}\left(k_{fz}\frac{\partial \mathrm{h}}{\partial \mathrm{z}}\right)=S_o\frac{\partial \mathrm{h}}{\partial \mathrm{t}}+W_o \quad (2)$$

where h = hydraulic head; k = permeability; So = storativity; and Wo = source/sink

Model Conceptualisation and Discretisation

The conceptualisation of the various components of this hydro system is shown in Figure 3. We considered a two-layered aquifer system. The top of Layer 1 is defined by the surface topography obtained from NASA's surface radar topography mission's (SRTM) digital elevation model (DEM), which was upscaled to the model grid. The top layer, which extends from the surface to approximately 35 m, is an unconfined layer that includes the Indus River, canals, drains, and shallow private tubewells. The thickness of Layer 2 is

between 22 and 306 m, which varies based on the bottom of the aquifer as defined by borelogs. This layer includes deep private tubewells, as well as deep scavenger tubewells, which extract groundwater for disposal into drains. These layers also interact through leakage between them.

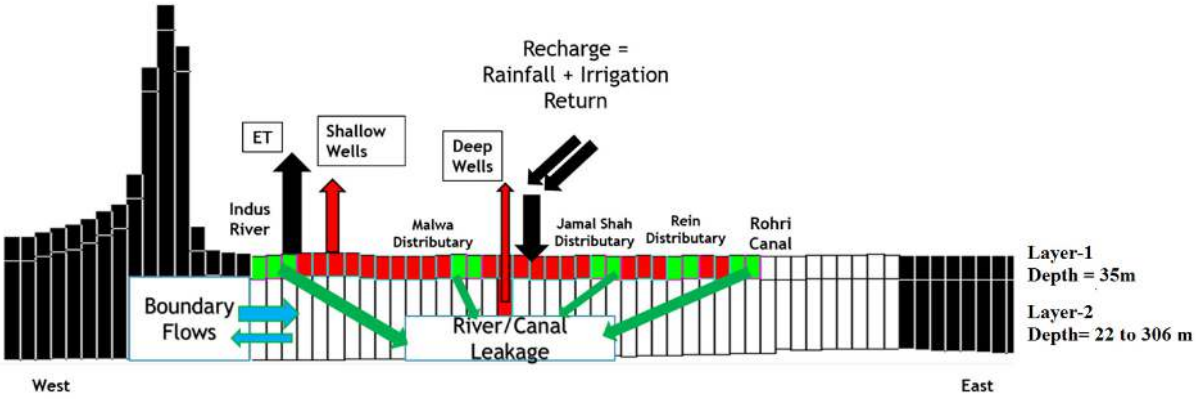

Figure 3. Model conceptualisation and typical cross-section of the model. Red cells are pumping cells, and green cells show river cells. Arrow shows the water balance components.

The sub-regional model of Sindh is bounded between 376,000 and 523,000 metres east and between 2,872,000 and 3,078,000 metres north. The spatial grid of the model is 1000 m (east) by 1000 m (north) size, with 206 rows and 147 columns. A monthly stress period divided into three time steps was considered for temporal discretisation. The model was calibrated from October 2010 to April 2014 to cover the Rabi and Kharif cropping seasons. Then, the model was simulated through to 2047 for impact assessment of climate change on the groundwater budget. Initial heads were assigned using the SMO dataset post-2015, and point data were interpolated on the model grid using kriging interpolation.

Aquifer Parameterisation

Aquifer parameterisation was performed for two-layer conceptualisation. Based on the material appearing in the borelogs, an initial value was assigned from the standard values for the material, and then kriging interpolation was performed to generate the gridded values. Based on the initial values, the distribution of conductivity and specific yield values is generally higher throughout the study area. There is also a prominent low value zone in the northeast section of the model which coincides with the outcrop areas. Table 2 shows the ranges for the initial values of the parameters. Zonation and adjustment were performed on these initial values during the calibration.

Table 2. Initial values of aquifer parameters assigned to the model.

	Kh [m/d]	Kh:Kv	Depth [m]	Sy [-]	Ss [1/m]
Layer-1	21.5 to 33	100	35	0.12 to 0.16.	1.84×10^{-4} to 8.92×10^{-6}
Layer-2	12 to 35	100	22–306	0.01 to 0.17	2.77×10^{-4} to 5.096×10^{-6}

Initial and Boundary Conditions

Initial water levels were assigned based on the initial values for October 2010. Initial water levels are generally shallow in the study area, particularly along the major canals. Therefore, direct evapotranspiration (EVT) from groundwater is expected to be high. In order to capture this phenomenon, evapotranspiration boundary condition based on extinction depth was applied. Monthly data was used for each stress period in the study area, and temporal EVT rates obtained by multiplying potential EVT with crop coefficients were used as a model input. In June and July, maximum EVT rates exceeded 300 mm per month, and varied spatially, with highest values occurring from farm fields. The extinction depth was

estimated by using 163 borelogs from the districts of Sukkur, Khairpur, Naushero Feroze, and Shaheed Benazirabad and interpreting the near surface borelog. The extinction depths assigned to each log were adopted from [32]. Major contributions to recharge are from rainfall and irrigation, so a recharge boundary was assigned to quantify these. This was estimated by aggregating recharge from rainfall, canal irrigation, and tubewell irrigation. Basin and furrow irrigation methods are widely used for supplying water to wheat, cotton, vegetable, fruit, and fodder crops during Rabi and Kharif seasons in the study area. The irrigation water supply of the canal command area was estimated for the modelled area on a monthly basis. Since surface irrigation methods are deemed to be 40 to 60 percent efficient, it was estimated that 50 to 60 percent of irrigation water in the modelled area contributed to the aquifer as recharge. The amount was adjusted spatially and temporally during the calibration process. Based on the water supply, each grid cell was assigned returns from irrigation for each monthly stress period.

The river and canals were taken as river boundary cells. The river and canal system in the model is defined by segmenting the river and canal into reaches, such that each reach resides in a single cell so that the area required for calculating conductance is taken for each grid cell. The thickness of bed material (m) is assumed to be 1, with riverbed conductivity included as a model calibration parameter. A similar approach was taken for the drainage boundary.

Calibration

Calibration is a process of varying the quantity and spatial distribution of uncertain model parameters within a probable range until a sufficient consistence of modelled and measured data is achieved. The procedure involves adjusting aquifer hydraulic properties, storage, boundary conditions, and system stresses (recharge, evaporation, river and canal–aquifer interactions) such that the model is capable of simulating both spatial and temporal responses. In this study, the strategy we adopted for calibration involved the following:

- In Step 1, we divided the aquifer into different zones based on the aquifer properties in the area. Zones were defined based on interpretation of aquifer parameters, and then units with similar properties were grouped.
- Each unit was assigned a zone number, in which a multiplier was used to adjust the input parameter values.
- In Step 2, we divided the model domain into different recharge/discharge zones based on irrigation divisions in the model domain. A multiplier was assigned for each parameter to adjust the sink and source terms in each zone, including: (i) rainfall recharge; (ii) irrigation recharge; (iii) evapotranspiration; and (iv) pumping.
- Fifty-nine observation wells were considered for calibration to compare the observed versus simulated water heads. Model calibration was performed for 42 stress periods from October 2010 to April 2014. The head measured in October 2010 (post-monsoon) was taken as the initial head condition. Observed heads were arranged for the post- and pre-monsoon season for each year from 2010 to 2014.

3.3.4. Scenario Assessment

Scenario assessment was performed to evaluate the impact of policy intervention to ensure the sustainable use of groundwater in Sindh. The starting point for these scenarios was the initial head conditions observed in October 2010. The following scenarios were assessed to establish future management policy for sustainable use of groundwater:

- Scenario 1: Baseline/no change. This scenario assumes that pumping will remain the same as for the calibrated model and is used as a base case to compare with other scenarios.
- Scenario 2: 10% decrease in surface water supply. This scenario was developed in consultation with SID to assist in understanding its impact on freshwater zones. In this scenario, water supply in the early Kharif period (i.e., April to July) was reduced by 10% of historical amounts.

- Scenario 3: 10% increased pumping. In this scenario, pumping was increased from the freshwater zone in the same early Kharif period to help identify threshold depth and time scale of depletion, thus helping to set extraction limits for the freshwater lens.
- Scenario 4: 10% increased pumping and 10% decrease in water supply. In this scenario, pumping was increased for freshwater zone while overall surface water supply was decreased for the early Kharif period to depict a water shortage scenario.
- Scenario 5: Climate change scenarios. Two scenarios were created where water balance assessment was performed using RCP 4.5 and RCP 8.5 time-series climatic predictions input data.

4. Results

4.1. Regionalisation

Given the significant climate variability across Sindh, the province was divided into five homogenous regions using the SKATER algorithm, drawing on two factors: the spatial contiguity of the dataset, and similarity of key parameters, being the average annual precipitation and PET. These five zones are shown in Figure 4a. Zone 1 (Central) covers the Khairpur, Naushero Feroze, Shaheed Benazirabad, Sanghar, Hyderabad, Dadu, Tando Allahyar, and Matiari districts. Zone 2 (South-Eastern) includes the desert districts of Umar Kot, Badin, and Tharparkar. Zone 3 (Upper) includes districts with high temperatures like Kashmore–Kandhkot, Jacobabad, Ghotki, Sukkur, Shikarpur, Larkana, and Qambar Shahdadkot. Zone 4 (South-Western) contains the districts of Sujawal, Thatta, and lower parts of Karachi. Zone 5 (West) includes Jamshoro and upper parts of the Karachi district. The following sections provide the statistical analysis of spatiotemporal variability for the two climate parameters. The focus of the study is on the intensively cultivated areas of northern Rohri, which includes the Central and Upper Zones (1 and 3).

4.2. Spatiotemporal Precipitation Trends for Northern Rohri CCA

Tables for precipitation trend analysis results are provided as Supplementary Material. The analysis shows future precipitation increasing in the south-eastern Zone 2 for both RCP scenarios, especially in the Tharparkar district. Our study area of interest (AOI), the Northern Rohri CCA, shows a non-significant increasing trend of precipitation in both scenarios. The RCP 4.5 scenario analysis for Zones 1 and 3, wherein our study area is located, reveals that maximum average precipitation (mm/day) and standard deviations are high for the months of July, August, and September, especially for Zone 1 (the southern areas of our study area). The Mann–Kendall (MK) monthly precipitation trends for both these zones show an increasing trend for March and for September to December and a decreasing trend for other months. There is a significantly decreasing trend early in the monsoon period (July and July) for both zones, which suggests a delay in the monsoon period that historically occurs from June to September towards the months of August to October. Sen's slope (Q) analysis shows the magnitude of the trends in mm/year, which for both zones are significantly negative for June to August, but positive for September to November. According to the RCP 8.5 high emission scenario analysis, the maximum average precipitation and standard deviations are again high in both Zones 1 and 3 for the months of August and September, and mostly higher than for the RCP 4.5 scenario. The Mann–Kendall monthly precipitation trends show an increasing trend for a longer period from January through to March as well as for September to December for both zones. The trend for the RCP 8.5 scenario again suggests a delay in the monsoon with a significantly decreasing trend in participation for June and July, coupled with a highly significant increase in future winter precipitation. Sen's slope (Q) analysis reveals that the magnitude of precipitation trend in the first five months of the year is approximately zero, significantly negative for June to August, and significantly positive for September to December.

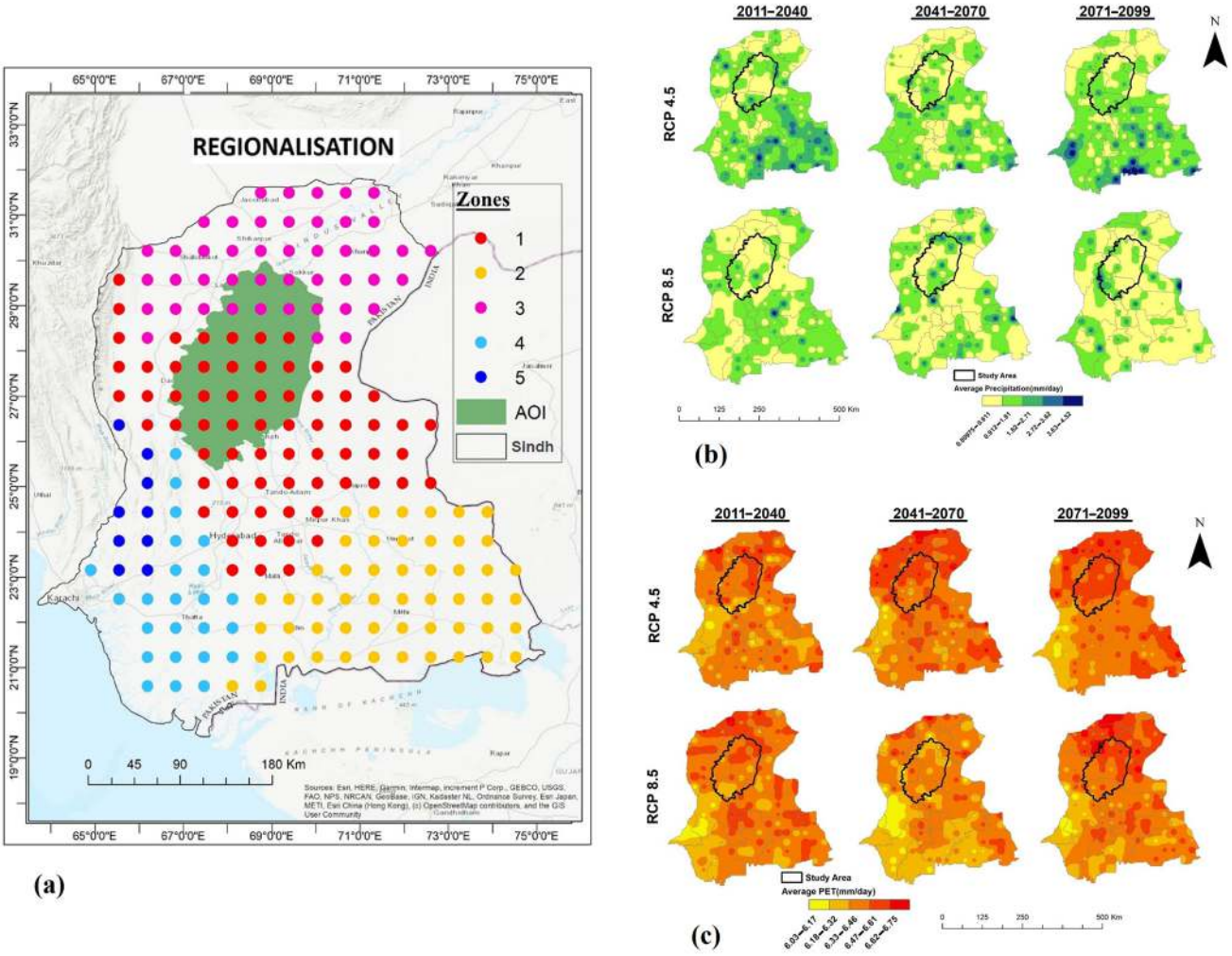

Figure 4. (**a**) Climate zones produced after running the SKATER algorithm; (**b**) spatiotemporal pattern of precipitation (mm); (**c**) spatiotemporal pattern of potential evapotranspiration. AOI refers to the Northern Rohri CCA as our area of interest and is replicated across all maps.

4.3. Spatiotemporal Potential Evapotranspiration Trends (PET) for Northern Rohri CCA

After calculating PET using Blaney Criddle's equation, the spatiotemporal trends for Sindh were analysed. Tables for PET trend analysis results are provided as Supplementary Material. Significantly increasing PET trends are observed in Zone 3 for all three future periods shown, and a generally increasing trend is observed for our study area under both scenarios. Under the RCP 4.5 scenario, the PET trends for Zones 1 and 3 greatly increased over time in summer, while they decreased during winter months. The Mann–Kendall (Z) and Sen's slope (Q) analyses both show negative PET trends from March to May for both zones.

Under the RCP 8.5 scenario, PET is at its maximum in June and July, with a high increase in PET across the summer months. The Mann–Kendall and Sen's slope analyses reveal negative trends for just two months (March and April), with a highly increasing PET trend for all remaining months.

4.4. Groundwater Model Calibration

Figure 5 shows spatial calibration for 59 observation points obtained at the end of the model calibration period (April 2014). At the end of the model calibration, most (39) piezometers in the study area showed a low residual value (i.e., a difference between the observed and the simulated water levels) in the range of 0–1 m, with 20 having a higher

residual, mostly located towards the northern end (18 in the range of 1–2 m, and two greater than 2 m). A root mean square value of 0.82 and absolute mean error of 0.62 m were obtained, suggesting an acceptable calibration of the simulated water levels over the model domain.

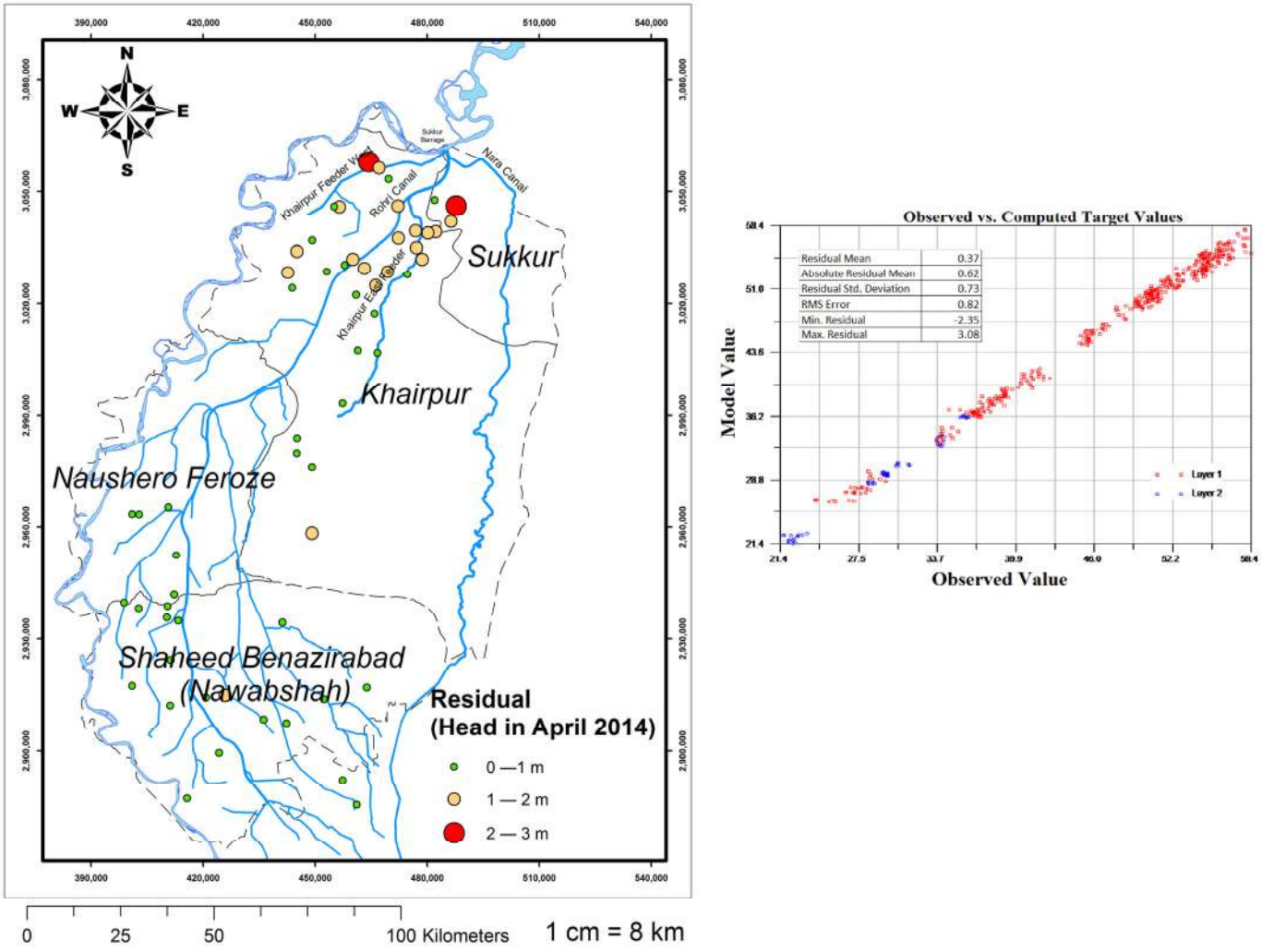

Figure 5. Calibration statistics.

The observed levels during the calibration in each irrigation division showed groundwater level declines in response to pumping as well as recovery following monsoonal rainfall recharge. Almost all pumping in the model domain is from the shallow (Layer 1) watertables that had developed due to rainfall, canal seepage, and irrigation return flows. These shallow freshwater lenses provide an opportunity for farmers to extract groundwater for irrigation. The bore responses show that water levels are either stable or declining by less than 1 m during the calibration period (October 2010 to April 2014). This result is reassuring given that approximately 3 BCM of groundwater is used annually in this area by farmers as supplementary irrigation when surface water supplies are inadequate. However, improved monitoring is required in areas with declining water levels to ensure the water quality of the freshwater lens does not decline at current extraction rates. Access to this groundwater allows farmers to maintain crop productivity and is an important supplementary source safeguarding their livelihoods.

4.5. Modelled Water Balance

The modelled water balance we undertook for Layers 1 and 2 for the period 2010 to 2014 confirms that the major inflow to Layer 1 is recharge (3.943 BCM) followed by an upward flow from Layer 2 (2.051 BCM), with the Indus contributing 1.16 BCM. Recharge from the Indus has been curtailed in recent times due to the construction of levies to control flooding during high flows, and significant upstream diversions. In its natural state, the Indus would have more frequently breached its banks during monsoon floods. The reduced recharge from the river has now been supplemented by increased recharge from canal seepage and irrigation. Significant outflows from Layer 1 are a result of pumped extractions (2.942 BCM) and the downward flow of groundwater to Layer 2 (2.48 BCM). The overall movement of water between Layers 1 and 2 indicates that Layer 1 is, on balance, contributing to inflows to Layer 2. It is important to ensure that an overall reversal of these gradient flows does not occur as this would lead to salinity transport from the lower layer to the upper layer, with the increased salinity in the upper layer likely to reduce crop productivity and thus undermine farming family livelihoods. The other significant loss from the top layer is through evapotranspiration (1.606 BCM), indicating the prevalence of shallow watertables in the model area.

In addition to the downward inflows to Layer 2 from Layer 1, there is a small amount of Layer 2 recharge occurring near the Kirther formation outcrop in the Khairpur district. However, the largest outflows from Layer 2 are actually upward flows to Layer 1, indicating that, in some areas of the model, groundwater pumping has become so significant that gradients between the layers may have reversed and an upward flow is occurring. This will need to be managed to avoid upward transport of deeper dissolved salts, reducing the useability of freshwater lenses in the upper layer. The other major outflow from Layer 2 involves boundary outflows (0.859 BCM) along the model's eastern boundary towards the Thar Desert. There is also a small amount of pumping by SCARP tubewells from Layer 2 (0.307 BCM) which is used for vertical drainage. This is where groundwater from the deeper layer is pumped into drainage channels so that the saline water can be removed via the Left Bank Outfall Drain (LBOD) to the sea.

4.6. Modelled Water Balance for the Longer-Term Scenario

The water balance for the scenarios based on historical climatic cycles is presented in Table 3. All values are in BCM and are averaged over the 32 years of simulation. In the baseline scenario, the two major components of the water balance inflows are recharge from irrigation and river/canal leakages (4.282 BCM). The major outflow is from wells (3.619 BCM) and evapotranspiration (1.754 BCM). The net loss for the baseline scenario is −1.244 BCM, which is equivalent to a 73 mm/year decline in average water levels. Reducing canal supplies by 10% during early Kharif (Scenario 2) will not have a significant change in the average groundwater recharge over the simulation period as compared with the baseline scenario. Net storage will only decrease slightly from −1.244 (baseline) to −1.343 BCM (Scenario 2). The 10% increase in pumping scenario will reduce net storage from −1.244 to −1.436 BCM, which represents an almost 15% decline in net storage compared with the baseline scenario. If both a 10% increase in pumping and 10% decrease in recharge were to take place simultaneously (Scenario 4), then the net loss in storage for the model increases from −1.244 (baseline) to −1.535 BCM, which is equivalent to a decline in water levels of 90 mm per year.

Under the climate change scenarios RCP 4.5 and RCP 8.5, the net loss in storage increases substantially to −2.815 and −2.214 BCM, respectively. This outcome results from the projected lower rainfall and higher temperatures, which would drive higher evapotranspiration, especially in the RCP 8.5 scenario. The recharge in the system decreases from 3.944 BCM to 3.769 (for RCP 4.5) and 3.732 BCM (for RCP 8.5) compared with the baseline scenario. In response to high projected temperatures, outflow due to evapotranspiration is seen to increase by approximately 36–38% in RCP 4.5 and RCP 8.5 scenarios compared with the baseline scenario. All other water balance terms remain unchanged, except drainage

outflows, which reduce from 0.47 (baseline) to 0.27 (RCP 4.5 and 8.5) due to a lowering of the watertables from higher rates of evapotranspiration.

Table 3. Water balance assessments for Scenario 1 (baseline); Scenario 2 (10% reduced canal supplies); Scenario 3 (10% increased pumping); Scenario 4 (10% reduced canal supplies and 10% increased pumping); and the RCP 4.5 and RCP 8.5 climate change scenarios. All values are in BCM and averaged over the simulation period.

Inflows	**Calibrated**	**Scenario 1**	**Scenario 2**	**Scenario 3**	**Scenario 4**	**RCP 4.5**	**RCP 8.5**
Boundary	0.071	0.077	0.079	0.079	0.081	0.128	0.131
Wells	0	0	0	0	0	0	0
Drains	0	0	0	0	0	0	0
River Leakage	1.16	1.094	1.096	1.099	1.101	1.153	1.16
ET	0	0	0	0	0	0	0
Recharge	3.944	4.282	4.162	4.282	4.162	3.769	3.732
Total Inflows	5.175	5.453	5.337	5.46	5.344	5.049	5.023
Outflows	**Calibrated**	**Scenario 1**	**Scenario 2**	**Scenario 3**	**Scenario 4**	**RCP 4.5**	**RCP 8.5**
Boundary	0.859	0.972	0.965	0.969	0.962	0.837	0.831
Wells	3.25	3.619	3.619	3.826	3.826	3.619	3.619
Drains	0.467	0.294	0.285	0.289	0.28	0.271	0.27
River Leakage	0.033	0.059	0.058	0.059	0.058	0.05	0.049
ET	1.606	1.754	1.754	1.754	1.754	2.458	2.468
Recharge	0	0	0	0	0	0	0
Total Outflows	6.215	6.697	6.68	6.897	6.879	7.234	7.237
Net	−1.04	−1.244	−1.343	−1.437	−1.535	−2.185	−2.214

4.7. Water Level Assessment under Different Scenarios

The spatial distribution of groundwater depths for the calibrated model and various scenarios is shown in Figure 6, with modelled temporal trends in watertable levels for selected piezometers shown in Figure 7. Depth to water (DTW) levels are divided into categories: waterlogged (dark blue in Figure 6); shallow watertables (0–1.5 m and 1.5–3.0 m—lighter blue); moderate water levels (3.0–10 m—yellow and orange); and deep water levels (>10 m—pink and red). For 2015, across all canal command areas, DTW is in the shallow or moderate watertable category. Shallow watertables can be seen at the head and mid reaches of distributaries, whereas DTW falls to moderate levels at the tail reaches, especially for canal command areas near the Indus River. This is because tail reaches near the Indus River comprise areas with more substantial reserves of non-saline groundwater that is extensively used for irrigation. DTW levels in non-irrigated areas are deeper as these areas are distanced away from where most of the recharge occurs (i.e., from irrigation return flows, canal leakage, and river inflows). In non-irrigated areas, the only source of recharge is from surrounding boundaries or from precipitation, which is minimal. For the baseline scenario, DTW levels by 2047 in the Khairpur East (KE) irrigation division are expected to change from moderate to deep, indicating declining trends. Most of KE will have DTW levels between 10 and 15 m, except the riverine area, which will maintain its moderate water levels. Such a large decline in DTW levels will deteriorate groundwater quality significantly. It is worth noting, however, that, in the simulation, the extent of groundwater extraction was not constrained. Realistically, farmers will stop pumping groundwater when its quality makes it unusable. If farmers continue pumping beyond this limit due to water shortages, then the resulting increased accumulation of salts in the root zone will have an adverse impact on agriculture land and productivity.

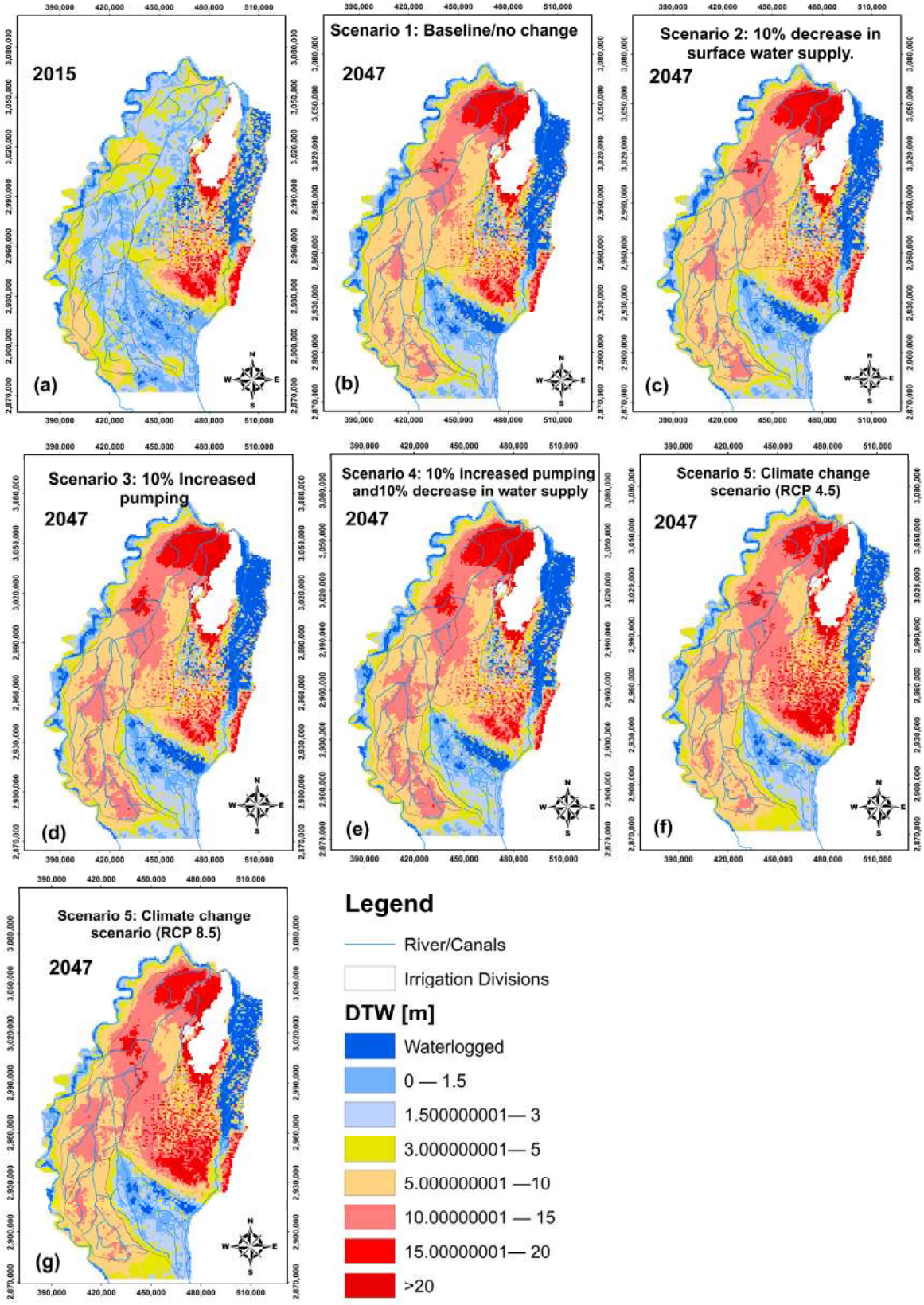

Figure 6. Spatial distribution of depth to groundwater level from top of natural surface in 2015 for: (**a**) depth to water level in 2015 for calibrated model; and in 2047 for (**b**) baseline scenario; (**c**) 10% decrease surface water supplies; (**d**) 10% increase in pumping; (**e**) increase in pumping and 10% decrease surface water supplies; (**f**) RCP 4.5; (**g**) RCP 8.5.

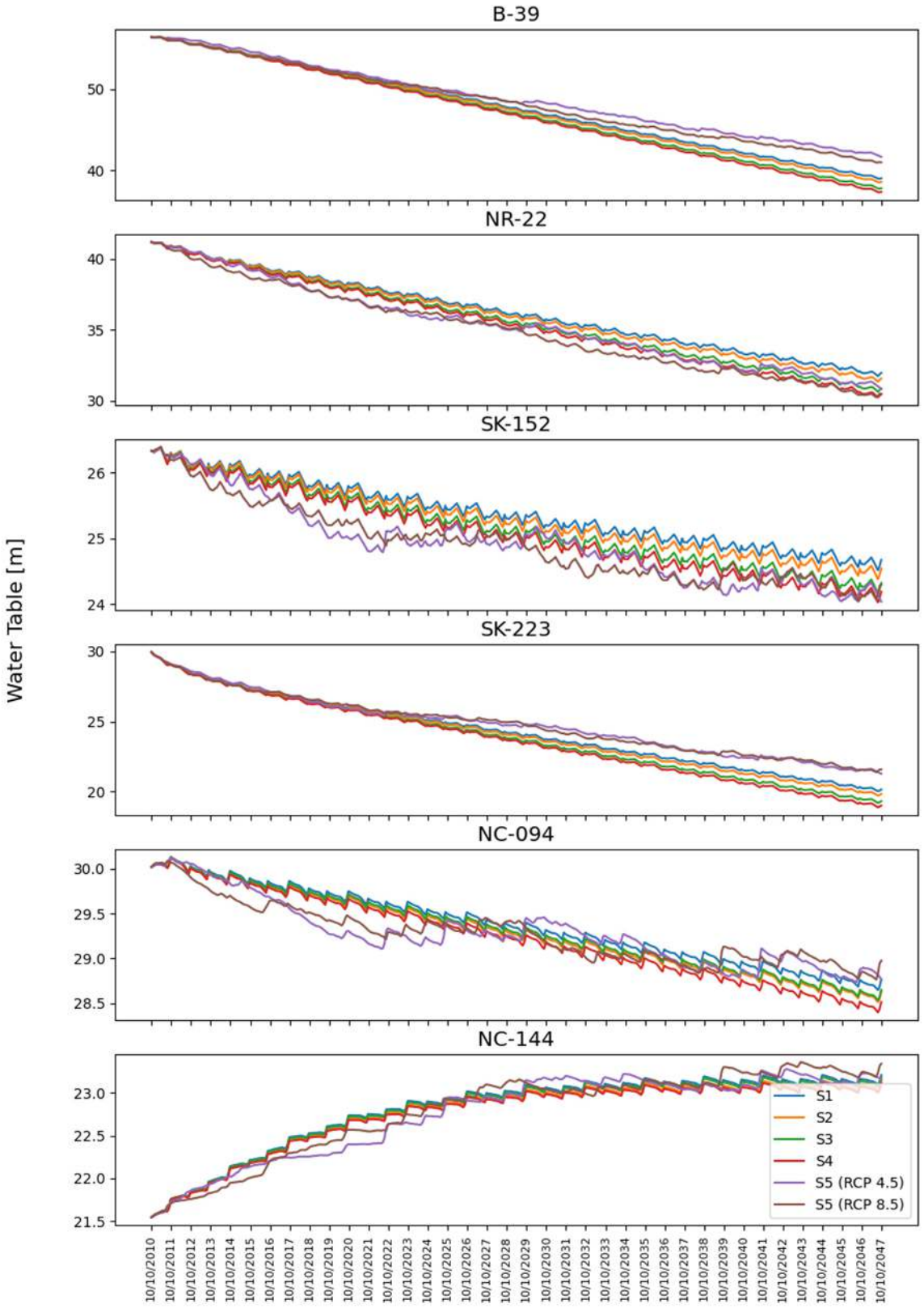

Figure 7. Simulated heads [mMSL] for selected monitoring points. The locations of these points are shown in Figure 1.

Climate change scenarios also showed lowering trends for DTW, but the gradient of decline was less constant (see purple and brown lines in Figure 7). For two monitoring locations (SK-152 and NC-094), the DTW trends over time sometimes increased but mostly

decreased, with the DTW in 2047 ending up similar to that for the baseline scenario. For two other monitoring locations (B-39 in the north and SK-223 in the south), the gradient diverges from that of the baseline scenario after the year 2028, showing a less pronounced decline, and DTW for the climate change scenarios, ending up 5 m higher than for the baseline scenario. One monitoring location in Nasrat irrigation division (NC-144) revealed a reverse trend, with DTW ending up at a higher level for all scenarios due to very low groundwater extractions at that location, an area of flat topography. This trend indicates that drainage will play an important role in such areas to minimise waterlogging from rising watertables and thus maintain agricultural productivity.

5. Discussion

Given climate variability in Sindh, the region was divided into five contiguous zones using the SKATER algorithm technique based on two climate parameters: precipitation and potential evapotranspiration. Analysis of the zones generated for the Northern Rohri CCA showed a negative trend for monsoon precipitation for both RCP 4.5 and RCP 8.5 climate scenarios and a delay in monsoon occurrence. Potential evapotranspiration showed a decreasing trend in winter season and a significantly increasing trend in summer in both scenarios.

The groundwater budget for the Norther Rohri CCA model indicated that river–aquifer connectivity, canal recharge, evapotranspiration, and groundwater pumping for irrigation were significant components for the upper layer of the aquifer, and, for the lower layer, interlayer leakage and pumping of saline water are important considerations. The results showed that the net loss in storage over the simulation period from October 2010 to April 2014 was -1.04 BCM/year. The net decline in storage in Layer 1 was -0.374 BCM and -0.665 in Layer 2. The sustainable yield was estimated at 3 ± 0.3 BCM to allow for adaptive management during times of drought and inadequate surface supplies and to safeguard livelihoods. For the RCP 4.5 scenario, the net loss in storage over the simulation period for 2010–2047 was -2.185 BCM/year (compared with -1.04 BCM/year for the baseline scenario). The net decline in storage was -0.625 BCM/year in Layer 1 and -1.558 BCM/year in Layer 2. For the RCP 8.5 scenario, the net loss in storage over the simulation period (2010–2047) was -2.214 BCM/year as compared with the baseline scenario (-1.04 BCM/year).

Groundwater level trends show an overall declining trend. This is concerning given that the freshwater lens in Sindh is a few metres thick and overlies deeper saline groundwater. A lack of access to groundwater in the future will force farmers to reduce cropping intensity with consequent adverse impacts on food security and the need to increase food imports. Continued use of groundwater in this environment will need to be accompanied by investments in water productivity to minimise adverse impacts of waterlogging and salinisation, and to preserve the freshwater lenses for the future of groundwater irrigation in Sindh. As climatic conditions become more challenging, management rules will be needed for pumping from the freshwater zones in the upper layer to avoid salinisation of the aquifer.

Our regionalised analysis, as exemplified by the Norther Rohri CCA groundwater model and budget, also provides implications for strategies that can be adopted to achieve the above-referred measures needed to secure groundwater yields that are sustainable and to avoid waterlogging and salinisation. This is the first time an estimate of sustainable yield has been made for this important agricultural region of Sindh and this will provide the irrigation authorities with guidance on groundwater planning, which in the past has largely been ignored. Our approach has led to recommendations that groundwater management strategies be developed at regional (irrigation division) scales [33,34], drawing on similar strategies adopted in Australia. In Australia, long-term sustainable yields are determined for specific groundwater management areas through agreement with users [35,36]. These area-specific sustainable yields can be revised after 5 to 10 years of application according to

agreements that have been made with groundwater users, or in response to droughts or increased development of groundwater use in the management area.

Such a regionalised process could be developed for groundwater management areas in Sindh, which would rely on having revised and improved groundwater models in place. These would enable SID, as the manager of these water resources, to develop an improved understanding of risks to groundwater from overexploitation and salinity intrusion, as well as to support SID's capacity to meet objectives of both the National and Sindh Water Policies. The importance that the National Water Policy has placed on groundwater will require significant investment in building capacity within SID to improve management of groundwater. With effective stakeholder engagement, this will ensure an equitable framework can be developed for sustainable management of groundwater [36,37].

Setting an allocation limit based on an assessment of sustainable yield does not necessarily mean hotspots will not occur, particularly in groundwater systems in the LIB. With increasing pressures on groundwater resources, resource managers recognise that despite an overall sustainable yield for a groundwater management area, localised areas of declining groundwater levels and quality would require water level response management, especially for systems nearing full allocation [35]. Future management of groundwater in the Indus Basin will thus require improved strategies focused on hotspots where sustainable future use of groundwater is critical.

The model simulated declining groundwater levels across all five SID divisions that traverse the area. Expansion of groundwater abstractions in all divisions except Nasrat should be monitored meticulously, with allocation limits adopted in consultation with users to manage hotspots and to ensure groundwater availability with suitable quality is maintained for future users. Most of the Nasrat division has poor groundwater quality, so the likelihood of additional pumping is low. However, shallow watertable management may be required to limit the spread of waterlogging and salinity. This could be achieved by adopting crops that use less water, improving irrigation management practices, and land management. Systematic monitoring of groundwater in the Northern Rohri CCA is essential to allow irrigation agencies and farming communities to improve the management of groundwater and to allow model extension to account for the increased number of tubewells and ensure the robustness of calibration.

6. Conclusions

The canal command areas supplied from the left bank of the Sukkur Barrage is considered the food basket for the people of Sindh province. Farmers across these areas add substantially to the provincial and national economy through their agricultural activities while also supporting the livelihoods of their families by making good use of the human, land, and water resources available to them. It is important, therefore, that use of these resources is managed sustainably, especially given the projected impacts of climate change, which is expected to be felt especially severely by Pakistan [11]. Our above regional assessment of the impacts from climate change and other factors on groundwater offers tangible benefits for planning and managing the resource for the Northern Rohri CCA in particular. Based on the assessment, it can be concluded that Sindh can be divided into five zones for future climate change assessment. In Upper Sindh and Central Sindh, there will be no significant changes in precipitation but evapotranspiration will increase. This increase will affect the groundwater use zones in the area. In order to sustain the groundwater resources of the Northern Rohri CCA, which is the most important groundwater extraction zone, a sustainable yield would need to be no greater than $3 \pm (0.3)$ BCM. In order to sustain agriculture land in shallow zones, we recommend that an allowance of 10% of the sustainable yield (0.3 BCM) would allow farmers to increase extraction during drought years, which could then be replenished when rainfall and surface water flows increase. As the impacts of climatic change intensify, groundwater managers will need to collaborate with users to modify how much is pumped from upper-level freshwater zones to avoid increased salinisation of the aquifer.

Supplementary Materials: The following supporting information can be downloaded at: https://www.mdpi.com/article/10.3390/su16010441/s1.

Author Contributions: Conceptualisation, J.F.P., M.M. and W.A.; methodology, J.F.P. and W.A.; validation, W.A., J.F.P. and M.S.E.; formal analysis, W.A. and S.A.; investigation, W.A., J.F.P. and S.A.; resources, A.L.Q.; data curation, S.A., W.A. and G.H.D.; writing—original draft preparation, W.A. and S.A.; writing—review and editing, M.M., J.F.P. and W.A.; visualisation, S.A., G.H.D. and W.A.; supervision, A.L.Q., G.H.D. and M.S.E.; project administration, A.L.Q.; funding acquisition, J.F.P. and M.M. All authors have read and agreed to the published version of the manuscript.

Funding: This research was funded by the Australian Centre for International Agricultural Research (ACIAR) (Project No. LWR-2015-036), with additional funds provided by Charles Sturt University.

Data Availability Statement: Model data and code can be made available on request.

Acknowledgments: We acknowledge that material and data were provided by SCARP's Monitoring Organization (SMO), WAPDA, Pakistan, and Sindh Irrigation Department, Government of Sindh, Pakistan. We also acknowledge the Numerical Modelling Group of Research and Development Division of the Pakistan Metrological Department (PMD) for providing access to precipitation and evapotranspiration data for Pakistan. Finally, we acknowledge with much gratitude the support and guidance provided by Evan Christen and Robyn Johnston, ACIAR's Water Research Program Managers, who had a deep understanding of the importance of groundwater in Pakistan.

Conflicts of Interest: The authors declare no conflict of interest.

References

1. Qazi, M.A.; Khattak, M.A.; Khan, M.S.A.; Chaudhry, M.N.; Mahmood, K.; Akhter, B.; Iqbal, N.; Ilyas, S.; Ali, U.A. Spatial distribution of heavy metals in ground water of Sheikhupura district Punjab, Pakistan. *J. Agric. Res.* **2014**, *52*, 99–110.
2. Qureshi, A.S.; Gill, M.A.; Sarwar, A. Sustainable groundwater management in Pakistan: Challenges and opportunities. *Irrig. Drain.* **2010**, *59*, 107–116. [CrossRef]
3. Qureshi, R.H.; Ashraf, M. *Water Security Issues of Agriculture in Pakistan*; Pakistan Academy of Sciences: Islamabad, Pakistan, 2019.
4. Qureshi, A.S. Groundwater governance in Pakistan: From colossal development to neglected management. *Water* **2020**, *12*, 3017. [CrossRef]
5. Watto, M.A.; Mitchell, M.; Akhtar, T. Pakistan's water resources: Overview and challenges. In *Water Resources of Pakistan: Issues and Impacts*; Watto, M.A., Mitchell, M., Bashir, S., Eds.; Springer: Cham, Switzerland, 2021; pp. 1–12.
6. Khattak, A.; Ahmed, N.; Hussain, I.; Qazi, M.A.; Khan, S.A.; Rehman, A.-U.; Iqbal, N. Spatial distribution of salinity in shallow groundwater used for crop irrigation. *Pak. J. Bot.* **2014**, *46*, 531–537.
7. Punthakey, J.F.; Khan, M.R.; Riaz, M.; Javed, M.; Zakir, G.; Usman, M.; Amin, M.; Ahmad, R.N.; Blackwell, J.; Richard, C.; et al. *Optimising Canal and Groundwater Management to Assist Water User Associations in Maximizing Crop Production and Managing Salinisation in Australia and Pakistan: Assessment of Groundwater Resources for Rechna Doab, Pakistan*; Ecoseal Developments Pty Ltd.: Roseville, Australia, 2015.
8. Watto, M.A.; Mugera, A.W.; Kingwell, R.; Saqab, M.M. Re-thinking the unimpeded tube-well growth under the depleting groundwater resources in the Punjab, Pakistan. *Hydrogeol. J.* **2018**, *26*, 2411–2425. [CrossRef]
9. Basharat, M.; Tariq, A.-u.-R. Groundwater modelling for need assessment of command scale conjunctive water use for addressing the exacerbating irrigation cost inequities in LBDC irrigation system, Punjab, Pakistan. *Sustain. Water Resour. Manag.* **2015**, *1*, 41–55. [CrossRef]
10. Bhutta, M.N.; Alam, M.M. Prospectives and limits of groundwater use in Pakistan, Groundwater research and management: Integrating science into management decisions. In Proceedings of the IWMI-ITP-NIH International Workshop, Roorkee, India, 8–9 February 2005; Sharma, B.R., Villholth, K.G., Sharma, K.P., Eds.; IWMI: Colombo, Sri Lanka, 2006; pp. 105–114.
11. Eckstein, D.; Hutfils, M.-L.; Winges, M. Global Climate Risk Index 2019. Who Suffers Most from Extreme Weather Events? Germanwatch Briefing Paper: Bonn, Germany, 2018.
12. Parry, M.L.; Canziani, J.P.; van der Linden, P.J.; Hanson, C.E. *Contribution of Working Group II to the Fourth Assessment Report of the Intergovernmental Panel on Climate Change 2007*; Cambridge University Press: Cambridge, UK, 2007.
13. Crosbie, R.S.; McCallum, J.L.; Harrington, G.A. *Diffuse Groundwater Recharge Modelling across Northern Australia. A Report to the Australian Government from the CSIRO Northern Australia Sustainable Yields Project. CSIRO Water for a Healthy Country Flagship, Australia*; CSIRO: Canberra, Australia, 2009.
14. Ashraf, A.; Ahmad, Z. Regional groundwater flow modelling of Upper Chaj Doab of Indus Basin, Pakistan using finite element model (Feflow) and geoinformatics. *Geophys. J. Int.* **2008**, *173*, 17–24. [CrossRef]
15. Khan, H.F.; Yang, Y.C.E.; Ringler, C.; Wi, S.; Cheema, M.J.M.; Basharat, M. Guiding groundwater policy in the Indus Basin of Pakistan using a physically based groundwater model. *J. Water Resour. Plan. Manag.* **2017**, *143*, 05016014. [CrossRef]

16. Ahmed, W.; Rahimoon, Z.A.; Oroza, C.A.; Sarwar, S.; Qureshi, A.L.; Punthakey, J.F.; Arfan, M. Modelling groundwater hydraulics to design a groundwater level monitoring network for sustainable management of fresh groundwater lens in Lower Indus Basin, Pakistan. *Appl. Sci.* **2020**, *10*, 5200. [CrossRef]
17. Chandio, A.S.; Lee, T.S.; Mirjat, M.S. The extent of waterlogging in the lower Indus Basin (Pakistan): A modeling study of groundwater levels. *J. Hydrol.* **2012**, *426–427*, 103–111. [CrossRef]
18. Kori, S.M.; Qureshi, A.L.; Lashari, B.K.; Memon, N.A. Optimum strategies of groundwater pumping regime under scavenger tubewells in Lower Indus Basin, Sindh, Pakistan. *Int. Water Technol. J.* **2013**, *3*, 138–145.
19. Hunting Technical Services Limited; Sir Mott MacDonald & Partners Ltd. *The Lower Indus Report*; West Pakistan Water and Power Development Authority: Lahore, Pakistan, 1965.
20. Bennett, G.D.; Rehman, A.U.; Sheikh, J.A.; Ali, S. *Analysis of Pumping Tests in the Punjab Region of West Pakistan, Geological Survey Water-Supply Paper 1608-G, Prepared in Cooperation with the W Pakistan Water & Power Dec Authority under US AID*; U.S. Government Printing Ofiice: Washington, DC, USA, 1969.
21. Sir Mott MacDonald & Partners Ltd. *LBOD Stage 1 Project, Mirpurkhas, Pilot Study: Hydrogeology, Special Wells, Preliminary Well Design, Well Numbers and Spacing*; Technical Report Annexes 1–6; Mott MacDonald: Croydon, UK, 1990.
22. Bonsor, H.C.; MacDonald, A.M.; Ahmed, K.M.; Burgess, W.G.; Basharat, M.; Calow, R.C.; Dixit, A.; Foster, S.S.D.; Gopal, K.; Lapworth, D.J.; et al. Hydrogeological typologies of the Indo-Gangetic basin alluvial aquifer, South Asia. *Hydrogeol. J.* **2017**, *25*, 1377–1406. [CrossRef] [PubMed]
23. MacDonald, A.M.; Bonsor, H.C.; Ahmed, K.M.; Burgess, W.G.; Basharat, M.; Calow, R.C.; Dixit, A.; Foster, S.S.D.; Gopal, K.; Lapworth, D.J.; et al. Groundwater quality and depletion in the Indo-Gangetic Basin mapped from in situ observations. *Nat. Geosci.* **2016**, *9*, 762–766. [CrossRef]
24. Iqbal, N.; Ashraf, M.; Imran, M.; Salam, H.A.; ul Hasan, F.; Khan, A.D. *Groundwater Investigations and Mapping the Lower Indus Plain*; Pakistan Council of Research in Water Resources (PCRWR): Islamabad, Pakistan, 2020.
25. Alamgir, A.; Khan, M.A.; Schilling, J.; Shaukat, S.S.; Shahab, S. Assessment of groundwater quality in the coastal area of Sindh province, Pakistan. *Environ. Monit. Assess.* **2016**, *188*, 78. [CrossRef] [PubMed]
26. Podgorski, J.E.; Eqani, S.A.M.A.S.; Khanam, T.; Ullah, R.; Shen, H.; Berg, M. Extensive arsenic contamination in high-pH unconfined aquifers in the Indus Valley. *Sci. Adv.* **2017**, *3*, e1700935. [CrossRef] [PubMed]
27. Burhan, A.; Waheed, I.; Syed, A.A.B.; Rasul, G.; Shreshtha, A.B.; Shea, J.M. Generation of high–resolution gridded climate fields for the Upper Indus River Basin by downscaling CMIP5 outputs. *J. Earth Sci. Clim. Change* **2015**, *6*, 1000254. [CrossRef]
28. Assunção, R.M.; Neves, M.C.; Câmara, G.; Da Costa Freitas, C. Efficient regionalization techniques for socio-economic geographical units using minimum spanning trees. *Int. J. Geogr. Inf. Sci.* **2006**, *20*, 797–811. [CrossRef]
29. Mann, H.B. Nonparametric tests against trend. *Econometrica* **1945**, *13*, 245–259. [CrossRef]
30. Sen, P.K. Estimates of the regression coefficient based on Kendall's Tau. *J. Am. Stat. Assoc.* **1968**, *63*, 1379–1389. [CrossRef]
31. Harbaugh, A.W. *MODFLOW-2005, the U.S. Geological Survey Modular Ground-Water Model—The Ground-Water Flow Process*; US Department of the Interior; US Geological Survey: Reston, VA, USA, 2005.
32. Shah, N.; Nachabe, M.; Ross, M. Extinction depth and evapotranspiration from ground water under selected land covers. *Groundwater* **2007**, *45*, 329–338. [CrossRef]
33. Punthakey, J.; Ashfaq, M.; Allan, C.; Mitchell, M. *Improving Groundwater Management to Enhance Agriculture and Farming Livelihoods in Pakistan: Final Report*; ACIAR Report No. FR2021-056; Australian Centre for International Agricultural Research: Canberra, Australia, 2021.
34. Ahmed, W.; Ejaz, M.S.; Memon, A.; Ahmed, S.; Sahito, A.; Qureshi, A.L.; Khan, M.R.; Memon, K.S.; Khero, Z.; Lashari, B.K.; et al. *Improving Groundwater Management to Enhance Agriculture and Farming Livelihoods: Groundwater Model for Left Bank Command of Sukkur Barrage in Khairpur, Naushero Feroze, and Shaheed Benazirabad Districts*; ILWS Report No 159; Institute for Land, Water and Society; Charles Sturt University: Albury, Australia, 2021.
35. Pierce, D.; Cook, P. Conceptual approaches, methods and models used to assess extraction limits in Australia: From sustainable to acceptable yield. In *Sustainable Groundwater Management: A Comparative Analysis of French and Australian Policies and Implications to Other Countries*; Rinaudo, J.-D., Holley, C., Barnett, S., Montginoul, M., Eds.; Springer: Cham, Switzerland, 2020; pp. 275–289.
36. Richardson, S.; Evans, R.; Harrington, G. Connecting science and engagement: Setting groundwater extraction limits using a stakeholder-led decision-making process. In *Basin Futures: Water Reform in the Murray-Darling Basin*; Connell, D., Grafton, R.Q., Eds.; ANU e-Press: Canberra, Australia, 2011; pp. 351–366.
37. Allan, C.; Mitchell, M.; Punthakey, J.F. Institutional pathways for transforming groundwater planning and management: Reflections from Pakistan and Sri Lanka. *World Water Policy* **2023**, *9*, 283–668. [CrossRef]

sustainability

MDPI

Article

Towards Affordable Precision Irrigation: An Experimental Comparison of Weather-Based and Soil Water Potential-Based Irrigation Using Low-Cost IoT-Tensiometers on Drip Irrigated Lettuce

Ahmed A. Abdelmoneim, Roula Khadra *, Angela Elkamouh, Bilal Derardja and Giovanna Dragonetti

Mediterranean Agronomic Institute of Bari, 70010 Bari, Italy; ayoub@iamb.it (A.A.A.); angela-kamouh@hotmail.com (A.E.); derardja@iamb.it (B.D.); dragonetti@iamb.it (G.D.)
* Correspondence: khadra@iamb.it

Abstract: Predictive weather-based models are widely used to schedule irrigation through the estimation of crop evapotranspiration. However, perceiving real-time crop water requirements remains a challenge. This research aims at field validating and exploiting a low-cost IoT soil moisture tensiometer prototype to consequently compare weather-based irrigation to soil water moisture-based irrigation in terms of yield and crop water productivity. The prototype is based on the ESP32 microcontroller and BMP180 barometric sensor. When compared to a mechanical tensiometer, the IoT prototype proved its accuracy, registering an average R^2 equal to 0.8 and an RMSE range of 4.25–7.1 kPa. In a second step, the irrigation of a Romaine lettuce field (*Lactuca sativa* L.) cultivated under a drip system was managed according to two different scenarios: (1) using the data feed from the IoT tensiometers, irrigation was performed to keep the soil water potential between −15 and −25 kPa; (2) using the data provided by the in-situ weather station to estimate the crop water requirements. When comparing the yield, no significant difference was registered between the two scenarios. However, the water productivity was significantly higher, registering a 36.44% increment in scenario 1. The experiment highlights the water-saving potential achievable through real-time monitoring of soil moisture conditions. Since it is a low-cost device (82.20 USD), the introduced prototype facilitates deploying and managing a fleet of sensors for soil water potential live mapping.

Keywords: precision irrigation; agriculture water management; water productivity; IoT Irrigation; ESP32; sensors

Citation: Abdelmoneim, A.A.; Khadra, R.; Elkamouh, A.; Derardja, B.; Dragonetti, G. Towards Affordable Precision Irrigation: An Experimental Comparison of Weather-Based and Soil Water Potential-Based Irrigation Using Low-Cost IoT-Tensiometers on Drip Irrigated Lettuce. *Sustainability* **2024**, *16*, 306. https://doi.org/10.3390/su16010306

Academic Editors: Xiao Lin Yang, Wenfeng Liu and Wen Yin

Received: 1 November 2023
Revised: 15 December 2023
Accepted: 22 December 2023
Published: 28 December 2023

1. Introduction

Water is fundamental for our existence. Although it covers 71% of the planet, only 2.5% is fresh water, out of which only 1% is accessible [1]. Thus, mismanagement is a luxury that cannot be afforded. Moreover, the combination of population growth and climate change is placing additional stress on the already limited water resources, particularly in the Mediterranean region and Eurasia. This is affecting livelihoods, food security, economic development, and even social stability [2].

On a global scale, 70% of freshwater consumption is attributed to irrigated agriculture, which serves as the main cause and causality of water scarcity [3,4]. Consequently, there is a significant need to prioritize and improve on-farm irrigation management to effectively address such challenges.

Precision irrigation stands as a cornerstone for advancing agricultural sustainability. By leveraging technologies like soil moisture sensors, weather data, and automated irrigation systems, it enables farmers to deliver water precisely where and when it is needed [5]. This targeted approach conserves water resources and mitigates the strain on increasingly scarce water supplies. Furthermore, precision irrigation allows for the optimization of nutrient delivery, thus reducing excess runoff and minimizing the risk of water pollution. This

practice not only enhances crop health and yields but also supports the long-term resilience of the soil, which is crucial for sustainable agriculture [6]. Overall, precision irrigation is a key strategy for promoting agricultural sustainability, ensuring that agriculture can meet the growing global demand for food while minimizing its environmental impact. Yet, the lack of affordable and dependable data monitoring systems poses a major barrier to such potential enhancements [7]. Considering the spatially variable and stochastic nature of agricultural systems, it becomes imperative to have access to cost-effective and energy-efficient data acquisition systems. Such systems could play a major role in more accurate scheduling, monitoring, and assessment of irrigation activities [8].

This research work aims to (i) field validate a low-cost prototype DIY soil moisture tensiometer and (ii) exploit its use by comparing soil moisture-based irrigation management to weather-based irrigation management in terms of yield and water productivity.

2. Materials and Methods

2.1. Irrigation Scheduling

Irrigation scheduling directly impacts water use efficiency as it involves making decisions regarding the timing and quantity of water application to the field [9]. To efficiently schedule irrigation events, one must comprehend the dynamics of the plant water continuum, which is influenced by the interaction between weather conditions, soil characteristics, and plant physiology, usually referred to as SPAC (Soil-Plant-Atmosphere-Continuum) [10]. Hence, the criteria on which irrigation scheduling approaches are based are divided into (i) weather-based scheduling, (ii) soil moisture-based scheduling, and (iii) plant status-based scheduling.

Coupled with the rapid development of solid-state sensors and cloud platform-based services, monitoring systems could be integrated into the three aforementioned approaches. In the next section, the first two main approaches and their comparisons in relation to monitoring systems will be briefly presented.

It is worth mentioning that other factors could impact the actual implementation of an irrigation schedule outside the SPAC [11], such as the water supply routine, existing irrigation infrastructure, irrigator preferences based on social behavior patterns, fertigation and leaching requirements, . . . etc. Yet, this study is based on on-farm irrigation events that target the full satisfaction of plant water requirements using an on-demand, supplied drip irrigation system.

2.1.1. Weather Conditions Based Scheduling

It implies estimating reference evapotranspiration (ET_0) using measured weather parameters for a well-irrigated theoretical Alfalfa grass with a height of 12 cm, settled and immovable plane resistance of 70 s m^{-1} and an albedo of 0.23, vigorously rising, effectively watered, and entirely covering the land [12]. Several models were developed to estimate ET_c. One of the most used models is the FAO 56—Penman–Monteith [12–14] (Equation (1)).

$$ET_0 = \frac{0.408\Delta(R_n - G) + \gamma \frac{900}{T+273} u_2(e_s - e_a)}{\Delta + \gamma (1 + 0.34u_2)} \pi r^2 \quad (1)$$

where ET_0 is the reference evapotranspiration (mm day^{-1}), R_n is the net radiation at the crop surface (MJ m^{-2} day^{-1}), G is the soil heat flux density (MJ m^{-2} day^{-1}), T is the air temperature at 2 m height (°C), u_2 is the wind speed at 2 m height (m s^{-1}), e_s is the saturation vapor pressure (kPa), e_a is the actual vapor pressure (kPa), $e_s - e_a$ is the saturation vapor pressure deficit (kPa), Δ is the slope vapor pressure curve (kPa $°C^{-1}$), and γ is the psychrometric constant (kPa $°C^{-1}$).

Once ET_0 is estimated, it must be corrected using an empirical factor to represent the crop evapotranspiration (ET_c) (mm day^{-1}) relative to ET_0 at each growth stage (crop coefficient K_c) where:

$$ET_c = ET_0 . K_c \quad (2)$$

ET_c represents the potential crop evapotranspiration, i.e., the crop water requirement. The objective of an efficient irrigation schedule based on this model is to replenish ET_c as readily available water (RAW) to be taken by the plant's effective root zone while minimizing the water losses that may occur along the distribution system. This could be represented by Equation (3) [15]:

$$RAW = MAD \,.\, \left(\theta_{fc} - \theta_{pwp}\right) \,.\, D_r \,.\, 10 \tag{3}$$

where MAD is the management allowed depletion (the fraction of total available water that is allowed to be depleted before the next event), θ_{fc} is volumetric water content at field capacity ($cm^3 \cdot cm^{-3}$), θ_{pwp} is volumetric water content at the permanent wilting point ($cm^3 \cdot cm^{-3}$), and Dr is the effective root zone depth in cm. RAW is expressed in mm.

Automated weather monitoring was one of the earliest systems to be integrated into irrigation management [16]. Currently, wireless weather stations are commercially available and equipped with sensors capable of measuring all the parameters mentioned in Equation (1) and automating ET_0 calculations using variable transmission protocols.

Yet, the main uncertainty of this method stems from the agronomic inputs needed to simulate crop evapotranspiration, mainly the estimation of K_c and yield response to stresses represented by the stress coefficient K_s [17]. Estimating K_c for crops is a complicated process that requires estimating the crop's ET_c using well-irrigated lysimeters and back-calculating K_c relative to ET_0 [18]. As it is not a feasible task for the majority of irrigators, K_c is usually assumed from pre-defined values that could be found in the literature for similar climatic zones and various crops [12,19,20]. Another significant challenge arises from the daily variation of K_c values, which can change as crops grow and their leaf area expands [21,22].

An additional important point to consider when scheduling irrigation based on weather conditions is the time frame of the weather data used to estimate ET_0. Two main methods are found in the literature:

1. Predictive weather-based models that use a probabilistic approach to generate a representative set from historical recorded data for the targeted period consider dry years re-occurrence with a certain predefined probability. In this case, the generated schedule should be adjusted while being implemented based on daily data, especially rain fall events [23–26].
2. Near-real-time weather-based models that use short forecasting for daily estimations of ET_0 to automate irrigation events accordingly [27].

In conclusion, accurate implementation of ET-based irrigation scheduling on a commercial basis can prove challenging for growers, even if a more accurate estimation of K_c is provided. The process involves retrieving daily ET_0 values from a representative weather station installed in a location with certain standard specifications [28]. Such limitations drive farmers towards using publicly available ET_0 coupled with predefined K_c from the literature, usually leading to overirrigation [21].

2.1.2. Soil Moisture Based Scheduling

When managing irrigation events, farmers tend to rely on experience by sensing the soil using their bare hands to judge its moisture condition based on its texture, structure, and wetness. This judgment intuition could be described scientifically by two main terms: (i) soil moisture content and (ii) soil water matric potential [29]. The first describes the amount of water stored in the soil relative to its dry mass in volumetric or gravimetric terms. The second is the energy that plant roots need to exert to draw water from the soil, or the forces exerted by the soil matrix to hold the water, usually measured by tensiometers [30]. Soil moisture condition sensors are commercially available for measuring both soil volumetric water content and soil water matrix potential. A comprehensive review of the most commonly used sensors and their working concepts can be found in [31].

Monitoring soil water potential is crucial for effective irrigation management as it provides more accurate information about the availability of water to plants and their

ability to extract it from the soil. While soil water content indicates the amount of water present in the soil, regardless of the plant's ability to access that water [32].

Soil moisture tensiometers are one of the earliest and most widely adopted devices for measuring soil water potential. They consist of a porous cup and a vacuum gauge for measuring the equivalent negative pressure or water tension in unsaturated soils [33]. Unlike soil water content sensors, tensiometers are not sensitive to variations in soil texture [34], so they do not require prior calibration to be used for determining the matric potential at the current moment. Yet, it is important to couple soil water content readings with soil water potential monitoring to avoid over-irrigation, as tensiometers are inaccurate under high tensions (-80 to -100 kPa), especially in fine-textured soils [30].

Soil water potential (SWP) could be described as follows:

$$\psi = \psi_m + \psi_o + \psi_p + \psi_g \quad (4)$$

where ψ (kPa) is the potential energy per unit mass, volume, or weight of water and the sub-scripts m, o, p, and g are the matric, osmotic, pressure, and gravitational potentials, respectively [35].

Irrigation scheduling based on soil water potential, typically obtained through soil moisture tensiometers, is a practical and profound approach to ensuring efficient and rational use of water resources in irrigated agriculture [36,37]. It implies defining a soil water potential threshold—or a comfortable zone—for a specific crop below which the plant begins to suffer [38]. A lot of predefined thresholds could be found in the literature for various crops [30,35,38–48].

Several studies reported potential improvements in water productivity when switching to soil water-based irrigation compared to other irrigation approaches [49]. However, few have compared soil water potential-based irrigation to the FAO method of estimating crop water requirements [12] or any other weather-based irrigation approach. Smajstrla and Locascio [50] Smajstrla and Locascio compared irrigation scheduling based on pan evaporation to soil water potential-based scheduling using tensiometers under tomato drip cultivation. Water productivity increased by 40 and 50% when soil water potential was kept at -10 and -15 kPa, respectively, compared to the pan-evaporation-based field. Also, in a tomato drip-irrigated field, [51] compared soil water potential-based irrigation management using two thresholds (-10 kPa and -15 kPa) to conventional farmer practices. The results showed up to 73% of potential water reduction when irrigation was based on the soil water potential with minimal impact on yield. In Green houses, Buttaro, et al. [52] reported water savings of 35% and 45% for tomato and cucumber, respectively, when setting an irrigation schedule based on tension threshold ranges of -10 to -40 kPa for tomato and -10 to -30 kPa for cucumber. Yang, et al. [53] reported an improvement of 43.1% to 50.3% in water productivity when switching to soil water potential-based irrigation management under rice cultivation, where the SWP was kept at -15 kPa.

2.2. Experimental Layout

The experiment was conducted in CIHEAM Bari's experimental field located in Valenzano, Puglia region, South of Italy (41°2′40.3872″ N, 16°53′3.8364″ E), during the period April–June 2023, under transplanted Romaine lettuce (*Lactuca sativa* L.).

The designed area was 15 m × 9 m divided into two plots, 7.5 m × 9 m each. Both plots were equipped with a drip irrigation system where the distance between lines was 1 m and the distance between the drippers (plants) was 0.25 m. Drippers were self-compensating with a designed flow rate of 2 L/h. All 16 mm laterals feeding the drippers were equipped with small butterfly valves to ensure precise control of each dripper line, an important design feature as the irrigation schedule will be different from one plot to the next. Figure 1 shows the experimental layout.

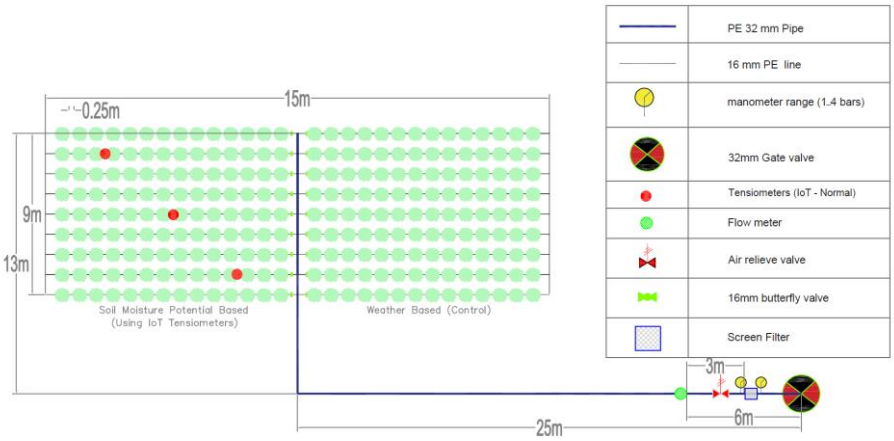

Figure 1. Layout of the irrigation network and the experimental field.

The first plot (Control) was irrigated according to the potential evapotranspiration derived from a weather station adjacent to the field using Penman–Monteith (Equation (1)) and adjusted using crop coefficients at variable growth stages based on FAO 56 [12] to calculate the potential crop water requirement as explained in Equation (2). Other agronomic and soil parameters are needed to simulate lettuce growth in the identified location. Table 1 summarizes all parameters used to generate the irrigation schedule, along with their sources and whether they were estimated or lab-measured. To facilitate the calculation process, Aquacrop [54] was used to generate the irrigation schedule.

Table 1. Climate, crop, management, and soil parameters are used to generate the weather-based irrigation schedule.

	Parameter		**Reference/Source**
Climate	Rainfall (mm)		Daily data for the past 3 years was provided from the weather station situated close to the field at CIHEAM Bari
	Evapotranspiration (mm)		
	Minimum and Maximum Temperature (°C)		
	Mean annual CO_2 concentration (ppm)		MaunaLoa.CO_2 file from Aquacrop data base
Crop	Calendar	Growing period	From 21 April to 21 June 2023
	Crop	Description	Display crop parameters: Full set
		Mode	Mode in: Growing Degree Days
		Development	• Initial canopy cover: 2.25% • Type of planting method: Transplanting • Maximum canopy cover: 60 days after transplant [55] • Root deepening: Shallow rooted crop (max 0.30 m) • Canopy growth coefficient (CGC): 15%/days
		Fertility stress	Not considered
		Salinity and cold stress	
		Temperature	• Base temperature for crop development: 7 °C • Upper temperature for crop development: 30 °C [55]
		Water	• Canopy expansion: Moderately tolerant to water stress • Upper threshold for canopy expansion: 0.25 • Lower threshold for canopy expansion: 0.55 • Shape factor for stress coefficient of canopy expansion: 3 • Stomatal closure: Moderately sensitive to water stress • Upper threshold for canopy expansion: 0.50 • Shape factor for stress coefficient for stomatal closure: 3 [55]

Table 1. *Cont.*

	Parameter		Reference/Source	
Crop	Crop	Type	• Annuals: Leafy vegetable crops • Type of photosynthetic pathways: C3 crop	From the FAO irrigation and drainage paper No. 56 "Crop evapotranspiration"
Management	Irrigation	Mode	Generation of irrigation schedule	Chosen by user preferences
		Irrigation method	• Drip irrigation • Percentage of soil surface wetted: 30%	
		Time and depth criteria	• Time criteria: Allowable depletion (20% of RAW) • Depth criteria: Back to field capacity • Irrigation water quality (Excellent)	
	Field	None		
Soil	Soil profile	Characteristic of soil horizons	• Description: Silt loam (clay 17.25%, silt 59.25%, sand 23.5%) • Thickness: 1.20 m • TAW: 130 mm/m • PWP: 13 vol % • FC: 26.0 vol % • SAT: 46 vol % • Hydraulic conductivity: 150 mm/day	Measured through a soil texture and structure analysis performed in the CIHEAM Bari soil lab
	Groundwater	None		

Irrigation management for this plot was implemented according to the generated irrigation schedule; however, the daily gross irrigation requirement was adjusted according to the measured daily rainfall during the season to avoid over-irrigation. All amounts of water supplied to the plot during the season were recorded using the water flowmeter installed upstream of the network.

On the other hand, the second plot was irrigated on demand using the data feed from three IoT soil moisture tensiometers developed by CIHEAMs Bari digital agriculture lab [33]. They measure the soil moisture and plot it on a cloud service platform (ThingSpeak™). ThingSpeak is a cloud-based IoT analytics platform service that enables the aggregation, visualization, and analysis of real-time data streams [56]. It was integrated into the IoT prototypes to visualize the data by linking a designated channel as a client using its identification number (ID) to receive strings from the devices (IoT tensiometers) identified by their internet protocol (Ips).

The three IoT prototypes were placed diagonally in rows no. 2, 5, and 8 at 15 cm depth (Figure 1). This depth was identified according to [57], as the ceramic cup was placed at half of the expected root zone during the season. In each measuring point, another conventional tensiometer with a mechanical manometer (JET FILL 2725) was added alongside the IoT one at the same depth (Figure 2). This was carried out to validate the developed IoT prototype and ensure its reliability.

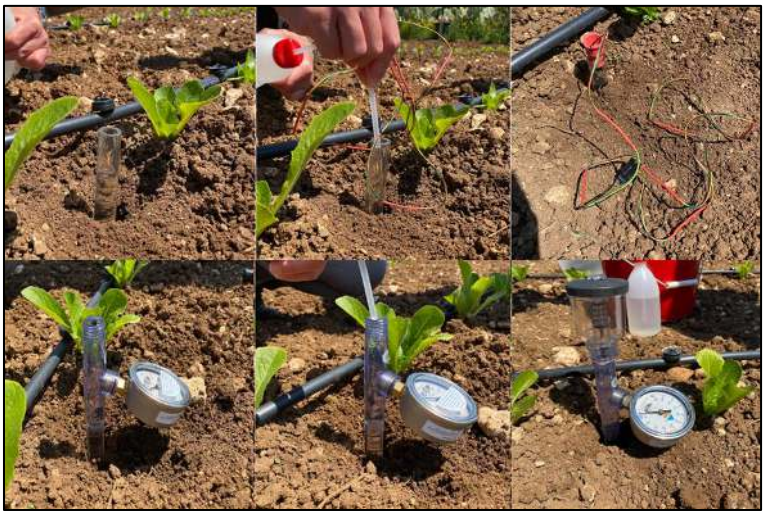

Figure 2. IoT and mechanical tensiometers as installed in the field.

Irrigation was managed according to the soil water potential in the root zoon. The comfortable range thresholds for the Romaine lettuce were investigated in previous studies. Michael and Barry [58] recommended −15 to −25 kPa in the establish phase and −25 to −35 kPa in the post-establish phase. Within the same range, Dessureault-Rompré, et al. [59] stated that −20 to −30 kPa is the ideal range. In this study, the threshold for initiating an irrigation event was set to −25 kPa, and the threshold to consider the field well irrigated was set to −15 kPa. This range was chosen based on literature and previous experience with soil water retention curves. The feed from the three tensiometers was received daily through the ThingSpeak platform. Once any of the three tensiometer readings exceeded −25 kPa, an irrigation event was triggered. The objective is to return that tensiometer within the comfortable zone. As the feedback from the tensiometers is not instant, continuous monitoring (each two hours) of the readings of the tensiometers was required in the initial events to ensure the return to the comfortable zone. During the irrigation season, the relationship between the amount of water needed and the tensiometer reading above the triggering threshold (−25 kPa) could be established, as shown in Table 2. All amounts of water supplied to the plot were recorded using the water flowmeter installed upstream of the network.

Table 2. Above-threshold tensiometer readings and the relative amount of water required and allocated to set back the reading.

Reading of Soil Water Tension (kPa)	Water Amount Allocated (mm)
−26 to −27	1.76
−27 to −28	2.64
−28 to −29	3.52
−29 to −30	4.4

2.3. Design and Development of the IoT Soil Moisture Tensiometer Prototype

The IoT-tensiometer integrates an isolated BMP180 barometric pressure sensor positioned near the top of the tensiometer tube, just beneath the closing cap. This sensor is linked to an ESP32 microcontroller through four slender wires (measuring 0.55 mm in diameter) utilizing an Inter-Integrated Circuit interface (I2C). The BMP180 operates on a logic voltage of 3.3 V and boosts the capability to detect barometric pressure up to 110 kPa with exceptional precision (2 Pa), making it well-suited for discerning even slight fluctuations in the tensiometer's vacuum. Serving as the prototype's central processing unit is the ESP32-WROOM MCU, a cost-effective and potent microcontroller module fea-

turing integrated WiFi and dual-mode Bluetooth capabilities. The detailed blueprints and description of the prototype can be found in [33].

In this study, the ESP32s deep sleep functionality was exploited to conserve power and ensure the prototype's self-sufficient operation. Figure 3 shows the algorithm flowchart. It works as follows: The ESP32 rouses itself every six hours (referred to as the "time slot" in the flowchart) to gauge the tension within the tensiometer's vacuum via the BMP180 sensors, then it transmits three data points to the ThingSpeak cloud service and reverts back to sleep mode.

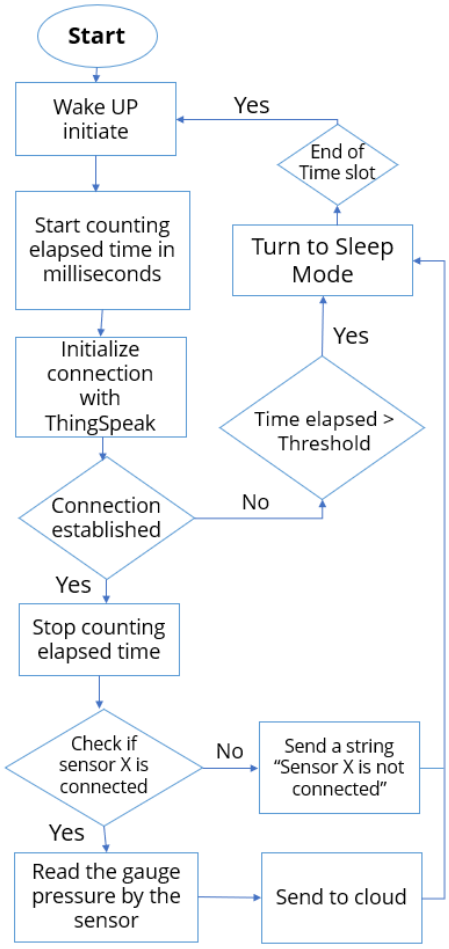

Figure 3. Algorithm Flowchart.

If the MCU is unable to locate an accessible network within 30 s (as denoted by the "threshold" on the flowchart), it returns to sleep mode. Similarly, if the MCU manages to establish a connection but is unable to detect the sensors, it subsequently returns to sleep mode, awaiting the next designated time slot. Figure 3 provides a visual representation of the code algorithm, scripted in the C++ language within the Arduino IDE environment.

The prototype is powered by two 3.7 V Li-Ion batteries connected in series, providing a combined voltage of 7.4 V. These batteries are recharged using a 1.1 W solar panel through an MT3608 DC-DC voltage regulator, which stabilizes the incoming charging voltage from the panels to 9 V. The MT3608 is a compact, cost-effective step-up booster converter module designed to elevate voltage from as low as 2 V up to a maximum of 28 V DC.

All components have been affixed to a designed platform and printed using Polyethylene Terephthalate Glycol material (PTEG). The design prioritized durability under outdoor conditions by minimizing openings or holes. The mounted electronic components are enclosed within an elongated sleeve-like box with two securely fitted side ducts (like a drawer), with the solar panel positioned on top as depicted in Figure 4.

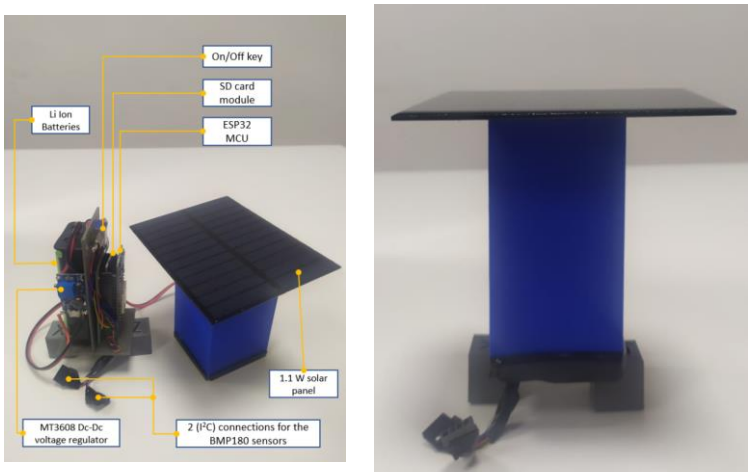

(**a**) (**b**)

Figure 4. The IoT tensiometer prototype: (**a**) The components; (**b**) the sealed prototype [33].

3. Results

The data feed from the three IoT prototyped tensiometers was compared to the readings of the mechanical tensiometers with a daily step along the season. Figure 5 shows the format of the data received on the ThingSpeak platform on a daily basis. The tool allowed for online and continuous soil water potential visualization and tracking, was easily accessed through personal devices, and could be downloaded as a .CSV file if needed.

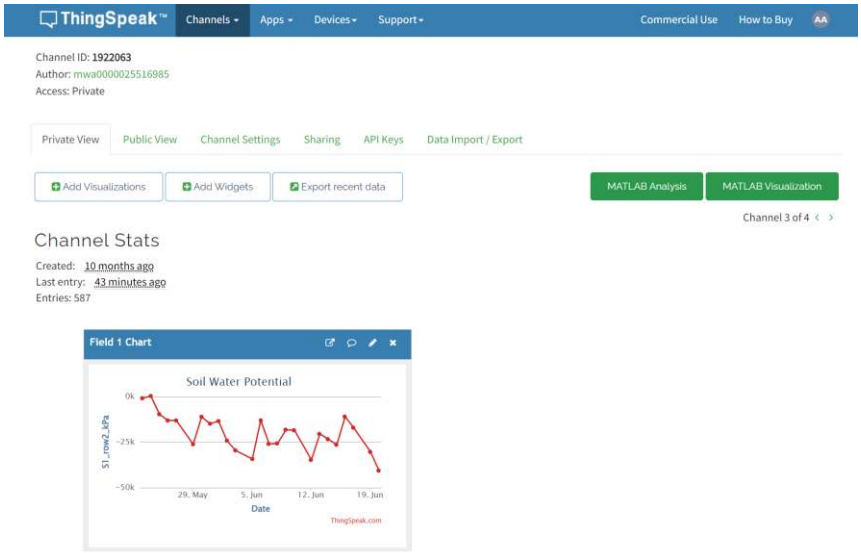

Figure 5. Data visualization is conducted on a daily basis, as shown on the ThingSpeak platform.

The deep sleep feature enabled the prototype to achieve a high degree of autonomy. It draws (0.8 µA) while in sleep mode and peaks at 50 mA for a duration of 5 s when uploading data. On days with ample sunlight, the solar panel generates a charging current ranging between 100 and 120 milliamperes. Thus, a 2400 mAh Li-ion battery was more than sufficient to supply the prototype on dim, cloudy days or at night during the test period (29 days from the 24th of May to the 21st of June in Valenzano, south Italy, 2023).

The deployed prototypes were able to detect the variation in soil water potential during the reported period. Figure 6 shows a high correlation between the three tested prototypes and their accompanied mechanical manometers, with an average R^2 of 0.8 while the root mean square error (RMSE) was insignificant, ranging from = 2.87 to 5.38. As the prototype was previously lab validated using bare soil pots [33], it is interesting to

discuss how repeating the validation process in the open field impacted the prototype's accuracy. Compared to the lab validation, R^2 is reduced from 0.99 to 0.8, while the RMSE range increased from 0.7–1.1 Kpa in the lab to 2.87–5.38 Kpa in the open field. Such results could be interpreted mainly as follows: (i) The medium scale: compared to large-scale open field soil structures, the soil pots (30 × 28 cm) provided a more confined environment, thus permitting the validation setup to be less prone to vertical and horizontal soil water movement and redistribution; (ii) The plant's effective root zone: unlike bare soil pots, the plant's roots (in this case Lettuce) were introduced in this validation setup. Despite considering the tensiometer placement to be as close as possible to the transplants (10–15 cm), it is not feasible to predict the effective root zone development and its impact on the prototype accuracy, yet it is an inevitable consequence.

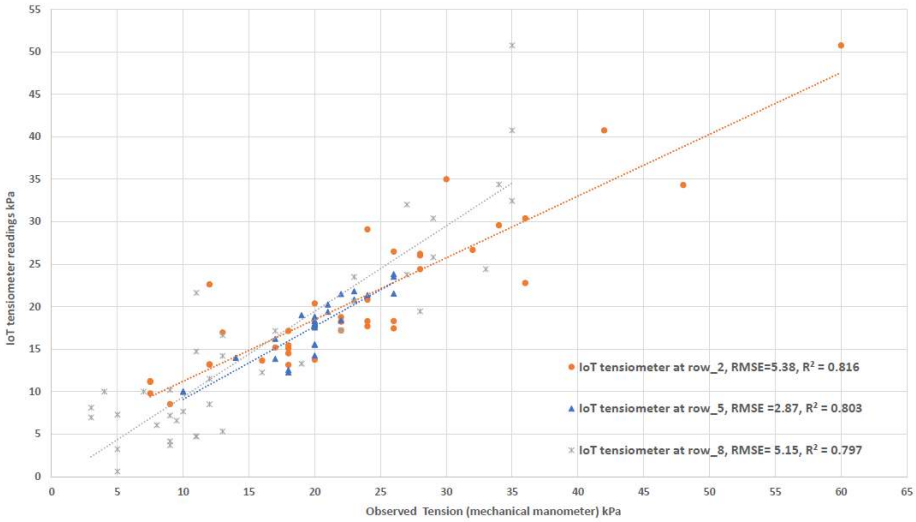

Figure 6. Validation of the three prototype sensors as compared to the mechanical manometers.

In terms of water productivity, fresh and dry yield were both weighed, while the amount of water allocated was registered using mechanical flowmeters. The fresh yield was almost the same: 149.7 kg in the weather-based plot and 146.9 kg in the soil-based one. On the other hand, the total amount of water allocated to the plots was 18.218 m^3 and 13.103 m^3 in the weather-based and soil-based plots, respectively, registering a reduction of 28%. Thus, the water productivity was higher by 36.44%, as shown in Figure 7.

Another result worth mentioning is the frequency of irrigation events. Figure 8 shows a comparison between the applied irrigation schedules. In the initial stage, both approaches were almost the same in terms of timing and quantity. However, after the initial stage (first week), the IoT soil-based plot maintained a soil water potential between −15 and −25 kPa, reducing the number of mandated irrigation events and spacing them apart. On the other hand, the gross irrigation requirements based on the simulated evapotranspiration from the adjacent weather station necessitated more irrigation events to meet the consumptive use. Overall, the weather-based plot required 32 irrigation events with a total of 26.7 irrigation hours. While the soil-based plot required only 22 irrigation events with 21.4 irrigation hours, a 28% reduction in the amount of water allocated. Although energy consumption was not measured in this study, the irrigation time implies that potential energy savings could be achieved.

One of the main advantages of the introduced prototype is its low cost, which does not only consider the initial cost of its components (82.20$) shown in Table 3 and compared to the readily available commercial versions (2023), whose costs range between 117 USD (Embsys Technologies Private Limited, Soil moisture tensiometer, Guindy, Chennai, Tamil Nadu, India) and 481 USD (METER, TEROS 32 Soil moisture tensiometer, 2365 NE Hopkins Ct. Pullamn, WA 99163, The United States of America). An important consideration instead is the subscription fee requested by the service provider to access data through the service

provider platform. Open source DIY prototypes—such as the one in hand—facilitate access to low-cost innovative solutions while overcoming the burden of data handling fees and service providers' ownership over data.

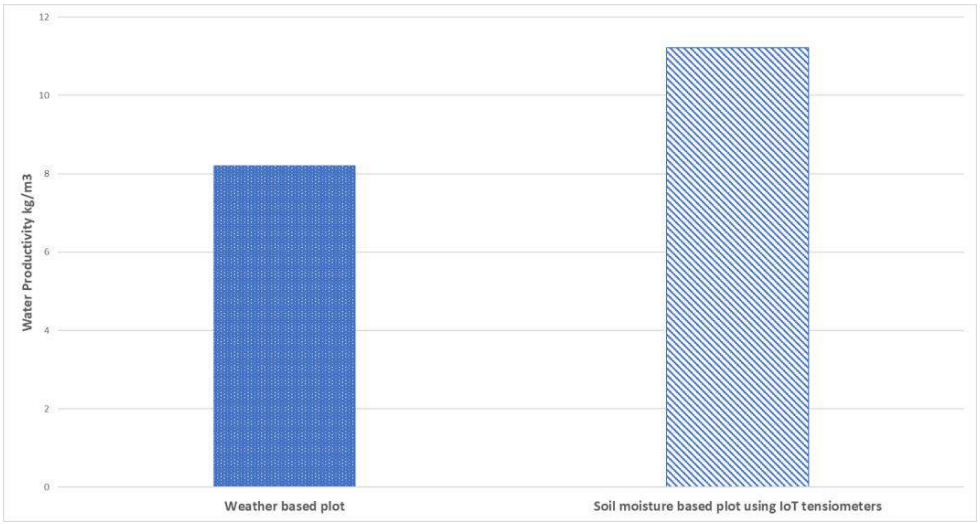

Figure 7. Water productivity as a result of irrigation scheduling based on weather and soil moisture using IoT tensiometers.

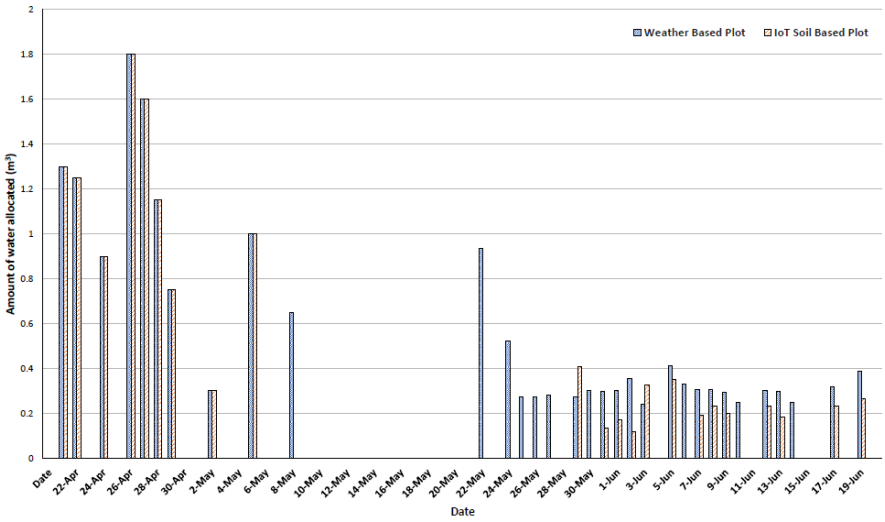

Figure 8. Applied irrigation schedules in both plots along the season.

Table 3. Breakdown of the cost of the prototype.

Item	Quantity	Cost ($)
ESP32 WROOM	1	10
BMP 180 sensor	1	2.5
MT3608 DC–DC	1	2
Tensiometer plexiglass tube	1	15
Permeable ceramic cup	1	15
2 cm airtight rubber cap	1	3.20
Li-ion batteries 3.7 volts	2	11
BMS 2S 10A charging model	1	4
1.1 W 6 V solar panel	1	14
Miscellaneous (Wires, isolation tape, pins. . .)	1	15
PTGE filament	0.5 kg	1.5
Total	**82.20**	

4. Conclusions

Progress in electronic technologies has granted researchers affordable access to solid-state sensors and programmable microcontroller-based circuits. Coupled with 3D printing potentials, prototyping for automating data collection has become much more feasible.

In this study, an easy-to-assemble, cost-effective, energy-autonomous prototype of an IoT tensiometer was field-validated. The IoT tensiometer proved to be reliable and was able to track the variation in the soil water potential with an average $R^2 = 0.8$ and RMSE ranging from 4.25 to 7.1. It was then used to compare weather-based to soil-based irrigation management under drip-irrigated lettuce cultivation.

In consistency with previous studies, irrigation scheduling based on soil water tension proved potential water savings when compared to a weather-based approach. Water productivity was improved by 36.44% when irrigation was based on the IoT tensiometer prototype, setting a threshold of (-15 to -25 kPa) relative to the FAO 56 weather-based approach [12].

Such a low-cost prototype (82.20$) contributes to an affordable, easy-to-access soil moisture monitoring system, which is an inherent problem when addressing soil moisture-based irrigation management.

It is worth mentioning that the field deployment of the sensors lasted for approximately 2 months, along with the whole cropping season of lettuce. This period served the objective of this study and allowed for soil-based on-farm irrigation management; however, it still remains a short period to test the sensors' durability and their long-term reliability. For the latter purpose, further investigation is needed, especially to set technical maintenance/replacement, and periodic recalibration requirements. The same applies for assessing the improvements in terms of energy consumption that accompany the irrigation time reduction.

Author Contributions: Conceptualization, A.A.A. and R.K.; methodology, A.A.A.; software, A.A.A. and A.E.; validation, G.D., A.E. and A.A.A.; formal analysis, A.A.A. and A.E.; investigation, G.D.; resources, R.K.; data curation, B.D.; writing—original draft preparation, A.A.A.; writing—review and editing, R.K.; visualization, A.A.A.; supervision, A.A.A.; project administration, R.K.; funding acquisition, R.K. All authors have read and agreed to the published version of the manuscript.

Funding: This research received no external funding.

Institutional Review Board Statement: This study did not require ethical approval.

Informed Consent Statement: This study did not involve humans.

Data Availability Statement: The data presented in this study are available on request from the corresponding author.

Acknowledgments: We extend our deepest gratitude to the dedicated and hardworking field workers who played a crucial role in the conclusion of this research experiment.

Conflicts of Interest: The authors declare no conflicts of interest.

References

1. Mishra, R.K. Fresh water availability and its global challenge. *Br. J. Multidiscip. Adv. Stud.* **2023**, *4*, 1–78. [CrossRef]
2. Fouial, A.; Khadra, R.; Daccache, A.; Lamaddalena, N. Modelling the impact of climate change on pressurised irrigation distribution systems: Use of a new tool for adaptation strategy implementation. *Biosyst. Eng.* **2016**, *150*, 182–190. [CrossRef]
3. FAO. *Water for Sustainable Food and Agriculture a Report Produced for the G20 Presidency of Germany*; FAO: Rome, Italy, 2017.
4. Hardie, M. Review of novel and emerging proximal soil moisture sensors for use in agriculture. *Sensors* **2020**, *20*, 6934. [CrossRef] [PubMed]
5. Anjum, M.N.; Cheema, M.J.M.; Hussain, F.; Wu, R.-S. Precision irrigation: Challenges and opportunities. *Precis. Agric.* **2023**, 85–101. [CrossRef]
6. Wu, H.; Zhang, L.; Lv, J.; Zhang, Y.; Zhang, Y.; Yu, N. Optimization of irrigation and N fertilization management profoundly increases soil N retention potential in a greenhouse tomato production agroecosystem of Northeast China. *Agric. Ecosyst. Environ.* **2022**, *340*, 108185. [CrossRef]

7. Khadra, R.; Sagardoy, J.A.; Taha, S.; Lamaddalena, N. Participatory irrigation management and transfer: Setting the guiding principles for a sustaining monitoring & evaluation system–a focus on the mediterranean. *Water Resour. Manag.* **2017**, *31*, 4227–4238.
8. Abdelmoneim, A.A.; Daccache, A.; Khadra, R.; Bhanot, M.; Dragonetti, G. Internet of Things (IoT) for double ring infiltrometer automation. *Comput. Electron. Agric.* **2021**, *188*, 106324. [CrossRef]
9. Koech, R.; Langat, P. Improving irrigation water use efficiency: A review of advances, challenges and opportunities in the Australian context. *Water* **2018**, *10*, 1771. [CrossRef]
10. García-Tejera, O.; López-Bernal, Á.; Orgaz, F.; Testi, L.; Villalobos, F.J. The pitfalls of water potential for irrigation scheduling. *Agric. Water Manag.* **2021**, *243*, 106522. [CrossRef]
11. Khadra, R.; Lamaddalena, N.; Inoubli, N. Optimization of on demand pressurized irrigation networks and on-farm constraints. *Procedia Environ. Sci.* **2013**, *19*, 942–954. [CrossRef]
12. Allen, R.G.; Pereira, L.S.; Raes, D.; Smith, M. *Crop Evapotranspiration-Guidelines for Computing Crop Water Requirements-FAO Irrigation and Drainage Paper 56*; FAO: Rome, Italy, 1998; Volume 300, p. D05109.
13. Penman, H.L. Natural evaporation from open water, bare soil and grass. *Proc. R. Soc. Lond. Ser. A Math. Phys. Sci.* **1948**, *193*, 120–145.
14. Monteith, J. Evaporation and environment. In *GE Fogg Symposium of the Society for Experimental Biology. The State and Movement of Water in Living Organisms*; Cambridge University Press: Cambridge, UK, 1965; Volume 19, pp. 205–234.
15. Huffman, R.L.; Fangmeier, D.D.; Elliot, W.J.; Workman, S.R.; Schwab, G. *Soil and Water Conservation Engineering*; American Society of Agricultural and Biological Engineers: St. Joseph, MI, USA, 2013.
16. Cabelguenne, M.; Debaeke, P.; Puech, J.; Bosc, N. Real time irrigation management using the EPIC-PHASE model and weather forecasts. *Agric. Water Manag.* **1997**, *32*, 227–238. [CrossRef]
17. Carr, M. *Crop Yield Response to Water*; Steduto, P., Hsiao, T.C., Fereres, E., Raes, D., Eds.; FAO Irrigation and Drainage Paper 66; Food and Agriculture Organization of the United Nations: Rome, Italy, 2012; p. 500. ISBN 978-92-5-107274-5. Available online: http://www.fao.org/docrep/016/i2800e/i2800e00.htm (accessed on 15 February 2023).
18. Piccinni, G.; Ko, J.; Wentz, A.; Leskovar, D.; Marek, T.; Howell, T. Determination of crop coefficients (Kc) for irrigation management of crops. In Proceedings of the 28th Annual International Irrigation Show, San Diego, CA, USA, 9–12 December 2007.
19. Guerra, E.; Ventura, F.; Snyder, R. Crop coefficients: A literature review. *J. Irrig. Drain. Eng.* **2016**, *142*, 06015006. [CrossRef]
20. Grattan, S.; Bowers, W.; Dong, A.; Snyder, R.; Carroll, J.; George, W. New crop coefficients estimate water use of vegetables, row crops. *Calif. Agric.* **1998**, *52*, 16–21. [CrossRef]
21. Cahn, M.D.; Johnson, L.F. New approaches to irrigation scheduling of vegetables. *Horticulturae* **2017**, *3*, 28. [CrossRef]
22. Lea-Cox, J.D. Using wireless sensor networks for precision irrigation scheduling. In *Problems, Perspectives and Challenges of Agricultural Water Management*; InTech Press: Rijeka, Croatia, 2012; pp. 233–258.
23. Gowing, J.; Ejieji, C. Real-time scheduling of supplemental irrigation for potatoes using a decision model and short-term weather forecasts. *Agric. Water Manag.* **2001**, *47*, 137–153. [CrossRef]
24. Wang, D.; Cai, X. Irrigation scheduling—Role of weather forecasting and farmers' behavior. *J. Water Resour. Plan. Manag.* **2009**, *135*, 364–372. [CrossRef]
25. Lorite, I.; Ramírez-Cuesta, J.; Cruz-Blanco, M.; Santos, C. Using weather forecast data for irrigation scheduling under semi-arid conditions. *Irrig. Sci.* **2015**, *33*, 411–427. [CrossRef]
26. Mahan, J.R.; Lascano, R.J. Irrigation analysis based on long-term weather data. *Agriculture* **2016**, *6*, 42. [CrossRef]
27. Yang, Y.; Cui, Y.; Bai, K.; Luo, T.; Dai, J.; Wang, W.; Luo, Y. Short-term forecasting of daily reference evapotranspiration using the reduced-set Penman-Monteith model and public weather forecasts. *Agric. Water Manag.* **2019**, *211*, 70–80. [CrossRef]
28. Yoder, R.; Ley, T.; Elliott, R. Measurement and reporting practices for automatic agricultural weather stations. In Proceedings of the 4th Decennial Symposium, Phoenix, AZ, USA, 14–16 November 2000; pp. 260–265.
29. Delgoda, D.; Saleem, S.K.; Malano, H.; Halgamuge, M.N. Root zone soil moisture prediction models based on system identification: Formulation of the theory and validation using field and AQUACROP data. *Agric. Water Manag.* **2016**, *163*, 344–353. [CrossRef]
30. Bianchi, A.; Masseroni, D.; Thalheimer, M.; Medici, L.; Facchi, A. Field irrigation management through soil water potential measurements: A review. *Ital. J. Agrometeorol.* **2017**, *22*, 25–38.
31. Yu, L.; Gao, W.; R Shamshiri, R.; Tao, S.; Ren, Y.; Zhang, Y.; Su, G. Review of research progress on soil moisture sensor technology. *Int. J. Agric. Biol. Eng.* **2021**, *14*, 32–42. [CrossRef]
32. Kassaye, K.T.; Boulange, J.; Saito, H.; Watanabe, H. Monitoring soil water content for decision supporting in agricultural water management based on critical threshold values adopted for Andosol in the temperate monsoon climate. *Agric. Water Manag.* **2020**, *229*, 105930. [CrossRef]
33. Abdelmoneim, A.A.; Khadra, R.; Derardja, B.; Dragonetti, G. Internet of Things (IoT) for Soil Moisture Tensiometer Automation. *Micromachines* **2023**, *14*, 263. [CrossRef] [PubMed]
34. Lieth, J.H.; Oki, L.R. Irrigation in soilless production. In *Soilless Culture*; Elsevier: Amsterdam, The Netherlands, 2019; pp. 381–423.
35. Campbell, G.S. Soil water potential measurement: An overview. *Irrig. Sci.* **1988**, *9*, 265–273. [CrossRef]
36. Richards, S. Soil suction measurements with tensiometers. In *Methods of Soil Analysis: Part 1 Physical and Mineralogical Properties, Including Statistics of Measurement and Sampling*; The American Society of Agronomy: Madison, WI, USA, 1965; Volume 9, pp. 153–163.

37. Freire, A.G.; de Alencar, T.L.; Chaves, A.F.; do Nascimento, Í.V.; de Assis Junior, R.N.; van Lier, Q.d.J.; Mota, J.C.A. Comparison of devices for measuring soil matric potential and effects on soil hydraulic functions and related parameters. *Agric. Water Manag.* **2018**, *209*, 134–141. [CrossRef]
38. Thompson, R.; Gallardo, M.; Valdez, L.; Fernández, M. Using plant water status to define threshold values for irrigation management of vegetable crops using soil moisture sensors. *Agric. Water Manag.* **2007**, *88*, 147–158. [CrossRef]
39. Dobriyal, P.; Qureshi, A.; Badola, R.; Hussain, S.A. A review of the methods available for estimating soil moisture and its implications for water resource management. *J. Hydrol.* **2012**, *458*, 110–117. [CrossRef]
40. Hubbell, J.; Sisson, J. Soil water potential measurement by tensiometers. In *The Encyclopedia of Water Science*; Marcel Dekker: New York, NY, USA, 2003; pp. 904–907.
41. Shock, C.C.; Wang, F.-X. Soil water tension, a powerful measurement for productivity and stewardship. *HortScience* **2011**, *46*, 178–185. [CrossRef]
42. Pardossi, A.; Incrocci, L. Traditional and new approaches to irrigation scheduling in vegetable crops. *HortTechnology* **2011**, *21*, 309–313. [CrossRef]
43. Thompson, T.L.; Doerge, T.A.; Godin, R.E. Subsurface drip irrigation and fertigation of broccoli: I. Yield, quality, and nitrogen uptake. *Soil Sci. Soc. Am. J.* **2002**, *66*, 186–192. [CrossRef]
44. Smittle, D.A.; Dickens, W.L.; Stansell, J.R. Irrigation regimes affect cabbage water use and yield. *J. Am. Soc. Hortic. Sci.* **1994**, *119*, 20–23. [CrossRef]
45. Thompson, T.L.; Doerge, T.A.; Godin, R.E. Nitrogen and water interactions in subsurface drip-irrigated cauliflower II. Agronomic, economic, and environmental outcomes. *Soil Sci. Soc. Am. J.* **2000**, *64*, 412–418. [CrossRef]
46. Gallardo, M.; Jackson, L.; Schulbach, K.; Snyder, R.; Thompson, R.; Wyland, L. Production and water use in lettuces under variable water supply. *Irrig. Sci.* **1996**, *16*, 125–137. [CrossRef]
47. Thompson, T.L.; Doerge, T.A. Nitrogen and water rates for subsurface trickle-irrigated romaine lettuce. *HortScience* **1995**, *30*, 1233–1237. [CrossRef]
48. Kukal, S.; Hira, G.; Sidhu, A. Soil matric potential-based irrigation scheduling to rice (*Oryza sativa*). *Irrig. Sci.* **2005**, *23*, 153–159. [CrossRef]
49. Gendron, L.; Letourneau, G.; Anderson, L.; Sauvageau, G.; Depardieu, C.; Paddock, E.; van den Hout, A.; Levallois, R.; Daugovish, O.; Solis, S.S. Real-time irrigation: Cost-effectiveness and benefits for water use and productivity of strawberries. *Sci. Hortic.* **2018**, *240*, 468–477. [CrossRef]
50. Smajstrla, A.G.; Locascio, S.J. Irrigation scheduling of drip-irrigated tomato using tensiometers and pan evaporation. *Proc. Fla. State Hortic. Soc. Am. Soc. Agric. Biol. Eng.* **1990**, *103*, 88–91.
51. Munoz-Carpena, R.; Bryan, H.; Klassen, W. Automatic soil moisture-based drip irrigation for improving tomato production. In Proceedings of the Florida State Horticultural Society, Sheraton World Resort, Orlando, FL, USA, 8–10 June 2003; pp. 80–85.
52. Buttaro, D.; Santamaria, P.; Signore, A.; Cantore, V.; Boari, F.; Montesano, F.F.; Parente, A. Irrigation management of greenhouse tomato and cucumber using tensiometer: Effects on yield, quality and water use. *Agric. Agric. Sci. Procedia* **2015**, *4*, 440–444. [CrossRef]
53. Yang, J.; Liu, K.; Wang, Z.; Du, Y.; Zhang, J. Water-saving and high-yielding irrigation for lowland rice by controlling limiting values of soil water potential. *J. Integr. Plant Biol.* **2007**, *49*, 1445–1454. [CrossRef]
54. Raes, D.; Steduto, P.; Hsiao, T.C.; Fereres, E. AquaCrop—The FAO crop model to simulate yield response to water: II. Main algorithms and software description. *Agron. J.* **2009**, *101*, 438–447. [CrossRef]
55. Amirouche, M.; Smadhi, D.; Zella, L. Calibration and validation of the AquaCrop model for the culture lettuce (*Lactuca sativa* L.) under fertilization levels in pluvial condition. *Agric. Water Manag.* **2018**, *208*, 107–119. [CrossRef]
56. Pasha, S. ThingSpeak based sensing and monitoring system for IoT with Matlab Analysis. *Int. J. New Technol. Res.* **2016**, *2*, 263492.
57. Peters, R.T.; Desta, K.G.; Nelson, L. *Practical Use of Soil Moisture Sensors and Their Data for Irrigation Scheduling*; Washington State University Extension: Washington, DC, USA, 2013.
58. Michael, C.; Barry, F. *Using Tensiometers for Scheduling Irrigations of Coastal Vegetables*; University of California US Cooperative Extension: Los Angeles, CA, USA, 2012.
59. Dessureault-Rompré, J.; Caron, J.; Plamondon, L.; Gaudreau, L.; Jutras, S.; Lafond, J.A. Growth and water-use characteristics of Romaine lettuce cultivated in Histosol as affected by irrigation management, compaction, and seeding type. *Can. J. Soil Sci.* **2020**, *100*, 278–288. [CrossRef]

sustainability

MDPI

Article

Sustainability of a Rainfed Wheat Production System in Relation to Water and Nitrogen Dynamics in the Soil in the Eyre Peninsula, South Australia

Vinod Phogat [1,2,3,*], Jirka Šimůnek [4], Paul Petrie [1,2,3,5], Tim Pitt [1,2,3] and Vilim Filipović [6,7]

[1] Crop Sciences, South Australian Research and Development Institute, GPO Box 397, Adelaide, SA 5001, Australia; paul.petrie@sa.gov.au or paul.petrie@adelaide.edu.au or paul.petrie@flinders.edu.au (P.P.); tim.pitt@sa.gov.au or tim.pitt@adelaide.edu.au or tim.pitt@flinders.edu.au (T.P.)
[2] School of Agriculture, Food and Wine, The University of Adelaide, PMB No.1, Glen Osmond, SA 5064, Australia
[3] College of Science and Engineering, Flinders University, Adelaide, SA 5042, Australia
[4] Department of Environmental Sciences, University of California, Riverside, CA 92521, USA; jiri.simunek@ucr.edu
[5] School of Mechanical and Manufacturing Engineering, The University of New South Wales, Sydney, NSW 2052, Australia
[6] Future Regions Research Centre, Federation University, Gippsland, VIC 3841, Australia; v.filipovic@federation.edu.au or vfilipovic@agr.hr
[7] Faculty of Agriculture, University of Zagreb, Svetošimunska Cesta 25, 10000 Zagreb, Croatia
* Correspondence: vinod.phogat@sa.gov.au or vinod.phogat@adelaide.edu.au or vinod.phogat@flinders.edu.au

Abstract: Rainfed wheat production systems are usually characterized by low-fertility soils and frequent droughts, creating an unfavorable environment for sustainable crop production. In this study, we used a processed-based biophysical numerical model to evaluate the water balance and nitrogen (N) dynamics in soils under rainfed wheat cultivation at low (219 mm, Pygery) and medium rainfall (392 mm, Yeelanna) sites in south Australia over the two seasons. Estimated evapotranspiration components and N partitioning data were used to calibrate and validate the model and to compute wheat's water and N use efficiency. There was a large disparity in the estimated water balance components at the two sites. Plant water uptake accounted for 40–50% of rainfall, more at the low rainfall site. In contrast, leaching losses of up to 25% of seasonal rainfall at the medium rainfall site (Yeelanna) indicate a significant amount of water evading the root zone. The model-predicted N partitioning revealed that ammonia–nitrogen (NH_4–N) contributed little to plant N nutrition, and its concentration in the soil remained below 2 ppm throughout the crop season except immediately after the NH_4–N-based fertilizer application. Nitrate–nitrogen (NO_3–N) contributed to most N uptake during both seasons at both locations. The N losses from the soil at the medium rainfall site (3.5–20.5 kg ha^{-1}) were mainly attributed to NH_4–N volatilization (N_v) and NO_3–N leaching (N_L) below the crop root zone. Water productivity (8–40 kg ha^{-1} mm^{-1}) and N use efficiency (31–41 kg kg^{-1}) showed immense variability induced by climate, water availability, and N dynamics in the soil. These results suggest that combining water balance and N modeling can help manage N applications to optimize wheat production and minimize N losses in rainfed agriculture.

Keywords: wheat; rainfed; water balance; nitrogen uptake; water productivity; nitrogen use efficiency; HYDRUS

Citation: Phogat, V.; Šimůnek, J.; Petrie, P.; Pitt, T.; Filipović, V. Sustainability of a Rainfed Wheat Production System in Relation to Water and Nitrogen Dynamics in the Soil in the Eyre Peninsula, South Australia. *Sustainability* **2023**, *15*, 13370. https://doi.org/10.3390/su151813370

Academic Editors: Wenfeng Liu, Xiao Lin Yang and Wen Yin

Received: 11 August 2023
Revised: 30 August 2023
Accepted: 4 September 2023
Published: 6 September 2023

1. Introduction

Water is one of the most limiting factors to increasing food and fiber production, especially in the arid and semi-arid regions of the world. In these regions, rainfall is insufficient and highly variable, often failing to satisfy the evapotranspiration demand of rainfed crop production. Low and sporadic rainfall in rainfed cultivated regions impacts crop water uptake and nutrient mineralization in soils of poor fertility [1,2]. Thus, crop production is

affected by the unpredictability of water availability at crucial crop growth stages, causing yield and quality loss. Numerous studies have shown that grain production in semi-arid rainfed cropping systems strongly depends on soil moisture and N supply, i.e., it is thus co-limited [3,4]. Therefore, water-saving technologies, water retention, and effective use of water and nutrients are of paramount importance in fragile rainfed production systems.

Wheat production in Australia is characterized by low to medium rainfall (<450 mm) and a very high evaporative demand relative to rainfall (>3:1), with a coefficient of variation of 25–30% [5], making it one of the driest rainfed cropping environments in the world [6]. Moreover, the soils in rainfed regions vary in texture, composition, water-holding capacity, and nutrient availability, which adds to the challenges of sustainable crop production. These factors lead to wide region-to-region and seasonal variability in wheat production. For example, wheat production during 2021-22 (36 Mt) was more than double that in 2019-20 [7], predominantly associated with favorable climatic conditions. However, a long-term yield assessment revealed that Australia's average annual wheat yield was only 50% (1.73 t ha^{-1}) of the potential yield [8]. Therefore, identifying yield-limiting constraints in the soil–plant–atmosphere continuum [9] can help devise ways and means to close this wide gap in the water-limited yield and year-to-year variability in wheat production.

Achieving potential yield with less water has always been an endeavor in increasing crop productivity and water use efficiency. One major stumbling block in this pursuit is limited and seasonally varying water availability for rainfed wheat. In this regard, the French and Schultz [10] model has provided a valuable benchmark for assessing the water-limited yield potential of grain crops based on seasonal rainfall. It is widely used by many farmers from rainfed regions in Australia and other parts of the world. For example, the model prediction for wheat is 20 kg grain ha^{-1} mm^{-1} of water transpired above 110 mm evaporation. This prediction has been revised numerous times to include various climatic factors such as rainfall distribution and evaporative demand of the environment [11,12] and co-limitation of water and nitrogen factors [13,14]. The co-limitation assessment raised the water-limited wheat yield to 24 kg ha^{-1} mm^{-1}, suggesting that low nutrient availability reduces water use efficiency and increases the gap between actual and water-limited yield potential. The major limitations of the French and Schultz [10] approach include its inability to account for the impact of the timing of growing season rain and water losses such as runoff or drainage and the assumption of constant seasonal evaporation [15]. These limitations can be addressed by more complex processed-based models commonly used for water balance studies under cropped conditions [16,17].

Water availability in the soils tremendously impacts nutrient availability and its uptake by the roots. The soil water content not only determines the crop N uptake but also controls biogeochemical N transformations, such as volatilization, nitrification, and urea hydrolysis. Therefore, water and N interactions in the soil affect crop growth and yield attributes, including photosynthesis, foliage growth, crop yield, protein content, leaf senescence, root-to-shoot water and N translocations, and microbial enzyme activity in the soil [4,18–21]. Benjamin et al. [22] reported that N uptake and N use efficiency were reduced with limited water availability during crop growth and corresponding limited N movement in the soil. On the other hand, N leaching and denitrification can occur when excessive water is applied [23,24]. Similarly, an appreciable amount of N can be lost to the atmosphere due to ammonium volatilization, especially when urea is top-dressed on the soil surface during the growing season [25–27].

Angus and Grace [1] reported that most grain cropping systems in Australia have a negative N balance, resulting from more N exported off-farm in agricultural products than applied as fertilizer or through biological nitrogen (N_2) fixation. Numerous studies found that the recovery efficiency of N in rainfed wheat production is as low as 30–50% [1,28–30]. Furthermore, Gastal et al. [28] reported that between 50 and 75% of the applied N is either retained in the crop residues, remains in the soil, or is lost from the system, leading to environmental problems. Other studies also revealed that N applications higher than the crop demand might result in leaching losses, which could contaminate groundwater and

trigger the eutrophication of freshwater and marine ecosystems [31,32]. Climate change further aggravates the problem and uncertainty regarding the supply of resources [33] and their optimum utilization [34]. Thus, maximization of water and N use is essential for ensuring long-term productive potential and maintaining the ecological functions of natural resources [35]. Hence, an increase in nitrogen use efficiency (NUE) will not only reduce the amount of applied N but also minimize N-related environmental pollution [36]. Therefore, accurate estimates of N reactive fluxes, plant uptake, and N losses (including gaseous) are required to fully understand N dynamics in the soil under rainfed wheat production systems.

Several process-based models (e.g., APSIM and HYDRUS) can provide estimates of effective water and N balances, use efficiencies, and losses from agricultural production systems. These models integrate the effect of rainfall, soil, weather, and other management practices to predict the dynamics of water and N movement in soils [37]. APSIM has been widely used in Australia to model the fate of water and nitrogen in rainfed farming systems (e.g., Keating et al. [16,38]). However, most of these studies have only used the bucket-type water balance module, the results of which can deviate from those provided by numerical simulations (e.g., HYDRUS), which provide more precise solutions of the partial differential equations describing non-linear water flow and convective–dispersive solute transport in soils [17].

Hence, the objectives of this investigation were to evaluate daily and seasonal soil water balances, including wheat's root water uptake and the dynamics of N in the soil (mineralization, transformation, plant uptake, and gaseous losses), using HYDRUS-1D. Water (WUE) and N use efficiency (NUE) of wheat were also estimated using the model-simulated water and N balance components. This information can help devise better guidelines for enhancing fertilizer use efficiency and reducing N losses in rainfed wheat production regions.

2. Materials and Methods

2.1. Description of Study Sites

This study was part of a project to evaluate soil moisture and N information to assist farmers on the Eyre Peninsula in south Australia in making better management decisions for profitable wheat production. Two sites, i.e., Pygery (−32.9838° S, 135.3642° E) and Yeelanna (−34.1369° S, 135.7665° E), representing different soils, climates, and N applications, were selected for this study to assess water and nitrogen dynamics in the soils under wheat production. These sites were selected based on large differences in the rainfall, soil, growing conditions, and fertilizer use, which enabled the evaluation of diverse rainfed wheat growing systems. The Pygery (Py) site is located in the west coast region of the Eyre Peninsula and is characterized as a low rainfall zone. Annual average rainfall and reference crop evapotranspiration (ET_0) at this site during the last 100 years amounted to 327 and 1397 mm, respectively. The Yeelanna (Ye) site is located in the lower Eyre Peninsula region, with annual average rainfall and ET_0 of 411 and 1172 mm, respectively. More details about this project and specific growing conditions can be found in [39].

Cereals (wheat, barley), rotated with canola or pasture legumes, are the widely grown crops in the study region. However, a wheat crop was grown at both locations during the study period (2018 and 2019). Details about wheat variety, spacing, density, sowing, harvesting, and fertilizer applications during the two seasons are given in Table 1. Notably, the amount of N fertilizer applied at Yeelanna was much higher than at Pygery. At Pygery, N was added only at the time of sowing. In 2018, 55 kg of mono ammonium phosphate (MAP) and 30 kg of a blend of urea and ammonium sulfate/ha was applied, while in 2019, 40 kg of urea and 60 kg of a blend of urea and ammonium sulfate/ha was applied. The basal dose at Yeelanna applied at the time of sowing was 100 kg urea + 66 kg MAP/ha and 75 kg urea/ha during the 2018 and 2019 seasons, respectively. Apart from the initial application, two doses of 100 kg of N were applied during the season as a top dressing at Yeelanna. An extra N application is typically added in medium rainfall environments to enhance yield and, thus, profitability [40]. This reflects a wide range of farmers' N use

practices in different rainfall regions. Essentially, the extent and timing of N applications in dryland wheat farming systems depend on the timing and intensity of rainfall, which provides the necessary water to dissolve the fertilizer in the soil and make it available for root uptake.

Table 1. Wheat sowing, fertilizer details, and wheat yield at the experimental sites.

	2018	**2019**
Pygery (Py)		
Variety	Mace	Mace
Sowing date	19 May	12 May
Row spacing (mm)		
Plant density (plants m^{-2})	140	160
Fertilizers (applied at sowing)		
MAP (kg ha^{-1})	55	-
Urea (kg ha^{-1})	-	40
Urea/ammonium sulfate blend	30	60
Yield (t ha^{-1})	1.45	1.6
Yeelanna (Ye)		
Variety	Emu Rock	Mace
Sowing date	12 May	22 May
Row spacing (mm)	307	305
Plant density (plants m^{-2})	150	150
Fertilizers (applied at sowing)		
MAP (kg ha^{-1})	66	
Urea (kg ha^{-1})	100	75
In-season fertilizer		
Urea (kg ha^{-1}) and date	50 on 16 July	100 on 28 June
	50 on 17 August	100 on 27 July
Yield (t ha^{-1})	5.67	3.84

Soil moisture probes (Sentek Sensor Technologies, Adelaide, SA, Australia) were installed in 2017, with sensors every 10 cm down to a depth of 40 cm and every 20 cm down to 100 cm. Soil samples were collected in triplicate from close to each sensor before crop sowing, and a representative composite sample from each layer was analyzed. The basic physicochemical properties of the soil were estimated following the standard procedures [41]. Data on soil texture, bulk density, pH, and organic carbon content are given in Table 2 for both sites. Soil texture at Pygery ranged from sandy loam to sandy clay, with clay contents increasing gradually with depth, while the texture at Yeelanna represents a typical duplex, sandy clay loam at the surface (0–10 cm) with heavy clay underneath. Both sites have soils with pH in the alkaline range and almost similar organic carbon contents (OC), except for a higher OC level (2.03%) in the surface soil at Yeelanna. The soil's cation exchange capacity (CEC) at different depths was almost double at Yeelanna than at Pygery except in the surface layer (0–15 cm). The soil nitrate (NO_3–N) and ammonium N (NH_4–N) contents were analyzed at 0–15, 15–30, 30–60, and 60–100 cm soil depths.

The particle size distribution and bulk density of different layers at the study sites were measured to estimate the soil hydraulic parameters, which were used as inputs into the HYDRUS-1D model [17]. Measured values of the air-dry (θ_r) and saturated (θ_s) water contents were used in the simulations. Typically, the θ_r values ($\approx$1500 kPa) were relatively high, a characteristic feature of heavy sub-soil clay commonly occurring in the dryland belt of the study region [42]. These parameters were further fine-tuned during the model calibration using water content dynamics data in the soil. Optimized parameters for both sites used in the numerical model are shown in Table 3.

Table 2. Physicochemical properties of soils at the experimental sites.

Depth (cm)	Soil Texture	Sand %	Silt %	Clay %	D_b (g cm^{-3})	OC (%)	pH (H_2O)	pH ($CaCl_2$)	CEC (Cmol (+) kg^{-1})
					Pygery (Py)				
0–15	SL	64.7	13.5	19.8	1.57	1.17	8.5	7.8	17.0
15–30	SCL	58.7	12.3	28.9	1.33	0.75	8.7	8.0	22.5
30–60	SCL	47.0	21.2	31.8	1.33	0.55	9.3	8.3	25.0
60–90	CL	42.7	21.2	36.0	1.42	0.34	9.5	8.5	26.2
90–100	SC	45.0	19.3	35.7	1.42	0.34	9.5	8.5	24.7
					Yeelanna (Ye)				
0–15	SCL	70.4	8.7	20.9	1.45	2.03	8.1	7.7	26.1
15–30	C	21.8	6.3	71.9	1.34	0.70	8.5	7.9	42.0
30–60	C	22.3	6.4	71.2	1.52	0.42	8.6	8.0	45.5
60–90	C	14.3	10.2	75.6	1.64	0.32	9.3	8.3	47.2
90–100	SC	51.5	3.0	45.5	1.64	0.32	9.3	8.3	51.5

S = sand; C = clay; L = loam; D_b = bulk density; OC = organic carbon; CEC = cation exchange capacity.

Table 3. Estimated soil hydraulic parameters at Pygery and Yeelanna used in the HYDRUS-1D modeling simulations.

Soil Texture	Soil Depth (cm)	θ_r (cm^3 cm^{-3})	θ_s (cm^3 cm^{-3})	a (cm^{-1})	n	K_s (cm d^{-1})	l	D_b (g cm^{-3})
				Pygery (Py)				
Loam	0–15	0.05	0.40	0.024	1.40	27.1	0.5	1.57
Loam	15–30	0.12	0.41	0.022	1.32	19.1	0.5	1.33
Clay loam	30–60	0.2	0.44	0.017	1.37	15.6	0.5	1.33
Clay loam	60–90	0.22	0.45	0.017	1.35	14.4	0.5	1.42
Cay loam	90–105	0.24	0.45	0.018	1.35	15.8	0.5	1.42
				Yeelanna (Ye)				
Loam	0–15	0.07	0.45	0.025	1.45	53.4	0.5	1.45
Clay	15–30	0.15	0.46	0.023	1.31	17.2	0.5	1.34
Clay	30–60	0.19	0.44	0.021	1.28	9.4	0.5	1.52
Clay	60–90	0.21	0.49	0.019	1.17	5.49	0.5	1.64
Silt loam	90–105	0.24	0.49	0.018	1.16	11.1	0.5	1.64

θ_r and θ_s are the residual and saturated water contents, respectively; K_s is the saturated hydraulic conductivity, D_b is the bulk density, and a, n, and l are shape parameters.

2.2. Climate Parameters

Local climate parameters were obtained from the SILO climate database [43] using the Wudinna Aero station (station 18083) for the Pygery site and the Yeelanna station (station 18,099) for the Yeelanna site. At Pygery, both 2018 and 2019 were dry years, with total rainfall during the wheat growing season (May to December) amounting to 208 and 190 mm, respectively (Figure 1). Most of the rain occurred during the winter period (May to August) when the crop water demand was low. Corresponding values of ET_0 at the Py and Ye sites were 829 and 886 mm, respectively (Figure 1).

At Yeelanna, average values of rainfall and ET_0 during the study period (2018–2019) and the wheat cropping season (May–December) were 365 and 693 mm, respectively (Figure 1). The ET_0 values were usually low during the winter season and then increased during the wheat's post-anthesis period, thus enhancing crop water demand between anthesis and harvest. Thus, low rainfall and high climate water demand at Pygery impose relatively adverse conditions for wheat cultivation compared to the Yeelanna site. Gradually

increasing trends in the daily ET_0 values suggest that the wheat growing season overlaps the winter season, slowly transitioning to summer under the Mediterranean climate.

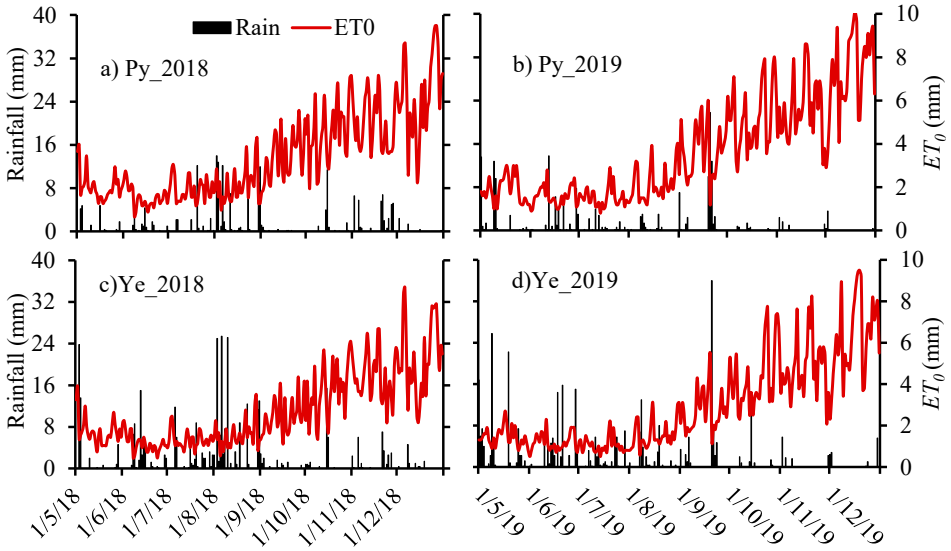

Figure 1. Daily values of rainfall and reference crop evapotranspiration (ET_0) at the Pygery (**a**,**b**) and Yeelanna (**c**,**d**) sites during the 2018 (**a**,**c**) and 2019 (**b**,**d**) wheat growing seasons (May–December).

Daily crop evapotranspiration (ET_C) values for wheat were estimated from daily reference crop evapotranspiration (ET_0) and crop coefficients (K_c) for different growth stages [44]. The daily ET_C values were divided into the evaporation (E_s) and transpiration (T_p) components based on the leaf area index (LAI) as follows [45]:

$$E_s = ET_c \cdot e^{-K_{gr} \times \mathrm{LAI}} \quad (1)$$

$$T_p = ET_c - E_s$$

where K_{gr} is the light extinction coefficient for wheat, and its value was set to 0.46 [46] for rainfed conditions. Estimated LAI values for wheat at both locations are shown in Figure 2. Daily wheat ETc values during the 2018 and 2019 seasons are shown in Supplementary Material (Figure S1a–d). Annual ETc values for wheat at Pygery and Yeelanna during 2018 and 2019 were 375.1 and 389.6 and 287.5 and 296.5 mm, respectively. These values and daily rainfall were then used as inputs into the HYDRUS-1D model to estimate the actual values of E_s and T_p ($E_{s\,act}$ and $T_{p\,act}$) for wheat at both locations.

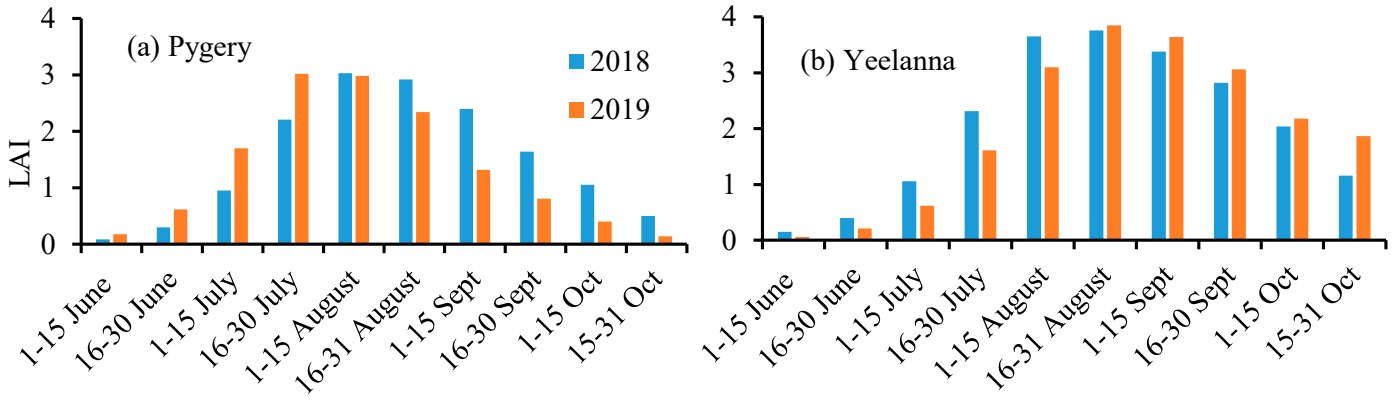

Figure 2. Estimated leaf area index (LAI) of wheat at the (**a**) Pygery and (**b**) Yeelanna sites during the 2018 and 2019 seasons.

2.3. Brief Description of HYDRUS-1D

The HYDRUS-1D software can simulate one-dimensional variably saturated water flow, heat movement, and transport of solutes involved in sequential first-order decay reactions [17]. The governing one-dimensional water flow equation is described as follows:

$$\frac{\partial \theta}{\partial t} = \frac{\partial}{\partial z}\left(K(h)\frac{\partial h}{\partial z} - K(h)\right) - R(h,z,t) \quad (2)$$

where θ is the soil water content (L^3L^{-3}), t is the time (T), h is the soil water pressure head (L), z is the vertical coordinate (L), $K(h)$ is the unsaturated hydraulic conductivity function (LT^{-1}), and $R(h,z,t)$ is the sink term accounting for an actual volume of water uptake by plant roots from a unit volume of soil per unit time ($L^3L^{-3}T^{-1}$). Water extraction $R(h,z,t)$ from the soil was computed using the Feddes model [47]. Different values of the stress response function for wheat were taken from the HYDRUS-1D data repository. In this method, the potential transpiration rate, T_p, is distributed over the root zone using the normalized root density distribution between 0 and 1 and multiplied by the dimensionless water stress response function. Hence, this model assigns plant root water uptake rates according to local soil water pressure heads at any point in the root zone. Therefore, potential transpiration (T_p) is reduced below its potential value when the soil can no longer supply the amount of water required by the plant under the prevailing climatic conditions.

The partial differential equations governing one-dimensional dynamics of N involved in sequential first-order decay chain reactions during transient water flow in a variably saturated rigid porous medium [17] are given as:

$$\frac{d\theta C_1}{dt} = \frac{d}{dz}\left(\theta D_1^w \frac{dC_1}{dz}\right) - \frac{dqC_1}{dz} - \mu'_{w,1}\theta C_1 \quad (3)$$

$$\frac{d\theta C_2}{dt} + \frac{d\rho S_2}{dt} + \frac{da_v g_2}{dt} = \frac{d}{dz}\left(\theta D_2^w \frac{dC_2}{dz}\right) + \frac{d}{dz}\left(a_v D_2^g \frac{dg_2}{dz}\right) - \frac{dqC_2}{dz} - \mu'_{w,2}\theta C_2 + \gamma_{s,2}\rho + \mu'_{w,1}\theta C_1 - r_{a,2} \quad (4)$$

$$\frac{d\theta C_3}{dt} = \frac{d}{dz}\left(\theta D_3^w \frac{dC_3}{dz}\right) - \frac{dqC_3}{dz} - \mu'_{w,3}\theta C_3 + \mu'_{w,2}\theta C_2 - r_{a,3} \quad (5)$$

where C is the solute concentration in the liquid phase (mg L^{-1}), S is the solute concentration in the solid phase (mg g^{-1}), g is the solute concentration in the gas phase (mg L^{-1}), ρ is the dry bulk density (g cm^{-3}), q is the volumetric flux density (cm day^{-1}), μ'_w is the first-order rate constant for the solute in the liquid phase (day^{-1}), providing connections between individual chain species, γ_s is a zero-order rate constant in the solid phase (day^{-1}), r_a is the root nutrient uptake (mg L^{-1} day^{-1}), D_w is the dispersion coefficient (cm^2 day^{-1}) for the liquid phase, and D_g is the diffusion coefficient (cm^2 day^{-1}) for the gas phase. The subscripts 1, 2, and 3 represent $(NH_2)_2CO$ (urea), NH_4^+–N (ammonium N), and NO_3^-–N (nitrate N), respectively. Adsorption/desorption of NH_4^+ is an instantaneous reaction between the soil solution and the exchange sites of the soil matrix [48].

2.4. Nitrogen Balance Parameters

Input parameters for the nitrogen transport in HYDRUS-1D are required to characterize the three main sets of processes: solute transport, solute reactions/transformations, and root solute uptake. Baldock et al. [49] defined the following N balance components in the soil, which are crucial to understanding and estimating the annual soil N dynamics.

$$\text{N balance} = (N_F + N_{Min} + N_{dfa} + N_{dep}) - (N_R + N_L + N_V + N_{Den} + N_E) \quad (6)$$

where N_F is N added to the soil in the form of chemical fertilizers, N_{Min} is N added to the soil in the form of organic amendments (e.g., manure, composts, etc.), N_{dfa} is N derived from atmospheric N_2 by symbiotic and non-symbiotic fixation, N_{dep} is the N deposition

from the atmosphere, N_R is N removed in harvested products, N_L is N leached from the root zone, N_V is N volatilized as ammonia from fertilizers and soils, N_{Den} is N lost as N_2 and N_2O by denitrification, and N_E is N lost by erosion.

In the N modeling study, all components of the N balance except for N_{dfa}, N_{dep}, N_{Den}, and N_E were considered. Neglected components were either present only in minute amounts (N_{dfa}, N_{dep}) in the wheat fields or represented negligible processes in dryland conditions (N_{Den}, N_E) [50,51]. Organic N mineralization (N_{Min}) was estimated based on the assumption of 3% annual mineralization estimated for the study region [49].

The following values of solute transport parameters were used in the simulation; the molecular diffusion coefficients in free water (D_w) for NH_4–N and NO_3–N were 1.52 and 1.64 cm^2 day^{-1}, respectively, the molecular diffusion coefficient in the air (D_g) for NH_3 was optimized as 18057.6 cm^2 day^{-1}, similar to other studies [52], the longitudinal dispersivity was considered equal to one-tenth of the profile depth [53], and Henry's law constant (K_H, at 25 °C) for NH_4–N was 2.95×10^{-4} [54]. The distribution coefficients (K_d) for NH_4 that varied from 1.0 to 1.8 cm^3 mg^{-1} in different soil layers were adapted from Li et al. [52]. These values fall within the range reported for different mixed and layered soils [55]. The urea hydrolysis rate (K_h) of 0.74 day^{-1} in the topsoil layer (0–10 cm) adapted in the current study is consistent with the reported values in numerous studies under different soils and climate conditions [52,56,57].

The nitrification rates were calibrated to vary from 0.02 to 0.25 day^{-1}, with higher surface soil values, then decreasing gradually with depths. The volatilization rate of 0.24 kg ha^{-1} day^{-1} reported under rainfed wheat cultivation in south Australia [27] was used in the current study. While some of these processes are temperature- and water-content-dependent, neglecting these dependencies is common [37,52] due to the lack of such information and measured data. Unlimited passive uptake of NO_3–N was allowed in the root solute uptake model [58] by specifying the maximum allowed uptake concentration exceeding NO_3–N concentrations in the root zone. In addition to passive uptake, active uptake of NH_4–N was also integrated into the simulations. The Michaelis–Menten constant for active uptake of NH_4 was assumed to equal the default value of 0.5 mg L^{-1}.

2.5. Initial and Boundary Conditions

The initial water contents at various depths were set using the soil water contents measured by the capacitance probe. Measured ammonium and nitrate contents in the soil, specified in terms of N concentrations (NH_4–N and NO_3–N), were set as the initial conditions for N simulations. The initial concentration representing the basal fertilizer application was calculated using the initial soil water content, assuming fertilizer was mixed within the surface 10 cm layer. An atmospheric boundary condition with surface runoff was specified at the soil surface for water flow. The free drainage boundary condition was imposed at the bottom of the domain (105 cm). Root water uptake was calculated using the potential transpiration rate, specified rooting depth and density, and the Feddes' stress response function [47]. The upper boundary condition for solute transport was set as a 'volatile' boundary condition [59] with a stagnant boundary layer of 2.5 cm. This boundary condition assumes a stagnant boundary layer (air) at the top of the soil profile and that upward solute movement through this layer is by solute diffusion in air, facilitating the simulation of volatilization losses of N. A third-type boundary condition was used at the lower boundary. The concentration fluxes of N for all fertilizer applications were calculated in N content terms. The top-dressed fertilizer application during the wheat season is represented in the model by converting the amount of applied urea into the boundary concentration using the known value of the water content in the topsoil layer (from the previous water flow simulation) at the time of fertilizer application.

HYDRUS-1D simulations were commenced on 1 May 2018 and continued until 31 December 2019 for both locations. Theoretical details and more information on the HYDRUS-1D software and related references can be found at https://www.pc-progress.com/en/Default.aspx?HYDRUS-3D (accessed on 30 August 2023).

2.6. Model Evaluation

The modeling performance for water balance was evaluated by comparing capacitance probe-measured (*O*) soil moisture values at various depths with those predicted by HYDRUS-1D (*P*) for the 2018 and 2019 crop seasons. The statistical error estimates, mean error (ME), mean absolute error (MAE), and root mean square error (RMSE), between the measured and simulated spatiotemporal water contents, were estimated as:

$$ME = \frac{1}{N}\sum_{i=1}^{N}(Oi - Pi) \quad (7)$$

$$MAE = \frac{1}{N}\sum_{i=1}^{N}|Oi - Pi| \quad (8)$$

$$RMSE = \sqrt{\frac{1}{N}\sum_{i=1}^{N}(Oi - Pi)^2} \quad (9)$$

3. Results

3.1. Soil Water Dynamics in the Soil

The capacitance probe measured daily soil water contents in 0–30 cm and 30–100 cm depths at the Pygery and Yeelanna sites, which were compared with corresponding HYDRUS-1D simulated values in Figure 3. The simulations showed small changes in the wetting of the upper horizon (<30 cm) at the Py site due to the instant depletion of soil moisture in response to soil evaporation and plant transpiration. However, at the medium rainfall site (Ye), the water content rapidly increased in the 0–30 cm horizon. In the second horizon (30–100 cm), both data sets showed only small changes in moisture content over the two wheat seasons. A close correspondence between the observed and modeled moisture distribution patterns exists in both horizons, despite the probe malfunction in 2018 during a short period from mid-February to mid-March 2019 (Figure 3). The moisture probe measured slightly lower values during the post-harvest wheat season, especially at deeper depths (>30 cm). The HYDRUS-1D results distinctly show two soil horizons with a boundary at a depth of 30 cm. It should be noted that measured and simulated moisture contents in the soil below 30 cm are consistently high during both seasons, especially at the Yeelanna site (between 0.25 and 0.35 cm^3 cm^{-3}). Similar values of soil water contents were observed in other regional studies [60]. This is a typical characteristic of sub-soil heavy clay in the study region, with the clay fraction at the Yeelanna site as high as 75% (Table 1). These soils can hold a large amount of water, varying between 0.2 and 0.25 cm^3 cm^{-3} at the wilting point (1500 kPa), which is unavailable to plants. In addition, these soils may have sub-soil constraints such as compaction, which further restricts the water movement and uptake by growing crop plants [60]. Hence, the water contents in the sub-soils (>30 cm depth) remained consistently static during the entire cropping season.

Statistical errors (ME, MAE, and RMSE) assessing the comparison between HYDRUS-1D simulated and measured soil water contents for the soil surface (0–30 cm) and deeper (30–100 cm) layers showed a varied response (Table 4). The RMSE, MAE, and ME values for the surface depth (0–30 cm) during 2018 and 2019 at Pygery remained between -0.02 and 0.03 cm^3 cm^{-3}, indicating a close agreement. The corresponding values for the 30–100 cm profile were between -0.06 and 0.07 cm^3 cm^{-3}, slightly higher than for the surface layer. At Yeelanna, the error estimates during 2018 ranged from -0.02 to 0.06 and from 0.03 to 0.04 cm^3 cm^{-3} in the 0–30 cm and 30–100 cm soil depths, respectively. During the validation period (2019), the error values varied from -0.04 to 0.07 cm^3 cm^{-3}. Wang et al. [61] reported RMSE and mean relative error (MRE) values of 0.07 cm^3 cm^{-3} and 21.6%, respectively, as accurate estimation of water content dynamics in the soil by SWAP model under wheat irrigated with varied levels of deficit irrigations. Error estimates reported in other studies [37,62] also corroborate well with the values estimated in the current study, which showed a good agreement between measured and simulated water content dynamics in the soil.

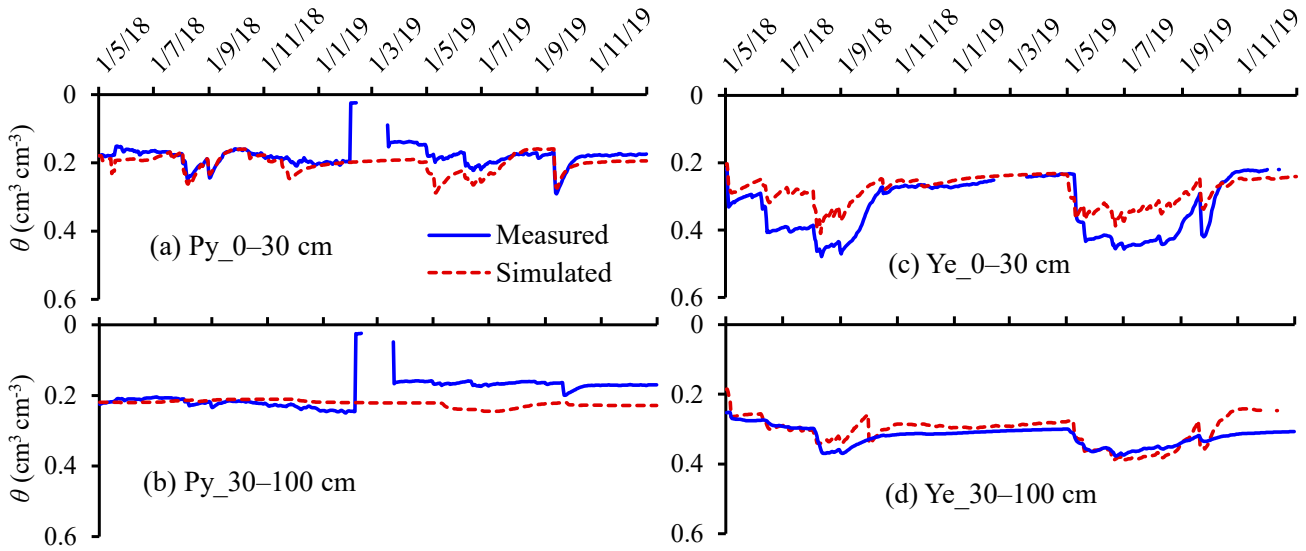

Figure 3. Comparison of measured soil water contents in the 0–30 cm (**top**) and 0–100 cm (**bottom**) (profile averaged) with the corresponding simulated values during the 2018 and 2019 wheat growing seasons at the Pygery (**a**,**b**) and Yeelanna (**c**,**d**) sites on the Eyre Peninsula.

Table 4. Estimated values of the root mean square error (RMSE), mean absolute error (MAE), and mean error (ME) between measured and model-predicted water content in the soil for the 0–30 cm and 30–100 cm soil layers at the Pygery and Yeelanna sites during 2018 and 2019.

Site	Year	Soil Depth (cm)	RMSE (cm^3 cm^{-3})	MAE (cm^3 cm^{-3})	ME (cm^3 cm^{-3})
Pygery	2018	0–30	0.02	0.01	−0.01
		30–100	0.04	0.03	0.02
	2019	0–30	0.03	0.03	−0.02
		30–100	0.07	0.06	−0.06
Yeelanna	2018	0–30	0.06	0.02	0.04
		30–100	0.04	0.03	0.03
	2019	0–30	0.07	0.07	−0.04
		30–100	0.05	0.04	−0.02

There are numerous possible reasons for the deviations in the behavior of water content dynamics in the soil. Apart from model assumptions, capacitance probes can induce significant errors in the water content measurements. Numerical modeling depends on three crucial factors: (a) the accuracy of model input parameters; (b) the precision of observed values compared with the model output; and (c) sensitivity in the initial conditions. Ramos et al. [62] showed that deviations between measured and model-predicted water content dynamics in the soils might be related to field measurements, model inputs, and model structural errors. The moisture probe's calibration and the inherent complexities of the soil [63] are additional crucial factors that immensely affect the extent of the divergence between observed and modeled data. These factors may contribute to a similar extent of deviations in water contents as obtained by modeling predictions. It is also likely that higher observed values of the water content at lower depths (>50 cm) at Yeelanna may have contributed to larger values of the error statistics. Overall, a good agreement between the measured and simulated data shows that the model can predict the effects of different weather and soil properties at different sites and respond to various field variations.

3.2. Soil Water Balance

Seasonal water balance components ($T_{p\,act}$ = actual plant water uptake, E_s = soil evaporation, D_r = drainage, ΔS = soil storage/depletion) for the wheat crop at Pygery (Py) and Yeelanna (Ye) predicted by HYDRUS-1D during 2018 and 2019 are shown in Table 5. At Pygery, evaporation losses during the crop season (May to October) varied from 44 to 57%, with an average of 50% of the rainfall received. The remaining water (43–58%) was attributed to plant uptake, while drainage losses were negligible. At Yeelanna, E_s losses varied from 29 to 42%, with an average value of 33%, significantly lower than at Pygery. Plant water uptake varied from 41 to 49%, with an average value of 40%. The drainage component (D_r) represents 12–26% (41–90 mm) of the rainfall received during the cropping season, which is the main difference between the two sites.

Table 5. Seasonal water balance components (mm) simulated by HYDRUS-1D during the 2018 and 2019 cropping seasons at the Pygery (Py) and Yeelanna (Ye) sites.

Site	Year	E_s	$T_{p\,act}$	D_r	ΔS	Rainfall (Season)	Rainfall (Annual)
Py	2018	76.6	95.2	0.03	6.4	175.6	235.3
	2019	98.6	85.0	0	−2.8	183.6	201.8
Ye	2018	96.3	140.5	40.8	54.9	333	407.6
	2019	104.3	140.6	90.4	9.2	348.3	375.5

$T_{p\,act}$ = actual plant water uptake, E_s = evaporation, D_r = drainage, ΔS = soil storage/depletion.

Daily $T_{p\,act}$ and E_s components of the water balance simulated by HYDRUS-1D during 2018 and 2019 at Pygery and Yeelanna are shown in Figure 4. At Pygery, daily plant water uptake varied from 0 to 2.6 mm during 2018, while the maximum value was 2.2 mm during the 2019 crop season. As expected, daily evaporation losses (Es) were higher before sowing and after the crop harvest. However, the magnitude remained low during 2018 (0–1.5 mm), reflecting the moisture availability in the surface soil layer. During 2019, spikes in daily evaporation (up to 2 mm) were similar to plant water uptake, especially during crop maturity and harvest (September and October).

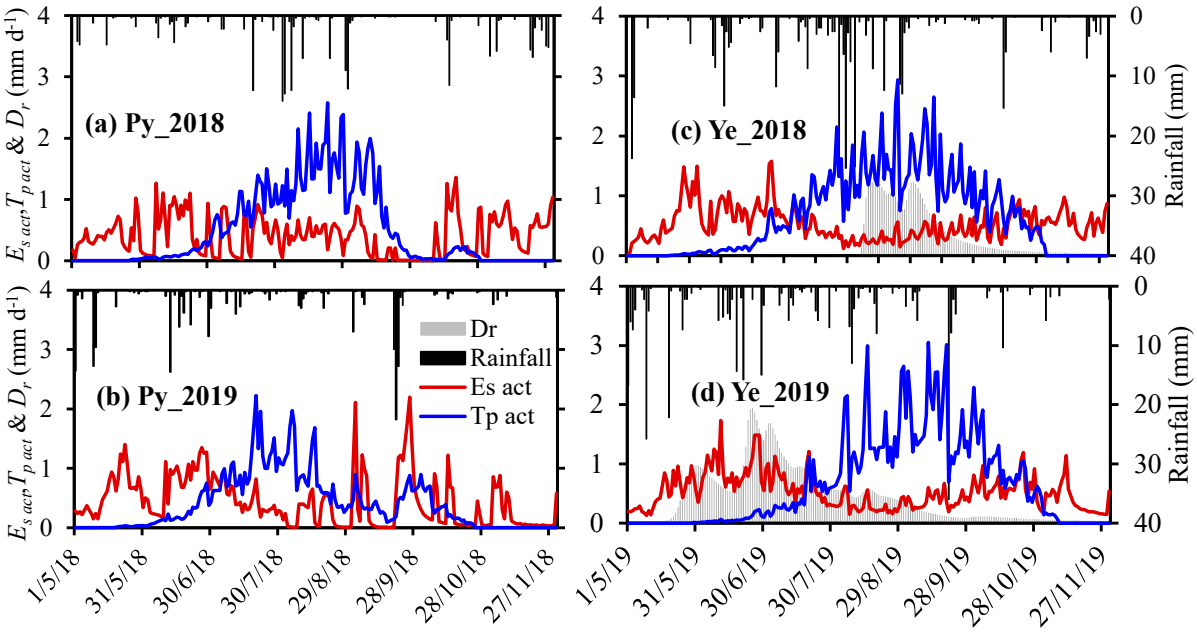

Figure 4. Daily rainfall and predicted values of actual evaporation ($E_{s\,act}$), actual plant water uptake ($T_{p\,act}$), and drainage (D_r) under wheat crop during the 2018 (**top**) and 2019 (**bottom**) growing seasons at the Pygery (**a**,**b**) and Yeelanna (**c**,**d**) sites on the Eyre Peninsula.

At Yeelanna, the maximum daily plant water uptake ($T_{p\,act}$) reached about 3 mm during the 2018 and 2019 seasons (Figure 4). The magnitude of daily $T_{p\,act}$ losses was similar to Pygery, but there was less fluctuation in the daily dynamics, probably due to the consistent availability of moisture in the surface layer. One of the important components of the water balance at Yeelanna is drainage (D_r), which was negligible at Pygery. Daily drainage (D_r) losses occurred in August–September of 2018, while these losses were higher early in the season (mid-May to August) during 2019.

3.3. Nitrogen Simulation in the Soils

Nitrogen species commonly occurring in a dissolved state in the soil solution are NH_4–N and NO_3–N. These species control the plant-available forms of N in the soils. The dynamics of these species depend on the number and magnitude of N pools in the soil, their interactions, transformations, and exchanges among them. The comparison of measured and simulated values of NH_4–N and NO_3–N in the soil at various depths at the time of wheat harvest is shown in Figure 5 for the Pygery site. Some inconsistencies include the higher simulated value of NO_3–N than measured in the surface soil (0–15 cm) during 2018, which subsequently increased in the second layer (15–30 cm) and then showed a similar pattern as measured values. Similarly, the measured NH_4–N value was higher than simulated, while the reverse was true for NO_3–N in the surface layer during the 2019 season. However, at other depths, the simulated values of both species matched well with the measured values. Furthermore, the profile-averaged measured NH_4–N values of 0.7 and 1.1 ppm were comparable to the corresponding simulated values of 0.8 and 0.9 ppm, respectively, during the 2018 and 2019 wheat seasons.

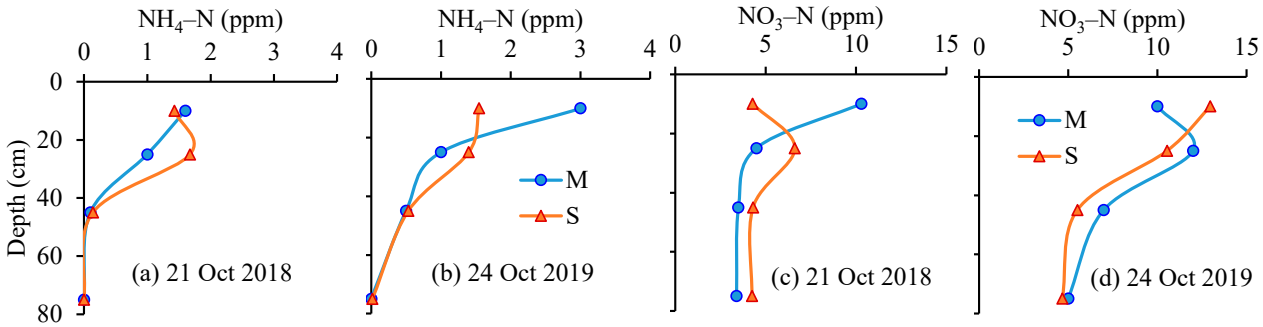

Figure 5. Comparison of measured (M) and simulated (S) values of NH_4–N (**a**,**b**) and NO_3–N (**c**,**d**) in the soil at wheat harvest time (as indicated) during the 2018 (**a**,**c**) and 2019 (**b**,**d**) seasons at the Pygery site.

Similarly, measured profile-averaged NO_3–N contents of 5.4 and 8.5 ppm matched well with the corresponding simulated values of 4.9 and 8.4 ppm, respectively, during 2018 and 2019. This indicates that the model has been able to simulate the N dynamics in the soil profile under wheat crop at the Pygery site. Modelled N dynamics in the soil at the Yeelanna site could not be compared in the absence of appropriate measured data. Overall, the patterns of NH_4–N and NO_3–N values in the soil indicate that the modeling approaches used to account for N mineralization, transformation, plant uptake, and conversions of N among different pools in the soils are reasonably sound. However, intensive soil observations for nitrogen transformations, losses, and soil solution species are required to improve the simulation at both field sites.

The spatiotemporal dynamics of the simulated concentrations of these species are shown in Figure 6 for both sites. The distribution pattern of N species revealed that a fraction of NH_4–N always remained in the soil due to the continuous decomposition of organic N to NH_4–N considered by the HYDRUS-1D model. High peaks of NH_4–N in the soil, especially in the surface layers (0–15 and 15–30 cm), corresponded to the fertilizer applications. However, the increasing presence of NH_4–N in low concentrations in the lower layers of the soil profile indicates a slow downward movement of NH_4–N in the soil

with time. However, NH_4–N concentrations in the soil remained below 2 ppm throughout the simulation except after applying the NH_4–N fertilizer.

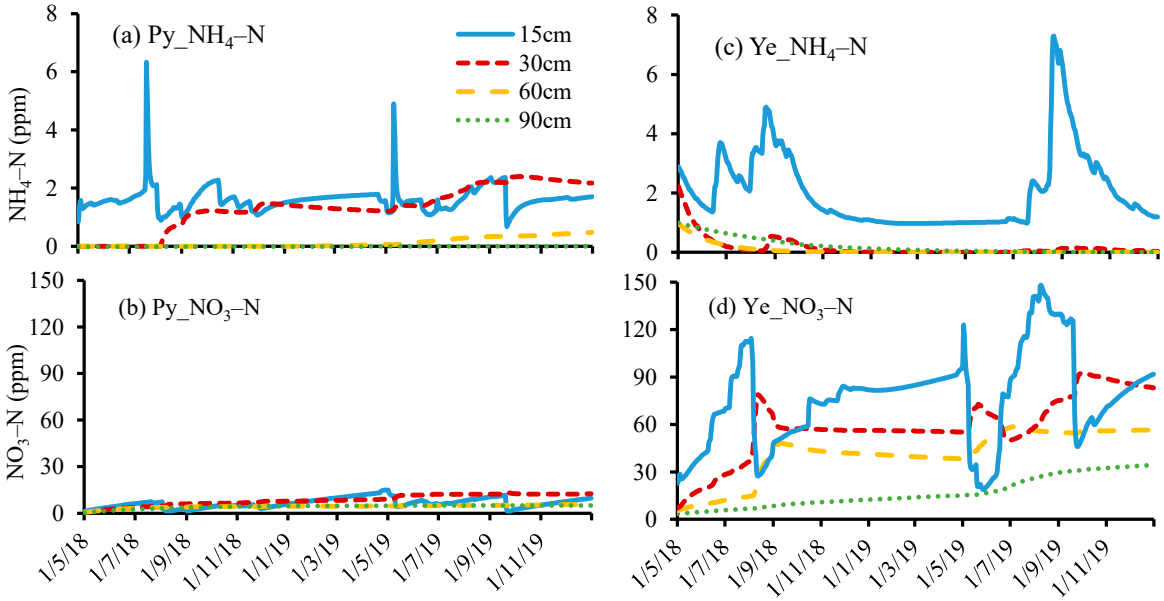

Figure 6. Simulated distribution of NH_4–N (**a**,**c**) and NO_3–N (**b**,**d**) in the soil at different depths (15, 30, 60, and 90 cm) at the Pygery (**a**,**b**) and Yeelanna (**c**,**d**) sites.

Simulated daily NO_3–N concentrations at the Pygery site gradually increased with time, especially in the surface soil layer (0–40 cm). They fluctuated between 1.2 and 14.9 ppm in the 0–15 cm layer (Figure 6b). The gradual peaks in the surface layer (0–15 cm) reveal the conversion of NH_4–N to NO_3–N via nitrification. These peaks subsequently moved to lower depths with lower concentrations and a lag time reflecting plant uptake. At deeper soil layers (below 50 cm), the NO_3–N concentrations were more or less stable around 5 ppm, indicating reduced N uptake and transformation activities in this zone. This also suggests a lack of deep drainage at Pygery, a crucial driver for transporting NO_3–N deeper into the soil. The water balance at the Pygery site strongly supports this observation (Table 4).

At Yeelanna, HYDRUS-1D predicted higher NH_4–N concentrations in the soil than at Pygery (Figure 6c). The NH_4–N concentrations in the surface layer (0–15 cm) reached high values of 4.8 and 7 ppm after the fertilizer application. The continued presence of NH_4–N in low concentrations in the surface zone indicates the continual production of NH_4–N by mineralizing organic matter. On the other hand, the peak NO_3–N concentration in the 0–15 cm soil depth at Yeelanna was almost 8–10 times higher than at Pygery. During 2018, the NO_3–N concentration increased to 112 ppm in response to fertilizer application and subsequently decreased in early September, likely due to leaching (Figure 6d). Later in the season, during the post-harvest summer period, the NO_3–N concentration in the upper soil layers (0–15 cm) increased with a decrease in the soil water content. The NO_3–N concentration in the soil peaked at 144 ppm in 2019 due to much higher N application and then decreased due to plant uptake and late-season leaching. At the end of the simulation in 2019 (31 December 2019), the NO_3–N concentration in the soil ranged from 34 to 91 ppm. Higher concentrations of NH_4–N and NO_3–N in the soil at Yeelanna were directly related to higher N applications. High levels of NO_3-N concentration were reported in other modeling studies under similar N fertilization and wheat production conditions [64].

3.4. Nitrogen Balance in Soils

3.4.1. Mineralization of Organic N in the Soil

The breakdown of organic matter in the soil (N_{Min}) at Pygery during the cropping season (May–December) added 37.3 kg N ha^{-1} during 2018 and almost a similar amount

during 2019 (Figure 7). HYDRUS-1D predicted higher N_{Min} (56.2 to 56.4 kg N ha^{-1}) for the soil at Yeelanna than at Pygery due to the higher organic carbon content in the soil at the former (2.03%) relative to the latter (1.17%) site. Additionally, relatively low rainfall at Pygery perhaps impacted the microbial decomposition of organic matter because the mineralization rate is only about two-thirds of that at Yeelanna. The absolute values of daily N_{Min} at Pygery ranged between 0.15 and 0.17 kg N ha^{-1}, whereas the corresponding values for Yeelanna ranged from 0.22 to 0.25 kg N ha^{-1}, with an average seasonal total of 37.5 and 56.3 kg N ha^{-1} at Pygery and Yeelanna, respectively. The conversion of NH_4–N to NO_3–N in the soil at Pygery was relatively poor compared to Yeelanna due to unfavorable moisture and temperature conditions. Therefore, relatively higher NH_4–N deposition/storage in the soil occurred at Pygery than at Yeelanna. There was a slight increase in the N_{Min} rate during the cropping/winter season at both locations. However, these estimates will vary over the years, depending on the substrate's content and quality, the C:N ratio, microbial activity, and climate variability, including rainfall and temperature variations [1,65].

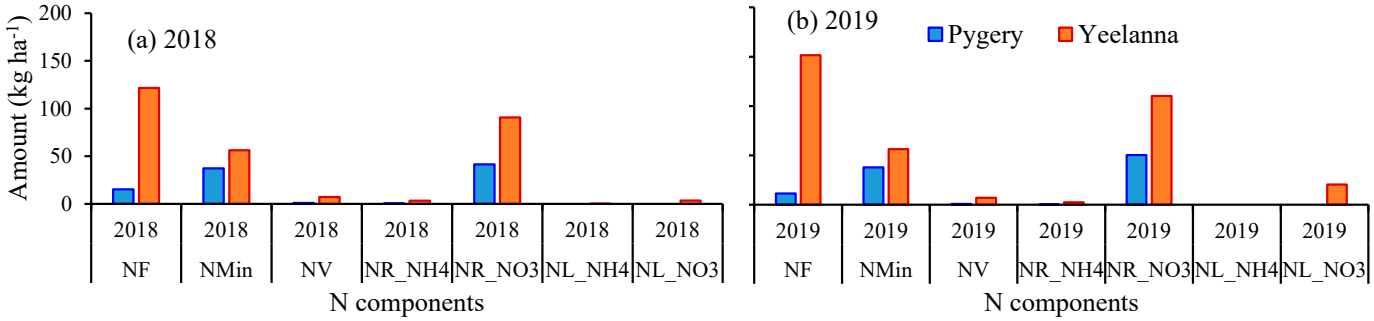

Figure 7. Predicted components of N balance ((N_F = fertilizer nitrogen; N_{Min} = N mineralization from organic matter; N_V = N volatilization; N_{R_NH4} = plant uptake of ammonium N; N_{R_NO3} = plant uptake of nitrate N; N_{L_NH4} = leaching of ammonium N; N_{L_NO3} = leaching of nitrate N) during the (**a**) 2018 and (**b**) 2019 at Pygery (Py) and Yeelanna (Ye).

3.4.2. Nitrogen Uptake by Wheat

Nitrogen available to wheat includes inorganic nitrogen (NH_4–N and NO_3–N), such as fertilizers, and soluble organic nitrogen. The amount of N delivered from soil to plants is location-specific due to the variations in the environmental conditions, soil types, and different agricultural management practices implemented at the two locations. Simulations showed that NH_4–N contributed very little to the plant N nutrition and that most N uptake was in the form of NO_3–N during both crop seasons (Figure 8). The simulated total N uptake at Yeelanna was more than twice that at Pygery. Daily NH_4–N and NO_3–N uptake by wheat at Pygery ranged from 0 to 0.16 mg L^{-1} and 0 to 13 mg L^{-1}, respectively. While at Yeelanna, maximum daily NH_4–N and NO_3–N uptakes were 0.9 and 0.8 mg L^{-1} in 2018 and 15.5 and 27.8 mg L^{-1} in 2019, respectively. Notably, wheat's maximum daily N uptake occurred from early August to late September, coinciding with the wheat's maximum growth period. Seasonal crop N uptake at Pygery ranged from 55 to 62% of the total N (N_F + N_{Min}+ N_S), whereas the corresponding N uptake at Yeelanna was only 40–44%. However, wheat N uptake during 2019 at Yeelanna was roughly double the amount of N mineralized in the soil (Figure 7). This implies that almost half of the N uptake by wheat was contributed by the N fertilizer.

3.4.3. Simulated Volatilization Losses of N

Volatilization N losses (N_V) usually occur when urea or ammonium fertilizers are top-dressed or applied on the soil surface. Typically, this is a regular feature of the dryland cropping system in Australia [27]. When there is not enough moisture in the soil to hydrolyze and move the dissolved fertilizer into the soil, NH_4–N is partially converted into NH_3 and escapes into the atmosphere. High temperatures, high wind, and low

water contents in the surface layer, commonly present during wheat sowing, create ideal conditions for N_V losses. Moreover, NH_4–N may move towards the soil surface via capillary rise with intense evaporative fluxes, contributing to gaseous losses. There is an even greater potential for NH_3 losses in areas with alkaline soils [66,67].

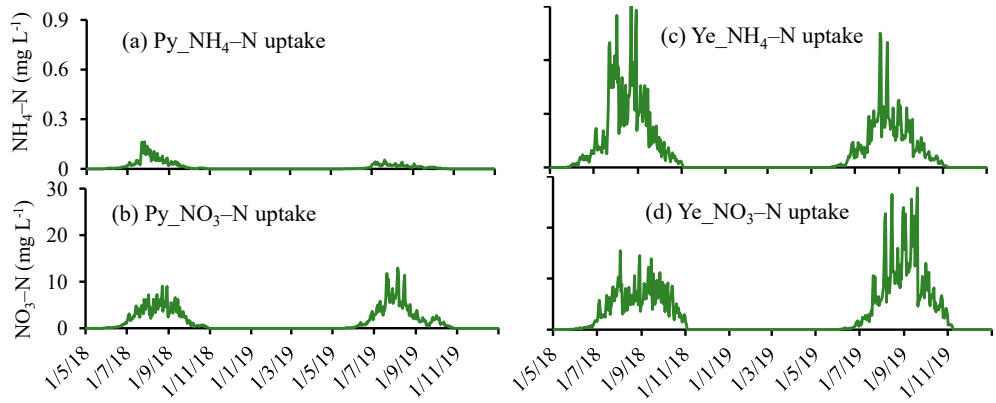

Figure 8. Daily NH_4–N (**a**,**c**) and NO_3–N (**b**,**d**) uptake by wheat at Pygery (**a**,**b**) and Yeelanna (**c**,**d**) during 2018 and 2019 simulated by HYDRUS-1D.

HYDRUS-1D simulations in the current study suggest that volatilization losses of N (N_v) at Pygery are smaller than at Yeelanna because fertilizer applications at the latter site (121–151 kg N ha^{-1}) are higher than at the former site (11–15 kg N ha^{-1}) for the same crop (Figure 9). The maximum daily N_V losses at Pygery were only 0.02 and 0.03 kg N ha^{-1} during 2018 and 2019, respectively (Figure 9a). Corresponding amounts at Yeelanna were 0.26 and 0.15 kg N ha^{-1}, respectively. At the Yeelanna site, daily N_V losses increased initially in response to fertilizer application and then rapidly dropped as the applied N was translocated deeper into the soil. This was due to high NH_4–N concentrations from the applied fertilizer in the surface soil layer with low water contents providing favorable conditions for N_v losses. Seasonal N_V losses at Pygery were 1.1 and 0.8 kg N ha^{-1} during the 2018 and 2019 cropping seasons (Figure 9), respectively. At Yeelanna, the corresponding losses were 7.3 and 6.9 kg N ha^{-1}, respectively. These losses represent 4.6 to 7.3% of the N applied. This amount falls within the range of N_V losses (1.8–23%) measured by Turner et al. [27] at different southern Australian locations involving fertilizers applied to rainfed crops, including wheat.

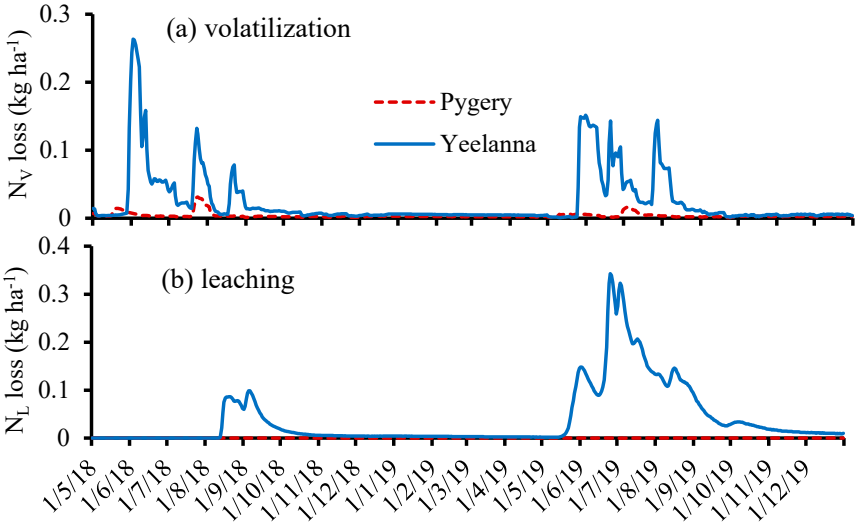

Figure 9. Daily nitrogen volatilization (N_v) (**a**) and leaching (N_L) (**b**) losses at the Pygery (Py, red line) and Yeelanna (Ye, blue line) sites simulated by HYDRUS-1D during the 2018 and 2019 wheat seasons.

3.4.4. Leaching Losses of Nitrogen

Leaching losses refer to the N losses induced by a drainage flux from the root zone to deeper soil layers and groundwater. These losses usually occur in the form of NO_3–N, a mobile component of N. At Pygery, leaching losses of NO_3–N (N_L) were negligible as there was not a sufficient drainage flux to trigger N losses. However, at Yeelanna, seasonal NO_3–N leaching amounted to 3.5 and 20.5 kg ha^{-1} during 2018 and 2019, respectively (Figure 9b). In 2018, drainage losses occurred during mid-season (mid-August to late September), even though drainage fluxes were low during that time. The maximum daily NO_3–N losses were 0.1 kg ha^{-1} (Figure 9b). On the other hand, N losses increased many folds during 2019. Most NO_3–N losses occurred early in the season when the T_p requirement was small. Heavy rain events during this period can leach an enormous quantity of NO_3–N from the root zone. Therefore, the daily rate of NO_3–N leaching increased to 0.35 kg N ha^{-1}, leading to N losses via off-site movement. On a percentage basis, N_L losses accounted for 3–13.5% of N applied by fertilizers and 1.5–7.6% of the total plant-available N in the soil.

3.5. Water Productivity and N Use Efficiency

Model-simulated seasonal water and nitrogen use and yield estimates for the experimental sites at Pygery and Yeelanna were used to estimate the water productivity in terms of transpiration (Wp_Tp) and evapotranspiration (Wp_ET), and nitrogen use efficiency (NUE) of dryland wheat (Figure 10). Both water productivities (Wp_Tp and Wp_ET) and NUE were higher at Yeelanna (high rainfall zone) as compared to Pygery (low rainfall zone). This explains a three times higher wheat yield at Yeelanna than the corresponding yield (1.52 t ha^{-1}) obtained at Pygery. The Wp_Tp and Wp_ET efficiencies at Pygery varied from 15 to 18 and 8 to 9 kg ha^{-1} mm^{-1}, respectively, while corresponding values at Yeelanna ranged from 27 to 40 and 16 to 24 kg ha^{-1} mm^{-1}. Different Wp values obtained at both sites signify the importance of rainfall quantities, soil's water retention properties, and farmers' management practices.

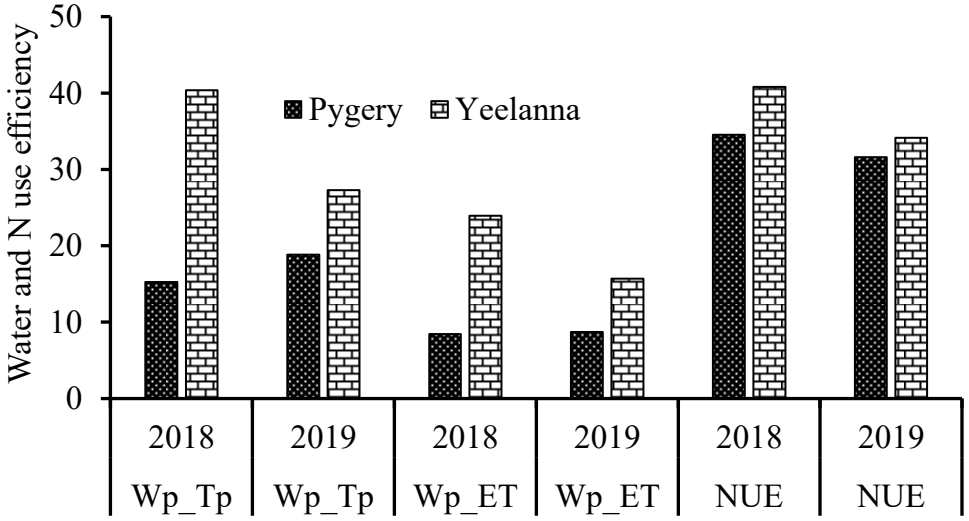

Figure 10. Estimated water productivity (kg ha^{-1} mm^{-1}) for transpiration (Wp_Tp) and evapotranspiration (Wp_ET), and nutrient use efficiency (NUE) (kg kg^{-1}) of wheat at Pygery (Py) and Yeelanna (Ye) during the 2018 and 2019 seasons.

Similarly, NUE varied from 31 to 34 and 34 to 41 kg grain yield kg^{-1} N uptake at Pygery and Yeelanna, respectively (Figure 8). Normally, the N use efficiency is relatively low, irrespective of crop type. For example, Hu et al. [68] found that about 40% of the N fertilizer is recovered in the aboveground parts of dryland wheat. The rest was either retained in the soil, denitrified, or lost by N leaching.

4. Discussion

4.1. Soil Water Balance and Wheat Water Uptake

Under rainfed conditions, the soil moisture regime is dictated by the timing, amounts, and intensity of rain, which are crucial for sustainable crop production. Therefore, accurate estimation of soil water balance helps understand the interrelationship among different hydrological components, including plant water availability and incipient water losses. Water content dynamics in the soil showed that most of the soil profile moisture regime variability occurred in the surface layer (0–30 cm), with a more static moisture regime in the deeper depths (Figure 3). The water content retained in the 0–30 cm horizon is crucial for seed germination and subsequent growth of crops, as the bulk of the fibrous roots of cereal crops mine this region for water and nutrient needs [69]. Wang et al. [61] reported that the root activity of winter wheat is concentrated within the 0–40 cm soil layer and reported small changes in water content dynamics at the deeper depths.

The model-simulated actual seasonal transpiration ($T_{p\,act}$) at both locations falls within the range estimated by French and Schultz [10] and Sadras and Angus [11] for the rainfed wheat crop. Site-specific climate, soil properties, and crop variety highly influence the extent of water uptake by wheat. In addition to low rainfall at Pygery, soils had low water holding capacity compared to Yeelanna, significantly influencing wheat's water availability in the soil. Indeed, soils with low water holding capacity and scanty rainfall during winter led to frequent terminal droughts [11]. Seasonal evaporation can tremendously impact the water availability for crop needs in the surface soils. Several studies [10,11] assumed a fixed value of the seasonal evaporation loss (110 mm) when determining water availability for rainfed wheat, which seems unreasonable. However, inter- and intra-season variabilities in the evaporation losses are common and are highly correlated with the diurnal and seasonal changes in the climate parameters and ground cover [61]. In the current study, seasonal E_s losses were 5–30% lower than a fixed value (110 mm) suggested by French and Schultz [10]. Numerous other studies [70–72] reported soil evaporation significantly lower (45–70 mm) than the proposed fixed value. Direct water loss from the soil surface can be reduced by adopting appropriate water storage and mulching practices, improving water retention in the soil [73]. Improved water regimes in surface soils can boost wheat growth and sustainable production in a water-limited environment.

Water uptake and crop yields of rainfed wheat are severely influenced by climate, soil and crop characteristics, and a large gap exists between the potential and actual crop yield [11,15]. These variabilities ultimately impact the water use efficiency of crops in rainfed environments. The average water productivity (WP_ET) values (8.6 kg ha^{-1} mm^{-1}) estimated in the current study are comparable to water use efficiency reported in other studies in the rainfed region of Australia [11,72]. Similarly, the transpiration efficiency (WP_Tp) values are similar to values reported by Harries et al. [72] and Sadras and Lawson [14] for the rainfed wheat production environments. However, the average values of WP_ET (19.8 kg ha^{-1} mm^{-1}) and WP_Tp (33.8 kg ha^{-1} mm^{-1}) obtained at the Yeelanna site were much higher than those reported in previous studies. Unlike the current study, these studies usually ignored the deep drainage component. The model predicted that 25% of rainfall received at Yeelanna is lost as deep drainage, a significant factor contributing to higher WP_ET and WP_Tp at this site. Thus, HYDRUS-1D has been able to predict the actual water balance fluxes, including deep drainage, depending on the climate, crop, and soil conditions [74], and provide an accurate assessment of water use efficiency and water-limited yield estimation for the rainfed wheat production system.

4.2. Nitrogen Losses and Recovery by Crop

Nitrogen supplement in the form of fertilizer is essential for profitable crop production. The fertilizer requirement of wheat may vary each season, depending on N_{Min} in the soil and climate variability. Angus and Grace [1] reported that the minimum level of N fertilizer applied to dryland wheat should be 45 kg N ha^{-1} for sustainable crop production. However, the long-term (15 years) application of the fixed amount of N fertilizer (45 kg ha^{-1}) at

50 farms resulted in a reduction in the wheat yield by 60% of the water-limited potential yield [75]. This suggests that the N fertilizer application at the Pygery site was much lower than required, significantly impacting obtaining a potential water-limited yield and N use efficiency. On the other hand, the amount of N applied was very high at Yeelanna (121–151 kg ha^{-1}), potentially leading to high N concentration in the soil and consequent losses of applied N. Therefore, blanket applications of N adopted by the growers in the current study can have varied impacts on crop growth and yield and may lead to potential N losses from the fields. Moreover, N transformation and loss mechanisms are highly influenced by climate variability and soil environment at different locations, impacting plant N uptake by rainfed crops. Angus et al. [76] reported that the average aboveground recovery of total N was around 36% at six commercial dryland wheat sites in south-eastern Australia. However, with improved management practices, the N recovery efficiency in grain production can be increased to 44% [1]. Thus, the wheat's NUE estimates in the current study corroborate well with other studies.

Soil factors such as texture, pH, and organic matter content, as well as soil constraints such as salinity and sodicity, also significantly impact the processes of N transformation in the soils [77]. Therefore, N recovery improvements require better temporal matching of N supply to periods of high crop demand and avoiding periods when risks of losses surge [37,65]. Monjardino et al. [78] concluded that adopting non-limiting or near-non-limiting nitrogen fertilizer practices could help close the wheat yield gap in the Australian rainfed cropping system. The results from this study indicate that site-specific water availability and N management play a crucial role in enhancing the efficient resource utilization of rainfed cropping systems. Thus, we recommend conducting further research on fertilizer-application timing and evaluating different fertilizer-application scenarios to increase crop recovery of fertilizers applied to dryland wheat production.

Ammonium volatilization (N_V), similar to ammonia and nitrate leaching (N_L) from the root zone, represents an important N loss for rainfed wheat cropping systems. The N_v losses from applied urea fertilizers typically contribute to greenhouse gas emissions from rainfed wheat production systems. However, in the present study, this fraction is lower than the emission threshold (10%) from the applied synthetic fertilizers considered by IPCC [79]. Nonetheless, N_V losses to the extent observed in the current study (4.6 to 7.3% of the N applied) still represent a major economic loss to farmers. Therefore, an accurate assessment of N_V losses could help devise better management practices for improving the productive and sustainable practices of rainfed wheat production systems.

Leaching drives the N_L losses due to rain events and the mass of N in the NO_3–N form in the soil. In sandy soils, N leaching (N_L) can be significantly higher [80], ranging between 6 and 20% of the total N flux (16–159 kg N ha^{-1} $year^{-1}$). Numerous other studies [81–84] have reported significant leaching losses of NO_3–N, varying from 4 to 59 kg ha^{-1} $year^{-1}$ for different cropping systems in Australia. This represents a financial loss to the growers and an increased risk of groundwater pollution. Indeed, NO_3 leaching occurs infrequently at most dryland cropping farms in Australia because the soil water-holding capacity is generally sufficient to retain the surplus rainfall over potential evapotranspiration.

The HYDRUS-1D simulations suggested that maintaining the N balance is crucial for the wheat production system, explaining how soil N storage changes over the years. Matching the supply of available N to the crop N demand will reduce the potential accumulation of available N and potential N losses. Although increasing N stocks is encouraged, it should be acknowledged that temporary periods of mining N stocks are acceptable, provided the extent of N mining is quantified and followed by a rebuilding phase, in which N stocks are replenished [49]. It is recommended that annual N balance calculations are performed. However, these values should be integrated and accumulated over time to define the full effect of applied management practices and temporal trends. Such information will allow grain growers to implement appropriate actions to maintain their production base in the future and continue to maximize profitable grain yield outcomes. Further optimization of N applications can reduce the N losses by linking them with soil water content, rainfall, and

meteorological data for a particular site. This requires more modeling efforts and intensive N estimation at the field site for developing rainfall-based guidelines.

5. Conclusions

Mathematical modeling tools can play a pivotal role in understanding the water and fertilizer used by the rainfed wheat production system. This study used the numerical model HYDRUS-1D to simulate the water balance and nitrogen dynamics under rainfed wheat cultivation at two locations (Pygery and Yeelanna) with varied climate and soil conditions. The model output of water and N balance was compared with measured data across various soil depths at both locations.

The modeled and measured water content suggested that plant water uptake by rainfed wheat mostly occurred in the top 30 cm of soil, signifying the importance of the surface soil layer, which stores water received by small rain events in rainfed environments. Nevertheless, moisture retained in the surface layer is vulnerable to evaporation imposed by hot and dry weather conditions in arid and semi-arid environments. In the current study, 50 and 30% of seasonal rainfall at low and medium rainfall sites were lost via evaporation. Significant leaching losses (25% of seasonal rainfall) at the medium rainfall site indicate considerable water loss in the rainfed wheat production system. Therefore, adopting appropriate water storage and mulching practices can reduce this direct water loss, enhancing water availability in the soil and improving the water-limited yield potential of rainfed wheat.

Assessing the off-site movement of N (leaching losses) can help devise better strategies for N fertilizer applications, which will reduce the environmental impacts of fertilizer use. This study showed that ammonium volatilization (N_V) and nitrate leaching (N_L) represent large potential N losses under the rainfed wheat system, depending on the seasonal rainfall and climate pattern. The N_V losses account for 4.6 to 7.3% of the added N fertilizer, while N_L losses ranged between 3 and 13.5% of N applied, especially at the medium rainfall site. Low N volatilization losses suggest that the contribution of dryland wheat farming to greenhouse N gas emissions is very low. This study evaluated water and N dynamics in the soil of the rainfed wheat production system for two years only. However, longer-term efforts are needed to reduce N leaching losses by managing the appropriate timing and dose of N applications in response to available soil moisture levels and crop needs.

Supplementary Materials: The following supporting information can be downloaded at https://www.mdpi.com/article/10.3390/su151813370/s1, Figure S1a–d: Daily values of estimated seasonal crop evapotranspiration (ETc) at the Pygery and Yeelanna sites during 2018 and 2019.

Author Contributions: Conceptualization, V.P.; methodology, V.P.; software, V.P. and J.Š.; formal analysis, V.P.; investigation, V.P.; resources and project management, P.P.; data curation, V.P.; writing—original draft preparation, V.P.; writing—review and editing, V.P., J.Š., P.P., V.F. and T.P.; visualization, V.P.; supervision, P.P. All authors have read and agreed to the published version of the manuscript.

Funding: The authors acknowledge the financial support provided by Grain Research Development Corporation (GRDC) vide Grant Number GRDC1911-004BXL for this investigation on using soil water information to make better decisions on the Eyre Peninsula.

Institutional Review Board Statement: Not applicable.

Informed Consent Statement: Not applicable.

Data Availability Statement: Data are available upon reasonable request to the corresponding author.

Acknowledgments: We acknowledge the collaboration with Amanda Cook and SARDI, Minnipa Agriculture Centre and the soil moisture probe landholders.

Conflicts of Interest: The authors declare no conflict of interest. The funders had no role in the study's design, in the collection, analyses, or interpretation of data, in the writing of the manuscript, or in the decision to publish the results.

References

1. Angus, J.F.; Grace, P.R. Nitrogen balance in Australia and nitrogen use efficiency on Australian farms. *Soil Res.* **2017**, *55*, 435–450. [CrossRef]
2. Sadras, V.O.; Denison, R.F. Neither crop genetics nor crop management can be optimised. *Field Crops Res.* **2016**, *189*, 75–83. [CrossRef]
3. Connor, D.J. Designing cropping systems for efficient use of limited water in southern Australia. *Eur. J. Agron.* **2004**, *21*, 419–431. [CrossRef]
4. Sadras, V.O.; Rodriguez, D. Modelling the nitrogen-driven trade-off between nitrogen utilisation efficiency and water use efficiency of wheat in eastern Australia. *Field Crops Res.* **2010**, *118*, 297–305. [CrossRef]
5. Cawood, R.M. (Ed.) Climate of south-eastern Australia. In *Climate, Temperature and Crop Production in South-Eastern Australia*; Principles of Sustainable Agriculture; Agriculture Victoria: Horsham, Australia, 1996; pp. 21–33.
6. Unkovich, M.; McBeath, T.; Llewellyn, R.; Hall, J.; Gupta, V.V.S.R.; Macdonald, L.M. Challenges and opportunities for grain farming on sandy soils of semi-arid south and south-eastern Australia. *Soil Res.* **2020**, *58*, 323–334. [CrossRef]
7. ABARES. *Wheat Forecast 20-22-23 Season*; Department of Agriculture, Fisheries and Forestry, Australian Government: Canberra, Australia, 2023.
8. Hochman, Z.; Gobbett, D.; Horan, H.; Garcia, J.N. Data rich yield gap analysis of wheat in Australia. *Field Crops Res.* **2016**, *197*, 97–106. [CrossRef]
9. Bodner, G.; Nakhforoosh, A.; Kaul, H.-P. Management of crop water under drought: A review. *Agron. Sustain. Dev.* **2015**, *35*, 401–442. [CrossRef]
10. French, R.; Schultz, J. Water use efficiency of wheat in a Mediterranean-type environment. I. The relation between yield, water use and climate. *Aust. J. Agric. Res.* **1984**, *35*, 743–764. [CrossRef]
11. Sadras, V.O.; Angus, J.F. Benchmarking water-use efficiency of rainfed wheat in dry environments. *Aust. J. Agric. Res.* **2006**, *57*, 847–856. [CrossRef]
12. Sadras, V.O.; Rodriguez, D. The limit to wheat water-use efficiency in eastern Australia. II. Influence of rainfall patterns. *Aust. J. Agric. Res.* **2007**, *58*, 657–669. [CrossRef]
13. Hochman, Z.; Gobbett, D.L.; Horan, H. Climate trends account for stalled wheat yields in Australia since 1990. *Glob. Chang. Biol* **2017**, *23*, 2071–2081. [CrossRef]
14. Sadras, V.O.; Lawson, C. Nitrogen and water-use efficiency of Australian wheat varieties released between 1958 and 2007. *Eur. J. Agron.* **2013**, *46*, 34–41. [CrossRef]
15. Angus, J.F.; van Herwaarden, A.F. Increasing Water Use and Water Use Efficiency in Dryland Wheat. *Agron. J.* **2001**, *93*, 290–298. [CrossRef]
16. Keating, B.A.; Carberry, P.S.; Hammer, G.L.; Probert, M.E.; Robertson, M.J.; Holzworth, D.P.; Huth, N.I.; Hargreaves, J.N.G.; Meinke, H.; Hochman, Z.; et al. An overview of APSIM, a model designed for farming systems simulation. *Eur. J. Agron.* **2003**, *18*, 267–288. [CrossRef]
17. Šimůnek, J.; van Genuchten, M.T.; Sejna, M. Recent developments and applications of the HYDRUS computer software packages. *Vadose Zone J.* **2016**, *15*, 1–25. [CrossRef]
18. Li, S.-X.; Wang, Z.-H.; Malhi, S.S.; Li, S.-Q.; Gao, Y.-J.; Tian, X.-H. Chapter 7 Nutrient and Water Management Effects on Crop Production, and Nutrient and Water Use Efficiency in Dryland Areas of China. *Adv. Agron.* **2009**, *102*, 223–265.
19. Cossani, C.M.; Slafer, G.A.; Savin, R. Co-limitation of nitrogen and water, and yield and resource-use efficiencies of wheat and barley. *Crop Pasture Sci.* **2010**, *61*, 844–851. [CrossRef]
20. Wang, Z.-H.; Li, S.-X. Nitrate N loss by leaching and surface runoff in agricultural land: A global issue (a review). *Adv. Agron.* **2019**, *156*, 159–217.
21. Osman, R.; Tahir, M.N.; Ata-Ul-Karim, S.T.; Ishaque, W.; Xu, M. Exploring the Impacts of Genotype-Management-Environment Interactions on Wheat Productivity, Water Use Efficiency, and Nitrogen Use Efficiency under Rainfed Conditions. *Plants* **2021**, *10*, 2310. [CrossRef] [PubMed]
22. Benjamin, J.G.; Porter, L.K.; Duke, H.R.; Ahuja, L.R. Corn Growth and Nitrogen Uptake with Furrow Irrigation and Fertilizer Bands. *Agron. J.* **1997**, *89*, 609–612. [CrossRef]
23. Lehrsch, G.; Sojka, R.; Westermann, D. Furrow irrigation and N management strategies to protect water quality. *Commun. Soil Sci. Plant Anal.* **2001**, *32*, 1029–1050. [CrossRef]
24. Smith, C.J.; Hunt, J.R.; Wang, E.; Macdonald, B.C.T.; Xing, H.; Denmead, O.T.; Zeglin, S.; Zhao, Z. Using fertiliser to maintain soil inorganic nitrogen can increase dryland wheat yield with little environmental cost. *Agric. Ecosyst. Environ.* **2019**, *286*, 106644. [CrossRef]
25. Keller, G.D.; Mengel, D.B. Ammonia Volatilization from Nitrogen Fertilizers Surface Applied to No-till Corn. *Soil Sci. Soc. Am. J.* **1986**, *50*, 1060–1063. [CrossRef]
26. Chien, S.; Prochnow, L.; Cantarella, A.H. Recent developments of fertilizer production and use to improve nutrient efficiency and minimize environmental impacts. *Adv. Agron.* **2009**, *102*, 267–322.
27. Turner, D.A.; Edis, R.E.; Chen, D.; Freney, J.R.; Denmead, O.T. Ammonia volatilization from nitrogen fertilizers applied to cereals in two cropping areas of southern Australia. *Nutr. Cycl. Agroecosystems* **2012**, *93*, 113–126. [CrossRef]
28. Gastal, F.; Lemaire, G.; Durand, J.-L.; Louarn, G. Chapter 8—Quantifying crop responses to nitrogen and avenues to improve nitrogen-use efficiency. In *Crop Physiology*, 2nd ed.; Sadras, V.O., Calderini, D.F., Eds.; Academic Press: San Diego, CA, USA, 2015; pp. 161–206.

29. Raun, W.R.; Johnson, G.V. Improving Nitrogen Use Efficiency for Cereal Production. *Agron. J.* **1999**, *91*, 357–363. [CrossRef]
30. Kubar, M.S.; Alshallash, K.S.; Asghar, M.A.; Feng, M.; Raza, A.; Wang, C.; Saleem, K.; Ullah, A.; Yang, W.; Kubar, K.A.; et al. Improving Winter Wheat Photosynthesis, Nitrogen Use Efficiency, and Yield by Optimizing Nitrogen Fertilization. *Life* **2022**, *12*, 1478. [CrossRef]
31. Galloway, J.N.; Townsend, A.R.; Erisman, J.W.; Bekunda, M.; Cai, Z.; Freney, J.R.; Martinelli, L.A.; Seitzinger, S.P.; Sutton, M.A. Transformation of the Nitrogen Cycle: Recent Trends, Questions, and Potential Solutions. *Science* **2008**, *320*, 889–892. [CrossRef]
32. Powlson, D.S.; Addiscott, T.M.; Benjamin, N.; Cassman, K.G.; de Kok, T.M.; van Grinsven, H.; L'Hirondel, J.L.; Avery, A.A.; van Kessel, C. When does nitrate become a risk for humans? *J. Environ. Qual.* **2008**, *37*, 291–295. [CrossRef]
33. Asseng, S.; Ewert, F.; Rosenzweig, C.; Jones, J.W.; Hatfield, J.L.; Ruane, A.C.; Boote, K.J.; Thorburn, P.J.; Rötter, R.P.; Cammarano, D.; et al. Uncertainty in simulating wheat yields under climate change. *Nat. Clim. Chang.* **2013**, *3*, 827–832. [CrossRef]
34. Ishaque, W.; Osman, R.; Hafiza, B.S.; Malghani, S.; Zhao, B.; Xu, M.; Ata-Ul-Karim, S.T. Quantifying the impacts of climate change on wheat phenology, yield, and evapotranspiration under irrigated and rainfed conditions. *Agric. Water Manag.* **2023**, *275*, 108017. [CrossRef]
35. Gonzalez-Dugo, V.; Durand, J.-L.; Gastal, F. Water deficit and nitrogen nutrition of crops. A review. *Agron. Sustain. Dev.* **2010**, *30*, 529–544. [CrossRef]
36. Norton, R.; Walker, C.; Farlow, C. Nitrogen removal and use on a long-term fertilizer experiment. In Proceedings of the 17th Australian Society of Agronomy Conference, Hobrt, Australia, 20–24 September 2015.
37. Phogat, V.; Skewes, M.A.; Cox, J.W.; Sanderson, G.; Alam, J.; Šimůnek, J. Seasonal simulation of water, salinity and nitrate dynamics under drip irrigated mandarin (*Citrus reticulata*) and assessing management options for drainage and nitrate leaching. *J. Hydrol.* **2014**, *513*, 504–516. [CrossRef]
38. Gaydon, D.S.; Balwinder, S.; Wang, E.; Poulton, P.L.; Ahmad, B.; Ahmed, F.; Akhter, S.; Ali, I.; Amarasingha, R.; Chaki, A.K.; et al. Evaluation of the APSIM model in cropping systems of Asia. *Field Crops Res.* **2017**, *204*, 52–75. [CrossRef]
39. Ware, A.; Spriggs, B.; Budarick, S.; Scholz, N. *Delivering Value from Soil Moisture Probes on Eyre Peninsula*; Minnipa Agriculture Centre: Minnipa, Australia, 2020.
40. Fabio, A.; Cook, A.; Richter, I.; King, N. *Benchmarking Water Limited Yield of Cereal Crops on Major Soil Types across Eyre Peninsula*; Minnipa Agriculture Centre: Minnipa, Australia, 2019.
41. Rayment, G.E.; Lyons, D.J.; Shelley, B. *Soil Chemical Methods—Australasia: Australasia*; CSIRO Publishing: Clayton, Australia, 2011.
42. ASRIS. Australian Soil Resource Information System. 2011. Available online: http://www.asris.csiro.au (accessed on 30 August 2023).
43. Jeffrey, S.J.; Carter, J.O.; Moodie, K.B.; Beswick, A.R. Using spatial interpolation to construct a comprehensive archive of Australian climate data. *Environ. Model. Softw.* **2001**, *16*, 309–330. [CrossRef]
44. Allen, R.G.; Pereira, L.S.; Raes, D.; Smith, M. *Crop Evapotranspiration: Guidelines for Computing Crop Water Requirements*; FAO: Rome, Italy, 1998.
45. Ritchie, J.T. Model for predicting evaporation from a row crop with incomplete cover. *Water Resour. Res.* **1972**, *8*, 1204–1213. [CrossRef]
46. Miralles, D.J.; Slafer, G.A. Radiation interception and radiation use efficiency of near-isogenic wheat lines with different height. *Euphytica* **1997**, *97*, 201–208. [CrossRef]
47. Feddes, R.A.; Kowalik, P.J.; Zaradny, H. *Simulation of Field Water Use and Crop Yield*; Pudoc for the Centre for Agricultural Publishing and Documentation: Wageningen, The Netherlands, 1978.
48. Nakasone, H.; Abbas, M.A.; Kuroda, H. Nitrogen transport and transformation in packed soil columns from paddy fields. *Paddy Water Environ.* **2004**, *2*, 115–124. [CrossRef]
49. Baldock, J.; Macdonald, L.; Farrell, M.; Welti, N.; Monjardino, M. *Nitrogen Dynamics in Modern Cropping Systems*; Grain Research and Development Corporation: Barton, Australia, 2018.
50. Barton, L.; Hoyle, F.C.; Stefanova, K.T.; Murphy, D.V. Incorporating organic matter alters soil greenhouse gas emissions and increases grain yield in a semi-arid climate. *Agric. Ecosyst. Environ.* **2016**, *231*, 320–330. [CrossRef]
51. Yang, Y.; Tong, Y.; Gao, P.; Htun, Y.M.; Feng, T. Evaluation of N(2)O emission from rainfed wheat field in northwest agricultural land in China. *Environ. Sci. Pollut. Res. Int.* **2020**, *27*, 43466–43479. [CrossRef]
52. Li, Y.; Šimůnek, J.; Zhang, Z.; Jing, L.; Ni, L. Evaluation of nitrogen balance in a direct-seeded-rice field experiment using Hydrus-1D. *Agric. Water Manag.* **2015**, *148*, 213–222. [CrossRef]
53. Phogat, V.; Mahalakshmi, M.; Skewes, M.; Cox, J.W. Modelling soil water and salt dynamics under pulsed and continuous surface drip irrigation of almond and implications of system design. *Irrig. Sci.* **2012**, *30*, 315–333. [CrossRef]
54. Renard, J.J.; Calidonna, S.E.; Henley, M.V. Fate of ammonia in the atmosphere—A review for applicability to hazardous releases. *J. Hazard. Mater.* **2004**, *108*, 29–60. [CrossRef] [PubMed]
55. Wang, S.; Chen, J. Study on the integrated distribution coefficient of ammonium N migration in layered soil. *Environ. Sci. Pollut. Res. Int.* **2020**, *27*, 25340–25352. [CrossRef]
56. Chowdary, V.M.; Rao, N.H.; Sarma, P.B.S. A coupled soil water and nitrogen balance model for flooded rice fields in India. *Agric. Ecosyst. Environ.* **2004**, *103*, 425–441. [CrossRef]
57. Yadav, D.; Kumar, V.; Singh, M.; Relan, P. Effect of temperature and moisture on kinetics of urea hydrolysis and nitrification. *Soil Res.* **1987**, *25*, 185–191. [CrossRef]
58. Šimůnek, J.; Hopmans, J.W. Modeling compensated root water and nutrient uptake. *Ecol. Model.* **2009**, *220*, 505–521. [CrossRef]

59. Jury, W.A.; Spencer, W.F.; Farmer, W.J. Behavior Assessment Model for Trace Organics in Soil: I. Model Description. *J. Environ. Qual.* **1983**, *12*, 558–564. [CrossRef]
60. Adcock, D. Soil Water and Nitrogen Dynamics of Farming Systems on the upper Eyre Peninsula, South Australia. Ph.D. Thesis, School of Earth and Environmental Sciences, University of Adelaide, Adelaide, Australia, 2005.
61. Wang, X.; Cai, H.; Li, L.; Wang, X. Estimating Soil Water Content and Evapotranspiration of Winter Wheat under Deficit Irrigation Based on SWAP Model. *Sustainability* **2020**, *12*, 9451. [CrossRef]
62. Ramos, T.B.; Šimůnek, J.; Gonçalves, M.C.; Martins, J.C.; Prazeres, A.; Pereira, L.S. Two-dimensional modeling of water and nitrogen fate from sweet sorghum irrigated with fresh and blended saline waters. *Agric. Water Manag.* **2012**, *111*, 87–104. [CrossRef]
63. Evett, S.R.; Schwartz, R.C.; Casanova, J.J.; Heng, L.K. Soil water sensing for water balance, ET and WUE. *Agric. Water Manag.* **2012**, *104*, 1–9. [CrossRef]
64. Shafeeq, P.M.; Aggarwal, P.; Krishnan, P.; Rai, V.; Pramanik, P.; Das, T.K. Modeling the temporal distribution of water, ammonium-N, and nitrate-N in the root zone of wheat using HYDRUS-2D under conservation agriculture. *Environ. Sci. Pollut. Res. Int.* **2020**, *27*, 2197–2216. [CrossRef] [PubMed]
65. Wallace, A.J.; Armstrong, R.D.; Grace, P.R.; Scheer, C.; Partington, D.L. Nitrogen use efficiency of 15N urea applied to wheat based on fertiliser timing and use of inhibitors. *Nutr. Cycl. Agroecosystems* **2020**, *116*, 41–56. [CrossRef]
66. Fenn, L.B.; Miyamoto, S. Ammonia Loss and Associated Reactions of Urea in Calcareous Soils. *Soil Sci. Soc. Am. J.* **1981**, *45*, 537–540. [CrossRef]
67. Freney, J.R.; Simpson, J.R.; Denmead, O.T. Volatilization of ammonia. In *Gaseous Loss of Nitrogen from Plant-Soil Systems*; Freney, J.R., Simpson, J.R., Eds.; Springer: The Hague, The Netherlands, 1983.
68. Hu, C.; Zheng, C.; Sadras, V.O.; Ding, M.; Yang, X.; Zhang, S. Effect of straw mulch and seeding rate on the harvest index, yield and water use efficiency of winter wheat. *Sci. Rep.* **2018**, *8*, 8167. [CrossRef] [PubMed]
69. White, R.G.; Kirkegaard, J.A. The distribution and abundance of wheat roots in a dense, structured subsoil—Implications for water uptake. *Plant Cell Environ.* **2010**, *33*, 133–148. [CrossRef]
70. Zhang, S.; Sadras, V.; Chen, X.; Zhang, F. Water use efficiency of dryland wheat in the Loess Plateau in response to soil and crop management. *Field Crops Res.* **2013**, *151*, 9–18. [CrossRef]
71. Lollato, R.P.; Edwards, J.T.; Ochsner, T.E. Meteorological limits to winter wheat productivity in the U.S. southern Great Plains. *Field Crops Res.* **2017**, *203*, 212–226. [CrossRef]
72. Harries, M.; Flower, K.C.; Renton, M.; Anderson, G.C. Water use efficiency in Western Australian cropping systems. *Crop Pasture Sci.* **2022**, *73*, 1097–1117. [CrossRef]
73. Bogunović, I.; Filipović, V. Mulch as a nature-based solution to halt and reverse land degradation in agricultural areas. *Curr. Opin. Environ. Sci. Health* **2023**, *34*, 100488. [CrossRef]
74. Krevh, V.; Filipović, L.; Petošić, D.; Mustać, I.; Bogunović, I.; Butorac, J.; Kisić, I.; Defterdarović, J.; Nakić, Z.; Kovač, Z.; et al. Long-term analysis of soil water regime and nitrate dynamics at agricultural experimental site: Field-scale monitoring and numerical modeling using HYDRUS-1D. *Agric. Water Manag.* **2023**, *275*, 108039. [CrossRef]
75. Hochman, Z.; Horan, H. Causes of wheat yield gaps and opportunities to advance the water-limited yield frontier in Australia. *Field Crops Res.* **2018**, *228*, 20–30. [CrossRef]
76. Angus, J.F.; van Herwaarden, A.F.; Fischer, R.A.; Howe, G.N.; Heenan, D.P. The source of mineral nitrogen for cereals in south-eastern Australia. *Aust. J. Agric. Res.* **1998**, *49*, 511–522. [CrossRef]
77. Cameron, K.C.; Di, H.J.; Moir, J.L. Nitrogen losses from the soil-plant system: A review. *Ann. Appl. Biol.* **2013**, *162*, 145–173. [CrossRef]
78. Monjardino, M.; Hochman, Z.; Horan, H. Yield potential determines Australian wheat growers' capacity to close yield gaps while mitigating economic risk. *Agron. Sustain. Dev.* **2019**, *39*, 49. [CrossRef]
79. IPCC. *Guidelines for National Greenhouse Gas Inventories*; Intergovernmental Panel on Climate Change: Geneva, Switzerland, 2006.
80. Siemens, J.; Kaupenjohann, M. Contribution of dissolved organic nitrogen to N leaching from four German agricultural soils. *J. Plant Nutr. Soil Sci.* **2002**, *165*, 675–681. [CrossRef]
81. Anderson, G.C.; Fillery, I.R.P.; Dunin, F.X.; Dolling, P.J.; Asseng, S. Nitrogen and water flows under pasture-wheat and lupin-wheat rotations in deep sands in Western Australia 2. Drainage and nitrate leaching. *Aust. J. Agric. Res.* **1998**, *49*, 345–361. [CrossRef]
82. Poss, R.; Smith, C.J.; Dunin, F.X.; Angus, J.F. Rate of soil acidification under wheat in a semi-arid environment. *Plant Soil* **1995**, *177*, 85–100. [CrossRef]
83. Ridley, A.M.; White, R.E.; Helyar, K.R.; Morrison, G.R.; Heng, L.K.; Fisher, R. Nitrate leaching loss under annual and perennial pastures with and without lime on a duplex (texture contrast) soil in humid southeastern Australia. *Eur. J. Soil Sci.* **2001**, *52*, 237–252. [CrossRef]
84. Ridley, A.M.; Mele, P.M.; Beverly, C.R. Legume-based farming in Southern Australia: Developing sustainable systems to meet environmental challenges. *Soil Biol. Biochem.* **2004**, *36*, 1213–1221. [CrossRef]

sustainability

MDPI

Article

Improving Wheat Yield and Water-Use Efficiency by Optimizing Irrigations in Northern China

Xin Zhang [1,2,†], Jianheng Zhang [3,†], Jiaxin Xue [2] and Guiyan Wang [1,2,4,5,*]

[1] College of Resources and Environmental Sciences, Hebei Agricultural University, Baoding 071000, China; zhangx@hebau.edu.cn
[2] State Key Laboratory of North China Crop Improvement and Regulation, Baoding 071000, China
[3] College of Horticulture, Hebei Agricultural University, Baoding 071000, China
[4] Key Laboratory of Crop Growth Regulation of Hebei Province, Baoding 071000, China
[5] Key Laboratory of North China Water-Saving Agriculture, Ministry of Agriculture and Rural Affairs, Baoding 071001, China
* Correspondence: wanggy@hebau.edu.cn; Tel.: +86-312-7528131
† These authors contributed equally to this work.

Abstract: Achieving the goal of increasing both crop yield and water-use efficiency with a better irrigation regime is a major challenge in semi-arid areas. In this study, we presented a two-season field experiment (October 2018–June 2019 and October 2019–June 2020) that considered drought stresses, i.e., no irrigation (W0), irrigated in jointing (W1), both in jointing and flowering (W2) after re-greening, and wheat varieties (S086; J22). The results showed that a 45.5% excess of irrigation water input did not promote wheat yield (W1 vs. W2). S086 was beneficial for the usage of soil water consumption under a low amount of irrigation water in both seasons. In addition, irrigation positively affected the activities of superoxide dismutase and catalase in flag leaves ($p < 0.05$). A decrease in irrigation helped to increase the concentrations of soluble sugar and proline and decrease the amount of malondialdehyde content for S086. For the water- and irrigation-water-use efficiency, W1 was significantly increased by 20.6–21.7% and 38.3–39.3% in 2018–2019 and 23.4–24.4% and 43.8–44.7% in 2019–2020, respectively, as compared to W2. Additionally, a higher yield for S086 than J22 was found under deficit irrigation. Consequently, our study suggested that the S086 variety combined with a total amount of irrigation water of 165 mm might be recommended to meet the win–win goal of high crop yields and water-use efficiency for reducing ground water depletion in the future.

Keywords: limited irrigation; drought stress; yield; water-use efficiency; northern China

Citation: Zhang, X.; Zhang, J.; Xue, J.; Wang, G. Improving Wheat Yield and Water-Use Efficiency by Optimizing Irrigations in Northern China. *Sustainability* **2023**, *15*, 10503. https://doi.org/10.3390/su151310503

Academic Editors: Wenfeng Liu, Xiao Lin Yang and Wen Yin

Received: 21 April 2023
Revised: 16 June 2023
Accepted: 28 June 2023
Published: 4 July 2023

1. Introduction

Intensified winter wheat planting is the primary cropping system in northern China, which produces >67% of the wheat in China [1]. Northern China is a typical semi-arid area with an average annual precipitation of 556 mm, but only 27–32% (150–180 mm) of this falls during the winter wheat growing season [2]. Consequently, precipitation cannot meet the requirements, and a lack of adequate water thus causes up to a 200–300 mm shortage of water during the whole winter wheat growing season [3,4]. The irrigation water for flood irrigation measurements, which is pumped from deep groundwater 3–5 times per wheat season, accounts for 80% of the total agricultural water used in this region [5]. In this region, flood irrigation that is used by many farmers causes up to 60% of the irrigation water lost by evaporation or leaching, and this poses a serious threat for sustainable agricultural production [6]. As a result, the groundwater level is declining rapidly at a rate of 0.8–1.5 m yr^{-1} in this region [3,7], which has become an important issue that is restricting sustainable development [8,9]. Therefore, formulating optimal irrigation approaches and improving water-use efficiency in northern China are essential for future agriculture. Since

the 1990s, limited irrigation methods have been implemented and proposed to reduce the use of groundwater without decreasing the wheat yield in this region [10]. Because of the important status of wheat in food consumption over the previous 40 years, a focus on improving the productivity of irrigation water is probably the most common strategy for resolving future water-related challenges by adapting proper agricultural management and implementing irrigation-water-saving measures [11,12].

Deficit irrigation, defined as the application of irrigation water below the full-crop evapotranspiration (ET) level, is an important practical strategy to affect water-use efficiency and wheat yields, its quality is based on the key growth stages in which the irrigation water is applied, and it has been globally applied for wheat and other crop fields, particularly in dry regions such as northern China [13–15]. A reduction in or a total loss of seasonal irrigation treatments may cause drought stress, which can stimulate wheat roots to grow into deeper soil (below the 80 cm soil layer) layers and then utilize the soil water and nitrogen found in the deep soil [8]. Additionally, an appropriate scheduling of irrigation minimizes the effects of water stress on crop yields and increases the productivity from water [16]. Li et al. [8] reported that irrigating after the flowering stage could reduce the consumption of pre-anthesis water and ensure the soil water supply at the critical stage, thus increasing water-use efficiency. Jha et al. [17] reported that plants that experienced water stress during the flowering and vegetative growth stages had significantly lower yields and biomass. However, Davarpanah and Ahmadi [12] reported that irrigation at the jointing stage was the most efficient irrigation event for achieving a high yield in all climate conditions. Zhang et al. [18] found that water-saving irrigation contributed to a high plant N-use efficiency and improved the mitigation of greenhouse gas emission and soil N losses. In addition, the physiological indicators of wheat leaf, for example, enzymes in flag leaves such as superoxide dismutase, peroxidase, catalase, and malondialdehyde (MDA), are directly affected by irrigation regimes. Moreover, the responses of crop yield production and the sensitivity of the physiological indicators of wheat leaf to irrigation regimes remain unclear. Thus, the main purpose of this study was to (1) assess the effects of irrigation on soil water consumption, winter wheat yield, water-use efficiency, and the sensitivity of the physiological indicators of wheat leaf; then to (2) determine the traits of two wheat varieties with high yields, such as the WUE and yield; and to (3) explore the influence of the interaction of year, variety, and irrigation events on wheat yield and water-use efficiency. Furthermore, this knowledge will aid in the development of appropriate irrigation management strategies and the selection of appropriate wheat varieties in accordance with future agriculture goals in northern China.

2. Materials and Methods

2.1. Experiment Area

This study was conducted in Quzhou County, Hebei Province (36°86′ N, 115°02′ E, Figure 1a) during the two wheat seasons of 2018–2019 and 2019–2020. Quzhou is a typical area with the most serious water shortage in northern China with an annual average temperature of 16.8 °C. The long-term average annual precipitation is 541.31 mm, and most of this rainfall occurs in the summer and comprises 65–80% of the total. The soil parameters, precipitation, and air temperature values are shown in detail in Table 1 and Figure 1b.

Table 1. Soil conditions of 0–20 cm soil layer.

Year	Bulk Density (g cm^{-3})	SOM (g kg^{-1})	TN (g kg^{-1})	Av-N (mg kg^{-1})	Av-P (mg kg^{-1})	Av-K (mg kg^{-1})
2018–2019	1.48	14.12	1.21	110.41	16.41	150.15
2019–2020	1.46	15.35	1.44	100.56	11.62	137.62

Note: SOM, soil organic matters content; TN, total nitrogen content; Av-N, the concentration of available nitrogen; Av-P, the concentration of available phosphorus; Av-N, the concentration of available potassium.

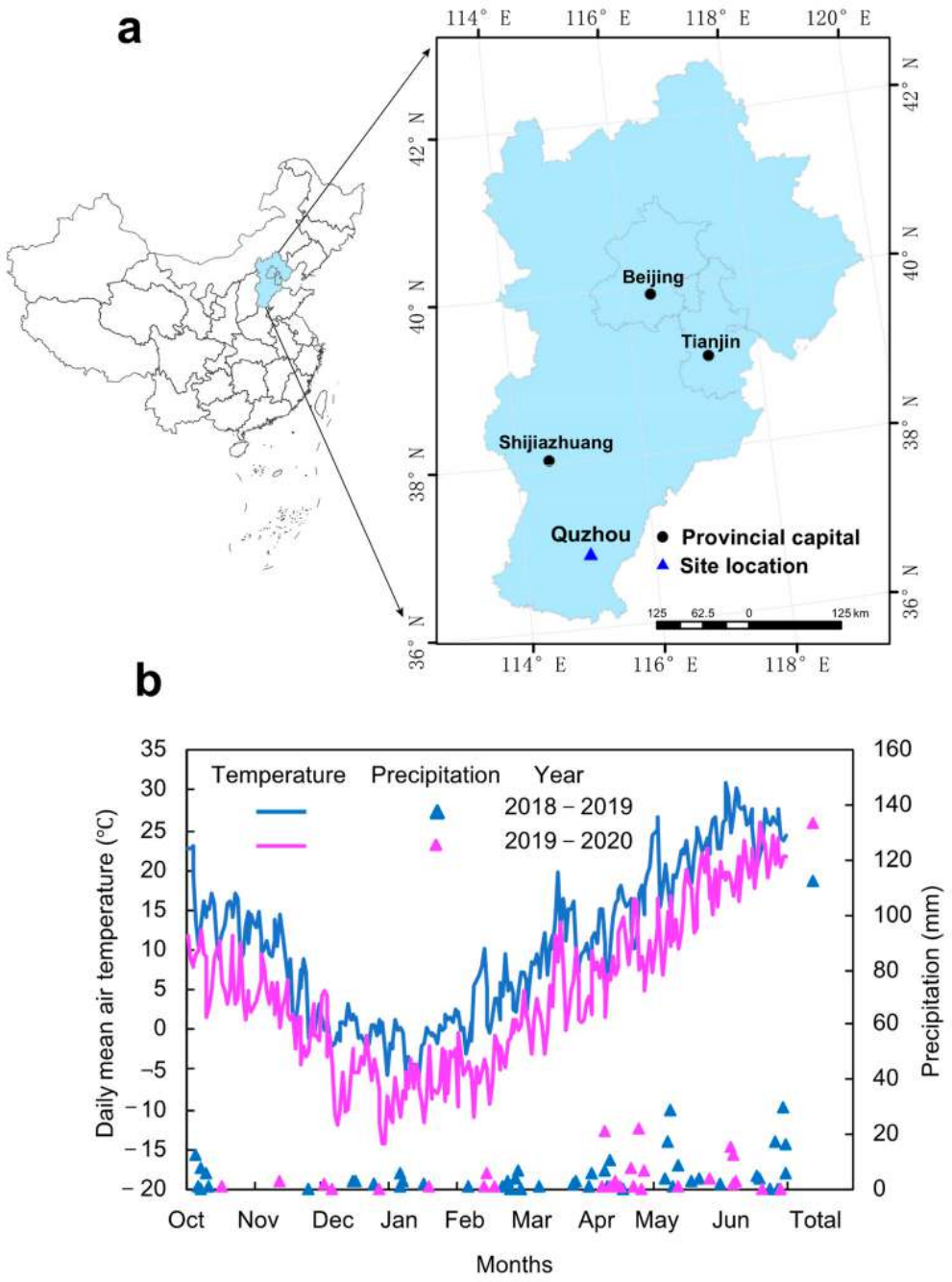

Figure 1. (**a**) The location map of the study area and (**b**) daily precipitation and average daily air temperature during the study period.

2.2. Experimental Design

First, we selected two popular local wheat varieties, i.e., J22 and S086. J22 is an extensively planted variety with steady yield especially in northern China, and S086 is a drought-resistant variety identified by the Institute of Dry Farming, Hebei Academy of Agricultural Sciences, Baoding, China (2015). Secondly, three limited irrigation treatments were considered, i.e., W0, no irrigation after re-greening; W1, irrigation during the jointing stage at 75 mm; W2, irrigation during the jointing and flowering stages at 75 mm for each irrigation, in a total of 150 mm. In this study, all the treatments were irrigated before the winter growth period with the same amount at 90 mm. More irrigation details are shown in Table 2. In this study, wheat variety was maintained in the main plot and irrigation treatments were allocated into sub-plots under a split-plot design. Therefore, six treatments with three

replicates, resulting in a total of 18 plots (each with an area of 10 m length × 6 m width), were considered. For fertilizer, 150 kg N ha^{-1}, 120 kg P_2O_5 ha^{-1}, and 90 kg K_2O ha^{-1} were applied along with the wheat sowing, and then 60 kg N ha^{-1} was top-dressed at the jointing stage. Wheat was sown with a row spacing of 15 cm after deep ploughing on 15 October 2018 and 20 October 2019 and harvested on 12 June 2019 and 13 June 2020. Precipitation during the wheat growth period between 2019 and 2020 was 133.7 mm, close to the annual average precipitation of this region.

Table 2. Irrigation amount (mm) in different growth stages during 2018–2020.

Year	Varieties	Treatment	Overwinter 18 December	Jointing 20 March	Flowering 15 May	Total
2018–2019/ 2019–2020	S086	W0	90	0	0	90
		W1	90	75	0	165
		W2	90	75	75	240
	J22	W0	90	0	0	90
		W1	90	75	0	165
		W2	90	75	75	240

Note: The dates cited are the time of irrigation events for each growth stage. W0, no irrigation events after overwintering stage; W1, irrigated in jointing stage; W2, irrigated in jointing and flowering stages.

2.3. Data Collection and Calculation

2.3.1. Crop Yield

To determine the crop yield, the spikes were all counted in one 1 m^2 area of each plot before harvest. The grain number per spike was then counted from 30 randomly selected plants in each plot. The 1000-grain weight was determined by weighing 1000 grains from each plot. At maturity, all the wheat plants in a 3 m^2 area in each plot were harvested, threshed, and then dried at 80 °C for crop yield calculation. In addition, the actual crop yield was calculated with a 12.5% moisture basis.

2.3.2. Soil-Water-Holding Consumption and Water-Use Efficiency

Three soil samples were collected in a 0–200 cm soil layer at 20 cm intervals and then mixed for soil water content analysis at sowing, overwintering, jointing, flowering, filling, and maturity stages. The soil gravimetric water content (%) was measured by oven-drying at 105 °C for 48 h. The soil-water-holding consumption (SWC, mm) was calculated as the final soil-water-holding amount (harvest stage) minus the initial one (seeding stage).

Crop evapotranspiration for a given stage (ET) was calculated according to the soil water balance equation:

$$ET = \Delta S + I + P - R - D + CR \quad (1)$$

where ΔS (mm) is soil water extraction based on the difference between two close growth stages, I (mm) is irrigation, P (mm) is rainfall, R (mm) is runoff, D (mm) is drainage deeper than the 200 cm soil profile, and CR (mm) is the capillary rise into the root zone. R and D can be ignored in northern China according to [19,20]. Additionally, the groundwater table at the experimental site is 5–6 m below the ground surface, which was deeper than the root activity depth of these two wheat varieties selected in this paper (0–2.5 m); therefore, the CR is negligible.

ΔS was calculated according to Equation (2):

$$\Delta S = 10\sum_{i=1}^{n} \gamma_i H_i(\theta_{i1} - \theta_{i2}) \quad (2)$$

where n (=10) is the number of soil layers from 0 to 200 cm; γ_i (g cm^{-3}) is the bulk density of the ith soil layer; H_i (cm) is the soil depth of the ith soil layer; θ_{i1} (%) and θ_{i2} (%) are the initial and final gravimetric water content of the ith soil layer, respectively.

The water consumption intensity (CD, mm d^{-1}) and percentage (CP, %) for a given stage are calculated as follows:

$$CD = \frac{ET}{D} \tag{3}$$

$$CP = \frac{ET}{ET_T} \tag{4}$$

where ET (mm) is the crop evapotranspiration for a given stage, D (d) is the duration days for a given stage, and ET_T (mm) is the total ET for the whole growth season.

The water-use efficiency was evaluated based on the use of the total and irrigation water by the crop, which was estimated as crop-water-use efficiency (WUE, kg m^{-3}) and irrigation-water-use efficiency ($IWUE$, kg m^{-3}), as described by Jha et al. [21].

$$WUE = \frac{GY}{ET_T \times 10} \tag{5}$$

$$IWUE = \frac{GY}{I \times 10} \tag{6}$$

where GY is the grain yield (kg ha^{-1}), ET_T is the total evapotranspiration during a growing season (mm), and I is irrigation (mm).

2.3.3. Plant Nitrogen Uptake and Utilization

The 6 wheat plants were collected at overwintering, jointing, flowering, filling, and maturity stages, and then oven-dried and sieved. The total nitrogen (N) content was determined using the Kjeldahl method. In this study, the NUE indicator was used through N partial factor productivity for fertilizer (PFP_N, kg grain kg^{-1} N_{fert}) [10].

PFP_N was defined as the ratio of crop yield to fertilizer N applied (7):

$$PFP_N = \frac{GY}{N_{fert}} \tag{7}$$

where GY is the grain yield (kg ha^{-1}) and N_{fert} is the fertilizer N application rate (kg ha^{-1}).

2.3.4. Physiological Factors of the Flag Leaf

Twenty flag leaves in each plot were randomly collected at 0, 7, 14, 21, and 24 days after the flowering stage in 2018–2019 and 2019–2020 and then stored at −20 °C before the biochemical analysis was conducted based on a previous study [19]. In this study, six related indicators were used: superoxide dismutase (SOD, U g^{-1} h^{-1}), peroxidase (POD, U g^{-1} h^{-1}), catalase (CAT, U g^{-1} h^{-1}), malondialdehyde (MDA, nmol g^{-1}), soluble sugar (SS, mg g^{-1}), and proline (Pro, mg g^{-1}) content of flag leaf according to Troll and Lindsley [22] and Zhang and Kirkham [23].

2.4. Statistical Analysis

The results in the table have been expressed as mean ± standard error of the three replicates of each treatment. Varieties (i.e., S086 and J22) and irrigation practices (i.e., W1, W2, and W3) were applied in the main and sub-plot, respectively. Microsoft Excel 2010 (Microsoft Co., Redmond, WA, USA) was used to arrange the experimental data. The effects of different years, wheat varieties, irrigation practices, and their interactions on crop yield, N and water consumption, and soil water content were analyzed by SPSS 22.0 software (SPSS Inc., Chicago, IL, USA) using a three-way ANOVA at a significance level of 0.05. Significant differences among different irrigation practices under S086 or J22 were tested using the least significant difference (LSD) test at a significance level of 0.05. Significant differences between S086 and J22 under W1, W2, and W3 were tested using an independent t-test at a significance level of 0.05. Simple correlation analysis was performed to determine

whether soil water characteristics, yield, and water-use efficiency were related to wheat physiological factors using Origin pro, 2021 (Origin lab, Northampton, MA, USA).

3. Results

3.1. Crop Water Consumption

Water consumption intensity (*CD*), percentage (*CP*), and total water consumption (TWC) were different in differing growth stages and treatments (Table 3). For the filling–mature stage, the CD of W2 was higher ($p < 0.05$) than those of W1 and W0.

Table 3. Crop water consumptions in different growth stages.

Year	Varieties	Treatment	Seeding to Jointing			Jointing to Flowering			Flowering to Filling			Filling to Mature		
			CD	CP	TWCl	CD	CP	TWC	CD	CP	TWC	CD	CP	TWC
			mm d^{-1}	%	mm	mm d^{-1}	%	mm	mm d^{-1}	%	mm	mm d^{-1}	%	mm
2018–2019	S086	W0	0.43 a	26.26 a	70.92 a	2.93 b	41.16 a	111.17 b	3.00 b	10.01 b	27.04 b	3.15 b	31.46 b	84.97 c
		W1	0.40 a	20.14 b	66.43 a	3.61 a	41.63 a	137.32 a	4.68 a	12.76 a	42.08 a	3.83 b	31.39 b	103.53 b
		W2	0.42 a	18.04 b	69.42 a	3.90 a	38.55 a	148.36 a	5.51 a	12.90 a	49.63 a	5.04 a	35.34 a	136.00 a
	J22	W0	0.45 a	27.43 a	72.34 a	3.16 b	44.33 a	116.92 b	2.92 b	8.86 b	23.38 b	2.83 b	29.02 b	76.53 b
		W1	0.46 a	23.32 b	74.92 a	3.84 a	44.18 a	136.93 a	7.12 a	17.73 a	56.98 a	2.98 b	25.06 b	80.51 b
		W2	0.47 a	20.08 b	76.92 a	3.97 a	38.35 a	146.94 a	7.31 a	15.27 a	58.50 a	5.36 a	37.79 a	144.76 a
2019–2020	S086	W0	0.54 a	22.84 a	88.98 a	0.89 b	8.65 b	33.69 b	7.32 c	16.92 b	65.90 c	3.28 b	22.71 b	88.48 c
		W1	0.51 a	18.94 b	84.99 a	1.77 a	15.01 a	67.32 a	16.96 b	34.03 a	152.65 b	4.30 b	25.85 b	115.99 b
		W2	0.56 a	19.28 b	93.02 a	1.83 a	14.40 a	69.48 a	22.24 a	41.50 a	200.19 a	5.39 a	30.15 a	145.43 a
	J22	W0	0.43 a	17.89 a	68.94 a	0.95 b	9.08 b	34.98 b	8.36 c	17.37 b	66.91 c	2.69 b	18.83 b	72.55 b
		W1	0.35 a	13.89 b	57.45 a	1.48 a	13.26 a	54.84 a	18.60 b	35.98 a	148.80 b	3.17 b	19.42 b	80.29 b
		W2	0.35 a	12.34 b	56.21 a	1.52 a	12.37 a	56.35 a	25.88 a	45.45 a	207.03 a	6.14 a	36.42 a	165.91 a

Note: CD: water consumption intensity; CP: water consumption percentage; TWC: total water consumption. Definitions of different irrigation treatments (i.e., W0, W1, and W2) are given in the caption of Table 2. The same letter in the same column denotes no significant difference in different irrigation treatments by LSD ($p < 0.05$) for these two varieties.

In 2018–2019, a 55.62% (W1) and 83.54% (W2) higher TWC for S086 and 143.71% (W1) and 150.21% (W2) higher TWC for J22 compared to the W0 treatment were found in the flowering–filling stage, respectively. Additionally, a 31.36% (S086) and 79.80% (J22) higher TWC in W2 compared to W1 was found in the filling–mature stage. Similar to 2018–2019, in 2019–2020, TWC in W2 was highest for all growth stages (Table 3).

The *CP* especially in jointing–flowering was highest during the whole season, comprising 38.6–41.6% (S086) and 38.4–44.4% (J22) in 2018–2019, while that in the flowering–filling stage was highest in all irrigation treatments except the seeding–jointing and filling–mature stages in 2019–2020. During the whole season, TWC was W2 > W1 > W0 during both years (Figure 2).

3.2. Soil-Water-Holding Consumption

For different irrigation treatments, TWC decreased along with the increase in amount of irrigation (as the main source of crop water demand). Additionally, the increase in irrigation amount is related to the increase in TWC and the decrease in soil-water-holding consumption (SWC). In 2018–2019, for S086, the order of SWC in the 20–100 cm soil layer was W0 > W1 > W2, while that in 100–180 cm was W1 > W0 > W2. For J22, the order of SWC in the 20–120 cm soil layer was W0 > W1 > W2, but there was no obvious regularity in the deeper soil layer (Figure 3).

In 2019–2020, the order of SWC in surface soil (0–20 cm) and the 40–120 cm soil layer was W0 > W1 > W2 for S086, although there was a lack of an obvious trend in the deeper soil layer, while that in 20–120 cm was W0 > W1 > W2 for J22 but was not apparently regulatory in the deeper soil layer.

3.3. Dynamics of the Physiological Factors of Flag Leaves

Irrigation increased the activities of superoxide dismutase (SOD), peroxidase (POD), and catalase (CAT) from 7 days and the contents of soluble sugar (SS) and proline (Pro) from 14 days after the flowering stage, but decreased the content of malondialdehyde (MDA) during the whole flowering stage (Figures S1–S6). Accordingly, in W2, the SS content increased by 9.1–19.0% (S086) and 4.3–19.8% (J22) during 2018–2019 and 3.4–8.4% (S086)

and 10.2–16.6% (J22) during 2019–2020, compared with the content of W1. The Pro content of W2 was 5.6–11.7% (S086) and 7.3–15.2% (J22) higher than those of W1 during 2018–2019, while it was 9.0–10.4% (S086) and 8.3–12.6% (J22) higher than those of W1 during 2019–2020 (Figures S5 and S6). Year and irrigation significantly affected the POD content ($p < 0.05$), but no interaction was found (Table 4). However, there was no significant effect of year, variety, irrigation, and their interactions on SOD, CAT, MDA, sugar, and Pro content.

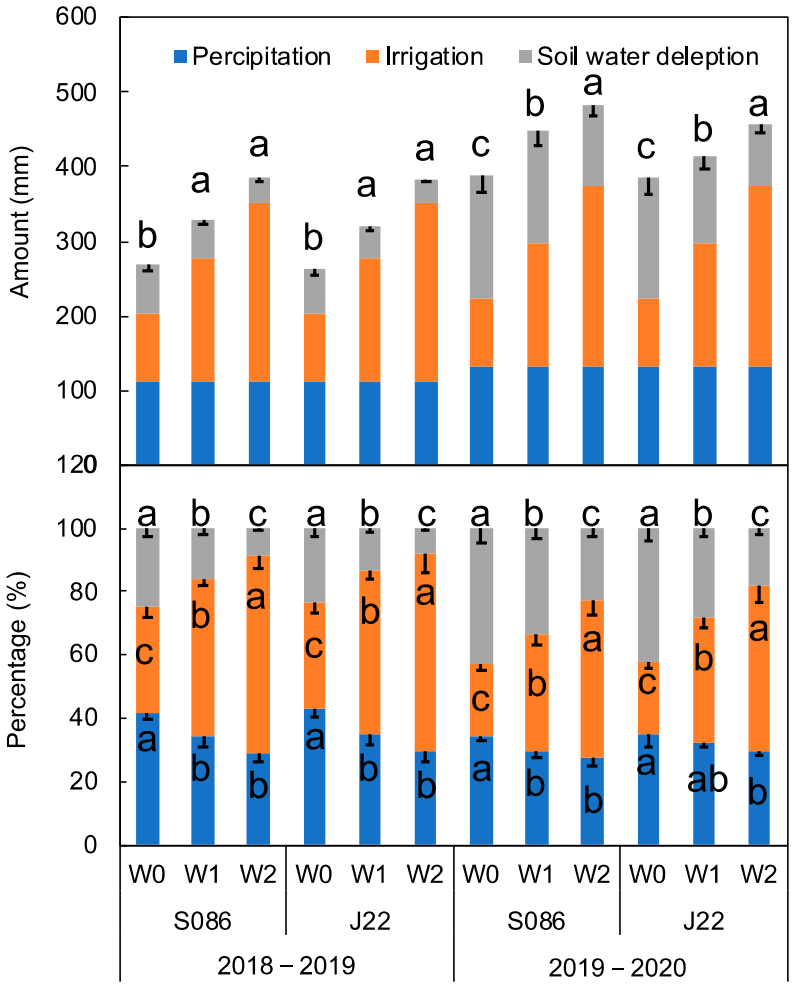

Figure 2. Water consumption and percentage from precipitation, irrigation, and soil water depletion in 0–200 cm soil layer under different treatments. Definitions of different irrigation treatments (i.e., W0, W1, and W2) are given in caption of Table 2. The same letter in each soil layer denotes no significant difference in different irrigation treatments by LSD ($p < 0.05$).

3.4. Crop Yield

Irrigation helped to cause an increase in the number of spikes and grains per spike in 2018–2019 (Table 5). Compared to W0, the spikes of S086 increased by 90.51% (W1) and 66.52% (W2). Similarly, the spikes of J22 increased by 75.63% (W1) and 83.90% (W2), respectively, compared to W0. In addition, the 1000-grain weight was significantly affected by year and variety, and their interaction. Additionally, the yield was significantly affected by irrigation practices and the highest wheat yield was found in S086 in all irrigation treatments during these two experimental seasons ($p < 0.05$, Table 4).

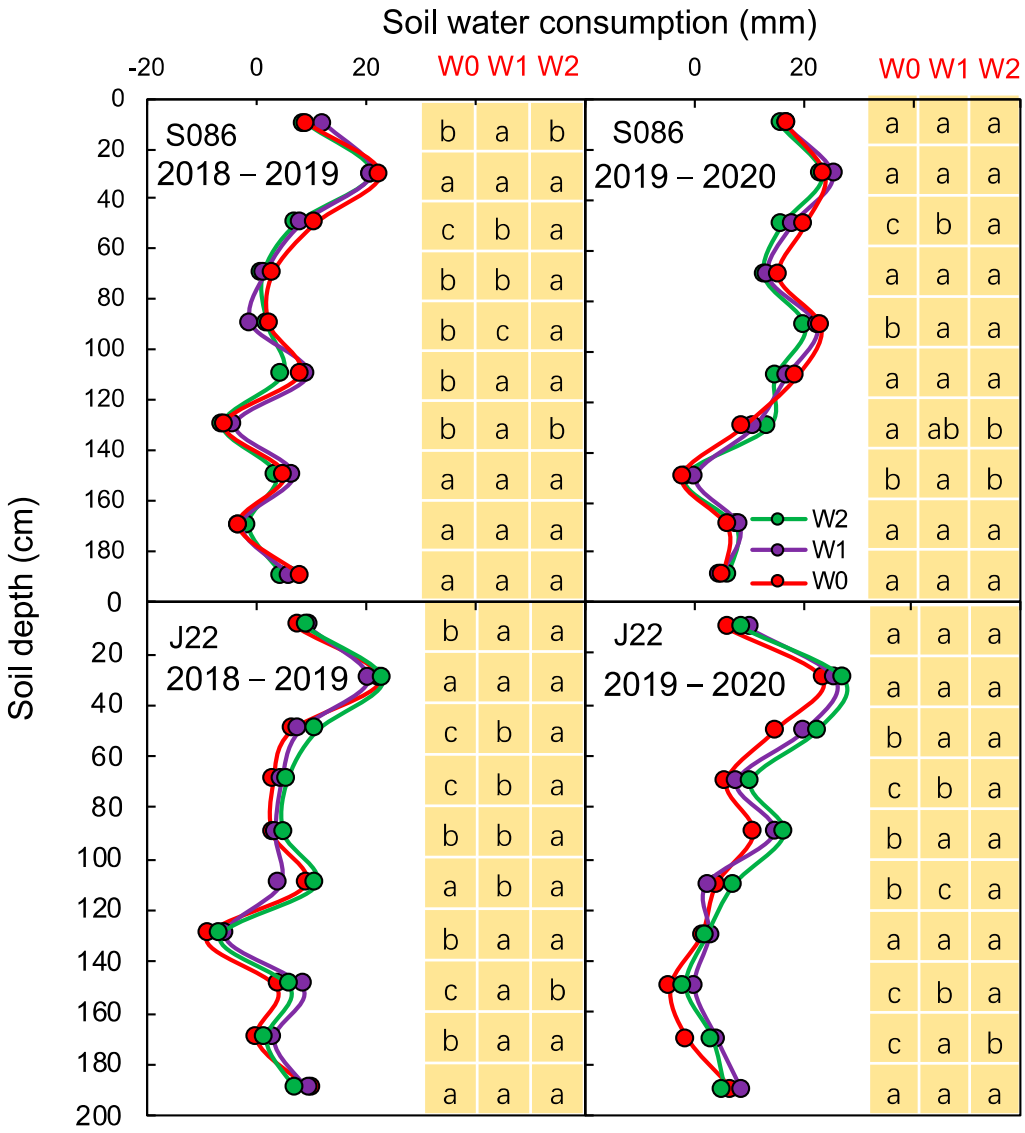

Figure 3. Soil water consumptions under different treatments in 0–200 cm soil layer. Definitions of different irrigation treatments (i.e., W0, W1, and W2) are given in caption of Table 2. The different letters in the same soil layer denote a significant difference in different irrigation treatments by LSD ($p < 0.05$).

3.5. Crop-Water-Use Efficiency

The water-use efficiency (WUE) and irrigation-water-use efficiency (IWUE) were significantly affected by year and irrigation, and their interactions (Table 6). In 2018–2019, the lowest WUE was found in W0 and the lowest IWUE was found in W2, while the highest WUE and IWUE were found in the W1 treatment for both varieties. In 2019–2020, the WUE of W1 was 15.5% ($p < 0.05$) and 9.4% ($p < 0.05$) higher than those in W0 and W2 for J22, respectively. However, the highest IWUE was found in W0, followed by W1 in 2019–2020, which was primarily owing to the higher yield caused by higher rainfall in comparison with that in 2018–2019.

Table 4. Two-way ANOVA of the effects of year, irrigation, and wheat variety on soil water consumption and plant physiological factors 7 days after flowering stage.

Year	Varieties	Irrigation	TWC	SWC	SOD	POD	CAT	MDA	Sugar	Pro
2018–2019	S086	W0	270.1 ± 88.2	67.5 ± 18.3	461.0 ± 1.6	188.4 ± 8.1	141.4 ± 6.1	20.9 ± 2.5	30.3 ± 2.3	289.5 ± 12.0
		W1	329.8 ± 76.5	52.2 ± 9.9	514.9 ± 12.6	202.0 ± 11.3	160.8 ± 10.1	16.1 ± 2.7	25.0 ± 0.5	259.8 ± 16.2
		W2	384.9 ± 45.2	32.3 ± 7.8	540.7 ± 15.3	225.3 ± 10.3	178.5 ± 2.3	14.7 ± 2.2	23.0 ± 0.5	238.3 ± 15.4
	J22	W0	263.7 ± 21.2	61.1 ± 1.2	473.9 ± 24.3	168.7 ± 5.5	150.0 ± 8.4	17.1 ± 2.1	34.9 ± 1.0	309.6 ± 10.6
		W1	321.3 ± 40.6	43.7 ± 3.9	553.0 ± 22.8	195.7 ± 16.9	176.3 ± 8.1	14.9 ± 1.4	31.3 ± 0.5	261.3 ± 8.4
		W2	383.1 ± 77.5	30.5 ± 11.5	573.5 ± 28.9	218.6 ± 12.4	183.7 ± 5.9	12.9 ± 1.6	28.3 ± 0.0	231.5 ± 4.2
2019–2020	S086	W0	389.6 ± 32.5	165.9 ± 6.1	485.6 ± 6.9	184.3 ± 8.1	125.3 ± 6.9	19.4 ± 1.0	32.0 ± 0.3	229.5 ± 10.6
		W1	448.6 ± 67.9	149.9 ± 13.1	540.3 ± 9.6	216.1 ± 11.3	144.0 ± 9.6	18.1 ± 0.1	26.5 ± 0.1	199.8 ± 11.3
		W2	482.4 ± 78.6	108.7 ± 10.8	563.1 ± 1.0	230.7 ± 10.3	150.0 ± 1.0	14.1 ± 1.2	24.3 ± 0.2	183.3 ± 15.5
	J22	W0	385.3 ± 22.5	161.6 ± 3.2	457.4 ± 8.8	188.1 ± 5.5	118.0 ± 8.8	15.0 ± 0.2	32.6 ± 0.2	229.6 ± 10.2
		W1	413.5 ± 55.2	114.8 ± 4.4	557.6 ± 7.9	206.8 ± 16.9	134.7 ± 7.9	16.8 ± 0.2	28.8 ± 0.3	193.3 ± 11.0
		W2	455.5 ± 49.3	81.8 ± 7.8	580.0 ± 9.5	228.1 ± 12.4	148.7 ± 9.5	22.5 ± 0.0	24.3 ± 0.3	171.5 ± 12.0
ANOVA *p* value										
Year (Y)			***	***	NS	*	NS	NS	NS	*
Variety (V)			NS	***	NS	NS	NS	NS	NS	NS
Irrigation (I)			***	***	NS	*	NS	NS	NS	NS
Y × V			NS	**	NS	NS	NS	NS	NS	NS
Y × I			NS	***	NS	NS	NS	NS	NS	NS
V × I			NS	NS	NS	NS	NS	NS	NS	NS
Y × V × I			NS	NS	NS	NS	NS	NS	NS	NS

Note: SWC, soil-water-holding consumption; TWC, total water consumption. SOD, superoxide dismutase; POD, peroxidase; CAT, catalase; MDA, malondialdehyde content; SS, soluble sugar content; Pro, proline content. *, **, and *** represent the 0.05, 0.01, and 0.001 significance levels, respectively. NS means no significant effect.

Table 5. Wheat yield and related factors under different irrigation treatments.

Year	Varieties	Irrigation	Spike ($\times 10^4$ ha^{-1})	Grains per Spike	Weight (1000-Grain) /g	Yield /kg ha^{-1}
2018–2019	S086	W0	331.95 b	26.33 b	36.68 b	3106.9 ± 212.7 d
		W1	632.41 a	33.00 a	40.79 a	7803.3 ± 413.3 a
		W2	552.75 a	33.67 a	39.57 a	8198.6 ± 178.3 a
	J22	W0	391.35 b	27.67 b	34.85 a	3512.9 ± 228.7 d
		W1	687.31 a	33.67 a	35.70 a	7773.7 ± 801.7 ab
		W2	719.70 a	32.00 a	34.69 a	8110.6 ± 85.0 a
2019–2020	S086	W0	527.67 a	30.61 b	49.28 a	6536.4 ± 206.7 bc
		W1	612.03 a	32.17 a	50.33 a	8182.3 ± 311.3 a
		W2	646.03 a	32.43 a	50.51 a	8286.0 ± 403.5 a
	J22	W0	567.01 a	29.81 b	48.50 a	6502.0 ± 359.2 c
		W1	598.36 a	34.47 a	49.08 a	8062.5 ± 211.8 a
		W2	601.03 a	35.37 a	48.97 a	8122.3 ± 204.5 a
ANOVA *p* value						
Year (Y)			**	**	***	***
Variety (V)			**	NS	***	NS
Irrigation (I)			***	***	NS	***
Y × V			***	NS	*	NS
Y × I			***	*	NS	***
V × I			NS	NS	NS	NS
Y × V × I			NS	*	NS	NS

Note: Definitions of different irrigation treatments (i.e., W0, W1, and W2) are given in caption of Table 2. The same letter in the same column denotes no significant difference in different irrigation treatments by LSD ($p < 0.05$) for these two varieties. *, **, and *** represent the 0.05, 0.01, and 0.001 significance levels, respectively. NS means no significant effect.

3.6. Combined Effects of Irrigation and Water Consumption on Grain Yield and Water Productivity

Along with the increase in SWC and TWC, POD increased ($p < 0.05$), but the contents of MDA and SS significantly decreased ($p < 0.05$, Figure 4). In addition, the crop yield was significantly affected by the content of SOD, CAT, and SS of flag leaves and then indirectly affected the WUE and PFP. Irrigation water productivity, such as IWUE, was positively correlated with SWC and TWC ($p < 0.05$). However, irrigation would decrease the consumption of soil water, which indicated that deficit irrigation could be beneficial for the increase in antioxidant activity of crops and water productivity.

Table 6. Crop-water- and N-use efficiency in different irrigation treatments.

Year	Varieties	Treatments	WUE (kg m^3)	IWUE (kg m^3)
2018–2019	S086	W0	1.53 ± 0.10 e	3.45 ± 0.24 d
		W1	2.81 ± 0.15 a	4.73 ± 0.25 bc
		W2	2.33 ± 0.05 bc	3.42 ± 0.07 d
	J22	W0	1.73 ± 0.11 de	3.90 ± 0.25 cd
		W1	2.80 ± 0.29 a	4.71 ± 0.49 bc
		W2	2.30 ± 0.02 bc	3.38 ± 0.04 a
2019–2020	S086	W0	2.92 ± 0.09 a	7.26 ± 0.23 b
		W1	2.74 ± 0.10 ab	4.96 ± 0.19 d
		W2	2.22 ± 0.11 c	3.45 ± 0.17 d
	J22	W0	2.91 ± 0.16 a	7.22 ± 0.40 a
		W1	2.70 ± 0.07 ab	4.89 ± 0.13 b
		W2	2.17 ± 0.05 cd	3.38 ± 0.09 d
ANOVA *p* value				
	Year (Y)		***	***
	Variety (V)		NS	NS
	Irrigation (I)		***	***
	Y × V		NS	NS
	Y × I		***	***
	V × I		NS	NS
	Y × V × I		NS	NS

Note: WUE, water-use efficiency; IWUE, irrigation-water-use efficiency. Definitions of different irrigation treatments (i.e., W0, W1, and W2) are given in caption of Table 2. The same letter in the same column denotes no significant difference in different irrigation treatments by LSD ($p < 0.05$) for these two varieties. *** represents the 0.001 significance levels. NS means no significant effect.

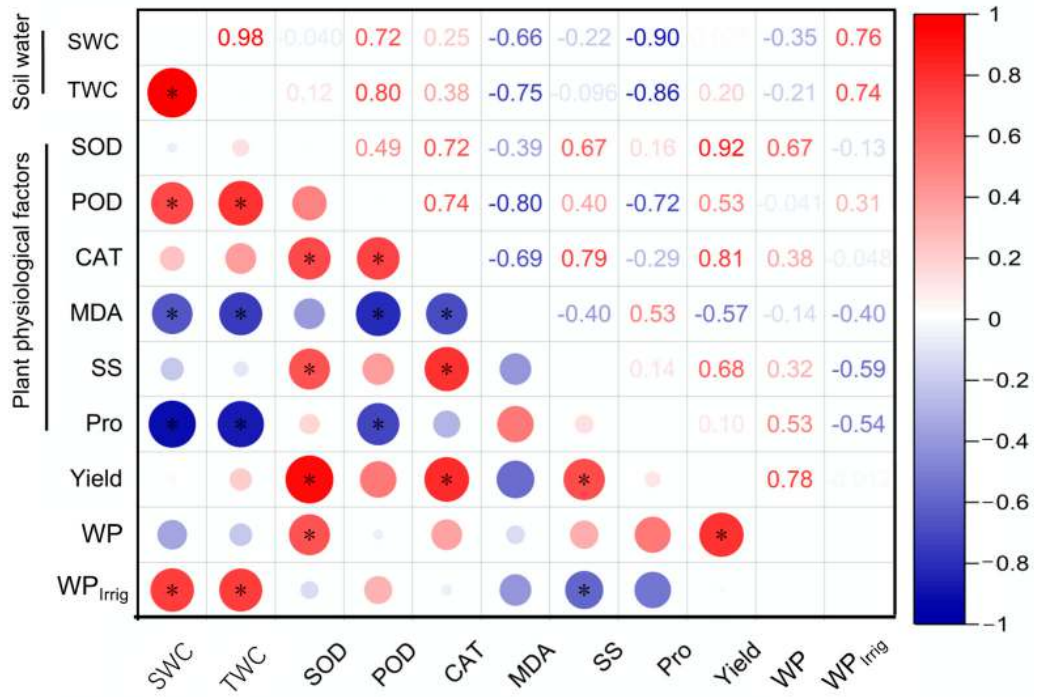

Figure 4. Correlation analysis of physiological factors of flag leaf, yield, and water-use efficiency with soil water consumptions ($p < 0.05$). SWC, soil-water-holding consumption; TWC, total water consumption; SOD, POD, CAT, MDA, SS, and Pro are given in caption of Table 4. * represents the significant correlation at 0.05 levels.

4. Discussion

4.1. Grain Yield and Water-Use Efficiency under Irrigation

Soil water is considered to be the main factor that affects crop yields. Irrigation has a direct impact on soil water content, as well as nutrient availabilities, physiological factors of the flag leaves, and water-use efficiency (Figure 4), which is in line with Ierna and Mauromicale [24].

In semiarid areas, like northern China, water is an important limiting factor in winter wheat yield production [25,26]. Rainfall could effectively supply the demands for crop water and soil water storage, particularly in the winter wheat season. Even though the water required in the winter wheat season still reached up to 200–300 mm [3,27], irrigation was still the main management method to maintain high crop yield production, e.g., the yield of S086 for W0 vs. W1 vs. W2 was 6536 vs. 8182 vs. 8286 kg ha^{-1}, respectively, in 2019–2020 (Table 5), which indicated that irrigation could increase crop yields by as high as 27–164%, and these results have been proven by previous studies [1,2], as Jha, Kumar, and Ines [17] reported that irrigation during dry spells could reduce the wheat yield losses caused by water stress. Additionally, the selection of drought-resistant varieties was also beneficial for irrigation water saving with high crop yield. In this study, the highest yield was found in S086 particularly under one irrigation after the re-greening stage, i.e., W1, owing to the higher drought resistance index in this plant compared to that of J22.

As expected, the grain yield was closely related to spikes, grain numbers per spike, and 1000-grain weight [28–30], as well as superoxide dismutase (SOD) and catalase (CAT) (Figure 4). However, the spikes and grain numbers per spike were highly influenced by irrigation practices ($p < 0.001$; Table 5), which is in line with Xu et al. [31]. As reported, the irrigation 10 days after the jointing stage could decrease the degradation of florets and improve the numbers per spike [32]. Different irrigation methods cause differences in water distribution and nitrogen accumulation, resulting in complex changes in the soil environment, thus altering the environmental responses of plant growth and water-/N-use efficiency [33]. A soil water deficit in the uppermost soil layers during the jointing to anthesis period would seriously decrease the grain numbers and reduce the aboveground biomass at anthesis [31]. The activities of SOD and the contents of malondialdehyde (MDA) and Pro were increased under the water deficit condition, but the activity of CAT was increased after irrigation events, particularly during the 14-day to 21-day period after the flowering stage (Figure S3), which is in line with Mu et al. [34]. Therefore, irrigation contributed to the antioxidant effect of crops in the pre-flowering stage and to nutrient transformations during the later stage of flowering. Moreover, the content of soluble sugar (SS) 14 days after the flowering stage in irrigation treatments contributed to osmoregulation and antioxidant ability in pre-flowering and then to the transformations of nutrients to increase the crop yield during the late-flowering stage (Figure 4), which is consistent with Hui et al. [35]. Above all, irrigation at the stem extension stage (i.e., the jointing stage) of winter wheat is the most effective time to increase grain yield, WUE, plant growth, and photosynthesis [31,32,36].

Compared to W1, the crop yield of W2 (increased one more irrigation event) increased without a significant difference but had a large decrease in the WUE (5.8–12.5%) and IWUE (27.8–30.7%, $p < 0.05$), which is not the appropriate approach to meet future sustainable agriculture [37]. In addition, irrigation was one of the key factors that influence enzymes (i.e., SOD, POD, and CAT) in flag leaves, which were related to the crop-water-use efficiency (Figure 4). Additionally, drought stress is often linked with increases in oxidative stress and decreases in the contents of SS and Pro, which are beneficial to increase the tolerance to drought [38,39]. Our study found that the increase in irrigation amount would improve the content of SOD, POD, CAT, SS, and proline (Pro) but decrease the content of MDA (Figure 4, $p < 0.05$), which might contribute to the resistance to crop oxidation [40]. However, increasing irrigation amount was inversely related to water productivity and use efficiency. Therefore, selections of drought-tolerant varieties were beneficial for the win–win goal of irrigation water reduction and steady yield under drought stress [41]. In our study, when

the S086 variety was considered, the reduction in irrigation water amount contributed to the increase in the content of SS and Pro, particularly 0–14 days after the flowering stage ($p < 0.05$, Figures S5 and S6), and then enhanced the ability of drought resistance [40].

As Liu et al. [42] reported, irrigation at 120 mm per wheat season is appropriate for future sustainable wheat production with high-yielding in the irrigation region. Additionally, limited irrigation (like deficit irrigation) could cause changes in the soil dry–wet conditions, which was beneficial to increase the drought resistance of crops (e.g., winter wheat, cotton), and then increase the transformation of plants to protein and increase crop yield and qualities, as well as water-use efficiency [14,43]. Thus, the plant system of S086 combined with W1 (165 mm per wheat season) that was recommended in this region was in accordance with the future agriculture goal.

4.2. Influence of Irrigation on Soil-Water-Holding Consumption

In our study, the crop water consumptions in these two winter wheat varieties were different between these two seasons (Table 3). Typically, after the re-greening stage, the physiological growth rate of winter wheat is fast with the increase in water and nutrients demanded. This is also the key period for plant nutrient transformation and grain formation [44]. Additionally, deficit irrigation could increase the SWC by winter wheat (Figure 2) as well, resulting in the increase in root activities and changes in soil microbial communities with more effective usage of the external water besides irrigation water [45].

Therefore, meeting the water requirement of winter wheat in the jointing–filling stage could be the key practice to ensure the normal growth and maintain the soil water storage, which has also been confirmed by other researchers [32,36]. However, SWC primarily differed in the 0–120 cm soil layer in these different irrigation treatments (Figure 2), which is in line with Zhang et al. [2]. In addition, the depletion of deeper soil water was increased when the irrigation water was reduced (i.e., W0 and W1). The SWC in 2019–2020 was higher than the one in 2018–2019, mainly because of the higher rainfall after winter wheat harvested in June 2019 and during April–May in 2020 (Figure 1). Previous studies have reported that severe drought could promote the growth of roots to extract the water in the deeper soil layers as deep as 160 cm for use, but with the cost of limited growth and lower biomass and crop yield [8].

In our study, for no irrigation after re-greening, i.e., W0, the soil water of S086 was higher than that of J22. When irrigated after re-greening, i.e., W1 and W2, the water required for crop growth primarily originated from irrigation water (36.8–62.7%) and increased along with the amount of irrigation amount. In addition, the percentage of irrigation amount to the TWC of S086 was lower than that of J22, which indicated that the S086 variety could be recommended in the regions with low irrigation amount inputs due to the high resistance to water stress. Accordingly, the use efficiency of rainfall and soil water decreased gradually and the irrigation water was still the primary process provided for the crop water demands. Also, the seasonal evapotranspiration would be increased when excessive water was irrigated [46,47].

In our study, during these two wheat seasons, we found no significant difference in crop yield, but a significant difference in total water consumption between W1 and W2 was found, indicating that improved irrigation practices (i.e., W1) can be considered suitable and is recommended for future agricultural production, but other optimized practices should be considered [48], for example, reasonably adjusting or reducing the single irrigation amount in combination with rainfall or delaying irrigation at the jointing stage [32], and improving irrigation strategies with drip irrigation [49,50].

Overall, the results of these two-season experiments indicated that the use of variety S086 under W1 treatment can realize high grain yield and water-use efficiency. However, some studies have pointed out that quantitative irrigation cannot fit the real demands of water for plant growth and have suggested that proper deficit irrigation methods should be carefully considered [15]. For example, our study found a significant influence of year on TWC and SWC mainly due to the different rainfalls between these two years (Figure 1),

which caused different soil water supplements for plant demands. Accordingly, further studies are still required to evaluate the combination effects of appropriate irrigation water amounts and rainfall on wheat growth and to maintain high yield for future sustainable agriculture as well as the changes in the micro-environment (e.g., rhizosphere environment, microbial communities) [25], and the interactions among plant physiology, root growth, and microbes.

5. Conclusions

The total water consumption (TWC) and soil water consumption (SWC) by winter wheat under different irrigation treatments all increased along with increasing amounts of irrigation water applied. However, the wheat yields for both W1 and W2 were not significantly higher than those of W0 in both 2018–2019 and 2019–2020 seasons; nonetheless, the highest yield was observed in the S086 variety in all irrigation treatments in both seasons. Also, the SWC in the 0–120 cm soil layer was highly related to wheat growth in all the treatments. During the whole growth period, the crop water consumption was primarily focused on the jointing to filling stage, particularly in the jointing–flowering stages (accounting for 38.4–44.3% of total crop water consumption). Additionally, the drought-resistant variety (i.e., S086) was beneficial for the usage of SWC under a lower amount of irrigation water applied. Meanwhile, irrigation after the re-greening stage might highly promote the physiological growth of flag leaves, i.e., superoxide dismutase and catalase, which could have highly affected crop yield production and water-use efficiency. This study recommended the combination usage of variety S086 and W1 to meet the win–win goal of high crop yield and water-use efficiency with low groundwater consumption. However, further studies are still needed to evaluate the combination effects of an appropriate irrigation water amount and rainfall on maintaining high wheat yield and growth for future sustainable agriculture.

Supplementary Materials: The following supporting information can be downloaded at: https://www.mdpi.com/article/10.3390/su151310503/s1, Figure S1: Superoxide dismutase (SOD) activities of flag leaf under different irrigation treatments. a, S086 in 2018~2019; b, J22 in 2018~2019; c, S086 in 2019~2020; d, J22 in 2019~2020; Figure S2: Peroxidase (POD) activities of flag leaf under different irrigation treatments. a, S086 in 2018~2019; b, J22 in 2018~2019; c, S086 in 2019~2020; d, J22 in 2019~2020; Figure S3: Catalase (CAT) activities of flag leaf under different irrigation treatments. a, S086 in 2018~2019; b, J22 in 2018~2019; c, S086 in 2019~2020; d, J22 in 2019~2020; Figure S4: Malondialdehyde (MDA) activities of flag leaf under different irrigation treatments. a, S086 in 2018~2019; b, J22 in 2018~2019; c, S086 in 2019~2020; d, J22 in 2019~2020; Figure S5: Soluble sugar (SS) activities of flag leaf under different irrigation treatments. a, S086 in 2018~2019; b, J22 in 2018~2019; c, S086 in 2019~2020; d, J22 in 2019~2020; Figure S6: Proline (Pro) activities of flag leaf under different irrigation treatments. a, S086 in 2018~2019; b, J22 in 2018~2019; c, S086 in 2019~2020; d, J22 in 2019~2020.

Author Contributions: Conceptualization, J.Z., X.Z. and G.W.; methodology, J.Z.; software, J.X.; formal analysis, X.Z. and J.Z.; investigation, J.X.; writing—original draft preparation, X.Z. and J.Z.; writing—review and editing, G.W.; funding acquisition, X.Z. and G.W. All authors have read and agreed to the published version of the manuscript.

Funding: This research was funded by the Key Research and Development Program of Hebei Province, grant numbers 21327001D, 22326402D, and 21327005D, State Key Laboratory of North China Crop Improvement and Regulation, grant number NCCIR2021ZZ–22.

Institutional Review Board Statement: Not applicable.

Informed Consent Statement: Not applicable.

Data Availability Statement: The data are available from the corresponding author on reasonable request.

Acknowledgments: We gratefully acknowledge the participating farmers at Quzhou Experimental Station, and other relevant help. We particularly thank Tinashe Zenda for helping to improve the language.

Conflicts of Interest: The authors declare no conflict of interest.

References

1. He, G.; Cui, Z.; Ying, H.; Zheng, H.; Wang, Z.; Zhang, F. Managing the trade-offs among yield increase, water resources inputs and greenhouse gas emissions in irrigated wheat production systems. *J. Clean. Prod.* **2017**, *164*, 567–574. [CrossRef]
2. Zhang, M.; Gao, Y.; Zhang, Z.; Liu, Y.; Han, M.; Hu, N.; Wang, Z.; Sun, Z.; Zhang, Y. Limited irrigation influence on rotation yield, water use, and wheat traits. *Agron. J.* **2020**, *112*, 241–256. [CrossRef]
3. Fang, Q.; Ma, L.; Yu, Q.; Ahuja, L.R.; Malone, R.W.; Hoogenboom, G. Irrigation strategies to improve the water use efficiency of wheat–maize double cropping systems in North China Plain. *Agric. Water Manag.* **2010**, *97*, 1165–1174. [CrossRef]
4. Sun, Z.; Zhang, Y.; Zhang, Z.; Gao, Y.; Yang, Y.; Han, M.; Wang, Z. Significance of disposable presowing irrigation in wheat in increasing water use efficiency and maintaining high yield under winter wheat-summer maize rotation in the North China Plain. *Agric. Water Manag.* **2019**, *225*, 105766. [CrossRef]
5. Deng, X.; Shan, L.; Zhang, H.; Turner, N.C. Improving agricultural water use efficiency in arid and semiarid areas of China. *Agric. Water Manag.* **2006**, *80*, 23–40. [CrossRef]
6. Rathore, V.S.; Nathawat, N.S.; Bhardwaj, S.; Sasidharan, R.P.; Yadav, B.M.; Kumar, M.; Santra, P.; Yadava, N.D.; Yadav, O.P. Yield, water and nitrogen use efficiencies of sprinkler irrigated wheat grown under different irrigation and nitrogen levels in an arid region. *Agric. Water Manag.* **2017**, *187*, 232–245. [CrossRef]
7. Zhao, Z.; Qin, X.; Wang, E.; Carberry, P.; Zhang, Y.; Zhou, S.; Zhang, X.; Hu, C.; Wang, Z. Modelling to increase the eco-efficiency of a wheat–maize double cropping system. *Agric. Ecosyst. Environ.* **2015**, *210*, 36–46. [CrossRef]
8. Li, J.; Xu, X.; Lin, G.; Wang, Y.; Liu, Y.; Zhang, M.; Zhou, J.; Wang, Z.; Zhang, Y. Micro-irrigation improves grain yield and resource use efficiency by co-locating the roots and N-fertilizer distribution of winter wheat in the North China Plain. *Sci. Total Environ.* **2018**, *643*, 367–377. [CrossRef]
9. Oort, P.; Wang, G.; Vos, J.; Meinke, H.; Baoguo, L.; Huang, J.K.; Werf, W. Towards groundwater neutral cropping systems in the Alluvial Fans of the North China Plain. *Agric. Water Manag.* **2016**, *165*, 131–140. [CrossRef]
10. Zhang, X.; Bol, R.; Rahn, C.; Xiao, G.; Meng, F.; Wu, W. Agricultural sustainable intensification improved nitrogen use efficiency and maintained high crop yield during 1980-2014 in Northern China. *Sci. Total Environ.* **2017**, *596–597*, 61–68. [CrossRef]
11. Sun, Q.; Wang, Y.; Chen, G.; Yang, H.; Du, T. Water use efficiency was improved at leaf and yield levels of tomato plants by continuous irrigation using semipermeable membrane. *Agric. Water Manag.* **2018**, *203*, 430–437. [CrossRef]
12. Davarpanah, R.; Ahmadi, S.H. Modeling the effects of irrigation management scenarios on winter wheat yield and water use indicators in response to climate variations and water delivery systems. *J. Hydrol.* **2021**, *598*, 126269. [CrossRef]
13. Pardo, J.J.; Martínez-Romero, A.; Léllis, B.C.; Tarjuelo, J.M.; Domínguez, A. Effect of the optimized regulated deficit irrigation methodology on water use in barley under semiarid conditions. *Agric. Water Manag.* **2020**, *228*, 105925. [CrossRef]
14. Ali, S.; Xu, Y.; Ma, X.; Ahmad, I.; Manzoor; Jia, Q.; Akmal, M.; Hussain, Z.; Arif, M.; Cai, T.; et al. Deficit irrigation strategies to improve winter wheat productivity and regulating root growth under different planting patterns. *Agric. Water Manag.* **2019**, *219*, 1–11. [CrossRef]
15. Yu, L.; Zhao, X.; Gao, X.; Siddique, K.H.M. Improving/maintaining water-use efficiency and yield of wheat by deficit irrigation: A global meta-analysis. *Agric. Water Manag.* **2020**, *228*, 105906. [CrossRef]
16. Lima, F.A.; Córcoles, J.I.; Tarjuelo, J.M.; Martínez-Romero, A. Model for management of an on-demand irrigation network based on irrigation scheduling of crops to minimize energy use (Part II): Financial impact of regulated deficit irrigation. *Agric. Water Manag.* **2019**, *215*, 44–54. [CrossRef]
17. Jha, P.K.; Kumar, S.N.; Ines, A.V.M. Responses of soybean to water stress and supplemental irrigation in upper Indo-Gangetic plain: Field experiment and modeling approach. *Field Crops Res.* **2018**, *219*, 76–86. [CrossRef]
18. Zhang, H.; Liang, Q.; Peng, Z.; Zhao, Y.; Tan, Y.; Zhang, X.; Bol, R. Response of greenhouse gases emissions and yields to irrigation and straw practices in wheat-maize cropping system. *Agric. Water Manag.* **2023**, *282*, 108281. [CrossRef]
19. Li, J.; Wang, Y.; Zhang, M.; Liu, Y.; Xu, X.; Lin, G.; Wang, Z.; Yang, Y.; Zhang, Y. Optimized micro-sprinkling irrigation scheduling improves grain yield by increasing the uptake and utilization of water and nitrogen during grain filling in winter wheat. *Agric. Water Manag.* **2019**, *211*, 59–69. [CrossRef]
20. Wang, D.; Yu, Z.; White, P.J. The effect of supplemental irrigation after jointing on leaf senescence and grain filling in wheat. *Field Crops Res.* **2013**, *151*, 35–44. [CrossRef]
21. Jha, S.K.; Ramatshaba, T.S.; Wang, G.; Liang, Y.; Liu, H.; Gao, Y.; Duan, A. Response of growth, yield and water use efficiency of winter wheat to different irrigation methods and scheduling in North China Plain. *Agric. Water Manag.* **2019**, *217*, 292–302.
22. Troll, W.; Lindsley, J. A photometric method for the determination of proline. *J. Fish Biol.* **1955**, *215*, 655–660. [CrossRef]

23. Zhang, J.; Kirkham, M.B. Drought-stress-induced changes in activities of superoxide dismutase, catalase, and peroxidase in wheat species. *Plant Cell Physiol.* **1993**, *35*, 785–791. [CrossRef]
24. Ierna, A.; Mauromicale, G. Tuber yield and irrigation water productivity in early potatoes as affected by irrigation regime. *Agric. Water Manag.* **2012**, *115*, 276–284. [CrossRef]
25. Li, J.; Dong, W.; Oenema, O.; Chen, T.; Hu, C.; Yuan, H.; Zhao, L. Irrigation reduces the negative effect of global warming on winter wheat yield and greenhouse gas intensity. *Sci. Total Environ.* **2019**, *646*, 290–299. [CrossRef] [PubMed]
26. Wang, D. Water use efficiency and optimal supplemental irrigation in a high yield wheat field. *Field Crops Res.* **2017**, *213*, 213–220. [CrossRef]
27. Sun, H.; Shen, Y.; Yu, Q.; Flerchinger, G.N.; Zhang, Y.; Liu, C.; Zhang, X. Effect of precipitation change on water balance and WUE of the winter wheat–summer maize rotation in the North China Plain. *Agric. Water Manag.* **2010**, *97*, 1139–1145. [CrossRef]
28. Serrago, R.A.; Alzueta, I.; Savin, R.; Slafer, G.A. Understanding grain yield responses to source–sink ratios during grain filling in wheat and barley under contrasting environments. *Field Crops Res.* **2013**, *150*, 42–51. [CrossRef]
29. Slafer, G.A.; Savin, R.; Sadras, V.O. Coarse and fine regulation of wheat yield components in response to genotype and environment. *Field Crops Res.* **2014**, *157*, 71–83. [CrossRef]
30. Bustos, D.V.; Hasan, A.K.; Reynolds, M.P.; Calderini, D.F. Combining high grain number and weight through a DH-population to improve grain yield potential of wheat in high-yielding environments. *Field Crops Res.* **2013**, *145*, 106–115. [CrossRef]
31. Xu, X.; Zhang, M.; Li, J.; Liu, Z.; Zhao, Z.; Zhang, Y.; Zhou, S.; Wang, Z. Improving water use efficiency and grain yield of winter wheat by optimizing irrigations in the North China Plain. *Field Crops Res.* **2018**, *221*, 219–227. [CrossRef]
32. Fan, Y.; Liu, J.; Zhao, J.; Ma, Y.; Li, Q. Effects of delayed irrigation during the jointing stage on the photosynthetic characteristics and yield of winter wheat under different planting patterns. *Agric. Water Manag.* **2019**, *221*, 371–376. [CrossRef]
33. Tari, A.F. The effects of different deficit irrigation strategies on yield, quality, and water-use efficiencies of wheat under semi-arid conditions. *Agric. Water Manag.* **2016**, *167*, 1–10. [CrossRef]
34. Mu, Q.; Cai, H.; Sun, S.; Wen, S.; Saddique, Q. The physiological response of winter wheat under short-term drought conditions and the sensitivity of different indices to soil water changes. *Agric. Water Manag.* **2021**, *243*, 106475. [CrossRef]
35. Hui, H.; Lin, Q.; Liu, Y.; Liu, J.; Zhang, H.; Zhai, Y. Effect of irrigation on sugar content in flag leaf and grain, and yield of super-high-yield wheat at grain-filling stage. *J. Triticeae Crops* **2011**, *31*, 887–893. (In Chinese)
36. Song, H.; Li, Y.; Zhou, L.; Xu, Z.; Zhou, G. Maize leaf functional responses to drought episode and rewatering. *Agric. For. Meteorol.* **2018**, *249*, 57–70. [CrossRef]
37. Si, Z.; Zain, M.; Mehmood, F.; Wang, G.; Gao, Y.; Duan, A. Effects of nitrogen application rate and irrigation regime on growth, yield, and water-nitrogen use efficiency of drip-irrigated winter wheat in the North China Plain. *Agric. Water Manag.* **2020**, *231*, 106002. [CrossRef]
38. Gupta, A.K.; Kaur, K.; Kaur, N. Stem reserve mobilization and sink activity in wheat under drought conditions. *Am. J. Plant Sci.* **2011**, *2*, 70–77. [CrossRef]
39. Kaur, K.; Kaur, N.; Gupta, A.K.; Singh, I. Exploration of the antioxidative defense system to characterize chickpea genotypes showing differential response towards water deficit conditions. *Plant Growth Regul.* **2013**, *70*, 49–60. [CrossRef]
40. Shahzad, A.; Xu, Y.; Jia, Q.; Irshad, A.; Ma, X.; Malak, H.; Ren, X.; Peng, Z.; Cai, T.; Zhang, J. Ridge-furrow mulched with plastic film improves the anti-oxidative defence system and photosynthesis in leaves of winter wheat under deficit irrigation. *PLoS ONE* **2018**, *13*, e0200277.
41. Ashraf, M. Inducing drought tolerance in plants: Recent advances. *Biotechnol. Adv.* **2010**, *28*, 169–183. [CrossRef]
42. Liu, Y.; Zhang, X.; Xi, L.; Liao, Y.; Han, J. Ridge-furrow planting promotes wheat grain yield and water productivity in the irrigated sub-humid region of China. *Agric. Water Manag.* **2020**, *231*, 105935. [CrossRef]
43. Liu, X.; Qi, Y.; Li, F.; Yang, Q.; Yu, L. Impacts of regulated deficit irrigation on yield, quality and water use efficiency of Arabica coffee under different shading levels in dry and hot regions of southwest China. *Agric. Water Manag.* **2018**, *204*, 292–300. [CrossRef]
44. Li, J.; Zhang, Z.; Liu, Y.; Yao, C.; Song, W.; Xu, X.; Zhang, M.; Zhou, X.; Gao, Y.; Wang, Z.; et al. Effects of micro-sprinkling with different irrigation amount on grain yield and water use efficiency of winter wheat in the North China Plain. *Agric. Water Manag.* **2019**, *224*, 105736. [CrossRef]
45. Jha, S.K.; Gao, Y.; Liu, H.; Huang, Z.; Wang, G.; Liang, Y.; Duan, A. Root development and water uptake in winter wheat under different irrigation methods and scheduling for North China. *Agric. Water Manag.* **2017**, *182*, 139–150. [CrossRef]
46. Liu, X.; Shao, L.; Sun, H.; Chen, S.; Zhang, X. Responses of yield and water use efficiency to irrigation amount decided by pan evaporation for winter wheat. *Agric. Water Manag.* **2013**, *129*, 173–180. [CrossRef]
47. Payero, J.O.; Tarkalson, D.D.; Irmak, S.; Davison, D.; Petersen, J.L. Effect of irrigation amounts applied with subsurface drip irrigation on corn evapotranspiration, yield, water use efficiency, and dry matter production in a semiarid climate. *Agric. Water Manag.* **2008**, *95*, 895–908. [CrossRef]
48. Zhao, J.; Han, T.; Wang, C.; Jia, H.; Worqlul, A.W.; Norelli, N.; Zeng, Z.; Chu, Q. Optimizing irrigation strategies to synchronously improve the yield and water productivity of winter wheat under interannual precipitation variability in the North China Plain. *Agric. Water Manag.* **2020**, *240*, 106298. [CrossRef]

49. Xu, J.; Cai, H.; Wang, X.; Ma, C.; Lu, Y.; Ding, Y.; Wang, X.; Chen, H.; Wang, Y.; Saddique, Q. Exploring optimal irrigation and nitrogen fertilization in a winter wheat-summer maize rotation system for improving crop yield and reducing water and nitrogen leaching. *Agric. Water Manag.* **2020**, *228*, 105904. [CrossRef]
50. Sandhu, O.S.; Gupta, R.K.; Thind, H.S.; Jat, M.L.; Sidhu, H.S.; Yadvinder, S. Drip irrigation and nitrogen management for improving crop yields, nitrogen use efficiency and water productivity of maize-wheat system on permanent beds in north-west India. *Agric. Water Manag.* **2019**, *219*, 19–26. [CrossRef]

sustainability

MDPI

Article

Sustainable Analysis of Maize Production under Previous Wheat Straw Returning in Arid Irrigated Areas

Pan Li [1,2], Wen Yin [1,2,*], Guiping Chen [1,2,*], Yao Guo [3], Zhilong Fan [1,2], Falong Hu [1,2], Fuxue Feng [1,4], Hong Fan [1] and Wei He [1]

[1] State Key Laboratory of Aridland Crop Science, Lanzhou 730070, China
[2] College of Agronomy, Gansu Agricultural University, Lanzhou 730070, China
[3] College of Life Sciences, Northwest Normal University, Lanzhou 730070, China
[4] College of Water Conservancy and Hydropower Engineering, Gansu Agricultural University, Lanzhou 730070, China
* Correspondence: yinwen@gsau.edu.cn (W.Y.); chengp@gsau.edu.cn (G.C.)

Abstract: Conservation tillage is widely recognized as an important way to improve soil quality, ensure food security and mitigate climate change. However, relatively little attention has been paid to the subject in terms of sustainable evaluation of environmental and economic benefits of the combination of no tillage and straw returning for maize production in arid irrigated areas. In this study, grain yield (GY) and water use efficiency based on grain yield (WUE_{GY}), soil carbon emission characteristics and economic benefits were investigated, and a sustainability evaluation index based on the above indicators was assessed in maize production under a wheat–maize rotation system from 2009 to 2012. Four wheat straw returning approaches were designed: no tillage with 25 to 30 cm tall wheat straw mulching (NTSMP), no tillage with 25 to 30 cm tall wheat straw standing (NTSSP), conventional tillage with 25 to 30 cm tall wheat straw incorporation (CTSP), and conventional tillage without wheat straw returning (CTP). The results showed that NTSMP treatment could effectively regulate water consumption characteristics of maize fields and meet the water conditions for high grain yield formation, thus gaining higher GY and WUE_{GY}. NTSMP increased GY and WUE_{GY} of maize by 13.7–17.5% and 15.4–16.7% over the CTP treatment, and by 5.6–9.0% and 2.3–11.2% over the CTSP treatment, respectively. Meanwhile, compared with CTP, the NTSMP treatment could effectively reduce carbon emissions from maize fields, where average soil carbon emission fluxes (AC_f), carbon emission (CE) and water use efficiency based on carbon emission (WUE_{CE}) were reduced by 17.7–18.9%, 11.1–11.2% and 8.8–12.8% and carbon emission efficiency (CEE) was increased by 10.2–14.7%. In addition, the NTSMP and NTSSP treatments could effectively increase total output and reduce human labor and farm machinery input, resulting in higher economic benefit. Among them, the NTSMP treatment was the most effective, net income (NI) and benefit per cubic meter of water (BPW) were increased by 16.1–34.2% and 19.1–31.8% over the CTP treatment, and by 13.2–13.3% and 9.8–15.6% over the CTSP treatment, respectively. The sustainability analysis showed that the NTSMP treatment had a high sustainability evaluation index and was a promising field-management strategy. Therefore, no tillage with 25 to 30 cm tall wheat straw mulching is a sustainable maize-management practice for increasing economic benefits and improving environmental impacts in arid irrigated areas.

Keywords: economic benefits; soil carbon emission; straw returning; sustainable evaluation; water use efficiency

Citation: Li, P.; Yin, W.; Chen, G.; Guo, Y.; Fan, Z.; Hu, F.; Feng, F.; Fan, H.; He, W. Sustainable Analysis of Maize Production under Previous Wheat Straw Returning in Arid Irrigated Areas. *Sustainability* **2023**, *15*, 8935. https://doi.org/10.3390/su15118935

Academic Editor: Imre J. Holb

Received: 23 April 2023
Revised: 23 May 2023
Accepted: 26 May 2023
Published: 1 June 2023

1. Introduction

Water resources are the main limiting factor for agricultural production [1]. Declining water resources available for agriculture in the context of global climate change poses a challenge to ensuring food security [2]. In particular, soil moisture during the crop-growing season is a key factor in ensuring the formation of crop yield and quality [3].

Thus, improving crop water use efficiency will help to ensure the sustainability of crop production. At the same time, the high consumption of fossil fuels contributes to global warming, but more fossil fuel inputs are often required in high-yield cropping systems [4,5]. As a result, the agricultural production sector is one of the major sources of greenhouse gas emissions, with agriculture and land use change accounting for about a quarter of total global greenhouse gas emissions [6]. In addition, a large amount of purchased resources are invested in conventional agricultural management [4], which in turn increases the cost of agricultural production and greenhouse gas emissions, making it possible to obtain poorer net income and ecological benefits [7]. Therefore, there is an urgent need to develop crop-management technologies that maintain and increase crop yield while reducing greenhouse gas emissions and improving crop water use efficiency to increase agricultural benefit.

Globally, conservation tillage practices such as reduced tillage or no tillage and straw returning play a key role in maintaining high soil moisture, increasing crop water use efficiency, and improving the ecological environment of farmland [8–10]. Straw returning has been regarded as an important agricultural water conservation technology for soil water storage and moisture retention, reducing ineffective evaporation and surface runoff [11,12]. At the same time, crop straws are a valuable renewable organic resource, which can effectively improve soil fertility and crop yield, thus obtaining higher crop productivity [13,14]. Published research showed long-term no tillage could improve crop water use efficiency by reducing deep soil root distribution and water uptake [9]. In addition, the combination of reduced tillage or no tillage and straw returning could further increase crop yield and water production benefit, and improve soil quality [11,15]. It has been shown that straw returning could increase water use efficiency by 5.5–36.4% over straw removal, with the combination of no tillage and straw returning having higher water use efficiency and economic benefit [11]. At the same time, conservation tillage has been widely adopted as an effective crop-management measure to reduce CO_2 emissions and ensure food security, with no tillage and straw covering combining the most prominent advantages [16,17]. Some studies found that no tillage plus straw mulching could increase crop yield and net income, reduce greenhouse gas emissions and carbon footprint, and ease the negative environmental impacts of crop production [18]. In addition, no tillage and maize residue covering integrated with suitable water and nitrogen supply could improve soil water storage capacity, reduce carbon emissions and increase soil carbon sequestration potential in arid irrigated areas [10]. Therefore, understanding how the combination of straw returning and reduced tillage or no tillage affects crop productivity and ecological environment of fields is important to improve crop yield and water use efficiency, reduce greenhouse gas emissions and increase economic benefit.

Northwestern China is a typical irrigated arid agricultural region [19], where wheat and maize are the main food crops [19]. Meanwhile, conservation tillage practices such as reduced tillage or no tillage and straw returning have positive effects on food security, improving soil fertility and water production benefit and reducing the environmental burden in this region [20,21]. However, the long-term continuous cropping pattern of maize in this region has seriously hampered maize production, resulting in massive damage to maize yield and soil quality [22]. Crop rotation is an agronomic practice that combines land use and land conservation, which can break the long-term continuous crop barriers, balance soil nutrients, improve the ecological environment of fields and ultimately achieve the purpose of increasing crop yield and net income [23,24]. At present, maize area accounts for more than 30% of the total food crop area in the region, and conservation tillage practices such as reduced tillage or no tillage and straw returning integrated in a wheat–maize rotation system are widely used [22]. It has been shown that long-term no tillage plus straw-management approaches could significantly reduce soil respiration rate and cumulative CO_2 emissions by increasing soil bulk density and reducing effective gas diffusivity in a wheat–maize rotation system, thereby reducing the net carbon flux of the wheat–maize rotation system, while improving the sustainability and carbon productivity of the wheat–maize rotation system [25]. In addition, several years of research showed that

the combination of conservation tillage practices and straw returning was conducive to sustained improvement of maize yields and water use efficiency in arid irrigated areas, and it significantly increased maize yield in drought years [20]. Therefore, reduced tillage or no tillage combined with straw returning is a more suitable crop-management practice for long-term sustainable development of wheat–maize rotation systems in arid irrigated areas. However, few of these studies have focused on evaluating the environmental and economic benefits of maize production systems under wheat–maize rotation systems, especially in arid irrigated areas, with respect to sustainability [10]. Therefore, an integrated study of water production benefits, environmental costs, agricultural production costs and net income of maize production in wheat–maize rotation systems based on the integration of no tillage and straw returning is beneficial to providing a sufficient economic and environmental basis for the promotion of sustainable agricultural production technologies.

The objective of this study was to investigate the economic and environmental sustainability of maize production in arid irrigated areas. We hypothesized that previous wheat straw mulching with no tillage under a wheat–maize rotation system in arid irrigated areas could be a sustainable maize-management practice without increasing the environmental risks.

2. Materials and Methods

2.1. Test Area Description

The field experiment was conducted at Wuwei City, Gansu province, in northwest China (29°51′41″ N, 105°59′53″ E) from 2009 to 2012. The average annual temperature of the area is 7.2 °C, the accumulated temperature of ≥10 °C is 2985.4 °C and the total number of sunshine hours is 2945 h. It is suitable for wheat and maize growth. Precipitation in the region occurs mainly from July to September, and the average annual precipitation is about 150 mm, but the potential evaporation is over 2000 mm per year. The region is representative of arid irrigated agriculture. The soil at the Research Station is classified as a type of desert land filled with calcareous particles. At planting time in 2010, the soil contained 11.2 g kg^{-1}, 1.78 mg kg^{-1}, and 12.5 mg kg^{-1} of organic C, NH_4^+–N, and NO_3–N, respectively, in the 0 to 30 cm soil layer; in 2012, these values were 12.0 g kg^{-1}, 1.88 mg kg^{-1}, and 12.8 mg kg^{-1}, respectively. The climatic conditions for the maize-growing season (April–September) in 2010 and 2012 are shown in Figure 1. In a typical wheat–maize rotation system in northwest China, a consecutive four-year field experiment was conducted using various wheat straw returning-management practices. The main research components were as follows: (1) elucidating the effects of wheat straw returning on maize yield, water consumption characteristics of crops during the growing season, and water use efficiency; (2) understanding the response of carbon emission characteristics and economic efficiency of maize field with respect to different wheat straw returning-management practices; and (3) exploring wheat straw returning-management practices for sustainable production of maize in rotation of arid irrigated areas.

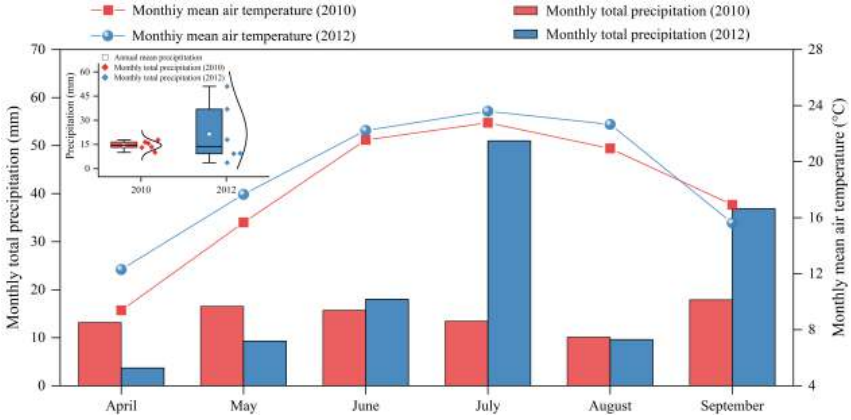

Figure 1. Monthly total precipitation and mean air temperature for the 2010 and 2012 maize-growing seasons at the Wuwei Experimental Station, northwest China.

2.2. Experimental Design

In 2009, different wheat straw returning approaches were established. This study used data related to maize farmland in 2010 and 2012. There were four treatments in the experiment: (1) no tillage with 25 to 30 cm tall wheat straw mulching (NTSMP), (2) no tillage with 25 to 30 cm tall wheat straw standing (NTSSP), (3) conventional tillage with 25 to 30 cm tall wheat straw incorporation (CTSP), and (4) conventional tillage without wheat straw returning (CTP) (Figure 2). Each treatment was arranged according to a completely randomized design and replicated three times. Maize (cultivar *Wu-ke* 2, a popular hybrid) was sown on 22 April 2010 and 20 April 2012, and harvested on 28 September 2010 and 2 October 2012, respectively. The planting density of maize was 82,500 plants ha^{-1} and the plot was 4.8 m^2 (10 by 4.8 m) with a 0.5 m wide by 0.3 m high ridge between two neighboring plots to eliminate the potential movement of irrigation water.

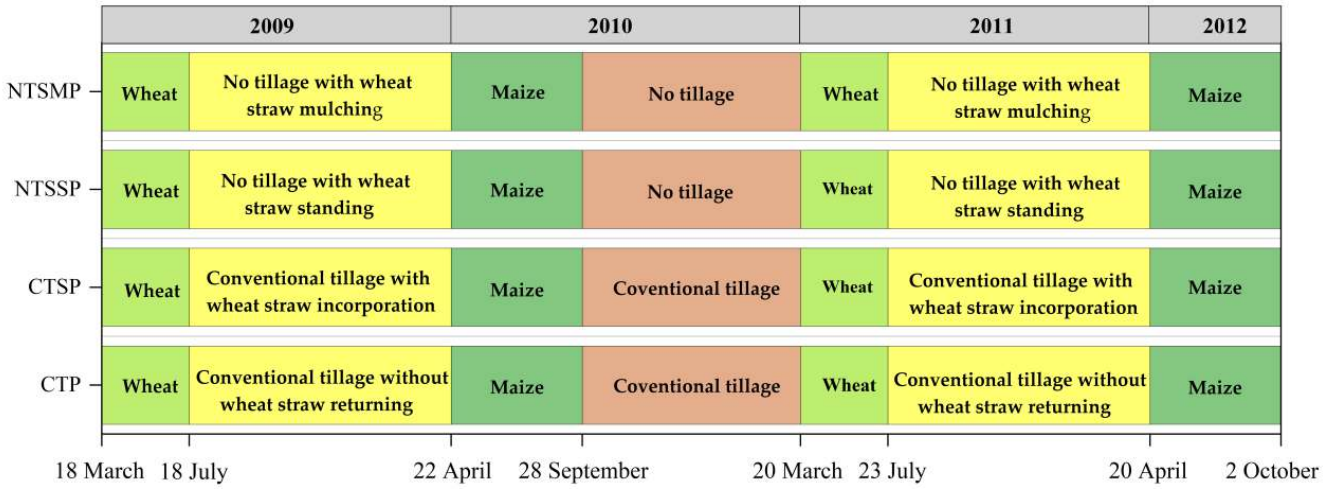

Figure 2. Schematic diagram of the annual wheat and maize rotation with crop types, wheat straw management, and the sowing and harvesting dates of wheat and maize at the arid regions in 2009–2010.

In 2009 and 2011, according to the experimental treatment, the corresponding straw returning approaches were adopted after wheat harvest. Maize was planted in 2010 and 2012, thus forming the wheat–maize rotation system, and the straw was removed from the maize field after the maize harvest. The CTSP and CTP treatments were tilled after wheat harvest at a depth of 30 cm; the following year, the base fertilizer was spread and harrowing and plastic mulching were carried out via machinery. The NTSMP and NTSSP treatments were no tillage practice after the tall wheat straw was harvested; the following year, the base fertilizer was spread, and rotary tillage, harrowing, and plastic mulching were carried out via machinery. Meanwhile, maize was sown in late April via a simple roller hole seeder. In addition, other field-management practices were the same as in the local high-yield maize field.

The irrigation and fertilization systems were the same as that of the local high-yield fields. The irrigation system was 120 mm of irrigation in late fall just before soil freezing, and 90, 75, 90, 75, and 75 mm of supplemental irrigation at the jointing, pre-heading, silking, flowering, and filling stages of maize. All treatments received 450 kg N ha^{-1} and 225 kg P_2O_5 ha^{-1}. Meanwhile, phosphorus and nitrogen fertilizers were applied as diammonium phosphate and urea. All of the P was applied as base fertilizer. The N was applied three times: 30, 60, and 10% of the total top-dressing before sowing and at the jointing and grain-filling stages of maize, respectively.

2.3. Data Collection

Evapotranspiration (ET): The approximate evapotranspiration was calculated using the following field water balance equation [10,26].

$$ET_i = P_i + I_i - \Delta S \quad (1)$$

where P and I are precipitation and irrigation, respectively, in each maize-growing stage (mm); ΔS is the difference value of soil water storage (mm) between the pre-growing and post-growing stages of maize; and i represents the various maize-growing stages. The upward and downward flows were measured previously at a nearby field, and these two items were found to be negligible in this semiarid area. Runoff was also negligible due to small rains, and irrigation was controlled via raised ridges between plots.

Grain yield (GY): The grain yield was determined by using a small combine harvester at the physiological maturity stage of maize. A sampling square of 5 m was selected to investigate the ear number for maize in each plot. The grain yield per unit area was converted to the standard grain water content of 13%.

Water use efficiency based on grain yield (WUE_{GY}):

$$WUE_{GY} = GY/ET \quad (2)$$

where WUE_{GY} (kg m^{-3}), GY (kg ha^{-1}), and ET (m^3 ha^{-1}) are water use efficiency based on grain yield, grain yield, and evapotranspiration, respectively.

Average soil CO_2 fluxes (AC_f): Soil CO_2 fluxes (C_f, μmol CO_2 m^{-2} s^{-1}) were measured using a CFX-2 system (Soil CO_2 Flux System, CFX-2, PP System, Hitchin, UK) connected with a proprietary respiration chamber. Before measuring, all crop residue and other refuse on the soil surface were removed, and a hole with a diameter the same as the respiration chamber size was made on the maize field to release the stored CO_2 efflux, at least 12 h before the measurement. The chamber, with a sharp edging point at the bottom, was placed on the soil surface and then pushed to a depth of 20 mm. Measurements were taken at three places randomly selected in each plot, five values were recorded for each place within 180 s, and the average value was used for each plot. The diurnal soil respiration was measured at 2 h intervals from 8:00 a.m. to 8:00 p.m. on the selected dates, the seasonal measurements started on 21 April 2011 and 22 April 2012, and the rest of the measurements were taken at 20-day intervals from April to September in each year. Average soil CO_2 fluxes (μmol CO_2 m^{-2} s^{-1}) could be obtained by calculating the average of C_f across the maize-growing season.

Soil carbon emission (CE): Soil carbon emission (CE) for the entire maize-growing season was based on C_f. CE was calculated with the following equation [5,10].

$$CE = \sum \left[\frac{C_{f(i+1)} + C_{fi}}{2} (t_{i+1} - t_i) \times 0.1584 \right] \times 0.2727 \times 24 \times 10 \quad (3)$$

where CE (kg C ha^{-1}) is soil carbon emission, C_f (μmol CO_2 m^{-2} s^{-1}) is soil CO_2 fluxes, i and j are the current and last monitoring dates, respectively, t is days after maize emergence, 0.1584 is the conversion factor between mol CO_2 m^{-2} s^{-1} and g CO_2 m^{-2} h^{-1}, and 0.2727 is the conversion factor between g CO_2 m^{-2} h^{-1} and g C m^{-2} h^{-1}.

Soil carbon emission efficiency (CEE): Soil carbon emission efficiency (CEE, kg kg^{-1}) indicates how many kg of grain yield are produced for every 1 kg of carbon emission from soil [10]. The calculation of carbon emission efficiency (CEE, kg kg^{-1}) quantifies the association between carbon emissions and grain yield, and it was described as follows.

$$CEE = GY/CE \quad (4)$$

where GY (kg ha^{-1}) and CE (kg C ha^{-1}) are grain yield and soil carbon emission, respectively.

Water use efficiency based on soil carbon emission (WUE_{CE}): Water use efficiency based on soil carbon emission (kg C m^{-3}) was determined using the following equation [26].

$$WUE_{CE} = CE/ET \quad (5)$$

where CE (kg C ha^{-1}) and ET (m^3 ha^{-1}) are soil carbon emission and evapotranspiration, respectively.

Economic benefit: In the two experimental years of this study, the inputs of agricultural materials such as human labor and farm machinery inputs (harrowing, mulching, fertilization, weeding, pest control, and harvesting), fertilizers, pesticides, seeds, mulch, drip irrigation tape, and irrigation volume were recorded in detail for the four wheat straw returning approaches. By combining the grain and straw yield of each plot, output, input, net income (NI), and input–output ratio were calculated for various wheat straw returning approaches. The price of grain, straw, agricultural materials, and labor costs were calculated according to the market price of the year. The benefit per cubic meter of water (BPW) was based on NI and ET. BPW was calculated with the following equation [27].

$$BPW = NI/ET \quad (6)$$

where BPW (¥ m^{-3}), NI (¥ ha^{-1}), and ET (m^3 ha^{-1}) are benefit per cubic meter of water, net income, and evapotranspiration.

Sustainable evaluation: the sustainability evaluation index (SEI) was based on GY, WUE_{GY}, CE, CEE, WUE_{CE}, NR, and BPW of various straw returning approaches. SEI was used to evaluate the straw returning approach with higher yield and efficiency, and a clean and friendly environment. A higher index indicates that the straw returning approach is more environmentally friendly and sustainable. To ensure that the evaluation component could be compared quantitatively, the variables were not dimensionalized. Three equations were used to determine the SEI, which was calculated as follows. Three equations were used to determine the SEI calculation equation. SEI was calculated with the following equation [4,5].

$$ax_{ij} = \frac{x_{ij}}{x_{max}} \begin{pmatrix} i = 1,2,3,4 \\ j = 1,2,3 \ldots\ldots 5 \end{pmatrix} or \frac{x_{min}}{x_{ij}} = \begin{pmatrix} i = 1,2,3,4 \\ j = 6,7 \end{pmatrix} \quad (7)$$

where ax_{ij} is a standardized value ($0 < ax_{ij} \leq 1$) at $i \times j$; ax_{ij} is the corresponding actual value for the treatment i and variable j; x_{max} and x_{min} are the maximum and minimum value for each variable.

$$bx_{ij} = \frac{1}{ax_{ij}} \sqrt{\frac{1}{m} \sum_{i=1}^{m} \left(ax_{ij} - \overline{ax_{ij}}\right)^2} \begin{pmatrix} i = 1,2,3,4 \\ j = 1,2,3 \ldots\ldots 7 \end{pmatrix} \quad (8)$$

where bx_{ij} is the coefficient of variation for each variable, the average of ax_{ij} repetitions, and m is the maximum number for i or j.

$$SEI = \sum_{j=1}^{m} \left(ax_{ij} \times \frac{bx_{ij}}{\sum_{j=1}^{m} bx_{ij}} \right) \begin{pmatrix} i = 1,2,3,4 \\ j = 1,2,3 \ldots\ldots 7 \end{pmatrix} \quad (9)$$

where SEI is the sustainability evaluation index of various wheat straw returning approaches, and the higher the value of this index, the better the sustainability of the approach.

2.4. Statistical Analysis

All data on various parameters were analyzed via analysis of variance (ANOVA) for treatments using SPSS software 24.0 (IBM, Chicago, IL, USA). The mean values of various

treatments were tested for statistical significance at a 5% ($p < 0.05$) level of probability using Duncan's multiple range test [27].

3. Results

3.1. Grain Yield and Water Use Efficiency Based on Grain Yield of Maize Affected by Various Wheat Straw Returning Approaches

3.1.1. Grain Yield of Maize

Wheat straw returning significantly increased grain yield (GY) of maize, but the difference between the test year, straw returning approaches, and their interaction were not significant (Figure 3). In 2010 and 2012, compared to conventional tillage without wheat straw returning (CTP), wheat straw returning (NTSMP, NTSSP, and CTSP) treatments increased GY by 13.7–17.5%, 12.0–13.9%, and 4.4–11.9%, respectively. Meanwhile, no tillage with wheat straw mulching (NTSMP) was the most productive treatment and increased GY by 5.6–9.0% compared to conventional tillage with wheat straw returning (CTSP). Therefore, no tillage with 25 to 30 cm tall previous wheat straw mulching can effectively increase the grain yield of maize on the following occasion.

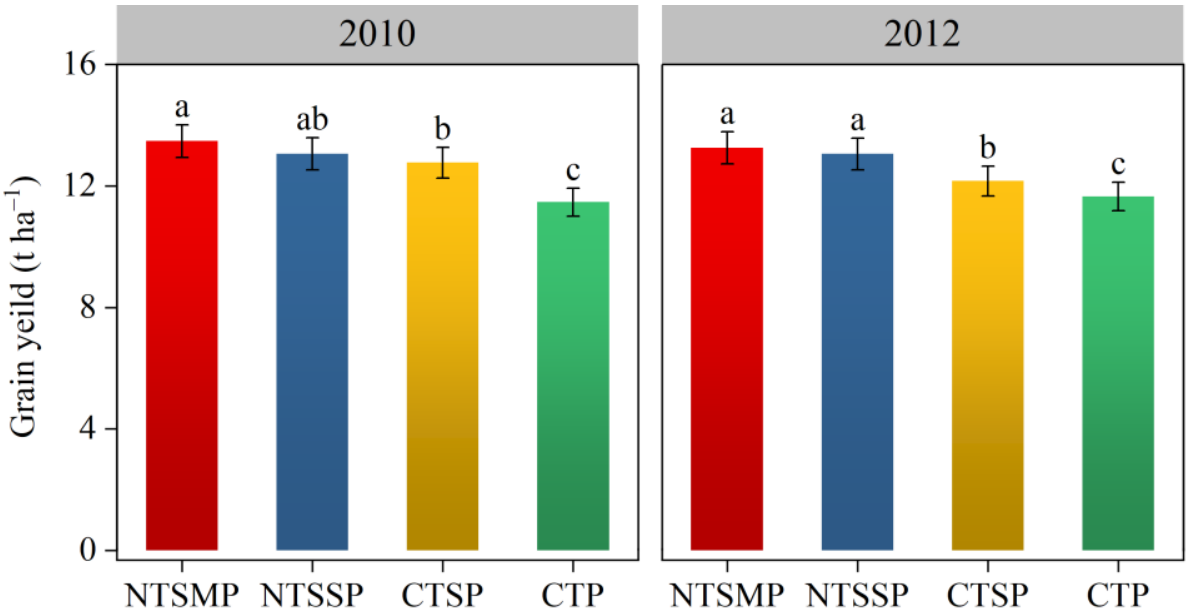

Figure 3. Grain yield of maize in wheat–maize rotation system under various wheat straw returning approaches in arid regions, in 2010 and 2012. NTSMP, no tillage with 25 to 30 cm tall wheat straw mulching; NTSSP, no tillage with 25 to 30 cm tall wheat straw standing; CTSP, conventional tillage with 25 to 30 cm tall wheat straw incorporation; CT, conventional tillage without wheat straw returning. The smaller bars are standard errors. Different letters indicate significant differences ($p < 0.05$) among treatments.

3.1.2. Evapotranspiration of Maize at Each Growth Stage

In 2012, NTSMP treatment had lower total evapotranspiration (ET) of maize during the whole growing period, reduced by 2.0%, 2.0%, and 2.5% compared to NTSSP, CTSP, and CTP treatments, respectively, but there was no significant difference between NTSSP, CTSP, and CTP treatments. While in 2010, NTSMP and NTSSP increased total ET by 3.2% and 3.7% over the CTSP treatments, but there was no significant difference between NTSMP and CTP treatments (Table 1).

Table 1. Evapotranspiration of maize at each growth stage under various wheat straw returning approaches in arid regions, in 2010 and 2012.

Year	Treatment	ET (m^3 ha^{-1})				Total (m^3 ha^{-1})
		Sowing To Jointing Stage	Jointing to Large Bell Mouth Stage	Large Bell Mouth to Silking Stage	Silking to Full-Ripe Stage	
2010	NTSMP	2181 ^{a}	539 ^{c}	1056 ^{c}	1774 ^{a}	5550 ^{ab}
	NTSSP	2075 ^{ab}	626 ^{b}	1137 ^{b}	1741 ^{a}	5580 ^{a}
	CTSP	1965 ^{bc}	665 ^{b}	1200 ^{a}	1550 ^{b}	5380 ^{b}
	CTP	1902 ^{c}	787 ^{a}	1230 ^{a}	1531 ^{b}	5450 ^{ab}
2012	NTSMP	1656 ^{c}	470 ^{b}	1511 ^{b}	2157 ^{a}	5794 ^{b}
	NTSSP	1746 ^{b}	433 ^{b}	1656 ^{a}	2080 ^{a}	5915 ^{a}
	CTSP	1656 ^{c}	473 ^{b}	1713 ^{a}	2074 ^{a}	5915 ^{a}
	CTP	1839 ^{a}	576 ^{a}	1706 ^{a}	1825 ^{b}	5945 ^{a}

Note: NTSMP, no tillage with 25 to 30 cm tall wheat straw mulching; NTSSP, no tillage with 25 to 30 cm tall wheat straw standing; CTSP, conventional tillage with 25 to 30 cm tall wheat straw incorporation; CT, conventional tillage without wheat straw returning. Different letters indicate significant differences ($p < 0.05$) among treatments.

At the sowing to jointing stage of maize, ET accounted for 29.3–37.0% of the total ET, and the difference was significant between test years. In 2010, no tillage wheat with straw returning significantly increased maize ET, and NTSMP and NTSSP increased ET by 14.4% and 9.1% over the CTP treatment, and by 11.0% and 5.6% over the CTSP treatment, respectively, but there was no significant difference between the NTSMP and NTSSP treatments. In 2012, wheat straw returning significantly had lower ET of maize, NTSMP, NTSSP, and CTSP decreased by 9.9%, 5.1%, and 9.9% over the CTP treatment, and NTSMP decreased by 5.2% over the NTSSP treatment, respectively, while there was no significant difference between NTSMP and CTSP treatments. This indicates that no tillage with wheat straw returning facilitated the reduction of evapotranspiration from the sowing to jointing stage in maize as the test year was extended.

At jointing to the large bell mouth stage of maize, the NTSMP, NTSSP, and CTSP treatments had lower ET, reduced by 18.4–31.5%, 20.5–24.9%, and 15.5–18.0%, compared to CTP treatment, respectively, with the smallest ET in the NTSMP treatment. Similarly, at the large bell mouth to silking stage of maize, NTSMP had lower ET by 7.2–8.8%, 11.8–12.0%, and 11.4–14.2% than that of NTSSP, CTSP, and CTP treatments, respectively. In addition, at the silking to full-ripe stage of maize, NTSMP and NTSSP increased by 15.9–18.2% and 13.8–14.0% over the CTP treatment, respectively, with the NTSMP treatment having higher ET, increased by 4.0–14.5% over the CTSP treatment, but there was no significant difference between NTSMP and NTSSP treatments.

Overall, no tillage with wheat straw returning reduced evapotranspiration before the silking stage, increased evapotranspiration after the silking stage, and met the water demand for the formation of higher grain yield in the later stage of maize, with the NTSMP treatment having the most prominent effect.

3.1.3. Water Use Efficiency Based on Grain Yield of Maize

Wheat straw returning had the effect of significantly improving water use efficiency based on grain yield (WUE_{GY}) throughout the growing season of maize; the NTSMP treatment in particular was outstanding (Figure 4). In both trial years, NTSMP, NTSSP, and CTSP increased WUE_{GY} by 15.4–16.7%, 11.3–12.6%, and 4.9–12.8% over the CTP treatment, respectively, and NTSMP increased by 2.3–11.2% over the CTSP treatment. In addition, in 2010, NTSMP increased WUE_{GY} by 3.7% over the NTSSP treatment; in 2012, NTSMP and NTSSP were not significant with respect to each other, but NTSMP treatment had the highest WUE_{GY} in both trial years.

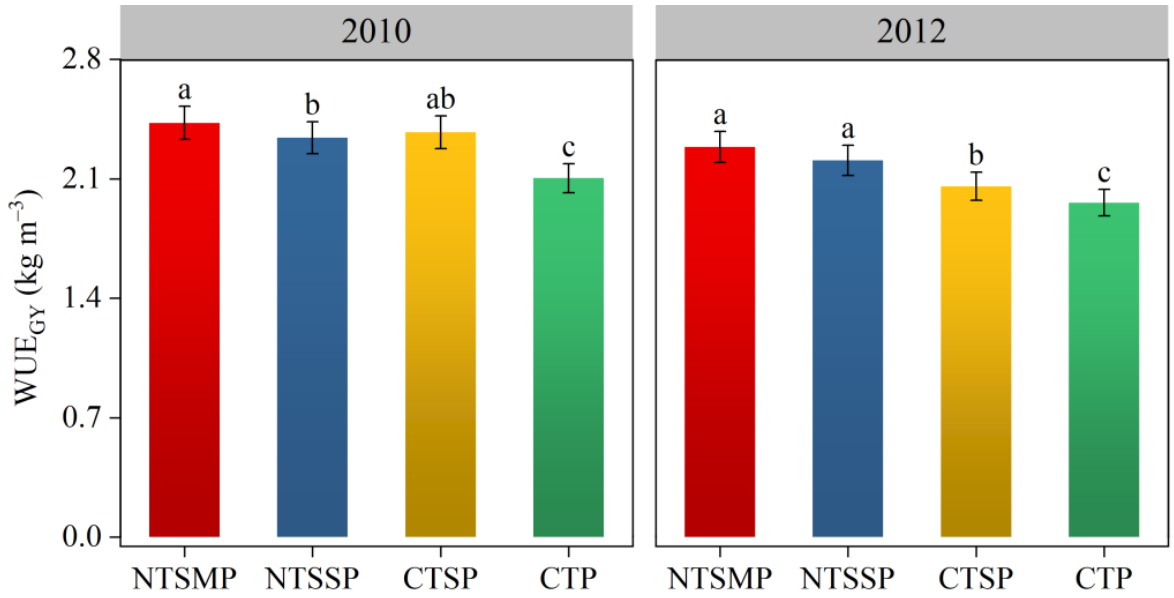

Figure 4. Effects of different wheat straw returning approaches on water use efficiency based on grain yield of maize in wheat–maize rotation system in arid regions, in 2010 and 2012. NTSMP, no tillage with 25 to 30 cm tall wheat straw mulching; NTSSP, no tillage with 25 to 30 cm tall wheat straw standing; CTSP, conventional tillage with 25 to 30 cm tall wheat straw incorporation; CT, conventional tillage without wheat straw returning. The smaller bars are standard errors. Different letters indicate significant differences ($p < 0.05$) among treatments.

3.2. Regulation Effect of Wheat Straw Returning Approaches on Soil Carbon Emission Characteristics of Maize Field

3.2.1. Average Soil CO_2 Fluxes and Soil Carbon Emissions during the Maize-Growing Season

Different wheat straw returning approaches had significant effects on soil carbon emissions during the maize-growing season (Figure 5). Compared to 2010, the average soil CO_2 emission fluxes (AC_f) and carbon emission (CE) of wheat straw returning treatments were lower in 2012, reduced by 3.1% and 4.8%, especially the NTSMP treatment of 2012 decreased by 4.9% and 5.7% over the NTSMP treatment of 2010, respectively. Overall, NTSMP reduced AC_f by 10.7–17.7%, 14.3–16.8%, and 17.7–18.9%, and CE decreased by 5.4–10.0%, 6.1–8.6%, and 11.1–11.2%, respectively. These values indicated that with the extension of the test year, the effect of wheat straw returning in reducing carbon emissions from maize field has gradually emerged, and the NTSMP treatment had the advantage of carbon reduction compared with other wheat straw returning approaches.

3.2.2. Soil Carbon Emission Efficiency and Water Use Efficiency Based on Soil Carbon Emission

The test years and wheat straw returning approaches had a significant effect on carbon emission efficiency (CEE) and water use efficiency based on carbon emissions (WUE_{CE}) of maize field (Figure 6). Compared to 2010, CEE decreased by 3.5% and WUE_{CE} increased by 12.9% in 2012. Wheat straw returning had a significant effect on CEE; NTSMP, NTSSP, and CTSP increased by 29.9–32.4%, 13.3–21.3%, and 10.2–14.7% over the CTP treatment, respectively, while NTSMP and NTSSP increased 15.4–16.1% and 2.9–5.8% over the CTSP treatment, respectively, with the NTSMP treatment having higher CEE by 9.1–12.8% over the NTSSP treatment. Meanwhile, NTSMP had lower WUE_{CE}, reduced by 4.9–8.2%, 4.2–11.4%, and 8.8–12.8% over the NTSSP, CTSP, and CTP treatments, respectively.

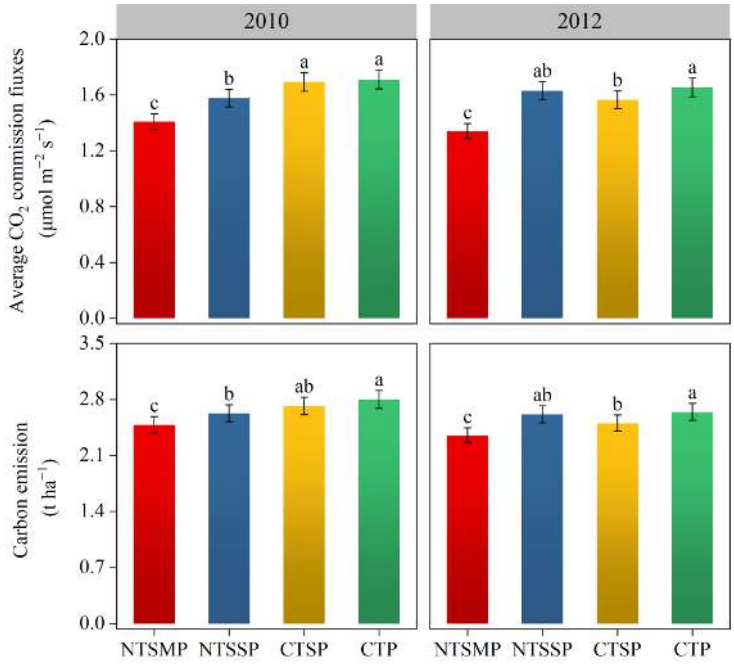

Figure 5. Effects of different wheat straw returning approaches on average soil CO_2 fluxes and soil carbon emission during the maize-growing season in arid regions, in 2010 and 2012. NTSMP, no tillage with 25 to 30 cm tall wheat straw mulching; NTSSP, no tillage with 25 to 30 cm tall wheat straw standing; CTSP, conventional tillage with 25 to 30 cm tall wheat straw incorporation; CT, conventional tillage without wheat straw returning. The smaller bars are standard errors. Different letters indicate significant differences ($p < 0.05$) among treatments.

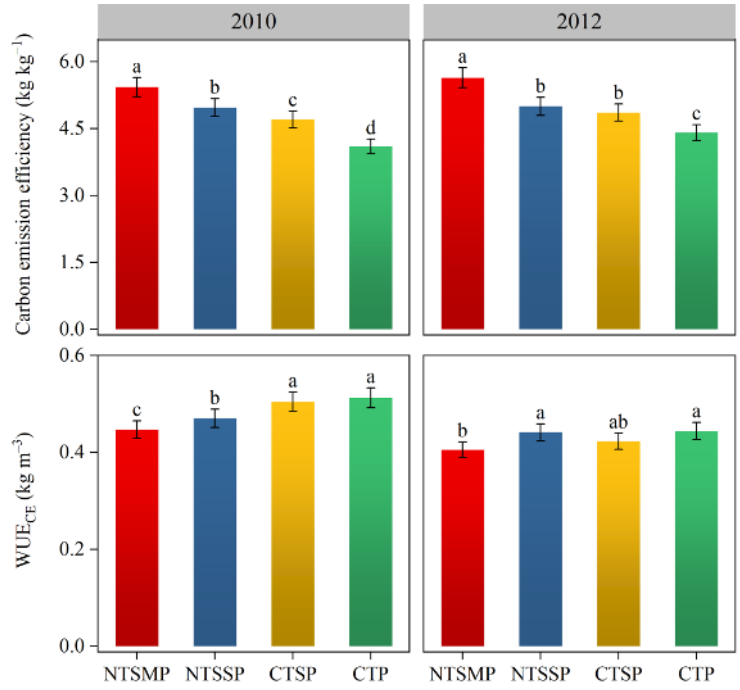

Figure 6. Effects of different wheat straw returning approaches on soil carbon emission efficiency and water use efficiency based on soil carbon emission of maize field in arid regions, in 2010 and 2012. NTSMP, no tillage with 25 to 30 cm tall wheat straw mulching; NTSSP, no tillage with 25 to 30 cm tall wheat straw standing; CTSP, conventional tillage with 25 to 30 cm tall wheat straw incorporation; CT, conventional tillage without wheat straw returning. The smaller bars are standard errors. Different letters indicate significant differences ($p < 0.05$) among treatments.

3.3. Economic Benefit Analysis of Maize Production System under Different Wheat Straw Returning Approaches

3.3.1. Input and Output Analysis

The test years and wheat straw returning approaches had a significant effect on grain output, straw output, and total output of maize production (Table 2). Compared to 2010, grain output, straw output, and total output were significantly higher in 2012, with increases of 3.7%, 27.8%, and 7.5%, respectively. In both years, NTSMP and NTSSP increased grain output by 13.5–17.5% and 12.0–13.9% over the CTP treatment, respectively, with the NTSMP treatment standing out in output addition, increased by 5.8–5.9% over the CTSP treatment, but there was no significant difference between NTSMP and NTSSP treatments. In terms of straw output, compared to CTSP and CTP, the NTSM treatment increased by 7.7% and 7.0% in 2010, respectively, but there was no significant difference between NTSMP and NTSSP treatments, while NTSM decreased by 4.2%, 7.4%, and 18.1% over the NTSSP, CTSP, and CTP treatments in 2012, respectively. Meanwhile, NTSMP increased total output by 6.7–15.8% over the CTP treatment and by 5.8–5.9% over the CTSP treatment. In addition, compared to NTSMP in 2010, the NTSMP treatment increased grain output, straw output, and total output by 3.3%, 14.1%, and 4.7% in 2012, respectively. It can be seen that no tillage with 25 to 30 cm tall wheat straw covering is beneficial with respect to increasing grain and straw output, thus increasing total output of maize production.

Table 2. Economic benefit analysis of maize production system under different wheat straw returning approaches in arid regions in China in 2010 and 2012.

Year	Treatment	Output (¥ ha^{-1})			Input (¥ ha^{-1})				Net Income (¥ ha^{-1})	Input–Output Ratio
		Grain	Straw	Total Output	Human Labor and Farm Machinery	Agricultural Supplies	Others	Total Input		
2010	NTSMP	26,940 ^{a}	4934 ^{a}	31,874 ^{a}	5538 ^{b}	4650 ^{a}	1817 ^{c}	12,005 ^{a}	19,869 ^{a}	2.655 ^{a}
	NTSSP	26,108 ^{ab}	5006 ^{a}	31,114 ^{ab}	5611 ^{b}	4650 ^{a}	1830 ^{bc}	12,091 ^{a}	19,023 ^{a}	2.573 ^{a}
	CTSP	25,520 ^{b}	4582 ^{b}	30,102 ^{b}	6055 ^{a}	4650 ^{a}	1863 ^{ab}	12,568 ^{b}	17,535 ^{b}	2.395 ^{b}
	CTP	22,920 ^{c}	4610 ^{b}	27,530 ^{c}	6203 ^{a}	4650 ^{a}	1875 ^{a}	12,728 ^{c}	14,802 ^{c}	2.163 ^{c}
2012	NTSMP	27,818 ^{a}	5628 ^{c}	33,446 ^{a}	5992 ^{b}	4923 ^{a}	1825 ^{b}	12,740 ^{a}	20,707 ^{a}	2.625 ^{a}
	NTSSP	27,405 ^{a}	5876 ^{b}	33,281 ^{a}	6071 ^{b}	4923 ^{a}	1840 ^{b}	12,834 ^{a}	20,448 ^{a}	2.593 ^{a}
	CTSP	25,529 ^{b}	6078 ^{b}	31,608 ^{b}	6529 ^{a}	4923 ^{a}	1865 ^{a}	13,317 ^{b}	18,292 ^{b}	2.374 ^{b}
	CTP	24,465 ^{c}	6870 ^{a}	31,335 ^{b}	6690 a	4923 ^{a}	1885 ^{a}	13,498 ^{b}	17,838 ^{b}	2.322 ^{b}

Note: NTSMP, no tillage with 25 to 30 cm tall wheat straw mulching; NTSSP, no tillage with 25 to 30 cm tall wheat straw standing; CTSP, conventional tillage with 25 to 30 cm tall wheat straw incorporation; CT, conventional tillage without wheat straw returning. Different letters indicate significant differences ($p < 0.05$) among treatments.

NTSMP and NTSSP had lower cost input of maize production, reduced by 5.6–5.7% and 4.9–5.0% over the CTP treatment, and reduced by 4.3–4.5% and 3.6–3.8% over the CTSP treatment, respectively (Table 2). In particular, NTSMP and NTSSP reduced human labor and farm machinery by 10.4–10.7% and 9.3–9.5% over the CTP treatment and by 8.2–8.5% and 7.0–7.3% over the CTSP treatment, respectively. However, there was no significant difference in agricultural supplies and others between the treatments. Meanwhile, due to higher market prices in 2012, compared to 2010, total input increased by 6.1% in 2012, human labor and farm machinery and agricultural supplies increased by 8.0% and 5.9%, respectively, while the difference in other inputs was not significant. Therefore, at the same market prices, the NTSMP treatment can effectively reduce human labor and farm machinery input, and thus a certain degree of reduction in cost input of maize production.

The effect of wheat straw returning approaches on input–output ratio of maize was significant, while the test year did not have a significant effect on input–output ratio (Table 2). In the two test years, no tillage with wheat straw returning had higher input–output ratio, with NTSMP and NTSSP increased by 13.1–22.8% and 11.7–19.0% over the

CTP treatment, and by 10.6–10.9% and 7.4–9.3% over the CTSP treatment, respectively, among which the NTSMP treatment had obvious advantages.

Analysis of the above results shows that no tillage with 25 to 30 cm tall wheat straw mulching could increase total output and reduce total input by increasing grain and straw output and reducing human labor and farm machinery input, thus obtaining a higher input–output ratio, which was conducive to improving the economic benefits of maize production.

3.3.2. Net Income

The test years and wheat straw returning approaches had a significant effect on net income (NI) of maize production (Table 2). Compared to 2010, NI increased by 7.8% in 2012. In both test years, no tillage with wheat straw returning had higher NI; NTSMP and NTSSP increased by 16.1–34.2% and 14.6–28.5% over the CTP treatment, and by 13.2–13.3% and 8.5–11.8% over the CTSP treatment, while the difference between NTSMP and NTSSP treatments was not significant, but the highest NI was observed with NTSMP treatment. Meanwhile, NTSMP improved NI by 4.2% in 2012 over the NTSMP treatment in 2010. Therefore, no tillage with 25 to 30 cm tall wheat straw mulching can gain higher net income, which helps farmers to increase their income, and the advantage become more and more prominent with the extension of the test year.

3.3.3. Benefit Per Cubic Meter of Water

No tillage with wheat straw returning had the effect of significantly increasing benefit per cubic meter of water (BPW) of maize production, with the most prominent advantage being with NTSMP treatment (Figure 7). In both trial years, NTSMP and NTSSP increased BPW by 19.1–31.8% and 15.2–25.2% over the CTP treatment, and by 9.8–15.6% and 4.6–11.8% over the CTSP treatment, respectively. In 2010, CTSP increased BPW by 20.0% over the CTP treatment, but the difference between CTSP and CTP treatment was not significant in 2012.

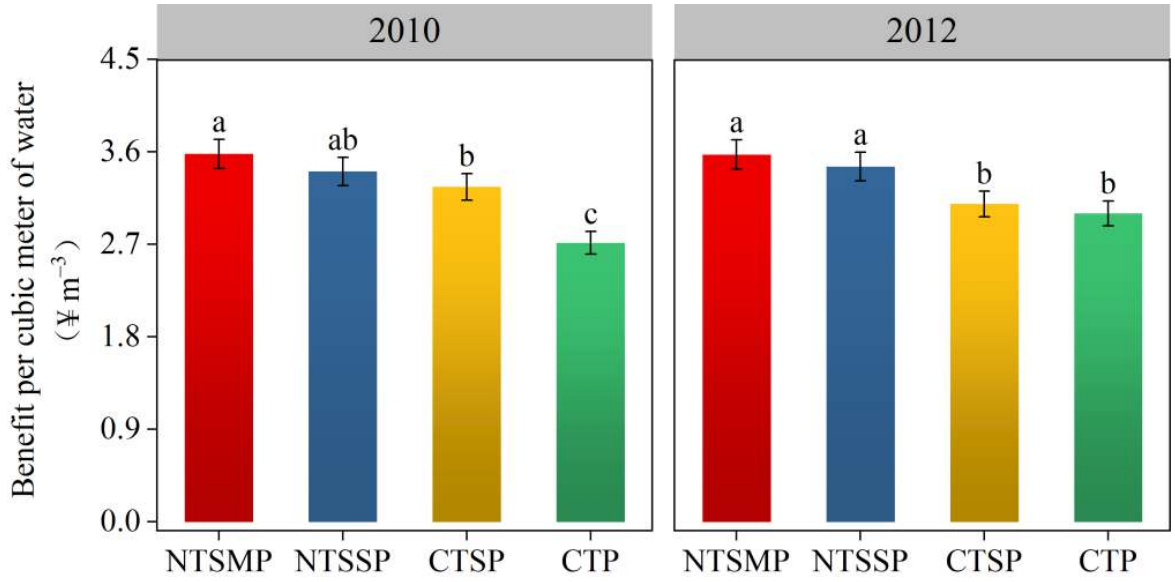

Figure 7. Effects of different wheat straw returning approaches with respect to benefit per cubic meter of water for maize in arid regions in China in 2010 and 2012. NTSMP, no tillage with 25 to 30 cm tall wheat straw mulching; NTSSP, no tillage with 25 to 30 cm tall wheat straw standing; CTSP, conventional tillage with 25 to 30 cm tall wheat straw incorporation; CT, conventional tillage without wheat straw returning. The smaller bars are standard errors. Different letters indicate significant differences ($p < 0.05$) among treatments.

3.4. Sustainable Evaluation of Maize Production in Arid Irrigated Areas

In this study, GY, WUE_{GY}, CE, CEE, WUE_{CE}, NI, and BPW were used to assess the sustainability of various wheat straw returning approaches (Figure 8a). Among the four

wheat straw returning approaches, the highest sustainable evaluation index (SEI) was found in the NTSMP treatment, where NTSMP, NTSSP, and CTSP increased by 21.1%, 14.7%, and 9.1% over the CTP treatment, respectively; NTSMP and NTSSP increased by 11.0% and 5.2% over the CTSP treatment, respectively; NTSMP increased by 5.6% over the NTSSP treatment (Figure 8b). In particular, the NTSMP treatment had higher CEE and BPW, mainly because of higher GY and NR, and lower CE and ET (Figure 8c).

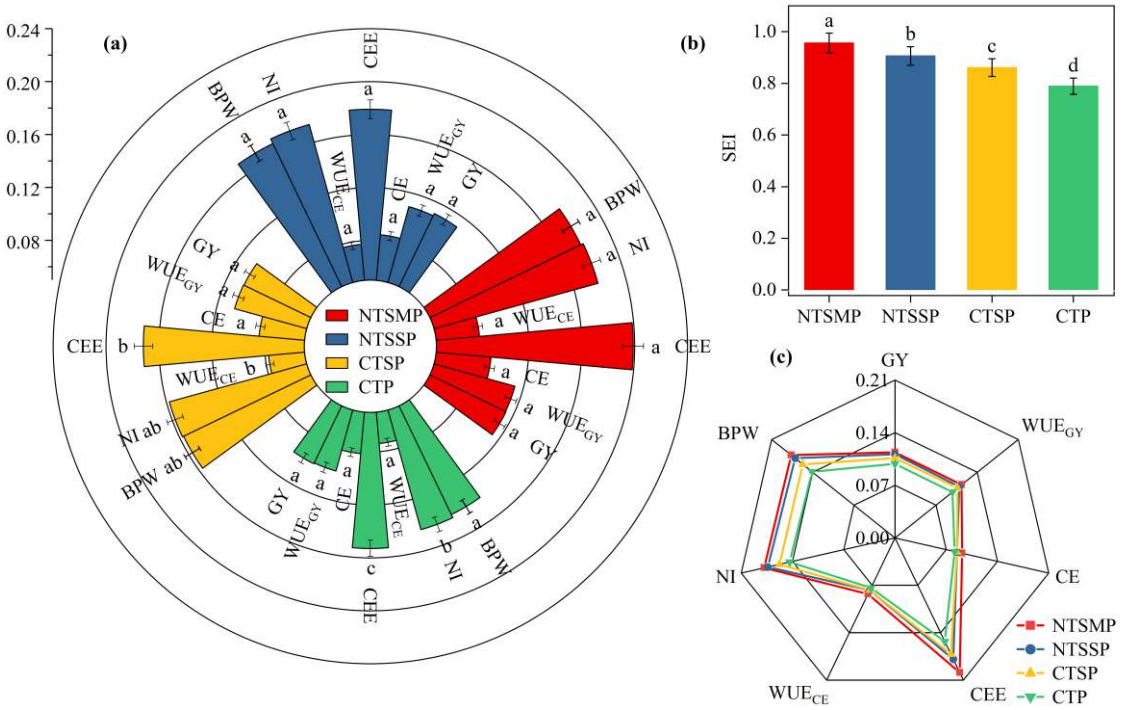

Figure 8. Functional components and the sustainable evaluation index for assessing the sustainability of various wheat straw returning approaches in arid regions in China in 2010 and 2012. Functional components of sustainable evaluation of maize production (**a**), the sustainability index of different wheat straw returning approaches (**b**), and performance of evaluated components for different wheat straw returning approaches using radar chart (**c**). GY, grain yield; WUE_{GY}, water use efficiency based on grain yield; CE, carbon emission; CEE, carbon emission efficiency; WUE_{CE}, water use efficiency based on carbon emission; NI, net income; BPW, benefit per cubic meter of water. NTSMP, no tillage with 25 to 30 cm tall wheat straw mulching; NTSSP, no tillage with 25 to 30 cm tall wheat straw standing; CTSP, conventional tillage with 25 to 30 cm tall wheat straw incorporation; CT, conventional tillage without wheat straw returning. The smaller bars are standard errors. Different letters indicate significant differences ($p < 0.05$) among treatments.

4. Discussion

4.1. Crop Yield and Water Use Efficiency of Maize Affected by Various Wheat Straw Returning Approaches

Different wheat straw returning approaches had different effects on maize yield [17]. At present, under the conditions of straw returning, tillage practices commonly used in China's maize production are conventional tillage (plow tillage), no tillage, and reduced tillage (subsoil tillage and rotary tillage) [17]. In this study, we found that maize yield under no tillage conditions was significantly higher for the wheat straw returning treatments (NTSMP and NTSSP) than the CTP treatment, with the highest yield in the NTSMP treatment, which was similar to the results of previous studies (Figure 3). Previous studies showed that 33% straw mulching, 67% straw mulching, and 100% straw mulching significantly increased maize yield under no tillage over the conventional tillage [28]. However, another study found that crop yield of no tillage without straw returning was

lower than plow tillage without straw returning, while no tillage with straw returning significantly increased crop yield compared to plow tillage without straw returning [29]. This suggests that no tillage can have a negative impact on crop yield to some extent under specific regions and climatic conditions [29]. Meanwhile, the combination of no tillage and straw returning could effectively increase soil organic carbon, effective potassium, effective nitrogen, and water storage [30,31], thus improving soil quality and offsetting this negative impact and contributing to higher crop productivity. Meanwhile, it has been shown that no tillage, straw mulching, and crop rotation (three important techniques in conservation agriculture) used in combination could maintain the same or significantly increase crop yield with conventional tillage practices [32,33], which was consistent with the crop-management practices in this study, i.e., combination of no tillage and wheat straw mulching applied in a wheat–maize rotation system (Figure 2). Therefore, the NTSMP treatment in a wheat–maize rotation system is an effective crop-management practice in arid irrigated areas that could improve maize yield. At the same time, this study found that the NTSMP treatment effectively regulated water consumption characteristics of maize during the growing season, which laid the foundation for grain yield formation in late maize reproduction, thus significantly improving water use efficiency based on grain yield (Table 1, Figure 4). It was also found that in semiarid areas, no tillage with straw mulching could retain and improve soil water and optimize crop water transfer compared to conventional tillage without straw returning, thus significantly improving crop yield and water use efficiency [34]. This was mainly because no tillage with straw mulching could effectively increase precipitation infiltration, reduce soil bulk density, and enhance soil water storage capacity, which was conducive to reducing field water consumption and increasing soil water content [35,36]. In addition, no tillage with straw mulching could also reduce ineffective evaporation of soil water, which contributed to the maintenance and regulation of field water and was conducive to improving crop water use efficiency [11]. Therefore, no tillage with wheat straw mulching can significantly improve maize yield and water use efficiency in a wheat–maize rotation system, thus ensuring food security in arid irrigated areas.

4.2. The Influence of Wheat Straw Returning Approaches on Soil Carbon Emission of Maize Field

Soil carbon sequestration is a clean and effective carbon emission mitigation strategy [37]. However, soil biodiversity had a strong influence on carbon sequestration and was influenced by factors such as temperature, rainfall, fossil fuels, and chemical fertilizers [38]. Rich substrates of renewable organic resources (crop straw) increased soil microbial and enzymatic activity related to carbon and nutrient cycling, and improved soil structure [39]. It has been shown that straw returning changed the community and function of soil bacteria and also increased the soil nutrient and soil organic carbon content in the subsoil [40], thus enhancing the carbon sequestration capacity of the crop field. However, numerous studies have shown that higher soil organic carbon content obtained through certain carbon sequestration measures might promote soil microbial respiration and lead to increased carbon emissions [25,41]. In terms of straw returning practices, previous studies have found that straw returning might also promote microbial decomposition of soil organic carbon, and accelerate soil carbon mineralization and acidification, thus significantly increasing carbon emissions from the field [42]. This process is mainly influenced by straw type, crop type, soil texture, temperature straw returning duration, and soil microbial species [38]. Nevertheless, straw returning had an important role in increasing crop yield and maintaining soil productivity [43,44]. Thus, there is an urgent need to optimize straw return methods to achieve a win–win situation in terms of increasing crop yield and reducing carbon emissions for crop production. At the same time, in our study, straw returning seems to reduce carbon emission from a field, as seen from the slightly reduced total soil carbon emission of CTSP compared to CTP, though this variation was not statistically significant in 2010 (Figure 5). Other studies have shown that no tillage practice could significantly reduce carbon emissions from the field by increasing soil bulk density and reducing the

effective oxygen diffusion coefficient due to reducing soil disturbance compared with conventional tillage, thus facilitating adaptation and mitigation of global climate change in the agricultural production sector [25,42]. In addition, a combination of conservation tillage practices such as straw returning and reduced tillage or no tillage in agricultural production could ensure food security, improve yield stability, and contribute to atmospheric CO_2 reduction through soil organic carbon sequestration [45]. It has been found that in arid irrigated areas, no tillage with straw mulching significantly reduced soil carbon emissions compared with conventional tillage, further improving carbon emission efficiency and having smaller carbon emissions per unit of water [26], which was similar to the results of this study. In this study, we found that the combination of no tillage and wheat straw mulching in wheat–maize rotation system had smaller average soil CO_2 fluxes, significantly reduced carbon emission from maize field, and lower water use efficiency based on carbon emission, which in turn improved carbon emission efficiency of maize fields in arid irrigated areas (Figures 5 and 6). Therefore, the combination of no tillage with straw mulching has the potential to mitigate climate change by reducing soil carbon emissions from crop production systems, providing an important theoretical basis for sustainable agriculture in arid irrigated areas.

4.3. The Sustainability of Maize Production by Wheat Straw Returning Approaches

In arid irrigated areas, the biggest challenge for maize production is to obtain maximum economic benefit with minimum risk input [46]. Previous studies have shown that no tillage with straw returning in maize production could achieve higher economic benefit and help increase farmers' income in the North China Plain [11]. Similarly, among the four treatments in this study, the NTSMP treatment had lower total input and higher total output, resulting in higher economic benefit (Table 2). This result was largely attributed to the reduction of resource inputs such as fossil fuels, human labor, and farm machinery with no tillage practices [46], and the NTSMP treatment had the highest maize yield, which in turn resulted in higher grain and straw output. However, some studies found no significant effect of straw returning on economic benefit, which was contrary to the results of this study [47]. This possibility was due to the apparent differences in straw returning approaches and other crop-management practices as well as soil characteristics and climatic conditions [42,45]. Meanwhile, in this study, the NTSMP and NTSSP treatments had higher benefit per cubic meter of water (Figure 7). This indicated that no tillage with wheat straw returning promoted transpiration of maize to a large extent and suppressed ineffective soil evaporation, thus increasing benefit per cubic meter of water [20]. Therefore, no tillage with wheat straw mulching can gain higher economic benefit for maize production under a wheat–maize rotation system with equal input of resources in arid irrigated areas.

From the sustainability analysis of the four wheat straw returning approaches, the NTSMP treatment had the highest sustainability evaluation index (Figure 8). This was mainly because no tillage with wheat straw mulching increased maize yield, and reduced water consumption and soil carbon emissions from maize field, and obtained higher net income, thus gaining higher carbon efficiency and benefit per cubic meter of water. Therefore, no tillage with wheat straw mulching is an effective crop-management practice with respect to achieving both economic and environmental win–win situations for maize production in arid irrigated areas. However, taking into account the great spatial heterogeneity of climate, soil characteristics, cropping systems, and agricultural management practices, it is not certain that the results obtained are fully applicable to other dry irrigated agricultural regions of the world. Future research is needed to evaluate the overall effectiveness of no tillage with wheat straw mulching at larger regional and even national scales to improve its application in sustainable maize production globally.

5. Conclusions

This study explored the effects of different wheat straw returning approaches on grain yield and water use efficiency based on grain yield, soil carbon emission characteristics,

and economic benefits in maize production and sustainability analysis under a wheat–maize rotation system in arid irrigated areas. The NTSMP treatment could effectively regulate water consumption characteristics of a maize field during the entire growing season and meet the water demand of maize in the late growing season, thus significantly improving maize grain yield and water use efficiency based on grain yield. Meanwhile, the NTSMP treatment reduced average soil CO_2 fluxes and soil carbon emissions for the maize-growing season compared to the other three treatments, thus reducing water use efficiency based on soil carbon emissions. In addition, the NTSMP and NTSSP treatments significantly increased total output of maize fields and reduced total input compared to CTP treatment, which gained higher net income and input–output ratio. Among them, the NTSMP treatment had higher soil carbon emission efficiency and benefit per cubic meter of water, and the sustainability evaluation index was higher than the other treatments. In conclusion, no tillage with 25 to 30 cm tall wheat straw mulching is an effective and feasible way to achieve higher yields and improved economic benefits for maize and to reduce soil carbon emissions in arid irrigated areas.

Author Contributions: W.Y., G.C., F.F. and F.H. conceived and designed the experiment. P.L. and W.Y. performed the statistical analyses. W.Y., G.C., F.F., Y.G. and F.H. were involved in field data collection. W.Y., Z.F., H.F. and W.H. critically reviewed the manuscript. All authors have read and agreed to the published version of the manuscript.

Funding: This research was funded by the Special Fund for Discipline Construction of Gansu Agricultural University (GSAU-XKJS-2018-078), the National Natural Science Foundation of China (32101857 and U21A20218), the Fuxi Young Talents Fund of Gansu Agricultural University (Gaufx-03Y10), and the Gansu Young Science and Technology Talents Supporting Project (2020-12), and the Important talent Project of Gansu province (204197083016).

Institutional Review Board Statement: Not applicable.

Informed Consent Statement: Not applicable.

Data Availability Statement: The entire set of raw data presented in this study is available upon request from the corresponding author.

Conflicts of Interest: The authors declare no conflict of interest.

References

1. Li, M.; Xu, Z.; Jiang, S.; Zhuo, L.; Gao, X.; Zhao, Y.; Liu, Y.; Wang, W.; Jin, J.; Wu, P. Non-Negligible Regional Differences in the Driving Forces of Crop-Related Water Footprint and Virtual Water Flows: A Case Study for the Beijing-Tianjin-Hebei Region. *J. Clean. Prod.* **2021**, *279*, 123670. [CrossRef]
2. Yu, L.; Zhao, X.; Gao, X.; Jia, R.; Yang, M.; Yang, X.; Wu, Y.; Siddique, K.H.M. Effect of Natural Factors and Management Practices on Agricultural Water Use Efficiency under Drought: A Meta-Analysis of Global Drylands. *J. Hydrol.* **2021**, *594*, 125977. [CrossRef]
3. Gao, Y.; Zhang, M.; Wang, Z.; Zhang, Y. Yield Sustainability of Winter Wheat under Three Limited-Irrigation Schemes Based on a 28-Year Field Experiment. *Crop J.* **2022**, *10*, 1774–1783. [CrossRef]
4. Yin, W.; Chai, Q.; Fan, Z.; Hu, F.; Fan, H.; Guo, Y.; Zhao, C.; Yu, A. Energy Budgeting, Carbon Budgeting, and Carbon Footprints of Straw and Plastic Film Management for Environmentally Clean of Wheat-Maize Intercropping System in Northwestern China. *Sci. Total Environ.* **2022**, *826*, 154220. [CrossRef] [PubMed]
5. Chai, Q.; Qin, A.; Gan, Y.; Yu, A. Higher Yield and Lower Carbon Emission by Intercropping Maize with Rape, Pea, and Wheat in Arid Irrigation Areas. *Agron. Sustain. Dev.* **2014**, *34*, 535–543. [CrossRef]
6. Laborde, D.; Mamun, A.; Martin, W.; Piñeiro, V.; Vos, R. Agricultural Subsidies and Global Greenhouse Gas Emissions. *Nat. Commun.* **2021**, *12*, 2601. [CrossRef]
7. Xian, Y.; Cai, G.; Sang, J.; Chen, Y.; Wang, X. Agricultural Environmental Footprint Index Based on Planetary Boundary: Framework and Case on Chinese Agriculture. *J. Clean. Prod.* **2023**, *385*, 135699. [CrossRef]
8. Huang, Y.; Tao, B.; Zhu, X.; Yang, Y.; Liang, L.; Wang, L.; Jacinthe, P.; Tian, H.; Ren, W. Conservation Tillage Increases Corn and Soybean Water Productivity across the Ohio River Basin. *Agric. Water Manag.* **2021**, *254*, 106962. [CrossRef]
9. Kan, Z.; Liu, Q.; He, C.; Jing, Z.; Virk, A.L.; Qi, J.; Zhao, X.; Zhang, H. Responses of Grain Yield and Water Use Efficiency of Winter Wheat to Tillage in the North China Plain. *Field Crops Res.* **2020**, *249*, 107760. [CrossRef]
10. Guo, Y.; Yin, W.; Chai, Q.; Fan, Z.; Hu, F.; Fan, H.; Zhao, C.; Yu, A.; Coulter, J.A. No Tillage with Previous Plastic Covering Increases Water Harvesting and Decreases Soil CO_2 Emissions of Wheat in Dry Regions. *Soil Tillage Res.* **2021**, *208*, 104883. [CrossRef]

11. He, C.; Wang, Y.; Yu, W.; Kou, Y.; Yves, B.N.; Zhao, X.; Zhang, H. Comprehensive Analysis of Resource Utilization Efficiency under Different Tillage Systems in North China Plain. *J. Clean. Prod.* **2022**, *347*, 131289. [CrossRef]
12. Zhang, K.; Wang, X.; Li, Y.; Zhao, J.; Yang, Y.; Zang, H.; Zeng, Z. Peanut Residue Incorporation Benefits Crop Yield, Nitrogen Yield, and Water Use Efficiency of Summer Peanut-Winter Wheat Systems. *Field Crops Res.* **2022**, *279*, 108463. [CrossRef]
13. Liu, N.; Li, Y.; Cong, P.; Wang, J.; Guo, W.; Pang, H.; Zhang, L. Depth of Straw Incorporation Significantly Alters Crop Yield, Soil Organic Carbon and Total Nitrogen in the North China Plain. *Soil Tillage Res.* **2021**, *205*, 104772. [CrossRef]
14. Huang, T.; Yang, N.; Lu, C.; Qin, X.; Siddique, K.H.M. Soil Organic Carbon, Total Nitrogen, Available Nutrients, and Yield under Different Straw Returning Methods. *Soil Tillage Res.* **2021**, *214*, 105171. [CrossRef]
15. Yin, W.; Chai, Q.; Guo, Y.; Fan, Z.; Hu, F.; Fan, H.; Zhao, C.; Yu, A.; Coulter, J.A. Straw and Plastic Management Regulate Air-Soil Temperature Amplitude and Wetting-Drying Alternation in Soil to Promote Intercrop Productivity in Arid Regions. *Field Crops Res.* **2020**, *249*, 107758. [CrossRef]
16. Yue, K.; Fornara, D.A.; Heděnec, P.; Wu, Q.; Peng, Y.; Peng, X.; Ni, X.; Wu, F.; Peñuelas, J. No Tillage Decreases GHG Emissions with No Crop Yield Tradeoff at the Global Scale. *Soil Tillage Res.* **2023**, *228*, 105643. [CrossRef]
17. Zhang, W.; Li, H.; Liang, L.; Wang, S.; Lakshmanan, P.; Jiang, Z.; Liu, C.; Yang, H.; Zhou, M.; Chen, X. An Integrated Straw-Tillage Management Increases Maize Crop Productivity, Soil Organic Carbon, and Net Ecosystem Carbon Budget. *Agric. Ecosyst. Environ.* **2022**, *340*, 108175. [CrossRef]
18. Wang, L.; Li, L.; Xie, J.; Luo, Z.; Zhang, R.; Cai, L.; Coulter, J.A.; Palta, J.A. Managing the Trade-Offs among Yield, Economic Benefits and Carbon and Nitrogen Footprints of Wheat Cropping in a Semi-Arid Region of China. *Sci. Total Environ.* **2021**, *768*, 145280. [CrossRef] [PubMed]
19. Gou, Z.; Yin, W.; Asibi, A.E.; Fan, Z.; Chai, Q.; Cao, W. Improving the Sustainability of Cropping Systems via Diversified Planting in Arid Irrigation Areas. *Agron. Sustain. Dev.* **2022**, *42*, 88. [CrossRef]
20. Zheng, J.; Fan, J.; Zhang, F.; Zhuang, Q. Evapotranspiration Partitioning and Water Productivity of Rainfed Maize under Contrasting Mulching Conditions in Northwest China. *Agric. Water Manag.* **2021**, *243*, 106473. [CrossRef]
21. Huang, F.; Liu, Z.; Zhang, P.; Jia, Z. Hydrothermal Effects on Maize Productivity with Different Planting Patterns in a Rainfed Farmland Area. *Soil Tillage Res.* **2021**, *205*, 104794. [CrossRef]
22. Yin, W.; Zhao, C.; Chai, Q.; Guo, Y.; Feng, F.; Yu, A. Effects of Previous Wheat Straw on the Yield of Maize in the Oasis Irrigation Region. *Crop Sci.* **2017**, *57*, 3217–3226. [CrossRef]
23. Yang, Y.; Ti, J.; Zou, J.; Wu, Y.; Rees, R.M.; Harrison, M.T.; Li, W.; Huang, W.; Hu, S.; Liu, K.; et al. Optimizing crop rotation increases soil carbon and reduces GHG emissions without sacrificing yields. *Agric. Ecosyst. Environ.* **2023**, *342*, 108220. [CrossRef]
24. Li, M.; Guo, J.; Ren, T.; Luo, G.; Shen, Q.; Lu, J.; Guo, S.; Ling, N. Crop Rotation History Constrains Soil Biodiversity and Multifunctionality Relationships. *Agric. Ecosyst. Environ.* **2021**, *319*, 107550. [CrossRef]
25. Zhang, X.; Xin, X.; Yang, W.; Ding, S.; Ren, G.; Li, M.; Zhu, A. Soil Respiration and Net Carbon Flux Response to Long-Term Reduced/No-Tillage with and without Residues in a Wheat-Maize Cropping System. *Soil Tillage Res.* **2021**, *214*, 105182. [CrossRef]
26. Hu, F.; Chai, Q.; Yu, A.; Yin, W.; Cui, H.; Gan, Y. Less Carbon Emissions of Wheat–Maize Intercropping under Reduced Tillage in Arid Areas. *Agron. Sustain. Dev.* **2015**, *35*, 701–711. [CrossRef]
27. Yin, W.; Guo, Y.; Hu, F.; Fan, Z.; Feng, F.; Zhao, C.; Yu, A.; Chai, Q. Wheat-Maize Intercropping With Reduced Tillage and Straw Retention: A Step Towards Enhancing Economic and Environmental Benefits in Arid Areas. *Front. Plant Sci.* **2018**, *9*, 1328. [CrossRef]
28. Chen, H.; Liu, Y.; Lü, L.; Yuan, L.; Jia, J.; Chen, X.; Ma, J.; Zhao, J.; Liang, C.; Xie, H.; et al. Effects of No-Tillage and Stover Mulching on the Transformation and Utilization of Chemical Fertilizer N in Northeast China. *Soil Tillage Res.* **2021**, *213*, 105131. [CrossRef]
29. Zhao, X.; Liu, S.; Pu, C.; Zhang, X.; Xue, J.; Ren, Y.; Zhao, X.; Chen, F.; Lal, R.; Zhang, H. Crop Yields under No-till Farming in China: A Meta-Analysis. *Eur. J. Agron.* **2017**, *84*, 67–75. [CrossRef]
30. Mondal, S.; Chakraborty, D. Soil Nitrogen Status Can Be Improved through No-Tillage Adoption Particularly in the Surface Soil Layer: A Global Meta-Analysis. *J. Clean. Prod.* **2022**, *366*, 132874. [CrossRef]
31. Liu, W..; Liu, W.; Kan, Z.; Chen, J.; Zhao, X.; Zhang, H. Effects of Tillage and Straw Management on Grain Yield and SOC Storage in a Wheat-Maize Cropping System. *Eur. J. Agron.* **2022**, *137*, 126530. [CrossRef]
32. Steward, P.R.; Dougill, A.J.; Thierfelder, C.; Pittelkow, C.M.; Stringer, L.C.; Kudzala, M.; Shackelford, G.E. The Adaptive Capacity of Maize-Based Conservation Agriculture Systems to Climate Stress in Tropical and Subtropical Environments: A Meta-Regression of Yields. *Agric. Ecosyst. Environ.* **2018**, *251*, 194–202. [CrossRef]
33. Pittelkow, C.M.; Linquist, B.A.; Lundy, M.E.; Liang, X.; van Groenigen, K.J.; Lee, J.; van Gestel, N.; Six, J.; Venterea, R.T.; van Kessel, C. When Does No-till Yield More? A Global Meta-Analysis. *Field Crops Res.* **2015**, *183*, 156–168. [CrossRef]
34. Qin, X.; Huang, T.; Lu, C.; Dang, P.; Zhang, M.; Guan, X.; Wen, P.; Wang, T.; Chen, Y.; Siddique, K.H.M. Benefits and Limitations of Straw Mulching and Incorporation on Maize Yield, Water Use Efficiency, and Nitrogen Use Efficiency. *Agric. Water Manag.* **2021**, *256*, 107128. [CrossRef]
35. Li, F.; Zhang, G.; Chen, J.; Song, Y.; Geng, Z.; Li, K.; Siddique, K.H.M. Straw Mulching for Enhanced Water Use Efficiency and Economic Returns from Soybean Fields in the Loess Plateau China. *Sci. Rep.* **2022**, *12*, 17111. [CrossRef] [PubMed]
36. Peng, Z.; Wang, L.; Xie, J.; Li, L.; Coulter, J.A.; Zhang, R.; Luo, Z.; Kholova, J.; Choudhary, S. Conservation Tillage Increases Water Use Efficiency of Spring Wheat by Optimizing Water Transfer in a Semi-Arid Environment. *Agronomy* **2019**, *9*, 583. [CrossRef]

37. Cui, H.; Wang, Y.; Luo, Y.; Jin, M.; Chen, J.; Pang, D.; Li, Y.; Wang, Z. Tillage Strategies Optimize SOC Distribution to Reduce Carbon Footprint. *Soil Tillage Res.* **2022**, *223*, 105499. [CrossRef]
38. Wang, X.D.; He, C.; Cheng, H.Y.; Liu, B.Y.; Zhang, H.L. Responses of Greenhouse Gas Emissions to Residue Returning in China's Croplands and Influential Factors: A Meta-Analysis. *J. Environ. Manag.* **2021**, *289*, 112486. [CrossRef]
39. Liu, B.; Arlotti, D.; Huyghebaert, B.; Tebbe, C.C. Disentangling the Impact of Contrasting Agricultural Management Practices on Soil Microbial Communities-Importance of Rare Bacterial Community Members. *Soil Biol. Biochem.* **2022**, *166*, 108573. [CrossRef]
40. Zhao, Y.; Wang, M.; Hu, S.; Zhang, X.; Ouyang, Z.; Zhang, G.; Huang, B.; Zhao, S.; Wu, J.; Xie, D.; et al. Economics and Policy-Driven Organic Carbon Input Enhancement Dominates Soil Organic Carbon Accumulation in Chinese Croplands. *Proc. Natl. Acad. Sci. USA* **2018**, *115*, 4045–4050. [CrossRef] [PubMed]
41. Tong, X.; Li, J.; Nolan, R.H.; Yu, Q. Biophysical Controls of Soil Respiration in a Wheat-Maize Rotation System in the North China Plain. *Agric. For. Meteorol.* **2017**, *246*, 231–240. [CrossRef]
42. Lin, H.; Zhou, M.; Zeng, F.; Xu, P.; Ma, S.; Zhang, B.; Li, Z.; Wang, Y.; Zhu, B. How Do Soil Organic Carbon Pool, Stock and Their Stability Respond to Crop Residue Incorporation in Subtropical Calcareous Agricultural Soils? *Agric. Ecosyst. Environ.* **2022**, *332*, 107927. [CrossRef]
43. Islam, M.U.; Guo, Z.; Jiang, F.; Peng, X. Does Straw Return Increase Crop Yield in the Wheat-Maize Cropping System in China? A Meta-Analysis. *Field Crops Res.* **2022**, *279*, 108447. [CrossRef]
44. Hao, X.; Han, X.; Wang, S.; Li, L. Dynamics and Composition of Soil Organic Carbon in Response to 15 Years of Straw Return in a Mollisol. *Soil Tillage Res.* **2022**, *215*, 105221. [CrossRef]
45. Li, S.; Hu, M.; Shi, J.; Tian, X.; Wu, J. Integrated Wheat-Maize Straw and Tillage Management Strategies Influence Economic Profit and Carbon Footprint in the Guanzhong Plain of China. *Sci. Total Environ.* **2021**, *767*, 145347. [CrossRef] [PubMed]
46. Wang, X.; Tan, W.; Zhou, S.; Xu, Y.; Cui, T.; Gao, H.; Chen, M.; Dong, X.; Sun, H.; Yang, J.; et al. Converting Maize Production with Low Emergy Cost and High Economic Return for Sustainable Development. *Renew. Sustain. Energy Rev.* **2021**, *136*, 110443. [CrossRef]
47. Li, S.; Chen, J.; Shi, J.; Tian, X.; Li, X.; Li, Y.; Zhao, H. Impact of Straw Return on Soil Carbon Indices, Enzyme Activity, and Grain Production. *Soil Sci. Soc. Am. J.* **2017**, *81*, 1475–1485. [CrossRef]

sustainability

MDPI

Article

A Simulation-Based Optimization Model for Control of Soil Salinization in the Hetao Irrigation District, Northwest China

Yunquan Zhang and Peiling Yang *

Center for Agricultural Water Research in China, China Agricultural University, Beijing 100083, China
* Correspondence: yang-pl@163.com

Abstract: The average annual water diversion of the Hetao Irrigation District (HID) from the Yellow River is 4.5 billion cubic meters, mainly used for surface irrigation. Because the groundwater depth is shallow, strong evaporation conditions and unmatched irrigation conditions lead to serious soil salinization in the area; thus, the irrigation area's ecological environment is fragile. Based on the current situation of the Yellow River irrigation project in the area, an interval two-stage robust stochastic optimization model is proposed to address the problem. In 2015, the Shuguang Experimental Station in the middle of the HID, Inner Mongolia, discussed the impact of different degrees of water–salt coordinated regulation on water consumption, yield and price of wheat, maize and sunflower under drip irrigation conditions. The obtained results provide the water shortage and water distribution targets of multiple water sources and multiple water levels in five irrigation areas of the HID. Those water distribution targets were used as the main input parameter and entered into the SALTMOD model based on the principle of water and salt balance. The output included data on groundwater mineralization and groundwater depth. It was observed that (1) integrated interval two-stage robust stochastic programming and the SALTMOD Model to couple optimization model under uncertainty can simulate a model together; (2) systemic risk issues were considered; and (3) the proposed method can be applied to the HID in northwest China to solve the soil salinization control problem. This approach is applicable to arid and semiarid regions that face similar problems.

Keywords: environmental simulation; pollution control; water resources management; eco-hydrology

Citation: Zhang, Y.; Yang, P. A Simulation-Based Optimization Model for Control of Soil Salinization in the Hetao Irrigation District, Northwest China. *Sustainability* **2023**, *15*, 4467. https://doi.org/10.3390/su15054467

Academic Editor: Jose Navarro Pedreño

Received: 1 February 2023
Revised: 27 February 2023
Accepted: 28 February 2023
Published: 2 March 2023

1. Introduction

China's saline-alkali land is distributed in 17 provinces including northeast China, north China, northwest China and coastal areas, where the total area of saline-alkali land and wasteland affecting cultivated land exceeds 500 million mu. Among them, the agricultural development potential accounts for more than 10% of the total cultivated land in China [1]. The Hetao Plain is located inland and is the most important agricultural and ecologically fragile area in northwestern China [2]. The rainfall in this area is relatively small, with the annual rainfall only 150~200 mm, while the annual evaporation is as high as 2000~3000 mm, 10~20 times the annual rainfall. Even though water from the Yellow River is introduced into this area, this water resource basically does not flow out through surface runoff. Instead, part of it evaporates and the other part is replenished by groundwater, which causes the salt contained in the water to accumulate in the area over a long time, causing salinization of the soil surface [3]. Moreover, with the gradual enhancement of groundwater evaporation in the region, soil salinization in the Hetao Irrigation District (HID) has aggravated, seriously affecting the ecological, agricultural and socio-economic development of the region [4]. Therefore, the joint application of surface water and groundwater with the optimal scheduling strategy of well and channel combinations can be used to control the groundwater level of the area below the critical depth, and reduce soil salinity in the irrigation area; this can be a reference for controlling soil salinization in the area [5].

In the regional agricultural water and soil resource management system, there are complexities such as runoff, rainfall, planning period supply and demand, and fluctuations in economic parameters, in the measures to control the salinization of surface land, water and salt migration, and droughts or floods, which intensify the work uncertainty. This leads to the use of traditional deterministic optimization methods, such as integer programming, multi-objective programming, dynamic programming, linear programming, and nonlinear programming, that cannot solve these problems. This requires uncertainty optimization technology that is widely used, including interval planning, fuzzy programming and stochastic programming methods [6]. These can be used to solve the problem of uncertainty in the prevention and control of surface land salinization by introducing the concepts of interval parameters, fuzzy number sets and probability density distribution. Among these methods, the interval two-stage robust stochastic programming (ITRM) model has a strong advantage in controlling soil salinization through the well-channel combination method. Its first stage decision must be made before the occurrence of uncertain events, and the second stage decision is a modification of the first stage decision, in order to minimize the "penalty" caused by the infeasible decision of the first stage [7].

Li and Huang et al. found an interval parameter multi-stage stochastic linear programming method (IMSLP) for uncertain water resources decision-making, combining probability density function and discrete interval in the optimization framework [8]. Li and Fu et al. created an interval linear multi-objective programming (ILMP) model for the uncertainty caused by climate change and human activities, and realized synergistic management of irrigated agricultural efficiency, yield increase and water saving [9]. Zhang and Tan et al. formed a multi-objective stochastic programming allocation model based on entropy methods combined with crop level prediction to analyze the ecological and economic trade-offs of irrigated agriculture [10]. The above optimization model is very effective in dealing with uncertain factors; if the optimization methods in the above references are applied to the treatment of saline-alkali land, the systemic risk problem is ignored. After application, it produces soil returning salt and agricultural production reduction. The model results are not absolutely feasible. The robust optimization method can effectively avoid risks in the planning process, and judge the relationship between variable random values and recourse costs in the system. For example, Li and Huang et al. built a two-stage fuzzy stochastic robust programming that represented uncertain parameters as probability density and/or fuzzy membership function, enhancing the robustness of the optimization results, and was used for regional air quality management [11]. Chen et al. set up a robust risk analysis method (RRAM) for uncertain water resources decision-making, combining interval parameter programming and robust optimization in a stochastic programming framework [12]. Tan and Zhang established a robust fractional programming (RFP) method that coupled fractional programming with robust optimization to improve agricultural water efficiency under uncertainty conditions [13].

Yao and Yang et al. utilized SALTMOD to investigate the effects of varying drainage and irrigation practices on root zone salinity and water table depth [14]. In Bahceci and Dinc et al.'s paper, the SALTMOD model was tested with data collected from the Karkin pilot area, and the effects of current irrigation–drainage practices on root zone salinity and drain discharge rate were evaluated [15]. Singh evaluated different options to solve the water-logging and soil salinization problem; the computer-based simulation model, SALTMOD, was applied in a waterlogged area of Haryana state in India [16]. There are uncertainties in the input parameters of crops, groundwater, irrigation and drainage reuse, which affect the simulation results of the SALTMOD model. The model cannot accurately describe the water and salt dynamics of a study area; therefore, combining it with a mathematical model can better solve this problem. In Mao and Yang et al.'s paper, two SALTMOD models are used to separately simulate canal- and well-irrigated areas, and an exchange flux is used as an additional mass balance term to calculate the mass balance of the canal- and well-irrigated areas [17]. In Sarangi and Singh et al.'s paper, comparative performance of artificial neural networks (ANNs) and the conceptual SALTMOD model

were used to simulate subsurface drainage effluent and root zone soil salinity in the coastal rice fields of Andhra Pradesh, India. The BPNN with the feed forward learning algorithm was a better model than SALTMOD in predicting salinity of drainage effluent from salt-affected subsurface drained rice fields. [18]. In Singh's paper, after successful calibration and validation, the computer-based simulation model, SALTMOD was applied in a waterlogged area of northwest India [19].

Complexity and uncertainty in agricultural irrigation planning based on soil salinization control at the irrigation district scale, uneven distribution of water resources in agriculture, industry, life and ecology, may result in high-risk water distribution for agriculture (such as lack of water during critical periods of crop growth, salt return to soil, etc.). The existing research has less consideration of systemic risk issues and cannot guarantee the absolute feasibility of model optimal solutions [15–19]. The robust optimization method can embody the function risk, effectively evaluate the risk, avoid the risk in the planning process, balance the relationship between the income and the risk in the regional agricultural water and land resource management system, and can effectively increase the feasibility of the model optimal solution and the stability of the system [20].

Therefore, the purpose of this study was to develop a method of coupling interval two-stage robust stochastic programming (ITRSP) with the SALTMOD model to jointly dispatch surface water and groundwater resources to deal with land salinization. The ITRSP model can address multiple concerns of two-level decision-makers and the robustness of runoff and obtained optimization schemes. Furthermore, by coupling with the SALTMOD model, the ecological and environmental impacts of irrigation and drainage measures, the objective and subjective factors of decision-making, and the environmental impacts of groundwater depth changes in the irrigation area are fully considered. Thus, the developed model can optimally allocate limited irrigation water, wells, and canals in a sustainable way. As shown in Figure 1, the developed method was then applied to a practical case for the HID of Inner Mongolia, northwest China. The results obtained from the model can help local decision-makers formulate a low-cost optimal allocation strategy under limited water supply that controls the groundwater burial depth below the critical depth, and further contribute to green agricultural development.

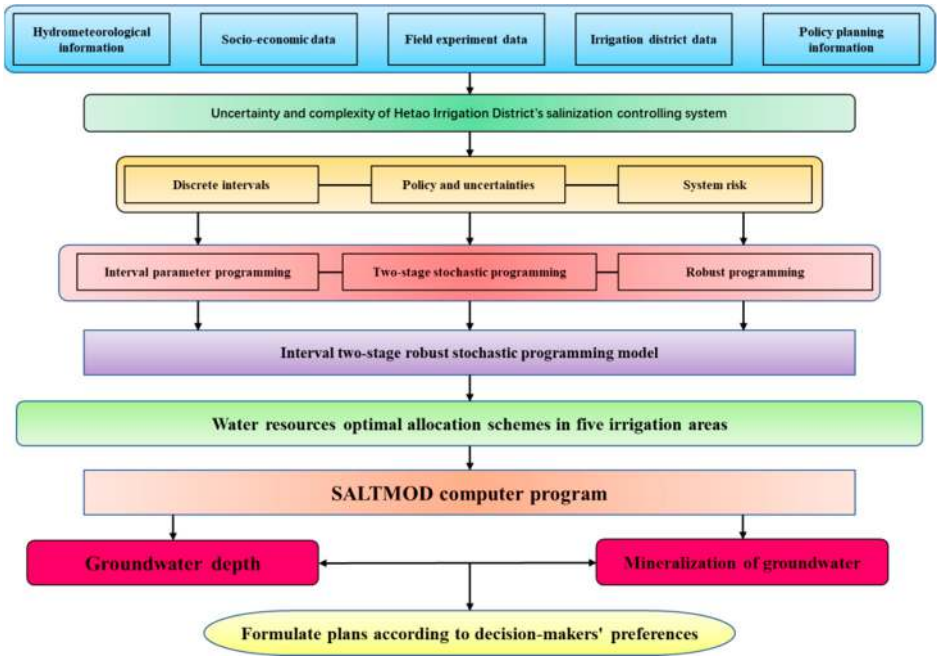

Figure 1. Framework of ITRSP and SALTMOD Coupled Model.

2. Modeling Formulation

2.1. Establishment of the Interval Two-Stage Robust Stochastic Programming Model

This study takes the water requirement of crops in the HID as the decision-making variable, introduces water cost and a water shortage penalty coefficient, and determines the optimal allocation of water resources in the HID in two stages [21–24].

To indicate the uncertainty, an interval parameter is introduced to represent the uncertainty parameter. "+" indicates the upper limit of the parameter, "−" indicates the lower limit of the parameter, then the interval two-stage robust stochastic programming (ITRM) model is established [25].

$$\min f^{\pm} = \sum_{i=1}^{m}\sum_{j=1}^{n} C_{ij}{}^{\pm} W_{ij}{}^{\pm} + \sum_{i=1}^{m}\sum_{j=1}^{n} D_{ij}{}^{\pm} \sum_{k=1}^{3} P_k S_{ijk}{}^{\pm} + \alpha \sum_{i=1}^{m}\sum_{j=1}^{n}\sum_{k=1}^{3} P_k \left(D_{ij}{}^{\pm} S_{ijk}{}^{\pm} - P_k \sum_{k=1}^{3} D_{ij}{}^{\pm} S_{ijk}{}^{\pm} + 2\theta_{ijk}{}^{\pm} \right) \quad (1)$$

subject to:

(1) Water demand constraint

$$W_{ijmax}{}^{\pm} \geq \sum_{i=1}^{m}\sum_{j=1}^{n} W_{ij}{}^{\pm} \geq W_{ijmin}{}^{\pm} \ (\forall i, j) \quad (2)$$

where

W_{ijmax}: the maximum water requirement for crop j normal growth
W_{ijmin}: the minimum water requirement for crop j normal growth

(2) Recourse variable constraint

$$\begin{cases} D_{ij}{}^{\pm} S_{ijk}{}^{\pm} - P_k \sum\limits_{k=1}^{3} D_{ij}{}^{\pm} S_{ijk}{}^{\pm} + \theta_{ijk}{}^{\pm} \geq 0 \ \ (\forall i, j, k) \\ \theta_{ijk}{}^{\pm} \geq 0 \end{cases} \quad (3)$$

(3) Water source maximum water supply constraint

$$W_{imax} \geq \sum_{j=1}^{n} W_{ij}{}^{\pm} \ \ (\forall i, j) \quad (4)$$

where W_{imax}: water source i maximum water supply, m^3

(4) Surface available water constraint and groundwater available constraint

$$Q_{ij}{}^{\pm} + q_{ik}{}^{\pm} - Q_{si}{}^{\pm} - \sum\nolimits_{j=1}^{n} \left(W_{ij}{}^{\pm} - S_{ijk}{}^{\pm} \right) = Q_{im}{}^{\pm} \geq Q_{imin} \ (i = 1, 2, \ldots, \mathrm{n}) \quad (5)$$

$$Q_{ij}{}^{\pm} + q_{ik}{}^{\pm} - Q_{si}{}^{\pm} - \sum_{j=1}^{n} \left(W_{ij}{}^{\pm} - S_{ijk}{}^{\pm} \right) = Q_{im}{}^{\pm} \geq Q_{imin} (i = n+1, n+2, \ldots, m) \quad (6)$$

(5) Groundwater depth constraint

$$\begin{cases} H_t \leq \overline{H} - Z_\alpha \\ H_t \geq \overline{H} - X_\alpha \end{cases} \ \forall t \quad (7)$$

where $\overline{H}$: average ground elevation

Z_α: critical depth of groundwater in each period
X_α: maximum allowable depth of groundwater at each time quantum

(6) Salt content constraint

$$S_{imax} \geq \sum_{j=1}^{n} {S_{ij}}^{\pm} \ (\forall i, j) \tag{8}$$

where S_{imax} : water source i maximum salt content

(7) Non-negative constraint

$$ {W_{ij}}^{\pm} \geq {S_{ijk}}^{\pm} \geq 0 \ \ (\forall i, j) \tag{9}$$

2.2. Solution of the Interval Two-Stage Robust Stochastic Programming Model

According to the characteristics of the interval two-stage robust stochastic programming model, the parameters are represented by intervals, and there are uncertainties in the ${W_{ij}}^{\pm}$. Huang and Loucks [26] found it difficult to judge what value is required to minimize the system cost; therefore, they introduced the decision variable z_{ij}, $z_{ij} \in [0, 1]$, and transformed ${W_{ij}}^{\pm} = {W_{ij}}^{-} + \Delta W_{ij} z_{ij}$. Among them $\Delta W_{ij} = {W_{ij}}^{+} - {W_{ij}}^{-}$, and it is a certain value.

When W_{ij} approaches its lower bound (when $z_{ij} = 0$), the water distribution costs for crops are minimum, but when the water allocation is less than the crop water requirement, the penalty cost of the crop will increase. Similarly, if the crop water requirement is met and W_{ij} is close to its upper limit (when $z_{ij} = 1$), the cost of crop penalties is reduced, but in order to meet the water demand of crops, the cost of water distribution will increase.

By introducing z_{ij}, the pre-target water distribution ${W_{ij}}^{\pm}$ and the decision variable optimal value z_{ijopt} can be obtained by using ${W_{ij}}^{\pm} = {W_{ij}}^{-} + \Delta W_{ij} z_{ijopt}$. When the value is a known condition, W_{ij} can be determined by this equation when the cost of the irrigation system is at a minimum. Using Matlab software to obtain ${f_{opt}}^{\pm}$ and ${S_{ijopt}}^{\pm}$, the final optimal allocation of water resources in the HID can be determined. According to the above solution and the interactive algorithm proposed by Xu and Diwekar [27], the ITRSP model was divided into two sub-models, since the goal of the model is to minimize the cost; therefore, the model corresponding to f^{-} was first solved:

$$\min f^{-} = \sum_{i=1}^{m}\sum_{j=1}^{n} {C_{ij}}^{-}({W_{ij}}^{-} + \Delta W_{ij} z_{ij}) + \sum_{i=1}^{m}\sum_{j=1}^{n} {D_{ij}}^{-} \sum_{k=1}^{3} P_k {S_{ijk}}^{-} + \alpha \sum_{i=1}^{m}\sum_{j=1}^{n}\sum_{k=1}^{3} P_k \left({D_{ij}}^{-} {S_{ijk}}^{-} - P_k \sum_{k=1}^{3} {D_{ij}}^{-} {S_{ijk}}^{-} + 2{\theta_{ijk}}^{-} \right) \tag{10}$$

subject to:

$$\begin{cases} {W_{ijmax}}^{-} \geq \sum\limits_{i=1}^{m}\sum\limits_{j=1}^{n} {W_{ij}}^{-} + \Delta W_{ij} z_{ij} \geq {W_{ijmin}}^{+} \ (\forall i, j) \\ {Q_{ij}}^{+} + {q_{ik}}^{+} - {Q_{si}}^{-} - \sum\limits_{j=1}^{n} \left({W_{ij}}^{-} + \Delta W z_{ij} - {S_{ijk}}^{-} \right) = {Q_{im}}^{-} \geq Q_{imin} (i = 1, 2, \ldots, n) \\ {Q_{ij}}^{+} + {q_{ik}}^{+} - {Q_{si}}^{-} - \sum\limits_{j=1}^{n} \left({W_{ij}}^{-} + \Delta W z_{ij} - {S_{ijk}}^{-} \right) = {Q_{im}}^{-} \geq Q_{imin} (i = n+1, n+2, \ldots, m) \\ \begin{cases} H_t \leq \overline{H} - Z_\alpha \\ H_t \geq \overline{H} - X_\alpha \end{cases} \forall t \\ W_{imax} \geq \sum\limits_{j=1}^{n} {W_{ij}}^{+} \ (\forall i, j) \\ S_{imax} \geq \sum\limits_{j=1}^{n} {S_{ij}}^{+} \ (\forall i, j) \\ {D_{ij}}^{-} {S_{ijk}}^{-} - P_k \sum\limits_{k=1}^{3} {D_{ij}}^{-} {S_{ijk}}^{-} + {\theta_{ijk}}^{-} \geq 0, \forall i, j, k \\ {\theta_{ijk}}^{-} \geq 0, \forall i, j, k \\ {W_{ij}}^{-} + \Delta W_{ij} z_{ij} \geq {S_{ijk}}^{-} \geq 0 \ \ (\forall i, j) \end{cases} \tag{11}$$

Among them, z_{ij} and ${S_{ijk}}^{-}$ are decision variables, and ${S_{ijopt}}^{-}$, z_{ijopt} , ${f_{opt}}^{-}$ are model solutions. Similarly, the objective function upper bound sub-model is obtained as:

$$\min f^{+} = \sum_{i=1}^{m}\sum_{j=1}^{n} {C_{ij}}^{+}({W_{ij}}^{-} + \Delta W_{ij} z_{ij}) + \sum_{i=1}^{m}\sum_{j=1}^{n} {D_{ij}}^{+} \sum_{k=1}^{3} P_k {S_{ijk}}^{+} + \alpha \sum_{i=1}^{m}\sum_{j=1}^{n}\sum_{k=1}^{3} P_k \left({D_{ij}}^{+}{S_{ijk}}^{+} - P_k \sum_{k=1}^{3} {D_{ij}}^{+}{S_{ijk}}^{+} + 2\theta_{ijk}{}^{+} \right) \quad (12)$$

subject to:

$$\begin{cases} {W_{ijmax}}^{+} \geq \sum_{i=1}^{m}\sum_{j=1}^{n} {W_{ij}}^{-} + \Delta W_{ij} z_{ij} \geq {W_{ijmin}}^{-} \ (\forall i, j) \\ {Q_{ij}}^{-} + {q_{ik}}^{-} - {Q_{si}}^{+} - \sum_{j=1}^{n} \left({W_{ij}}^{-} + \Delta W z_{ij} - {S_{ijk}}^{+} \right) = {Q_{im}}^{+} \geq Q_{imin} (i = 1, 2, \ldots, n) \\ {Q_{ij}}^{-} + {q_{ik}}^{-} - {Q_{si}}^{+} - \sum_{j=1}^{n} \left({W_{ij}}^{-} + \Delta W z_{ij} - {S_{ijk}}^{+} \right) = {Q_{im}}^{+} \geq Q_{imin} (i = n+1, n+2, \ldots, m) \\ \begin{cases} H_t \leq \overline{H} - Z_\alpha \\ H_t \geq \overline{H} - X_\alpha \end{cases} \forall t \\ W_{imax} \geq \sum_{j=1}^{n} {W_{ij}}^{-} \ (\forall i, j) \\ S_{imax} \geq \sum_{j=1}^{n} {S_{ij}}^{-} \ (\forall i, j) \\ {D_{ij}}^{+}{S_{ijk}}^{+} - P_k \sum_{k=1}^{3} {D_{ij}}^{+}{S_{ijk}}^{+} + \theta_{ijk}{}^{+} \geq 0, \forall i, j, k \\ \theta_{ijk}{}^{+} \geq 0, \forall i, j, k \\ {W_{ij}}^{-} + \Delta W_{ij} z_{ij} \geq {S_{ijk}}^{+} \geq 0 \ (\forall i, j) \\ {S_{ijk}}^{+} \geq {S_{ijk}}^{-} \ \forall i, j, k \end{cases} \quad (13)$$

After solving and calculating ${S_{ijopt}}^{+}$ and ${f_{opt}}^{+}$, and combining the two sub-models, the solution of the interval two-stage robust stochastic programming model was as follows:

$${f_{opt}}^{\pm} = \left[{f_{opt}}^{-}, {f_{opt}}^{+} \right]$$

$${S_{ijopt}}^{\pm} = \left[{S_{ijopt}}^{-}, {S_{ijopt}}^{+} \right] (\forall i, j)$$

$$z_{ij} = z_{ijopt} \ (\forall i, j)$$

The water optimal distribution target is:

$${O_{ij}}^{\pm} = {W_{ijopt}}^{\pm} - {S_{ijopt}}^{\pm} \ (\forall i, j)$$

where O_{ij}: the water optimal distribution target for water source i to crop j.

2.3. Introduction of the SALTMOD Model

The SALTMOD model was developed by Professor Oosterbaan and Senna of the Netherlands International Institute for Land Reclamation and Improvement (ILRI) based on the principle of water–salt balance, in the irrigation district of arid and semi-arid areas. The obtained irrigation and drainage measures showed that water and salinity change regularly in the aeration zone and phreatic water in different seasons of the year [28]. The model is mainly used to simulate and predict displacement and drainage salinity, groundwater depth, mineralization of soil water, groundwater and drainage, etc. Idris and Nazmi et al. [29] found it can also simulate farmers' responses to soil salinity, waterlogging, water scarcity, etc., and is suitable for different agricultural types, such as irrigated or non-irrigated agriculture, paddy fields or dry crops. The model has been successfully applied to the plains of Mashtul in Egypt and the coastal plains of Leziria Grande in Portugal.

The SALTMOD model is based on the principle of water and salt balance. The main input parameters include meteorology, soil, crops, irrigation and drainage, groundwater, etc.; the main output data includes groundwater depth, groundwater mineralization, soil salinity, and displacement. Based on local climatic conditions, crop growth, etc., the SALTMOD model can be divided into one to four simulation seasons, and the water–salt balance in the vertical direction of the soil is divided into four layers: aquifer, transition

layer, root layer and surface layer; for each layer both water balance and salt balance are entered as seasonal data and all factors are assumed to be evenly distributed throughout the study area.

The water–salt model has some shortcomings. For example, it is not flexible in inputting irrigation water or salinity data. Only one salinity value can be set, and the salinity of irrigation water for each season cannot be distinguished. Therefore, in the simulation study alternate irrigation of brackish and fresh water is limited [30].

In this research, based on the current situation of the Yellow River irrigation project in the HID of Inner Mongolia, the interval two-stage robust stochastic programming model is proposed to address the surface land salinization problem. The obtained results provide water shortage and water distribution targets of multiple water sources and multiple water levels in five irrigation areas. Those water distribution targets are used as main input parameters, and are substituted into the SALTMOD model based on the principle of water balance and salt balance, the output includes data on groundwater mineralization and groundwater depth.

3. Application

3.1. Regional Overview

The HID of Inner Mongolia is located in the western part of the Inner Mongolia Autonomous Region. It is one of the three largest irrigation districts in China and the largest one song artesian irrigation district in Asia. As shown in Figure 2, it is located between 105°12′ to 109°53′ east longitude and 40°13′ to 42°28′ north latitude. The total land area of the irrigation area is 11 million mu, and the existing irrigation area is 574,000 hm^2. From south to north, it can be divided into five irrigation areas, namely Yigan, Jiefangzha, Yongji, Yichang and Urad irrigation areas. The HID is located on a plateau, far from the ocean. It is affected by the Mongolian high pressure, with a large amount of wind and sand and less rainfall, forming a more typical continental monsoon climate. It is also an important commodity grain and oil production base in China. The main food crops are wheat, maize and sunflower, as well as cash crops such as processed tomato, watermelon and pepper. The irrigation area is located in an arid and semi-arid zone. Tainfall is sparse and the evaporation intensity is large. Without irrigation from the Yellow River, there would be no agricultural development [31].

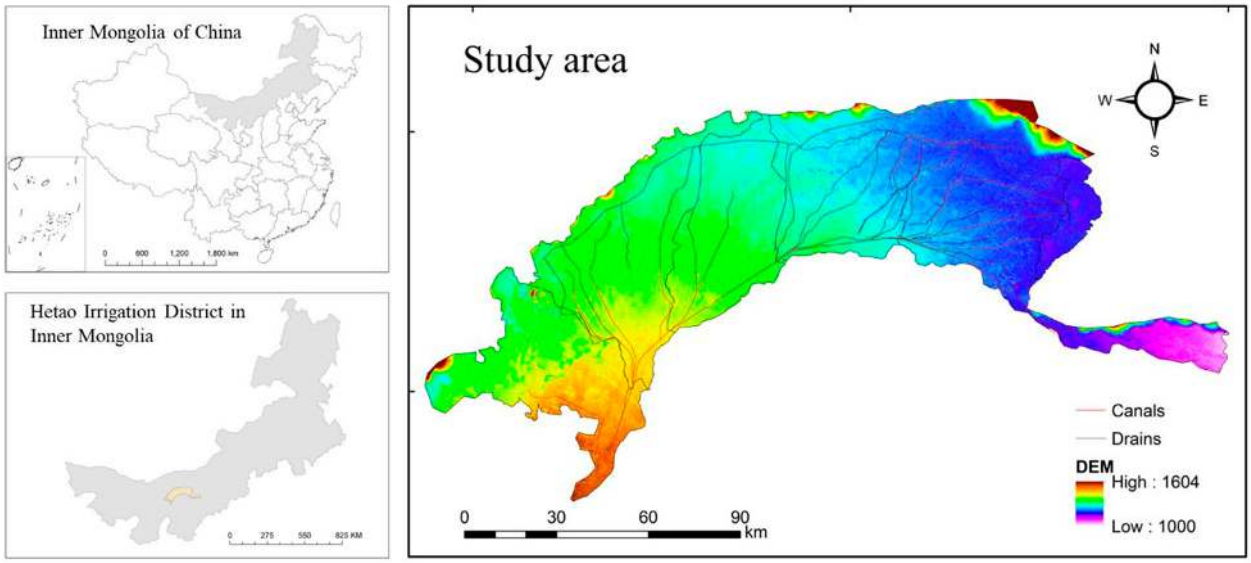

Figure 2. The geographical position of the study area.

The northeastern part of the Hetao Plain, where the HID is located, is the Yinshan Mountains. Rocks in the mountain area are strongly weathered and the salt is decomposed.

The low-lying areas of the plain have poor drainage, the water level is elevated, and the shallow groundwater has a high salt content. Water and salt rise to the surface through the soil capillary water, the water evaporates, and the salt remains on the surface. In addition, the formation of saline-alkali is supplemented by drought and waterlogging disasters. Long-term salinity has resulted in barren land and long-term stagnant food production. The lives of the masses are miserable. They eat red sorghum and wild vegetables, drink bitter and salty water, and live in earthen houses and cottages, strongly affected by the ecological, agricultural, and socio-economic development of the region [32].

3.2. Data Collection and Analysis

Three crops, wheat, corn and oil sunflower, were selected as research objects. Based on data from the 1985 to 2015 *Inner Mongolia Statistical Yearbook*, *Bayannaoer Statistical Yearbook*, and *Bayannaoer Water Resources Bulletin*, as well as data obtained from field surveys, water levels were divided into three categories: low, medium, and high [33]. According to the historical statistics of runoff and rainfall in the HID, it was concluded that the probability of occurrence of medium flow is greater than that of high flow and low flow, and the probability of occurrence of high flow and low flow is basically the same, consistent with the normal distribution law. Therefore, this study assumed that the probability of occurrence for three incoming water levels in the forecast year are 0.2, 0.6, and 0.2, respectively [34]. According to statistical data, Table 1 lists the upper and lower limits of the amount of surface and groundwater available for each administrative area under different incoming water levels in the forecast year.

Table 1. Allowable water of each district under different water levels.

Administrative Region	Inflow Level	Available Water (10^8 m^3)		Probability
		Surface Water	Groundwater	
LinHe	Low	[10.4, 10.6]	[3.5, 3.7]	0.2
	Middle	[10.5, 11.2]	[3.6, 4.2]	0.6
	High	[10.7, 12.8]	[4.0, 4.8]	0.2
DengKou	Low	[5.7, 5.9]	[4.5, 4.8]	0.2
	Middle	[8.2, 8.6]	[5.2, 5.9]	0.6
	High	[12.0, 12.7]	[8.3, 9.8]	0.2
HangJinHou banner	Low	[9.2, 9.6]	[3.3, 3.6]	0.2
	Middle	[10.0, 10.8]	[4.1, 4.8]	0.6
	High	[11.3, 12.2]	[7.7, 8.2]	0.2
Wuyuan	Low	[9.9, 10.8]	[3.0, 3.5]	0.2
	Middle	[10.5, 10.9]	[4.2, 4.6]	0.6
	High	[11.3, 12.8]	[5.2, 5.8]	0.2
Urad Front banner	Low	[5.9, 8.2]	[2.7, 3.2]	0.2
	Middle	[9.8, 13.2]	[4.4, 5.8]	0.6
	High	[12.2, 16.5]	[6.6, 7.2]	0.2

Data on the area of the three crops planted in the typical year of 2015 were selected as known conditions. It was also assumed that the planting structure of the three crops in the forecast year would not change to determine the optimal water supply target [35]. Table 2 shows the planting area of three crops in different administrative regions and the water demand data under sufficient irrigation conditions for different crops under advanced decision. Both were determined based on the survey data provided by the HID Administration and the measured data collected at the Shuguang Experimental Station in the middle reaches of the HID, Inner Mongolia in 2015.

Table 2. Water demand prediction analysis of each administrative region.

Administrative Region	Crop Acreage/10^3 hm^2				Water Demand of Crop/mm			
	Wheat	Maize	Sunflower	Total	Wheat	Maize	Sunflower	Total
LinHe	19.93	3.24	3.69	26.86	[300, 310]	[635, 650]	[320, 335]	[1255, 1295]
DengKou	85.77	9.28	10.16	105.21	[252, 268.5]	[580, 595.5]	[232.5, 250]	[1064.5, 1114]
HangJinHou banner	52.40	14.35	13.19	79.94	[286.5, 302.5]	[590.5, 600.5]	[300, 308.5]	[1177, 1211.5]
Wuyuan	60.51	15.85	33.62	109.98	[296.5, 305.5]	[630, 645]	[303, 315.5]	[1229.5, 1266]
Urad Front banner	34.29	6.98	10.52	51.79	[295, 302.5]	[628, 635]	[305, 325.5]	[1228, 1263]

In the planning and utilization of agricultural water resources, if the estimated water availability meets the crop water demand, there will only be the cost of Yellow River water diversion; if the crop water demand is not met, the water shortage penalty will result [36]. Table 3 shows the maximum and minimum original water volume of each administrative area of the HID, and the corresponding diversion costs and water shortage penalty coefficients, in combination with relevant references.

Table 3. Cost of water delivery and water shortage penalty coefficient under different water conditions.

Region	Headwaters	Max. Original Water/10^8 m^3	Min. Original Water/10^8 m^3	Net Benefit	Penalty Coefficient
LinHe	Surface water	13.27	10.44	[2.6, 3.2]	[3.2, 4.2]
	Groundwater	4.65	3.55	[2.8, 3.5]	[3.5, 4.8]
DengKou	Surface water	13.42	5.70	[3.5, 5.0]	[4.5, 6.2]
	Groundwater	5.20	4.46	[3.9, 4.8]	[4.8, 6.5]
HangJinHou banner	Surface water	12.60	10.18	[6.3, 7.9]	[7.2, 8.5]
	Groundwater	4.37	3.62	[7.8, 8.5]	[8.3, 9.6]
Wuyuan	Surface water	13.25	10.00	[3.2, 4.2]	[3.8, 7.2]
	Groundwater	5.52	3.01	[4.8, 5.5]	[5.8, 7.0]
Urad Front banner	Surface water	17.24	5.90	[7.9, 9.2]	[8.6, 9.6]
	Groundwater	2.94	2.70	[8.6, 9.8]	[9.5, 10.8]

4. Results Analysis

4.1. Optimized Water Distribution Plan

Using Matlab 7 software and Lingo 11 programming, the ITRSP model for multi-water source allocation in the HID of Inner Mongolia was robustly solved. The water shortage under different robust coefficients in the forecast year was obtained according to the calculation results of the sub-model, followed by the optimal allocation water volume at different flow levels [37]. The results are shown in Table 4.

Table 4 shows that for the Linhe District, the optimal decision variable $z_{ijopt0.2}$ was 0.2, and the corresponding optimal water supply for surface water and groundwater were 4.12×10^8 m^3 and 2.26×10^8 m^3, respectively. The optimal allocation of water was close to the lower limit of the predicted water demand, and the water shortage was 0, indicating that for this region, the benefit of increased crop yield is less than the cost of water caused by increased water consumption. Therefore, in selecting the risk of crop yield increase or decrease, the model can be selected to meet the basic water requirements of the crop; the optimal allocation of surface water and groundwater was equal to the optimal water supply target and was less than the minimum original water volume of Linhe District, 1.044×10^9 and 3.55×10^8 m^3, respectively, indicating that no external water was used [38].

Table 4. Results of optimal allocation of water resources at different water levels of each administrative region.

Administrative Region	Headwaters	Inflow Level	Pk	Optimal Water Supply Target/10^8 m^3	Water Shortage/m^3	Optimal Allocation of Water/m^3	Decision Variable
LinHe	Surface water	Low	0.2	4.12	0	4.12	0.2
		Middle	0.6	4.12	0	4.12	0.2
		High	0.2	4.12	0	4.12	0.2
	Groundwater	Low	0.2	2.26	0	2.26	0.2
		Middle	0.6	2.26	0	2.26	0.2
		High	0.2	2.26	0	2.26	0.2
DengKou	Surface water	Low	0.2	12.64	[2.23, 4.31]	[8.15, 10.02]	0.15
		Middle	0.6	12.64	[1.68, 3.35]	[8.28, 10.68]	0.15
		High	0.2	12.64	0	12.64	0.15
	Groundwater	Low	0.2	7.15	0	7.15	0.15
		Middle	0.6	7.15	0	7.15	0.15
		High	0.2	7.15	0	7.15	0.15
HangJinHou banner	Surface water	Low	0.2	15.34	[4.45, 6.72]	[8.62, 10.15]	0.35
		Middle	0.6	15.34	[3.18, 5.92]	[8.87, 10.37]	0.35
		High	0.2	15.34	[2.62, 5.59]	[9.18, 11.12]	0.35
	Groundwater	Low	0.2	5.58	[1.12, 2.15]	[3.05, 3.56]	0.35
		Middle	0.6	5.58	[1.03, 2.12]	[3.11, 3.69]	0.35
		High	0.2	5.58	[0, 0.87]	[4.42, 5.14]	0.35
Wuyuan	Surfacewater	Low	0.2	10.02	[5.68, 7.76]	[4.44, 5.36]	0.48
		Middle	0.6	10.02	[3.34, 6.15]	[5.86, 6.82]	0.48
		High	0.2	10.02	0	10.02	0.48
	Groundwater	Low	0.2	5.18	[2.12, 3.35]	[2.28, 3.47]	0.48
		Middle	0.6	5.18	[2.01, 3.28]	[2.46, 3.52]	0.48
		High	0.2	5.18	0	5.18	0.48
Urad Front banner	Surface water	Low	0.2	20.50	[8.62, 12.14]	[10.08, 12.25]	0.52
		Middle	0.6	20.50	[7.28, 10.62]	[11.14, 12.98]	0.52
		High	0.2	20.50	0	8.65	0.52
	Groundwater	Low	0.2	8.65	0	8.65	0.52
		Middle	0.6	8.65	0	8.65	0.52
		High	0.2	8.65	0	8.65	0.52

Table 4 shows that for Dengkou County, the optimal decision variable $z_{ijopt0.15} = 0.15$, then the corresponding optimal water supply for surface water and groundwater is 1.264×10^9 and 7.15×10^8 m^3, respectively. With $z_{ijopt0.52} = 0.52$ in Urad Front Banner, the corresponding optimal amounts of surface water and groundwater are 2.05×10^9 and 8.65×10^8 m^3, respectively. For Dengkou County and Urad Front Banner, the water shortage for both groundwater and surface water was 0 at the high water level. As can be seen in Table 3, the cost of surface water is lower than of groundwater. In order to ensure maximum benefits, in the process of water resources allocation, the surface water allocation is prioritized. Dengkou County had a small amount of water shortage at low and medium water levels. The surface water shortages reached 2.23×10^8~4.31×10^8 and 1.68×10^8~3.35×10^8 m^3, respectively, which indicates that the crop water demand in this area is relatively low compared to the soil salinization in this area. At the low incoming water level in Dengkou County, the optimal allocation of surface water and groundwater was 8.15×10^8~1.002×10^9 and 7.15×10^8 m^3, respectively, both larger than the minimum original water volume of 5.7×10^8 and 4.46×10^8 m^3, respectively, indicating that some external water was used. However, because the amount of groundwater resources was less than the amount of surface water resources, and the cost of mining is high, the optimal allocation of water should mainly come from surface water [39].

As seen in Table 4, for HangJinHou banner, the optimal decision variable $z_{ijopt0.35} = 0.35$, and the corresponding optimal water supply for surface water and groundwater was 1.534×10^9 and 5.58×10^8 m^3, respectively. The water shortage in HangJinHou banner was relatively large at low incoming water levels. The surface and groundwater shortages

reached 4.45×10^8~6.72×10^8 and 1.12×10^8~2.15×10^8 m^3, respectively. This shows that the region needs a larger amount of crop water, which is related to the larger crop cultivation area in the region. At a low incoming water level, the optimal allocation of surface water and groundwater in HangJinHou banner was 8.62×10^8~1.015×10^9 and 3.05×10^8~3.56×10^8 m^3, respectively, both less than the minimum original water volume of 1.018×10^9 and 3.62×10^8 m^3, respectively, indicating that water resources were scarce at low water supply levels; considering the higher cost of water, the amount of water allocated to crops should be relatively reduced [40].

As seen in Table 4, for Wuyuan County, the optimal decision variable $z_{ijopt0.48} = 0.48$, and the corresponding optimal water supply for surface water and groundwater was 1.002×10^9 and 5.18×10^8 m^3, respectively. In Wuyuan County, the surface water and groundwater shortage were only at the high water supply level, which means that at the high water supply level, water resources basically meet the water demand.

Based on the calculation results, the overall water supply structure of the HID was further calculated. At the low incoming water level of the forecast year, the ratio of surface water use was 63.2%, and the proportion of groundwater was 36.8%. At the middle incoming water level of the forecast year, the ratio of surface water use was 65.8%, and the proportion of groundwater was 34.2%. At the high incoming water level of the forecast year, the ratio of surface water use was 67.9%, and the proportion of groundwater was 32.1%. This suggests that the optimized proportion of surface water consumption increased, which has certain practical significance for mitigating groundwater over-exploitation, controlling groundwater below a critical depth, and preventing soil salinization in the HID.

4.2. Salt Control Analysis

The SALTMOD model was calibrated and validated using 1990–2010 field data for groundwater table depth and groundwater salinity (Figures 3 and 4). For groundwater table depth, the Nash–Sutcliffe efficiency (NSE) values were 0.68 (in calibration) and 0.65 (in validation), and the coefficient of correlation (R^2) 0.71 (in calibration) and 0.74 (in validation). For groundwater salinity, the NSE values were 0.66 (in calibration) and 0.58 (in validation), and the R^2 0.72 (in calibration) and 0.65 (in validation); thus, the SALTMOD modeling simulated the water and salt transport law in the HID very well. Multi-source, multi-region and different water-supply targets obtained from the two-stage robust stochastic optimization model as main parameters were input into the SALTMOD model based on the principle of water and salt balance. The output includes data such as groundwater mineralization and groundwater burial depth [41].

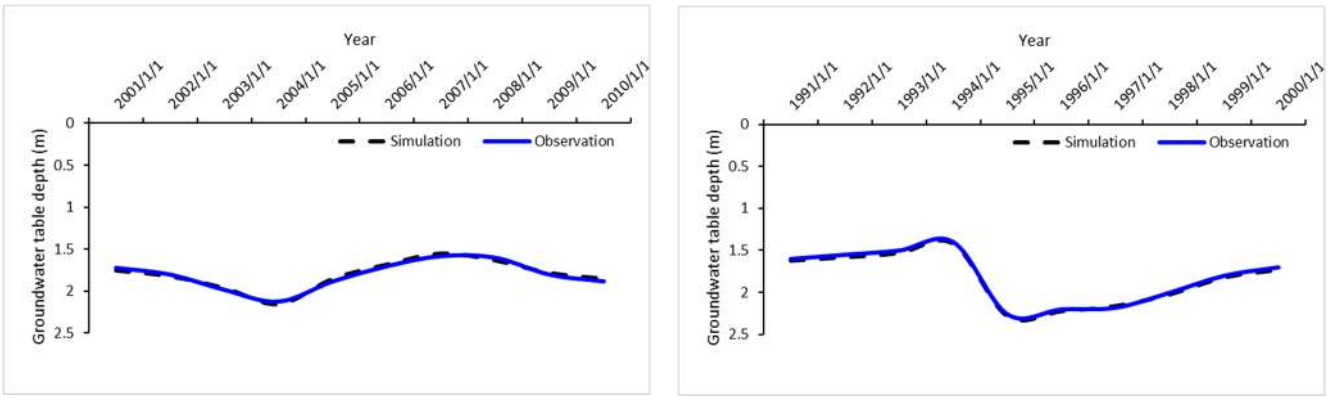

(**a**) (**b**)

Figure 3. Simulated versus observed groundwater table depths during (**a**) calibration from January 2001 to January 2010, and (**b**) verification from January 1991 to January 2000.

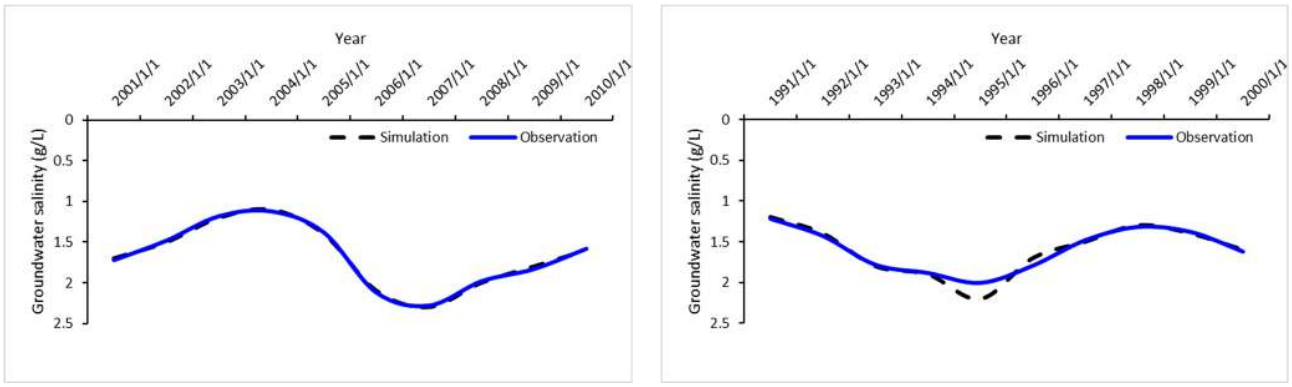

(**a**) (**b**)

Figure 4. Simulated versus observed groundwater table values during (**a**) calibration from January 2001 to January 2010, and (**b**) verification from January 1991 to January 2000.

From 2010 to 2014, the combination of wells with canals was not implemented, and from 2015 to 2019, surface water and groundwater joint scheduling was implemented in the HID.

The HID has low precipitation and high evaporation, the movement of groundwater belongs to the type of vertical infiltration and evaporation, and the salt content of irrigation water is about 0.5 g/L; this leads to serious secondary soil salinization in the HID. As shown in Figures 5 and 6, with the implementation of combined measures of wells with canals in the HID in 2015, for many years the groundwater table depth increased by approximately 0.3 m on average, and the groundwater salinity decreased by approximately 0.2 g/L on average. These two phenomena have a synergistic effect. However, the promotion of the combined measures of wells with canals should increase the area and extend the time to prevent the occurrence of salt return in the Wu Yuan irrigation area.

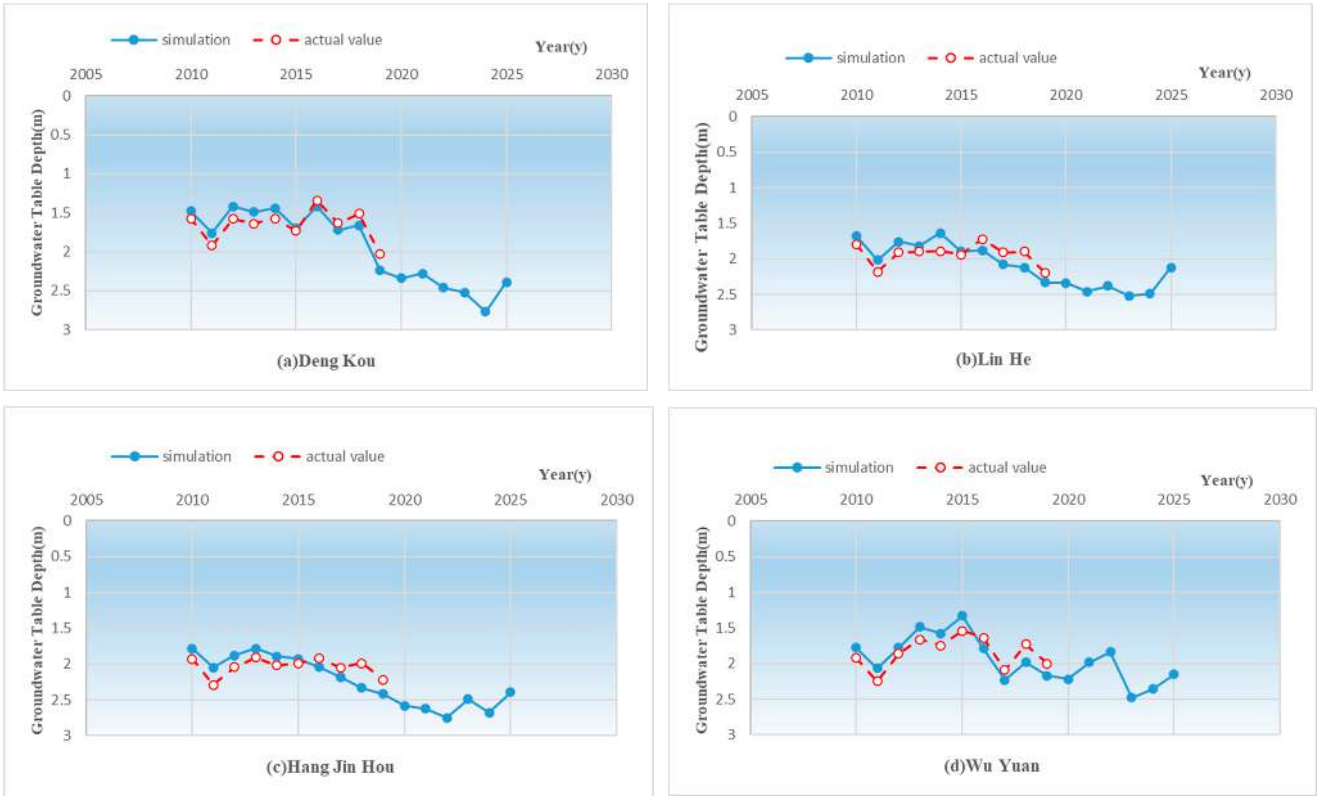

Figure 5. *Cont.*

Figure 5. Comparison of simulated and measured values of groundwater depth.

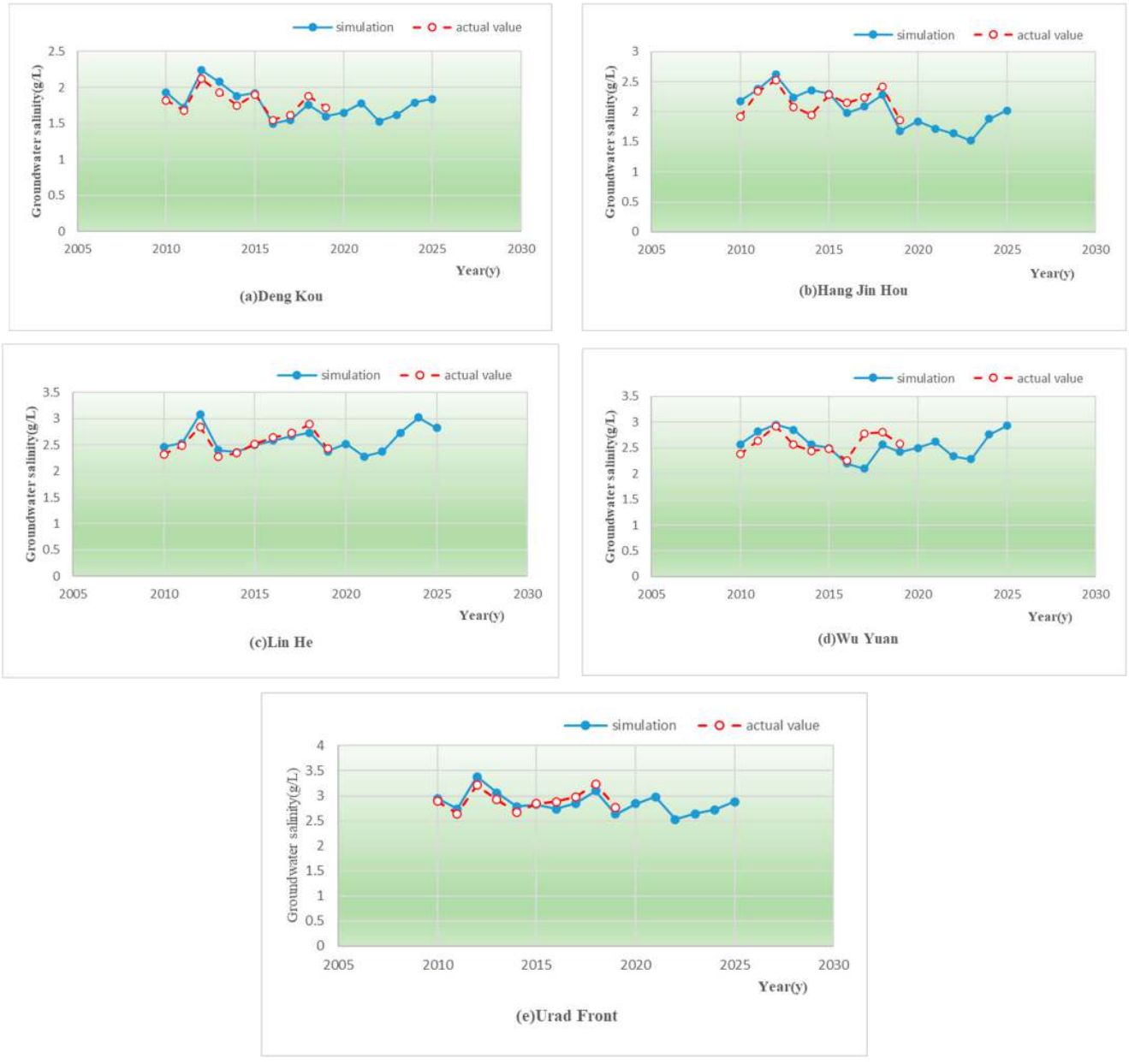

Figure 6. Comparison of simulated and measured values for water mineralization.

The measured groundwater depths in the different administrative areas of the HID were compared with the groundwater depth data output by the SALTMOD model. It was concluded that after combining wells and canals, over many years of pumping, the groundwater levels in the different administrative areas of the HID decreased by approximately 0.3 m [42].

The measured values of groundwater salinity in different administrative areas of the HID were also compared with those of groundwater salinity output by the SALTMOD model. It was concluded that after combining the wells and canals, the soil salt content in the different administrative areas of the HID will decrease slightly. The wheat, corn and oil sunflower roots have larger growth space, wider distribution, and enhanced stress resistance, which promote the high quality and yield of the three crops.

4.3. Risk Analysis under Different Incoming Water Conditions

The model was solved to obtain the minimum comprehensive cost of surface water and groundwater in the five irrigation areas in the case of joint dispatch f_{opt} = 1.38 × 10^9 ~3.24 × 10^9 yuan. Due to the different water distribution forms and the uncertainty of the system, the final cost was given as an interval value to accommodate different water distribution decisions [43]. In order to illustrate the effect of the robustness coefficient on the objective function value, the change of the objective function value of the water cost with the robustness coefficient at the three levels of low-medium-high water supply was calculated. The calculation results are shown in Figure 7.

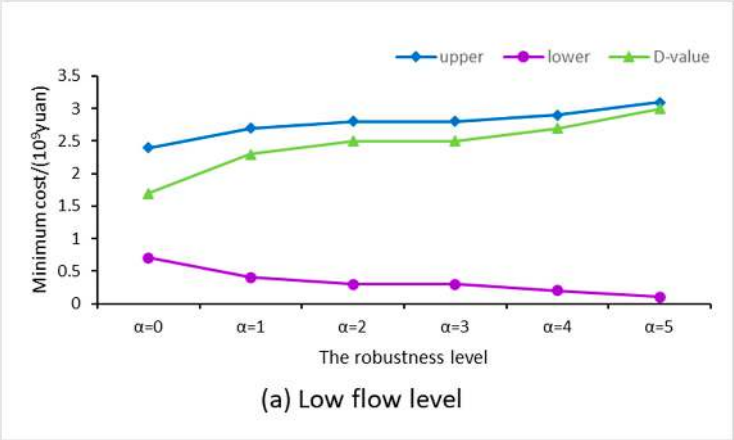

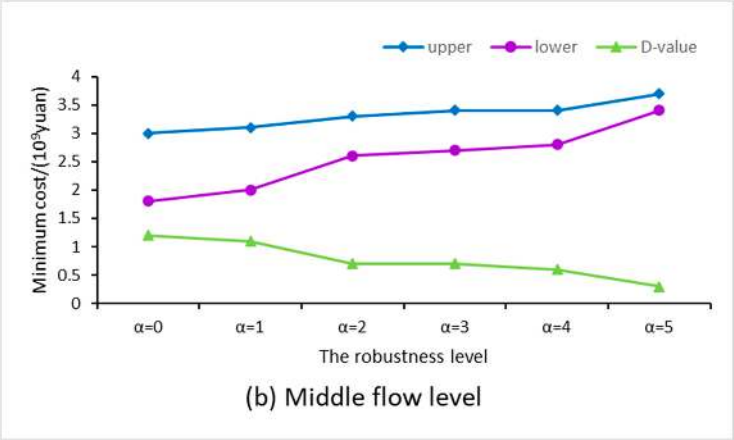

Figure 7. *Cont.*

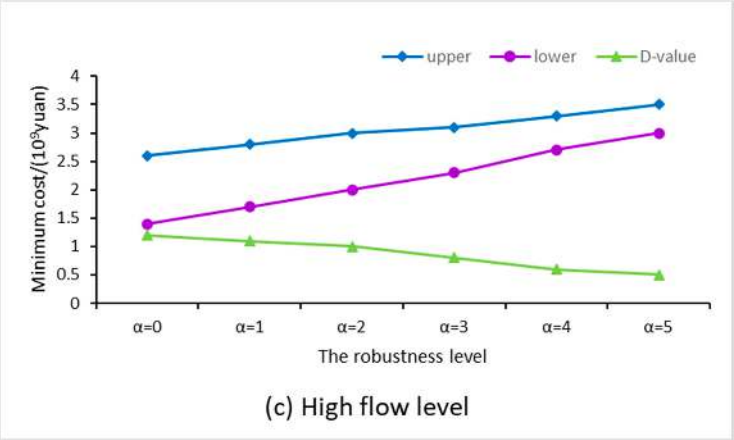

Figure 7. Minimum cost of water optimal allocation of different water levels under different α.

Under three types of incoming water probability, the robust coefficient α changes from 0 to 5 [44]. From Figure 7, it can be seen that the minimum cost of optimal allocation of water resources varies with α: (1) at the low water supply level: when $\alpha = 0$, the model is an ordinary interval two-stage stochastic programming model, which means that decision-makers think more about the economics of the system and ignore the system risks. The minimum cost is 1.7×10^9~2.4×10^9 yuan; as α increases, the objective function gradually increases. When $\alpha = 5$, the minimum cost is between 3×10^9~3.1×10^9 yuan. (2) At the middle water supply level: the objective function value gradually increases with the increase of α, and the minimum cost increases from 1.8×10^9~3×10^9 yuan to 3.4×10^9~3.7×10^9 yuan. (3) At the high water supply level: the objective function value also gradually increases with the increase of α, and the minimum cost increases from 1.4×10^9~2.6×10^9 to 3×10^9~3.5×10^9 yuan.

With the change of optimal allocation of water resources [45], the system cost shows a certain change law: (1) the increase of the robust coefficient causes the system cost to increase. When $\alpha \geq 2$, the cost is almost unchanged, indicating that the system has stabilized. (2) With the increase of the robust coefficient, the difference between the upper and lower limits of the cost becomes smaller, the stability of the system increases, and the economy and stability are well balanced.

5. Discussion

The interval two-stage stochastic optimization model is very effective in dealing with uncertain factors, but it ignores the risk issues in a saline-alkali land management system. After application, it can cause problems, such as soil salt return, agricultural production reduction and water shortage, in key periods of crop growth; thus, model results are not absolutely feasible. The robust optimization method can effectively avoid risks during the planning process and weigh the relationship between variable random values and recourse costs in the system. It is introduced into the interval two-stage stochastic programming model and coupled with the SALTMOD model. The results obtained can make the economy and stability of the saline-alkali land treatment system better balanced [46].

5.1. Precision Analysis of Water Distribution Model with the Actual Situation

Taking the agricultural water situation of HangJinHou banner in 2017 as an example, the model accuracy analysis was performed [47]. According to the statistics 2017 was calculated as the middle level of water supply. From the agricultural water in HangJinHou banner, the actual surface water and groundwater use was compared with the calculation results in the model. The results are shown in Table 5. The relative errors of the optimal allocation of surface water and groundwater were within 10%, the RMSE was approximately 30% and the d-index was smaller than 0.5. Overall, the model optimization results were consistent with the actual situation.

Table 5. Actual value and error analysis of water.

Administrative Region	**Surface Water**				
	Calculated Value/10^8 m^3	**Actual Value/10^8 m^3**	**Relative Error/%**	**RMSE**	**d-Index**
HangJinHou banner	[8.87, 10.37]	11.48	9.40	0.32	0.42
Administrative Region	**Groundwater**				
	Calculated Value/10^8 m^3	**Actual Value/10^8 m^3**	**Relative Error/%**	**RMSE**	**d-Index**
HangJinHou banner	[3.11, 3.69]	3.90	4.60	0.35	0.49

Through analysis, it is known that the planting structure data of the typical year 2015 was used as the known conditions when the model was optimized and solved, and the planting structure was adjusted accordingly in 2017, resulting in certain errors in the model [48]. However, the planting structure in the model can be adjusted through related parameters to reduce the error; surface water has a slightly larger error because the runoff cycle is more complicated than groundwater.

5.2. Precision Analysis of the Salt Control Model

The 2014–2016 output of the HID's Urat irrigation area through the SALTMOD model was used to compare the groundwater depth and mineralization of the groundwater with the measured values [49,50]. Among them, the combination of wells and canals was not implemented before 2015. After 2015, surface water and groundwater joint dispatching was implemented in the Urat irrigation area.

The comparison of the annual groundwater depth and actual measured values of the Urat irrigation area from 2014 to 2016 is shown in Table 6. The changing process of groundwater depth is shown in Figure 5e. Only the relative error of the simulation in 2014 was slightly greater than 15%, the rest were within 10%, and the RMSE for three years was smaller than 0.2. The simulation accuracy was high [51,52]. The comparison of the measured and simulated groundwater mineralization in the Urat irrigation area from 2014 to 2016 is shown in Table 7 and Figure 6e. The average relative error of mineralization of groundwater in the Urat irrigation area was between 12% and15%, and the RMSE for three years was within 0.1. The simulated values better reflect the dynamic changes of root salinity for main crops in the HID, and more accurately simulated the process of salt reduction due to the combination of wells and canals from 2015 to 2019 [53,54].

Table 6. Comparison of measured and simulated groundwater levels in the Urat irrigation area from 2014 to 2016.

	Measured Value (m)	**Simulated Value (m)**	**Relative Error**	**RMSE**	**d-Index**
2014	1.81	1.55	16.90%	0.18	0.13
2015	1.62	1.60	1.10%	0.01	0.997
2016	2.02	2.21	6.34%	0.13	0.01
The annual average	1.82	1.79	2.26%	0.02	0.002

Table 7. Comparison of measured and simulated groundwater mineralization in the Urat irrigation area from 2014 to 2016.

	Measured Value (g/L)	**Simulated Value (g/L)**	**Mean Relative Error**	**RMSE**	**d-Index**
2014	2.67	2.79	13.52%	0.08	0.002
2015	2.84	2.83	5.18%	0.01	0.988
2016	2.88	2.74	14.78%	0.10	0.002
The annual average	2.80	2.79	5.06%	0.007	0.002

6. Conclusions

In this study, an interval two-stage robust stochastic programming (ITRSP) and SALTMOD coupling model was established to coordinate agricultural irrigation and environmental protection under a variety of uncertainties, and to address risk issues in saline-alkali land management systems. The developed ITRSP-SALTMOD model can reflect the interaction of agricultural irrigation and salt control issues into a framework to support policy makers in developing comprehensive plans at the irrigation district scale. It can support agricultural irrigation and drainage under different robust coefficients, and then formulate related current policies to control the groundwater burial depth of irrigation districts below a critical depth while reducing groundwater mineralization. At the same time, it can also be used to reduce the cost of saline-alkali land management systems and realize considerable social and economic system benefits. In addition, it can provide solutions for protecting the agro-ecological environment of the HID and achieve green development in the region. The ITRSP-SALTMOD coupling model is a good example that can be applied and extended to salinized areas mainly distributed in Xinjiang, Gansu, Qinghai, Inner Mongolia, Ningxia and other areas in northwest China, as well as the eastern coastal areas.

With the aid of the model, several discoveries were found, as follows: (a) combining uncertainty and risk can avoid the shortcomings of the traditional interval two-stage stochastic programming method, and introduce robust optimization to seek the minimum water cost of optimal water resources allocation to prevent and control soil salinity, avoiding the situation of concentrating risk losses in a certain irrigation area. (b) Through an interval two-stage robust stochastic optimization model, from 2015, the implementation of combined surface water and groundwater use of optimal dispatching schemes had a positive significance for regulating groundwater depth and changing soil water and salt dynamics. (c) The SALTMOD model can better simulate the dynamic changes of the groundwater burial depth and soil root layer salinity in the irrigation districts of different administrative areas in the HID, providing a basis for decision-makers to reasonably control salt in the future. Correspondingly, specific suggestions for decision-makers can be summarized as follows: based on the existing "Three North" shelter forest system construction project in the HID, the crop planting structure should be adjusted, and the resistance to drought, smoke and salt-alkali crops, such as Sophora japonica, increased, improving salt control efficiency, while promoting local economic growth; governmental support and financial subsidies should be advocated, and the optimal dispatching scheme for expanding the combined use of surface water and groundwater promoted and applied in arid and semi-arid areas. Furthermore, consciousness and robust methods for identification of risk adoption should be considered in decision-making, such as the conditional value at risk (CVaR) method, which could fortify the reliability of interval two-stage (ITS) strategies. Since there are interactive relationships between water supply, irrigation, precipitation, water consumption and water demand in the irrigation district, multi-stage programming should be considered; due to the particularity of the complex system of water resources, it is necessary to introduce intuitionistic fuzzy sets to obtain the water resources allocation scheme based on group decision-making. These are worthy of further research in the future.

Author Contributions: The study and writing of the manuscript were carried out with contributions from all the authors. Writing—original draft preparation, Y.Z.; supervision, P.Y. All authors have read and agreed to the published version of the manuscript.

Funding: This research was financially supported by the National Natural Science Foundation of China's continuation of funding projects for innovative research groups (No. 51621061), the Discipline Innovation and Talent Introduction Plan of China Agricultural University (111 Plan), the Planning and Design of Donghui Ten Thousand Mu Modern Agricultural Science and Technology Demonstration Park in Lancang County, Yunnan Province (No. 69190031), and the Research on multi-dimensional regulation model of water resources in ecological farmland in southern Xinjiang (No. 69112002).

Institutional Review Board Statement: Not applicable.

Informed Consent Statement: Not applicable.

Data Availability Statement: Not applicable.

Conflicts of Interest: The authors declare no conflict of interest.

References

1. Xiao, B. Saline land is a devil who can become an angel. *Chin. Natl. Geogr.* **2011**, *4*, 146–151. (In Chinese)
2. Yang, P.L. *Modern Water Conservancy and Hydropower Project Management Theory and Practice*; China Water Conservancy and Hydropower Press: Beijing, China, 2014. (In Chinese)
3. Li, Y.; Huang, G.; Nie, S. An interval-parameter multi-stage stochastic programming model for water resources management under uncertainty. *Adv. Water Resour.* **2006**, *29*, 776–789. [CrossRef]
4. Li, M.; Fu, Q.; Singh, V.P.; Liu, D. An interval multi-objective programming model for irrigation water allocation under uncertainty. *Agric. Water Manag.* **2018**, *196*, 24–36. [CrossRef]
5. Zhang, S.; Tan, Q.; Cai, Y.; Zhang, T.; Song, G. Mathematical analyses of ecological and economic tradeoffs in irrigated agriculture based on inexact optimization principles and hierarchical crop projections. *J. Clean. Prod.* **2019**, *235*, 69–84. [CrossRef]
6. Li, Y.; Huang, G.H.; Veawab, A.; Nie, X.; Liu, L. Two-stage fuzzy-stochastic robust programming: A hybrid model for regional air quality management. *J. Air Waste Manag. Assoc.* **2006**, *56*, 1070–1082. [CrossRef]
7. Chen, C.; Huang, G.H.; Li, Y.P.; Zhou, Y. A robust risk analysis method for water resources allocation under uncertainty. *Stoch. Environ. Res. Risk Assess.* **2012**, *27*, 713–723. [CrossRef]
8. Tan, Q.; Zhang, T. Robust fractional programming approach for improving agricultural water-use efficiency under uncertainty. *J. Hydrol.* **2018**, *564*, 1110–1119. [CrossRef]
9. Yao, R.-J.; Yang, J.-S.; Zhang, T.-J.; Hong, L.-Z.; Wang, M.-W.; Yu, S.-P.; Wang, X.-P. Studies on soil water and salt balances and scenarios simulation using SaltMod in a coastal reclaimed farming area of eastern China. *Agric. Water Manag.* **2014**, *131*, 115–123. [CrossRef]
10. Bahçeci, I.; Dinç, N.; Tarı, A.F.; Ağar, A.İ.; Sönmez, B. Water and salt balance studies, using SaltMod, to improve subsurface drainage design in the Konya–Cumra Plain, Turkey. *Agric. Water Manag.* **2006**, *85*, 261–271. [CrossRef]
11. Ajay, S. Validation of SaltMod for a semi-arid part of northwest India and some options for control of waterlogging. *Agric. Water Manag.* **2012**, *115*, 194–202.
12. Mao, W.; Yang, J.; Zhu, Y.; Ye, M.; Wu, J. Loosely coupled SaltMod for simulating groundwater and salt dynamics under well-canal conjunctive irrigation in semi-arid areas. *Agric. Water Manag.* **2017**, *192*, 209–220. [CrossRef]
13. Sarangi, A.; Singh, M.; Bhattacharya, A.K.; Singh, A.K. Subsurface drainage performance study using SALTMOD and ANN models. *Agric. Water Manag.* **2006**, *84*, 240–248. [CrossRef]
14. Ajay, S. Evaluating the effect of different management policies on the long-term sustainability of irrigated agriculture. *Land Use Polic.* **2016**, *54*, 499–507.
15. Laguna, M. Applying Robust Optimization to Capacity Expansion of One Location in Telecommunications with Demand Uncertainty. *Manag. Sci.* **1998**, *44*, 101–110. [CrossRef]
16. Yu, C.-S.; Li, H.-L. A robust optimization model for stochastic logistic problems. *Int. J. Prod. Econ.* **2000**, *64*, 385–397. [CrossRef]
17. Huang, G.; Loucks, D.P. An inexact two-stage stochastic programming model for water resources management under uncertainty. *Civ. Eng. Environ. Syst.* **2000**, *17*, 95–118. [CrossRef]
18. Xu, W.; Diwekar, U.M. Multi-objective integrated solvent selection and solvent recycling under uncertainty using a new genetic algorithm. *Int. J. Environ. Pollut.* **2007**, *29*, 70–89. [CrossRef]
19. Oosterbaan, R.J.; Senna, M.A. Using SALTMOD to Predict Drainage and Salinity in the Nile Delta. In *Annual Report 1989*; ILRI: Wageningen, The Netherlands, 1990.
20. Zhang, Y.Q.; Yang, P.L.; Liu, X.; Adeloye, A.J. Simulation and Optimization Coupling Model for Soil Salinization and Waterlogging Control in the Urad Irrigation Area, North China. *J. Hydrol.* **2021**, *607*, 127408. [CrossRef]
21. Niu, G.; Li, Y.; Huang, G.; Liu, J.; Fan, Y. Crop planning and water resource allocation for sustainable development of an irrigation region in China under multiple uncertainties. *Agric. Water Manag.* **2015**, *166*, 53–69. [CrossRef]
22. Lu, H.W. Inexact Mathematical Programming Methods for Water Resources Management. Ph.D. Dissertation, Institute for Energy, Environment and Sustainable Communities, The University of Regina, Regina, SK, Canada, 2010.
23. Zeng, S.X.; Li, S.S. Decomposition and coordination model for large-scale irrigation water distribution system. *J. Hohai Univ.* **1990**, *18*, 67–75, (In Chinese with English Abstract).
24. Tan, Q. Inexact Programming Methodologies for Water Resources and Environmental Management under Compound Uncertainty. Ph.D. Dissertation, Institute for Energy, Environment and Sustainable Communities, The University of Regina, Regina, SK, Canada, 2011.
25. Peng, S.Z.; Zhang, Y.Y.; Shen, J.Q. Optimized irrigation model for combined use of wells and canals in Hetao Irrigation District. *Adv. Water Sci.* **1992**, *3*, 199–206, (In Chinese with English Abstract).

26. Guo, P. Inexact Mathematical Programming for the Management of Water Resources and Environmental Systems under Multiple Uncertainties. Ph.D. Dissertation, Institute for Energy, Environment and Sustainable Communities, The University of Regina, Regina, SK, Canada, 2009.
27. MWR. China's Agricultural Water Development. 2000. Available online: http://www.irrigate.com.cn/hangyegaikuang/ (accessed on 1 January 2023).
28. Inner Mongolia Autonomous Region Statistics Bureau. *Inner Mongolia Statistical Yearbook*; China Statistics Press: Beijing, China, 2014.
29. Bayannaoer City Statistics Bureau. *Bayannaoer Statistical Yearbook*; China Statistics Press: Beijing, China, 2014.
30. Bayannaoer Water Conservancy Bureau. *Bayannaoer Water Resources Bulletin*; China Statistics Press: Beijing, China, 2014.
31. Subbaiah, R. A review of models for predicting soil water dynamics during trickle irrigation. *Irrig. Sci.* **2013**, *31*, 225–258. [CrossRef]
32. Kourgialas, N.N.; Koubouris, G.C.; Dokou, Z. Optimal irrigation planning for addressing current or future water scarcity in Mediterranean tree crops. *Sci. Total Environ.* **2019**, *654*, 616–632. [CrossRef] [PubMed]
33. Communar, G.; Friedman, S.P. Relative Water Uptake Rate as a Criterion for Trickle Irrigation System Design: I. Coupled Source-Sink Steady Water Flow Model. *Soil Sci. Soc. Am. J.* **2010**, *74*, 1493–1508. [CrossRef]
34. Singh, D.; Rajput, T.; Sikarwar, H.; Sahoo, R.; Ahmad, T. Simulation of soil wetting pattern with subsurface drip irrigation from line source. *Agric. Water Manag.* **2006**, *83*, 130–134. [CrossRef]
35. Cote, C.M.; Bristow, K.L.; Charlesworth, P.B.; Cook, F.J.; Thorburn, P.J. Analysis of soil wetting and solute transport in subsurface trickle irrigation. *Irrig. Sci.* **2003**, *22*, 143–156. [CrossRef]
36. Han, M.; Zhao, C.; Feng, G.; Yan, Y.; Sheng, Y. Evaluating the Effects of Mulch and Irrigation Amount on Soil Water Distribution and Root Zone Water Balance Using HYDRUS-2D. *Water* **2015**, *7*, 2622–2640. [CrossRef]
37. Ben-Gal, A.; Lazorovitch, N.; Shani, U. Subsurface drip irrigation in gravel-filled cavities. *Vados. Zone J.* **2004**, *3*, 1407–1413. [CrossRef]
38. Li, J.; Zhang, J.; Rao, M. Wetting patterns and nitrogen distributions as affected by fertigation strategies from a surface point source. *Agric. Water Manag.* **2004**, *67*, 89–104. [CrossRef]
39. Autovino, D.; Rallo, G.; Provenzano, G. Predicting soil and plant water status dynamic in olive orchards under different irrigation systems with Hydrus-2D: Model performance and scenario analysis. *Agric. Water Manag.* **2018**, *203*, 225–235. [CrossRef]
40. Lu, P.; Zhang, Z.; Sheng, Z.; Huang, M.; Zhang, Z. Assess Effectiveness of Salt Removal by a Subsurface Drainage with Bundled Crop Straws in Coastal Saline Soil Using HYDRUS-3D. *Water* **2019**, *11*, 943. [CrossRef]
41. Ziogas, V.; Tanou, G.; Morianou, G.; Kourgialas, N. Drought and Salinity in Citriculture: Optimal Practices to Alleviate Salinity and Water Stress. *Agronomy* **2021**, *11*, 1283. [CrossRef]
42. Yang, T.; Li, D.; Clothier, B.; Wang, Y.; Duan, J.; Di, N.; Li, G.; Li, X.; Jia, L.; Xi, B. Where to monitor the soil-water potential for scheduling drip irrigation in Populus tomentosa plantations located on the North China Plain? *For. Eco. Manag.* **2019**, *437*, 99–112. [CrossRef]
43. Nazari, E.; Besharat, S.; Zeinalzadeh, K.; Mohammadi, A. Measurement and simulation of the water flow and root uptake in soil under subsurface drip irrigation of apple tree. *Agric. Water Manag.* **2021**, *255*, 106972. [CrossRef]
44. Xi, B.; Bloomberg, M.; Watt, M.S.; Wang, Y.; Jia, L. Modeling growth response to soil water availability simulated by HYDRUS for a mature triploid Populus tomentosa plantation located on the North China Plain. *Agric. Water Manag.* **2016**, *176*, 243–254. [CrossRef]
45. Elmaloglou, S.; Diamantopoulos, E. Simulation of soil water dynamics under subsurface drip irrigation from line sources. *Agric. Water Manag.* **2009**, *96*, 1587–1595. [CrossRef]
46. Zhang, Y.; Yang, J.; Yao, R.; Wang, X.; Xie, W. Short-term effects of biochar and gypsum on soil hydraulic properties and sodicity in a saline-alkali soil. *Pedosphere* **2020**, *30*, 694–702. [CrossRef]
47. Wei, C.; Ren, S.; Yang, P.; Wang, Y.; He, X.; Xu, Z.; Wei, R.; Wang, S.; Chi, Y.; Zhang, M. Effects of irrigation methods and salinity on CO_2 emissions from farmland soil during growth and fallow periods. *Sci. Total Environ.* **2020**, *752*, 141639. [CrossRef]
48. Zhang, C.; Li, X.; Guo, P.; Huo, Z.; Huang, G. Enhancing irrigation water productivity and controlling salinity under uncertainty: A full fuzzy dependent linear fractional programming approach. *J. Hydrol.* **2022**, *606*, 127428. [CrossRef]
49. Guo, L.; Nie, Z.; Zhou, J.; Zhang, S.; An, F.; Zhang, L.; Tóth, T.; Yang, F.; Wang, Z. Effects of Different Organic Amendments on Soil Improvement, Bacterial Composition, and Functional Diversity in Saline–Sodic Soil. *Agronomy* **2022**, *12*, 2294. [CrossRef]
50. Lu, H.; Li, H.; Wang, J.; Zheng, H.; Cao, X.; Tong, C. Optimal water and land resource allocation in pastoral areas based on a water-land forage-livestock balance: A case study of Otog Front Banner, Inner Mongolia, China. *Environ. Sci. Pollut. Res.* **2020**, *27*, 10328–10341. [CrossRef] [PubMed]
51. Bughici, T.; Skaggs, T.H.; Corwin, D.L.; Scudiero, E. Ensemble HYDRUS-2D modeling to improve apparent electrical conductivity sensing of soil salinity under drip irrigation. *Agric. Water Manag.* **2022**, *272*, 107813. [CrossRef]
52. Zhang, Y.Q.; Yang, P.L. Agricultural Water Optimal Allocation Using Minimum Cross-Entropy and Entropy-Weight-Based TOPSIS Method in Hetao Irrigation District, Northwest China. *Agriculture* **2022**, *12*, 853. [CrossRef]

53. Hardie, M.; Ridges, J.; Swarts, N.; Close, D. Drip irrigation wetting patterns and nitrate distribution: Comparison between electrical resistivity (ERI), dye tracer, and 2D soil–water modelling approaches. *Irrig. Sci.* **2018**, *36*, 97–110. [CrossRef]
54. Zhang, Y.Q.; Yang, P.L. Agricultural Productive Carrying Capacity Improve and Water Optimal Allocation under Uncertainty Based on Remote Sensing Data in Lancang County, Southwest China. *Water* **2022**, *14*, 3641. [CrossRef]

MDPI AG
Grosspeteranlage 5
4052 Basel
Switzerland
Tel.: +41 61 683 77 34

Sustainability Editorial Office
E-mail: sustainability@mdpi.com
www.mdpi.com/journal/sustainability

Academic Open
Access Publishing

mdpi.com

ISBN 978-3-7258-3731-1